Czech Technical University in Prague
Faculty of Electrical Engineering

Department of Electrical Power Engineering
Field of study: Electrical Power Engineering

Decomposition of organic and waste substances in a thermal plasma reactor

Rozklad organických a odpadních látek v reaktoru s termickým plazmatem

MASTER'S THESIS

Author:	Bc. Jakub Pilař
Supervisor:	prof. Ing. Stanislav Pekárek, CSc.
Year:	2023

ZADÁNÍ DIPLOMOVÉ PRÁCE

I. OSOBNÍ A STUDIJNÍ ÚDAJE

Příjmení: **Pilař** Jméno: **Jakub** Osobní číslo: **474462**

Fakulta/ústav: **Fakulta elektrotechnická**

Zadávající katedra/ústav: **Katedra elektroenergetiky**

Studijní program: **Elektrotechnika, energetika a management**

Specializace: **Elektroenergetika**

II. ÚDAJE K DIPLOMOVÉ PRÁCI

Název diplomové práce:

Rozklad organických a odpadních látek v reaktoru s termickým plazmatem

Název diplomové práce anglicky:

Decomposition of organic and waste substances in a thermal plasma reactor

Pokyny pro vypracování:

Cílem práce je analýza dat z experimentů na plazmochemickém reaktoru určeném k tepelnému zpracování různých organických a odpadních látek. Energie pro probíhající endotermické reakce je dodávána pomocí termického plazmatu generovaného obloukovými a mikrovlnnými plazmatrony. V reaktoru typicky probíhají tři základní typy reakcí: 1. zplyňování (gazifikace) za přístupu stechiometrického množství kyslíku nutného k vytvoření oxidu uhelnatého, 2. pyrolýza bez přístupu kyslíku a 3. různé kombinace prvních dvou. Úkolem studenta je zúčastnit se celého experimentálního procesu, který zahrnuje:

1. Přípravu materiálu pro zpracování včetně kalibrace jeho podávání do reaktoru.
2. Přípravu zdroje plazmatu, jeho testování a pochopení jeho vlastností.
3. Přípravu reaktoru a diagnostických zařízení, zejména spolehlivého měření složení a vlastností výstupných produktů.
4. Účast na experimentu, sledování a kontrolu všech měřících zařízení.
5. Zpracování a vyhodnocení naměřených dat.

Na základě vyhodnocení dat z jednoho nebo více experimentů by měl student samostatně dospět k závěrům, které se mohou soustředit na různé aspekty dané problematiky. Příkladem může být podrobná energetická bilance procesu a posouzení, zda je konkrétní způsob zpracování určité látky (například gazifikace nemocničního odpadu) konkurenceschopný zejména z pohledu vysoké energetické náročnosti plazmatu. Také je možné zaměřit se na porovnání odlišných zdrojů termického plazmatu – obloukového a mikrovlnného – a pokusit se najít optimální podmínky vhodné pro zpracování daného materiálu daným typem plazmatu. Jinou možností je podrobné zkoumání konkrétního produktu reakce, například pokusit se maximalizovat množství produkovaného vodíku při zachování jeho co nejvyšší čistoty. Velkým tématem je třeba také minimalizace produkce $CO2$, a současně smysluplné využití pevného uhlíku, který vzniká v různých podobách při pyrolýze.

Seznam doporučené literatury:

[1] Huang H, Tang L (2007) Treatment of organic waste using thermal plasma pyrolysis technology. Energy Conversion and Management 48, 1331–1337.
[2] Heberlein J, Murphy A (2008) Thermal plasma waste treatment. J. Phys. D: Appl. Phys. 41, 053001.
[3] Fabry F, Rehmet C, Rohani V, Fulcheri L (2013) Waste gasification by thermal plasma: A review. Waste Biomass Valor, Vol. 4, 421–439.
[4] Hrabovský M, van der Walt, I J (2018) Plasma Waste Destruction. In: Handbook of Thermal Science and Engineering, Springer Nature, 1st Edition.
[5] Sikarwar V S, Hrabovský M, Van Oost G, Pohořelý M, Jeremiáš M (2020) Progress in waste utilization via thermal plasma. Prog. Energy Combust. Sci., vol. 81, p. 100873.

Jméno a pracoviště vedoucí(ho) diplomové práce:

prof. Ing. Stanislav Pekárek, CSc. katedra fyziky FEL

Jméno a pracoviště druhé(ho) vedoucí(ho) nebo konzultanta(ky) diplomové práce:

Datum zadání diplomové práce: **16.02.2023** Termín odevzdání diplomové práce: ______________

Platnost zadání diplomové práce: **22.09.2024**

prof. Ing. Stanislav Pekárek, CSc. podpis vedoucí(ho) práce	doc. Ing. Zdeněk Müller, Ph.D. podpis vedoucí(ho) ústavu/katedry	prof. Mgr. Petr Páta, Ph.D. podpis děkana(ky)

III. PŘEVZETÍ ZADÁNÍ

Diplomant bere na vědomí, že je povinen vypracovat diplomovou práci samostatně, bez cizí pomoci, s výjimkou poskytnutých konzultací.
Seznam použité literatury, jiných pramenů a jmen konzultantů je třeba uvést v diplomové práci.

. Datum převzetí zadání	Podpis studenta

Sworn statement

I hereby declare that I have prepared the submitted thesis independently and that I have listed all the sources of information used in accordance with the Guidelines for the observance of ethical principles in the preparation of university final theses.

Prague, ...

Bc. Jakub Pilař

Acknowledgements

I would like to thank prof. Ing. Stanislav Pekárek, CSc. for cooperation with the Department of Electrical Power Engineering, allowing me to devote to this topic in my master's thesis and for his general guidance. Furthermore, I am very grateful to Mgr. Alan Mašláni, Ph.D., who was practically my second supervisor and provided me valuable feedback for most of the thesis content.

Similarly, I thank Ing. Michal Jeremiáš, Ph.D. that he enabled me to work on the master's thesis at the Institute of Plasma Physics, Ing. Václav Březina for his tireless help with technical aspects, Ing. Dominik Kralik for his advice concerning chemical engineering and Mgr. Oldřich Živný, Ph.D. for his suggestions about the formal requirements of the thesis.

Also, I express my gratitude to Ing. Petr Kočárník, Ph.D. for advice on models and gas mixtures, doc. Dr. Ing. Jan Kyncl for consultations about the issue of heat transfer and Ing. Tomáš Králík, Ph.D. for discussion and inspiration regarding some of the economic aspects.

Last but not least, I would like to thank all my other friends and colleagues who in any way contributed to the enrichment of this thesis, and my close ones, especially family, for their support and trust during my studies.

Bc. Jakub Pilař

Title:
Decomposition of organic and waste substances in a thermal plasma reactor

Author: Bc. Jakub Pilař

Study program: Electrical Engineering, Power Engineering and Management
Field of study: Electrical Power Engineering
Type of work: Master's thesis

Supervisor: prof. Ing. Stanislav Pekárek, CSc.
Department of Physics

Abstract: This thesis is devoted to the issue of waste treatment using thermal plasma. From the beginning, it is focused on a brief description of the plasma theory, technology of plasma torches and reactors, including their types and mutual differences. This is followed by a practical part related to the experiments, which is divided into a summary of the preparatory activities before the experiments and the results obtained by measurements, calculations, and analyses. The main pillars of the quantitative assessment of individual experimental processes are discrete numerical models of energy balances, on which the discussion regarding the achieved results is based. The next part is a brief summary of the electricity market in relation to the opportunities for this technology to become competitive. Finally, specific projects utilizing this technology are presented, which are already in operation or have the potential to become commercially and industrially successful.

Key words: thermal plasma, plasma torch, plasma reactor, waste treatment, energy accumulation, energy balance, energy efficiency, electricity market

Název práce:
Rozklad organických a odpadních látek v reaktoru s termickým plazmatem

Autor: Bc. Jakub Pilař

Abstrakt: Tato práce je věnována problematice zpracování odpadů termickým plazmatem. Úvodem je soustředěna na stručný popis teorie plazmatu, technologie plazmových hořáků a reaktorů, včetně jejich typů a vzájemných odlišností. Následuje praktická část týkající se experimentů, která je rozdělena na shrnutí přípravných aktivit před experimenty a na výsledky obdržené měřením, výpočty a analýzami. Hlavními pilíři kvantitativního posouzení jednotlivých experimentálních procesů jsou diskrétní numerické modely energetických bilancí, ze kterých vychází diskuse ohledně dosažených výsledků. Další částí je stručné shrnutí energetického trhu v souvislosti s příležitostmi této technologie stát se konkurenceschopnou. Nakonec jsou představeny konkrétní projekty využívající této technologie, které již v provozu fungují nebo mají potenciál se komerčně a průmyslově prosadit.

Klíčová slova: termické plazma, plazmový hořák, plazmový reaktor, zpracování odpadu, akumulace energie, eneretická bilance, energetická účinnost, energetický trh

Contents

List of abbreviations

AB	Aggregation block
aFRR	Automatic Frequency Restoration Reserve
AMM	Automated Meter Management
BL	Boundary layer
BS	Black Start
CAPEX	Capital expenditure
CAS	Czech Academy of Sciences
CEPS	Czech electricity transmission system (ČEPS, a.s.)
CEZ	CEZ Group (České energetické závody, a.s.)
CHA	Chemical analysis
CHP	Combined heat and power generation
CNG	Compressed natural gas
CZK	Czech crown
DC	Direct current
DS	Distribution system
DSO	Distribution system operator
EAN	European Article Number
EMO	Energy market operator
ERO	Energy Regulatory Office
EU	European Union
EUW	Energetically usable wastes
FCR	(Frequency Containment Reserve
FGP	Flue Gas Pipe
GDP	Gross domestic product
GPS	Global Positioning System
HHV	Higher heating value
HPT	Hybrid plasma torch
HV	High voltage
HW	Hazardous waste

IPP Institute of plasma physics
LHV Lower heating value
LNG Liquified natural gas
LRW Low level radioactive waste
LTE Local thermodynamic equilibrium
LV Low voltage
mFRR Manual Frequency Restoration Reserve
MWPT Microwave plasma torch
MSW Municipal solid waste
NAP National Action Plan
OG Off-Grid
OPEX Operating expense
P2G Power-to-Gas
P2X Power-to-X
PBS Power balancing services
PCC Point of Common Coupling
PCHT Plasma chemical technologies
POP Persistent organic pollutants
PT Plasma torch
QT Quenching Tower
RDF Refuse derived fuel
RE Reactor
RES Renewable energy sources
RP Reserved power
RR Restoration Reserve
SMW Simulated medical waste
SRUQ Secondary regulation of U & Q
SuS Support services
SyS System services
TCHR Thermochemical reactions
TS Transmission system
TSO Transmission system operator
TWD Traveling wave discharge
UHHK University Hospital Hradec Králové
USD United States dollar ($)
VHV Very high voltage
W2E Waste-to-energy
W2H Waste-to-heat

List of Figures

Introduction

With industrial and scientific development, outdated technologies are getting replaced by more modern and advanced ones. An example is electrical power engineering, where rapid changes and evolution can be observed, particularly during recent decades. This transformation includes building new power plants, using renewable energy sources, modernizing existing network structures, increasing efficiency, or implementing smart measurement and control methods to make use of electrical energy more effective and to ensure bigger reliability of supplies.

These processes are motivated by many factors, particularly the efforts to protect the environment and reduce the impacts of climate change like global warming or extreme weather, growing demand for energy, increasing prices of primary commodities, the desire for a transition to sustainable and cost-effective energy sector, and accomplishing the maintenance of economic growth.

The solution to many of the mentioned problems could be potentially provided by thermal plasma waste treatment technology. It is an efficient way of processing waste and producing secondary raw materials (or also energy) from most waste materials. Although this approach may be more efficient than traditional combustion methods, its operation is practically emission-free. Plasma waste treatment also enables waste to be decomposed into its primary components and used for further production, which can contribute to sustainability and reduce waste by transitioning to a circular economy. The main output products are synthesis gas (known as syngas), solid carbon black, and slag. All of these by-products are possibly reusable.

Despite its undeniable advantages, the operation is still usually commissioned mostly in laboratory conditions, especially in current middle Europe. Commercial use of this technology remains restrained. This may be caused by the technical and technological complexity, and relatively short history of development compared to other conventional technological processes.

The construction and technical realization of a plasma reactor facility, including the used plasma torch, can vary for different applications. In this thesis, mainly the PLASGAS reactor at the IPP CAS will be considered. Experiments of plasma waste treatment will be realized under different operating conditions, particularly in terms of the input materials and plasma torches used. The material samples will be simulated medical waste (SMW) and refuse-derived fuel (RDF). The tested plasma torches will be a hybrid arc plasma torch and a microwave plasma torch.

Motivation

This thesis is based on a persisting effort in cooperation with colleagues from the IPP CAS and an author's long-term interest in this field of study. The content is partly a wide extension of the author's already completed Bachelor's thesis and in the final scale, it may probably represent the main pillars for the upcoming research on plasma waste treatment technology.

Other major motivating factors for choosing this topic are the constantly deteriorating situation with waste management and the current situation in the energy sector. The effort to take a more ecological approach to energy production or the threat of a shortage of some fossil fuels (for example natural gas, which was supposed to be a transitional source for electricity production while coal-fired power plants would be getting replaced by renewable sources) is mainly concerned. This is strongly caused especially by the current intense geopolitical situation.

Although it is only an indirect part of the thesis assignment, the author's personal goal for completing the thesis is to make research about the real possibility of commercializing this technology and integrating plasma reactors into the electrical power system.

The overall objective is to perform a series of experiments on the semi-operational PLASGAS testing facility within various operating conditions, measure and evaluate relevant data, compare the individual experiments, and discuss the possible optimal conditions for different cases of a potential operation. Consequently, focus on the possible commercialization of the technology, evaluate the viability of a plasma gasification aggregates construction project, and assess for which application would the system be most suitable or which services would be optimal to provide. In case of multiple alternatives, it will be appropriate to compare the proposals respectively in terms of feasibility, difficulty, profitability, or general operation.

In addition to the theoretical part describing the topic and the practical part including the experiments and data analysis, the expected outcome of this thesis could be the proposal of possible project implementations and their comparison. The real project should be designed and assessed based on technical, logistical, economic, and legislative possibilities.

Chapter 1

Plasma aggregate

This chapter briefly describes the basics of the plasma theory, the technology of plasma torches and the plasma reactor, and briefly explains the properties and principle of thermal plasma generation. Further, the possibilities of this type of plasma utilization are explained, with an emphasis on material and waste processing. The basic chemical reactions and advantages of this material treatment approach compared to conventional methods are also summarized. Finally, the technology used at the IPP CAS is described and the different configurations for the two types of plasma torches are explained.

1.1 Plasma

Generally, plasma is known as the fourth state of matter, composed of electrons, ions, neutrals, excited species, and photons. In more detail, when talking about matter and its current state (solid, liquid, gas, plasma), it depends on the thermal kinetic energy of its particles and interparticle forces. The transitions between these phases occur within a constant pressure at a constant temperature, releasing (or absorbing) energy in the form of heat, known as latent heat. For solids, liquids, and gases, these changes only affect the kinetic energy of the particles and their intermolecular binding energy. If a molecular or atomic substance (usually a gas) absorbs enough energy, ionization will occur. During ionization, molecular or atomic particles surpass their binding energy with their kinetic energy and if a sufficient number of free charged particles is attained a plasma is formed. The ionization potential energy U (eV) of some atoms for the first electron is summarized in table 1.1. Under the table 1.1 is also an explanation of eV units (and their conversion from K units). The three main conditions that plasma must satisfy can be summarized as: [1, 2, 3, 4, 5]

$$\begin{aligned} &\lambda_{\mathrm{D}} << L \\ &N_{\mathrm{D}} >>> 1 \\ &\omega \cdot \tau > 1 \end{aligned} \tag{1.1}$$

where λ_{D} (m) is the Debye length, L (m) is the dimension of the plasma system, N_{D} $(-)$ is the number of particles in the Debye sphere, ω (s^{-1}) is the frequency of typical plasma oscillations and τ (s) is the mean time between collisions of charged particles and neutral particles (usually atoms). [5]

The Debye length determines the distance over which the electric field of individual charged particles (or a surface with a non-zero potential) affects other charged particles within the plasma. Because of the collective phenomena of plasma, charged particles organize themselves in a way to effectively shield electrostatic fields at the distance of Debye length. This shielded surrounding is called the Debye sphere. (The Debye length also represents the distance over which fluctuating electrical potentials can appear in the plasma. This corresponds to the conversion of the thermal kinetic energy of the particles into potential energy.) A more detailed definition of the Debye length and sphere is not necessary. [1, 5]

Ionized particles interact with the surrounding charged particles and the electromagnetic field of the environment. Although plasma contains a large amount of free charged particles, it macroscopically appears as electrically neutral, which is called quasi-neutrality. The state of quasi-neutrality can be simply expressed as follows: [6, 7, 8]

$$-q_\mathrm{e} \cdot n_\mathrm{e} \approx q_\mathrm{i} \cdot n_\mathrm{i} \tag{1.2}$$

where q_e (C) and q_i (C) are the elementary charges of electrons and ions, n_e (m^{-3}) and n_e (m^{-3}) is the particle density of electrons and ions (amount of particles in the unit of volume).

In fact, plasma represents over 99 % of the observed universe and naturally, it is possible to encounter it in the form of lightning strikes, Aurora Borealis, solar corona, or flames. However, humanity has also managed to create many types of plasma, which can be divided according to their properties or the way they are generated or utilized. The basic classification of types of plasma is described in figure 1.1. [2]

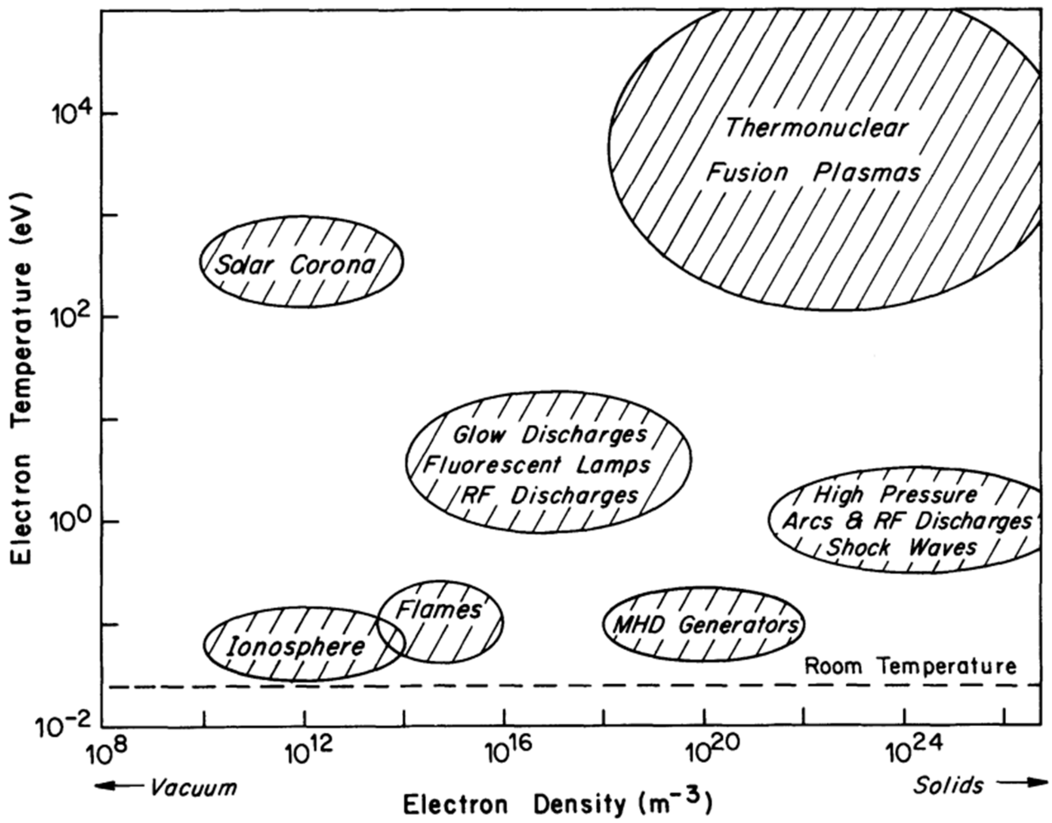

Figure 1.1: Classification of plasmas [2]

Overall, plasma can be distinguished between high-temperature and low-temperature plasma. By high-temperature plasma is meant thermonuclear fusion plasma, which is not important for the subject of this thesis and will not be discussed much further. Low-temperature plasma can be further divided into thermal (also called quasi-equilibrium) plasma and non-thermal (also called non-equilibrium or cold) plasma. [4]

Unlike fusion plasma, low-temperature plasmas are not in a (total) thermal equilibrium state, which is characterized by the same temperatures of all plasma particles, but only in the local thermal equilibrium (LTE). Particle kinetic temperatures (similarly like in gases) can be defined by the average particle kinetic energies: [2, 4]

$$\frac{1}{2} \cdot m_{\text{par}} \cdot v_{\text{avg}}^2 = \frac{3}{2} \cdot k \cdot T \tag{1.3}$$

where m_{par} (kg) is the particle mass, v_{avg} $(\text{m} \cdot \text{s}^{-1})$ is the effective particle velocity, k $(\text{J} \cdot \text{K}^{-1})$ is the Boltzmann constant and T (K) is the thermodynamic temperature.

Among the particles, energy and momentum are transferred by elastic collisions. Information about these collisions is important for example for the transport coefficients calculation, because there is a close functional relationship between these quantities. For thermal plasma, as a result of large electron number density during operation at pressures close to atmospheric, collision frequency is high and thermal equilibrium can be reached very fast. In most real cases, when the mixtures are more complex, the transport coefficients are often unknown or suffer from big uncertainty. Although most gases are electrically non-conductive, because of the presence of free charged particles, plasma has an electrical (and also thermal) conductivity comparable to metals (or even higher). [2, 7, 9]

When talking about plasma, the main important physical parameter is its temperature. It is a macroscopic quantity describing the behavior of particles on a microscopic scale, or rather their kinetic energy, as shown in equation 1.3. The term v_{avg} includes the different velocities of individual particles. Most plasmas behave classically, in other words, the distribution of particle velocities follows Boltzmann statistics and the velocity distribution known as Maxwell-Boltzmann (also Maxwellian). The Maxwellian distribution is described by the equation: [1, 5, 8]

$$f(v) = n \cdot \left(\frac{m_{\text{par}}}{2 \cdot \pi \cdot k \cdot T}\right)^{3/2} \cdot e^{\left(-\frac{m_{\text{par}} \cdot v^2}{2 \cdot k \cdot T}\right)} \tag{1.4}$$

where f (m^{-3}) is the number of particles per unit volume with velocities between v and $v + dv$ and n (m^{-3}) is the particle density. This equation depends only on the magnitude of the velocities of individual particles. The following equation also includes their direction. [1]

$$F(v) = 4 \cdot \pi \ v^2 \cdot n \cdot \left(\frac{m_{\text{par}}}{2 \cdot \pi \cdot k \cdot T}\right)^{3/2} \cdot e^{\left(-\frac{m_{\text{par}} \cdot v^2}{k \cdot T}\right)} \tag{1.5}$$

The density n (m^{-3}) (number of particles per unit volume) is thus defined: [1, 5]

$$n = \int_{-\infty}^{\infty} f(v)\, dv = \int_{0}^{\infty} F(v)\, dv \tag{1.6}$$

The Maxwell-Boltzmann distribution differs not only in relation to temperature but also to the type of substance (respectively gas) forming plasma and can be graphically expressed for example by figure 1.2. [10]

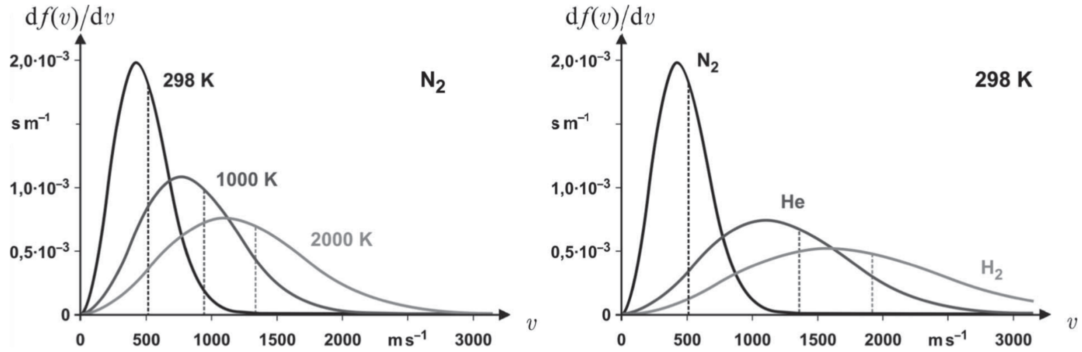

Figure 1.2: Maxwell-Boltzmann distribution for different gases and temperatures [10]

Element	U (eV)
Helium	24.59
Argon	15.76
Nitrogen	14.53
Oxygen	13.62
Hydrogen	13.60
Mercury	10.44
Iron	7.87
Sodium	5.14
Potassium	4.34
Cesium	3.98

Table 1.1: Ionization potential energy of some atoms for the first electron [1]

Combustion of fossil fuels can heat substances to temperatures of around 2000 °C, but plasma generated for example by electric thermal plasma torches can reach over 20000 °C. This offers much wider options from the perspective of operating conditions. When over temperatures of 10000 °C, radiation transfer starts to have an important role. Usually (including the case of experiments of this thesis), the plasma inside the reactor has a lower temperature, and the heat transfer between the plasma and the environment is dominated by convection (or a combination of convection and conduction in direct contact with the processed material). [11]

However, plasma temperatures can generally reach more than millions of Kelvin, and therefore the conversion from the temperature in K to energy in eV using the Boltzmann constant is more often used to classify plasmas in practice. The basic conversion factor therefore corresponds to: 1 eV = 11600 K. [1, 5]

1.1.1 Thermal plasma

The difference between non-thermal and thermal plasma is defined by the temperature difference between electrons and other particles. By definition, when a low-temperature plasma achieves (or gets close to) a local thermodynamic equilibrium (LTE), it is considered thermal plasma (and may be described as fluid with specific properties, for instance). Currently, it is known that the existence of actual LTE is rather exceptional. In order to achieve this state, similar temperatures of the plasma particles are necessary. The major impact on the kinetic equilibrium state has the parameter E/p, where E $(\mathrm{V \cdot m^{-1}})$ is the electric field intensity and

p (kPa) is the pressure in plasma. Kinetic equilibrium relation is expressed by 1.7. For small values of E/p a state of (or close to) kinetic equilibrium can be reached. The degree of ionization α_{doi}, defined by the ratio of ionized (n_{ionized}) and all particles ($n_{\mathrm{ionized}} + n_{\mathrm{neutral}}$) as shows equation 1.8, is also closely related to kinetic equilibrium and temperature. The direct ratio between ionized and neutral particles can be expressed by Saha's equation 1.9. [1, 2, 3, 12]

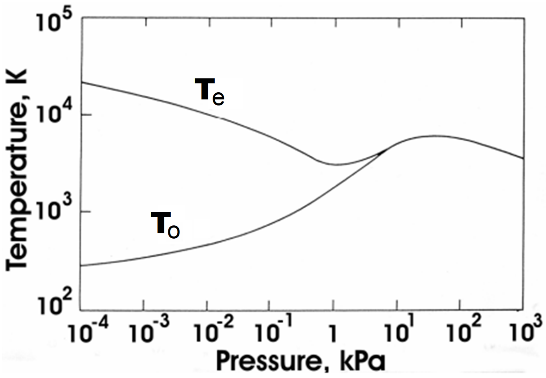

Figure 1.3: Relation between temperatures of plasma electrons (T_{e}) & other particles (T_{o}) and pressure [2, 12]

$$\frac{T_{\mathrm{e}} - To}{T_{\mathrm{e}}} \approx \left(\frac{E}{p}\right)^2 \tag{1.7}$$

T_{e} (K) and T_{o} (K) are the temperatures of electrons and other particles. The relation between temperature and pressure in plasma is shown in figure 1.3. It is conspicuous that a working pressure of at least 10 kPa is necessary to achieve LTE. Thermal plasma usually reaches temperatures around 10^4 K and electron densities from 10^{21} to 10^{26} m^{-3} during operation. [2]

$$\alpha_{\mathrm{doi}} = \frac{n_{\mathrm{ionized}}}{n_{\mathrm{ionized}} + n_{\mathrm{neutral}}} \tag{1.8}$$

Depending on the degree of ionization, plasma can be distinguished between weakly and strongly ionized plasma. For a weakly ionized plasma, charge-neutral interactions are dominant over the multiple Coulomb interactions. When the Coulomb interactions begin to prevail, the plasma can be considered strongly ionized. In other words, as the impact of the multiple Coulomb interactions (and forces) increases, the degree of ionization rises. [1]

$$\frac{n_{\mathrm{ionized}}}{n_{\mathrm{neutral}}} = 2.405 \cdot 10^{21} \cdot T^{3/2} \cdot \frac{1}{n_{\mathrm{ionized}}} \cdot e^{(-U/k \cdot T)} \tag{1.9}$$

Important thermodynamic properties of plasma are density, internal energy, specific heat, enthalpy, and entropy. Additionally, there exist derived thermodynamic functions for free energy and free enthalpy (or chemical potential): Helmholtz and Gibbs functions. If the composition is known, the thermodynamic properties can be also determined using partition functions, for example. [2]

Real plasma is characterized by gradients, which represent driving forces for individual flows of physical quantities within certain limits. To the basic relations describing the behavior of plasma, force relations (momentum equations respectively) can be added, which describe the external forces acting on the plasma and its particles, for example gravitational, pressure, electric and magnetic forces. The plasma behavior is also subject to Maxwell's equations for electric field intensity and magnetic induction. All sets of examples of previously mentioned equations are summarized in table 1.2. [2, 3]

When it comes to computational models of plasma, it is not that complicated to describe the behavior of individual particles (electrons and ions) in the surrounding electromagnetic field. On a larger scale, these calculations require the solution of continual changes in the electromagnetic field caused by the mutual forces of all particles, including their collisions. If the number of these particles and collisions increases, the calculation becomes very tedious and demanding on computing power and memory (and very often impossible). From a practical point of view, it is possible to describe plasma as a fluid in most cases. More detailed research about the theory of plasma physics is not needed for the purposes of this thesis and the subsequent practical part. [5, 8]

Gradient equations	**Force equations**	**Maxwell's equations**
$\mathbf{\Gamma} = -D \cdot \nabla n$	$\mathbf{F_g} = m_k \cdot \mathbf{g}$	$\nabla \cdot \mathbf{B} = 0$
$\mathbf{J} = -\sigma_{\mathrm{el}} \cdot \nabla \varphi_{\mathrm{el}}$	$\mathbf{F_e} = e_k \cdot \mathbf{E}$	$\nabla \cdot \mathbf{E} = \frac{\rho}{\varepsilon_0}$
$\mathbf{q} = -\kappa \cdot \nabla T$	$\mathbf{F_m} = e_k \cdot (\mathbf{v_k} \times \mathbf{B})$	$\nabla \times \mathbf{B} = \mu_0 \left(\mathbf{J} + \varepsilon_0 \frac{\partial \mathbf{E}}{\partial t} \right)$
$\mathbf{f_x} = -\mu \cdot \nabla v_x$	$\mathbf{F_p} = \frac{m_k}{\rho_k} \cdot \nabla p_k$	$\nabla \times \mathbf{E} = -\frac{\partial \mathbf{B}}{\partial t}$

Table 1.2: Summary of basic equations in plasma theory [1, 2, 3]

$\mathbf{\Gamma}$ ($\mathrm{m}^2 \cdot \mathrm{s}^{-1}$) is the particle flux, D ($\mathrm{m}^2 \cdot \mathrm{s}^{-1}$) is the diffusion coefficient, n (m^{-3}) is the number density of particles, $\mathbf{J}$ ($\mathrm{A} \cdot \mathrm{m}^{-2}$) is current density, σ_{el} ($\mathrm{S} \cdot \mathrm{m}^{-1}$) is electrical conductivity, φ_{el} (V) is electric potential, $\mathbf{q}$ ($\mathrm{W} \cdot \mathrm{m}^{-2}$) is heat flux, κ ($\mathrm{W} \cdot \mathrm{m}^{-1} \dot{\mathrm{K}}^{-1}$) is thermal conductivity, T (K) is thermodynamic temperature, $\mathbf{f_x}$ ($\mathrm{N} \cdot \mathrm{m}^{-2}$) is frictional force in direction x, μ ($\mathrm{kg} \cdot \mathrm{m}^{-1} \cdot \mathrm{s}^{-1}$) is dynamic viscosity, v_x ($\mathrm{m} \cdot \mathrm{s}^{-1}$) is velocity in direction x.

$\mathbf{F_g}$ (N), $\mathbf{F_e}$ (N), $\mathbf{F_m}$ (N) and $\mathbf{F_p}$ (N) are gravitational, electric, magnetic and pressure forces, m_k (kg) is mass of the component k, $\mathbf{g}$ ($\mathrm{m} \cdot \mathrm{s}^{-2}$) is acceleration due to gravity, e_k (C) is electric charge of component k, $\mathbf{v_k}$ ($\mathrm{m} \cdot \mathrm{s}^{-1}$) is velocity of component k, ρ_k ($\mathrm{kg} \cdot \mathrm{m}^{-3}$) is mass density of component k and p_k (Pa) is partial pressure of component k.

$\mathbf{B}$ (T) is magnetic induction, $\mathbf{E}$ ($\mathrm{V} \cdot \mathrm{m}^{-1}$) is electric field intensity, ρ ($\mathrm{C} \cdot \mathrm{m}^{-3}$) is the total electric charge density, ε_0 ($\mathrm{F} \cdot \mathrm{m}^{-1}$) is the vacuum permittivity and μ_0 ($\mathrm{H} \cdot \mathrm{m}^{-1}$) is the vacuum permeability.

1.1.2 Thermal plasma utilization

Plasma technology and its applications are not recent. Plasma processes were already used in the nineteenth century to provide extreme temperatures in the furnaces of the metalworking industry. In the twentieth century, plasma was used in the chemical industry for the production of acetylene from natural gas. Highly reactive species, high enthalpy and extreme temperatures of thermal plasma enable its use in a wide range of industrial applications. Furthermore, high thermal conductivity and radiation intensity result in extensive heat transfer. [6, 7, 13]

Currently, potential possibilities of thermal plasma utilization for technological or industrial purposes can be, for example: [2, 9]

- plasma deposition and coating,
- plasma synthesis of fine powders,
- plasma decomposition and destruction (of hazardous wastes),
- plasma metallurgy and clean melting,
- plasma densification,
- plasma welding and cutting.

Coating technology includes plasma spraying, wire arc spraying, and thermal plasma chemical vapor deposition (TPCVD). In thermal plasma synthesis, either the discharge itself or the plasma flame behind the discharge can be used to synthesize powders. [12]

Furthermore, thermal plasma can be used for material recovery, for example, aluminum recovery from dross or metal recovery from baghouse dust. Also, in combination with the quenching process, thermal plasma can be used for various depolymerization processes for monomer recovery from polymer waste. However, the subject of this thesis will mainly be the plasma material decomposition, respectively of waste. From the perspective of simple waste processing, this approach is attractive because of the reduction of the waste volume to non-leachable residues and the destruction of hazardous wastes, which is by far one of the most important applications. [4]

1.1.2.1 Thermal plasma material processing

The general opinion on the use of plasma technologies for waste management was initially highly skeptical. Potential commercial use was considered suspicious and unreliable from the very beginning of the research and development of plasma torches and reactors. It was enhanced by the attitude of research and scientific workers, promoting and emphasizing this method of waste treatment without considering the limiting circumstances outside the laboratory environment. [3]

A necessary strategy for sustainable waste management with the aim of reducing landfilling and minimizing the impact on the environment is the improvement of waste management. Waste is slowly becoming one of the renewable resources that can be significant when considering renewable energy sources. Recently, plasma waste processing methods have made significant progress, and since 1980 the technology of plasma gasification of waste is considered to be a very attractive way of processing MSW with the simultaneous disposal of dangerous harmful materials (for example asbestos, radioactive waste, and toxic chemicals). [13]

Currently, according to the literature, plasma gasification of waste appears to be one of the most promising technologies. It is more than desirable to try to promote them, as long as the problems associated with waste and its safe disposal increase each decade. There have already been examples of successful plasma reactors operating for many years for the industrial and energy use of waste in various parts of the world. Companies taking participation include InEnTec, PEAT, Alter NRG, CHO-Power, Advanced Plasma Power, Hitachi Metals Ltd., Plasco Energy Group Inc, EnviroParks Limited, Sunbay Energy Corporation, Green Power Systems, and many others. [3, 13]

Operating conditions of waste treatment by thermal plasma depend on many factors, for example, the plasma torch power, temperature inside the reactor, flow rates of plasma and material (or/and gases), type of stabilization medium, residence time, or properties of processed material (especially chemical and physical). The effects of all individual factors on specific types of operations have been and continue to be the subject of research all over the world. [7]

The controlled waste decomposition processes can offer significant advantages. In addition to obtaining valuable products that are useful for various industrial sectors, the problem of waste disposal is solved at the same time. This applies especially to waste with a largely organic character like RDF, medical waste, or municipal solid waste.

The great benefit is usually the ratio between the values of the output products compared to the input products. Waste as an input has a very low value (often even negative) and secondary raw materials as an output can have a very high value, defined by its quality and demand for individual industrial sectors such as energy, chemical, construction, and automotive. Wastes most attractive for thermal plasma treatment can be summarized as follows: [14]

- hazardous liquids and gases,
- municipal solid waste,
- medical (solid) waste,
- contaminated soil & sewage sludge waste,
- low level radioactive waste (LRW),
- manufacturing wastes.

Types of plasma waste treatment processes consist of plasma pyrolysis (thermal breakdown of chemicals with no oxidation), gasification (incomplete oxidation of organic component and reforming to synthesis gas), compaction and vitrification (inorganic material melting and binding hazardous substances), and combinations of all these processes. These reaction processes are described in the subsection *Chemical reactions*, so they will not be specified in more detail now. [14]

Working power has a great influence on material processing conditions. Higher powers increase the energy density and also the length of the plasma discharge zone, which increases the contact time of the material with the extreme temperatures of the plasma (and this increases the chances of a higher gas yield). In order to achieve the optimal synthesis gas composition (maximum yield of hydrogen and carbon monoxide and minimum yield of other compounds) while processing organic waste, it is necessary to reach temperatures above 900-1000 °C in the reactor. [11]

As it turned out, the specific energy consumption increases sharply above the critical temperature limit, when the temperature of the reactor no longer increases much due to significantly increased discharge losses in the form of radiation. Also, rather than the excessive increase in power, the ratio between the input carbon and hydrogen has a crucial impact on the resulting synthesis gas yield. In theory, at perfect stoichiometry, no solid carbon and no carbon dioxide should come out of the reactor. [4]

In the Czech Republic, there are companies that focus on the issue of plasma waste processing, for instance, Millennium Technologies. Currently, the company offers a promising system with the possibility of processing wastewater sludge from wastewater treatment plants using high-temperature pyrolysis. The system includes a dryer that reduces water content in the sludge from 65-75 % to 10 %, creating granulate which can be fed and processed in the plasma reactor. [3]

The investments into plasma waste treatment technology and its expansion, especially in the Czech Republic, are important to take into consideration. Stricter limitations of waste storage in landfills are expected soon, since their capacities are slowly getting fulfilled, also for the reason that almost half of the national waste ends up landfilled. Appropriate regulations regarding landfill management have already been implemented in foreign regions. If Czech waste management is not sufficiently prepared for this change, the costs of garbage collection could increase steeply, influencing practically every citizen. [3]

Currently, plasma vitrification systems (the vitrification of amorphous noncrystalline material through thermal transformation) are considered feasible and viable technologies for processing hazardous waste. Systems for processing MSW are very complicated in terms of industrial implementation and viability, and the output synthesis gas needs to be further cleaned, especially from contaminating elements like chlorine, mercury, lead, cadmium, zinc, or sulfur. [3]

This presents a big challenge in the fields of development, logistics, power engineering, and waste management. In consideration of current conditions, expanding research, and the advancement of plasma technologies in particular, plasma waste treatment as an important contribution to a circular economy is expected. A block diagram of the process layout of a typical thermal plasma waste gasification (W2E) facility designed by Westinghouse is shown in figure 1.4. [11]

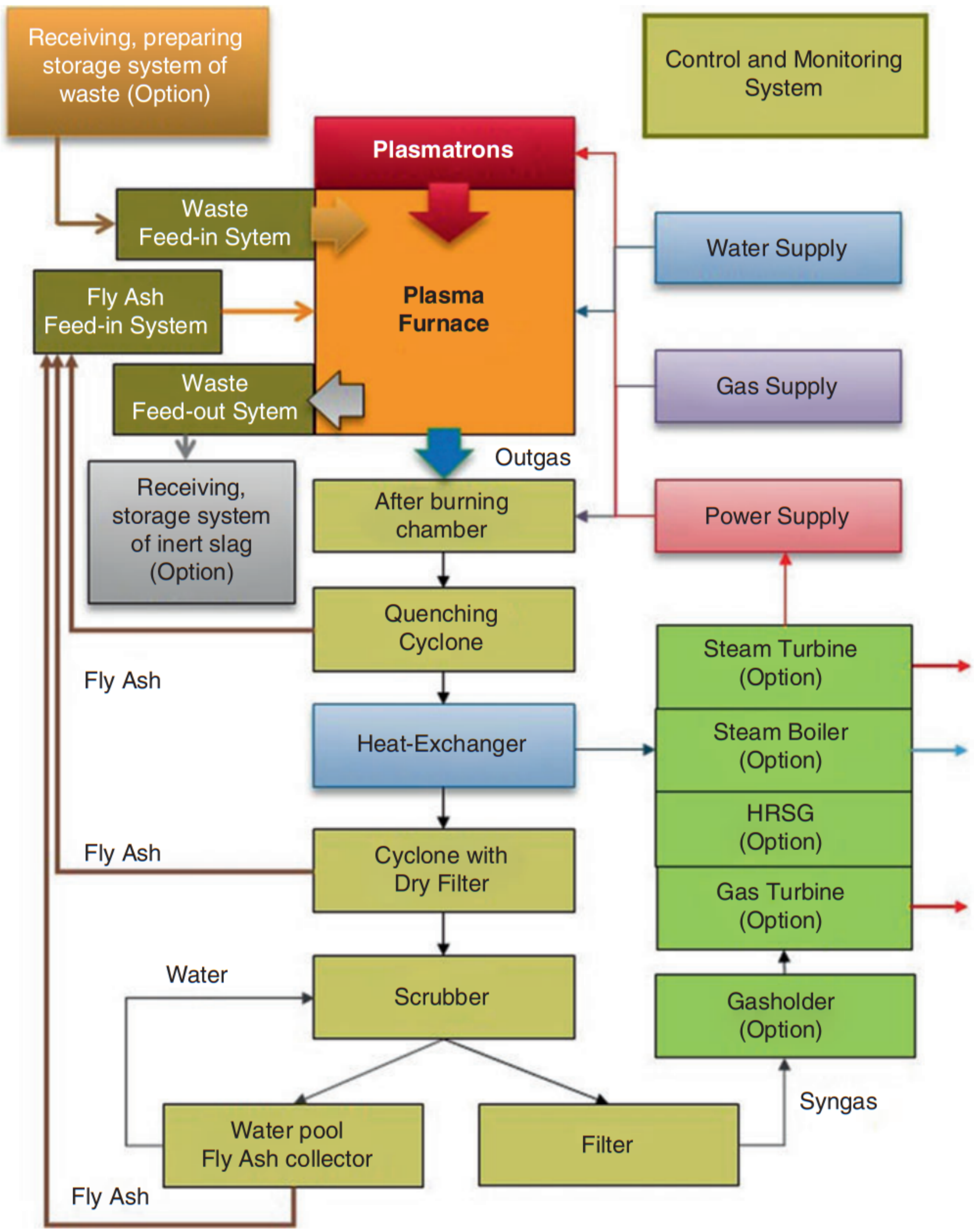

Figure 1.4: Schematic diagram of thermal plasma W2E facility [11]

1.1.2.2 Advantages of plasma gasification

In general comparison with incineration processes, industrial thermal power plants can have between 20 and 40 % conversion efficiency using a single steam cycle. Based on performance, a plasma gasification facility connected to a combined power plant cycle can theoretically achieve an efficiency of over 45 %. Although the conventional combined cycle can achieve an efficiency of around 60 %, there is an absence of advantages brought by the plasma gasification of waste. [13]

Thermal plasma reactors offer many unique advantages for potential waste disposal, namely: [9, 13, 14]

- the high energy density and temperatures, steep thermal gradients in the reactor,
- minimization of reformation of persistent organic pollutants (the non-energy part of the output is inert),
- treatment of all kinds of wastes including liquids, solids, and gases,
- relatively fast attainment of steady-state conditions (and related rapid start-ups and shutdown times, compared to other thermal treatments),
- oxidizing agents are not required, more options for the process chemistry,
- gas stream volume is smaller than during combustion,
- easier and less expensive to manage (the hazardous wastes),
- smaller dimensions of facility compared to conventional methods,
- precise control of enthalpy injected into the reactor (by electrical power).

Synthesis gas properties from the perspective of fueling gas engines are for instance: [11]

- independent power supply, greater predictability, and stability (compared to conventional bulk electricity supply),
- reduced energy costs, efficient and economic combined heat and electricity supply,
- substitute to conventional fuels, low gas pressure required,
- best suited for electrical output of hundreds of kW to 20-30 MW,
- environmental benefits, greenhouse gas reduction or,
- disposal of a problem gas by its utilization as an energy source.

1.2 Thermal plasma sources

Plasma can be generated in various ways by achieving the electrical breakdown of the stabilizing medium, for example by using direct current, alternating current, or pulsed discharge. The most widespread methods of thermal plasma generation include high-intensity electric arcs, inductively coupled high-frequency discharges, or recently even microwave discharges. Alternating and transient arcs or laser discharges are also possible to use as sources. For most case scenarios, the thermal plasma flow is highly turbulent. This complicates the plasma diagnostics, similar to extreme fluxes (for instance light or thermal fluxes), high gradients (including temperature), or fluctuations of dissipated power (often more than 50 %). [2, 12]

The method often depends on the design of the plasma torch or the purpose for which the plasma is intended. Technologies that are not dependent on the electrical energy supply for producing plasma also exist. Plasma generation is provided by chemical and other thermodynamic processes, for instance with flame or adiabatic compression of gas. Only electric arc plasma torches and microwave plasma torches will be further described, as the experimental part of this thesis was conducted with these two types of plasma torches. [3]

1.2.1 Electric arc plasma torch

A very common source of thermal plasma (especially for waste treatment applications) is the DC arc plasma torch because it is not sensitive to condition changes during the process. Their main advantage is lesser (electrical) noise, more stability, easier control, and regulation. Electrode arrangement can differ for diverse applications. Both electrodes being a part of the torch construction is the typical option. In this configuration, the plasma jet flows out from the output nozzle and extends beyond the anode part. This configuration is probably better for most organic material treatment scenarios. DC arc plasma torches have commonly power from units of kW up to units of MW (up to 6 MW). In some cases, one of the electrodes can be the processed material. This is referred to as a transferred arc device, often used for inorganic materials treatment in purposeful applications. Transferred arc reactors can range from powers of hundreds of W to tens of MW. [4, 14]

Although DC plasma torches are the most common devices used for material treatment or waste processing, the technology can be technically and financially problematic. The major issue is the short lifespan of the electrodes (approximately 300 - 500 hours, up to 1000 for non-aggressive media). The equipment of the torch including electronic components is more sensitive to DC current, which can lead to malfunction. For this reason, higher acquisition and operational costs need to be considered, specifically for the need for regular inspections or repairs and devices like rectifiers, that can complicate the power supply. [14]

The high-intensity arcs are defined by current levels of $I > 50$ A and pressures $p > 10$ kPa and can be distinguished by the way of stabilization (free-burning, wall-stabilized, convection-stabilized, magnetically stabilized, or self-stabilized). [2]

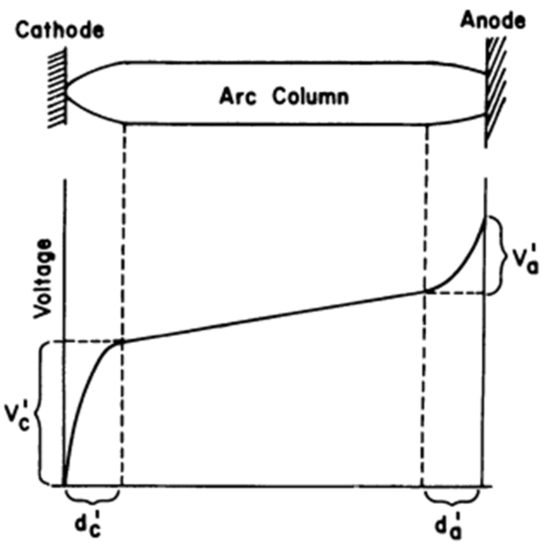

Figure 1.5: Typical potential distribution along an arc [2]

The principle of a DC plasma torch function is the creation of a constant electrical arc that passes through a stabilization chamber with a stabilizing medium (suitable liquid or gas, for example, water, air, or argon) between the electrodes. The gaseous or liquid medium is exposed to electrical breakthrough and plasma is generated, which forms a conductive path between the electrodes. The electric arc area can be divided into the cathode, anode, and column sections. The largest voltage drops occur in the peripheral parts as can be seen in figure 1.5. Closest to LTE is the central part of the plasma arc. [2]

While the arc current is drawn by the anode, the plasma jet continues to flow out of the plasma torch outlet nozzle, enabling its technical utilization. The stabilizing medium and energy should be maintained continuously to prevent the ionized particles from recombining back to a neutral gas. During the reaction, it is necessary to adequately cool the plasma torch to avoid damage, particularly the active parts – electrodes. To initiate the whole process, a strong impulse in the form of a voltage peak is required. This results in the arc penetrating the stabilizing medium by exceeding the electrical strength limit and thermal plasma is formed. [3]

The scientists and engineers from IPP designed their own concept of a hybrid plasma torch with a maximum power of approximately 160 kW. The technology of DC plasma torches differs from design to the choice of stabilization medium, which usually consists of gas or water. Recently, the IPP CAS has also been testing a microwave plasma torch with a maximum power of 100 kW.

1.2.1.1 Gas stabilized plasma torch

The most usual way of creating a plasma jet with an electrical plasma torch is to decompose the gas using an external electric field. Water is often used for the operation of the torch, but it only serves as a cooling and not as the plasma stabilizer, unlike in the case of water-stabilized and hybrid torches. [3]

The most commonly used neutral gases for ionization are air, argon, or nitrogen, because of their cost and availability. The properties of a plasma torch and its operation depend on the type of stabilizing gas used. Examples of different plasma properties for different stabilization media can be seen in the 1.6 figures, where the enthalpy and thermal conductivity are depicted as functions of temperature. [12]

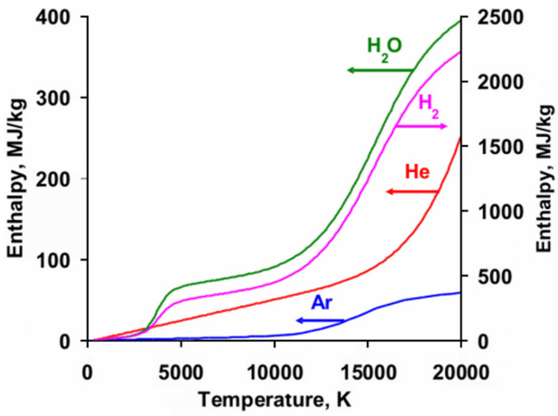

(a) Enthalpy

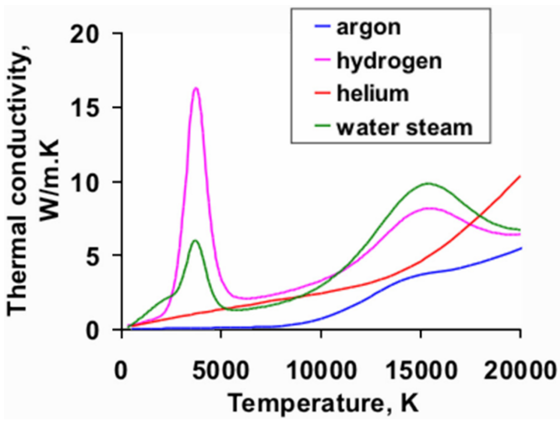

(b) Thermal conductivity

Figure 1.6: Plasma properties depending on the stabilization medium [12]

If air as an input stabilizing gas is used, the costs are lower, but the output synthesis gas is diluted with a significant amount of nitrogen, contributing to undesirable nitrogen oxides formation. If the stabilizing gas contains oxygen vapors, the oxidation and erosion of the electrodes are expedited. In contrast, argon plasma is less aggressive to plasma torch components but has a low enthalpy, low thermal conductivity, and low transmission capacity resulting in a lower ability to transfer energy to the processed material. In some cases, the stabilizing gas is water steam, but this steam is created externally (outside the torch), so this type is not considered as a water-stabilized torch.

An example of a gas-stabilized plasma torch is shown in figure 1.7. The plasma from this torch has peak temperatures of 10000-20000 K, depending on the power level, stabilization gas, and design. In practice, however, the plasma behind the exit nozzle deteriorates and loses its extreme properties, so the processed material is not exposed to such extreme temperatures. [7]

Arc behavior is strongly dependent on operating parameters such as arc electric current and voltage (which is also dependent on the nature of the medium used and its mass flow rates) and the design features of the nozzle, especially the diameter. This applies to all types of arc plasma torches. [7, 12, 14]

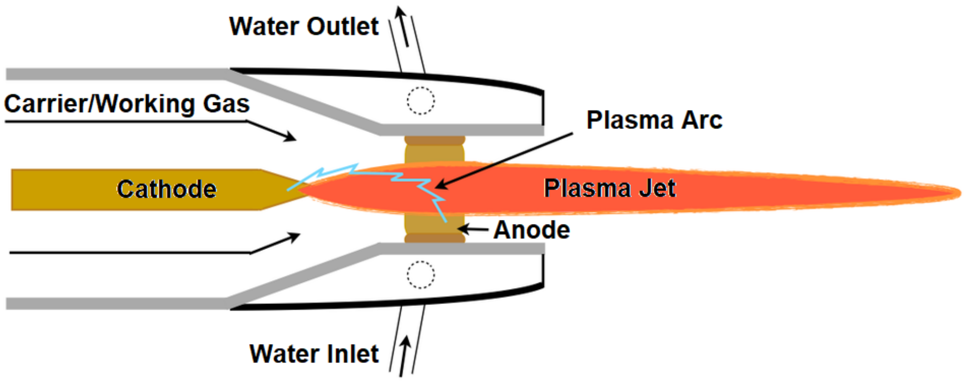

Figure 1.7: Schematic diagram of a gas-stabilized plasma torch - modified [15]

1.2.1.2 Water stabilized plasma torch

Another way of generating plasma is through the ionization of liquid water, which mainly consists of oxygen and hydrogen. The advantage of this method is the decomposition of water into hydroxyl and oxygen molecules. These molecules behave as active molecules in thermal plasma and effectively neutralize potentially dangerous, toxic, and volatile substances. This is the main benefit of water as a stabilizing medium, especially during the pyrolysis reaction of processed materials and waste. Unlike gas-stabilized plasma torches, water (and hybrid) plasma torches have significantly lower flow rates of the stabilizing medium and a very high specific enthalpy (over 200 $\mathrm{MJ \cdot kg^{-1}}$). [16]

Figure 1.8 presents a diagram of a water-stabilized plasma torch. Hot arc plasma is surrounded by a rotating vortex of liquid water, which cools the torch and creates a stabilizing environment for the plasma. This type of torch was developed at the IPP and has been successfully used for plasma spray applications. The biggest issue was the rapid erosion of the carbon cathode. The solution was using a cathode sliding system, which gradually inserted the eroding cathode into the torch. [3]

Therefore, the lifetime (operability) of this plasma torch depended on the length of the cathode (thus the time it burned out). The anode part was a rotating copper disk. The rotation resulted in slower anode degradation during the plasma generation process. [3]

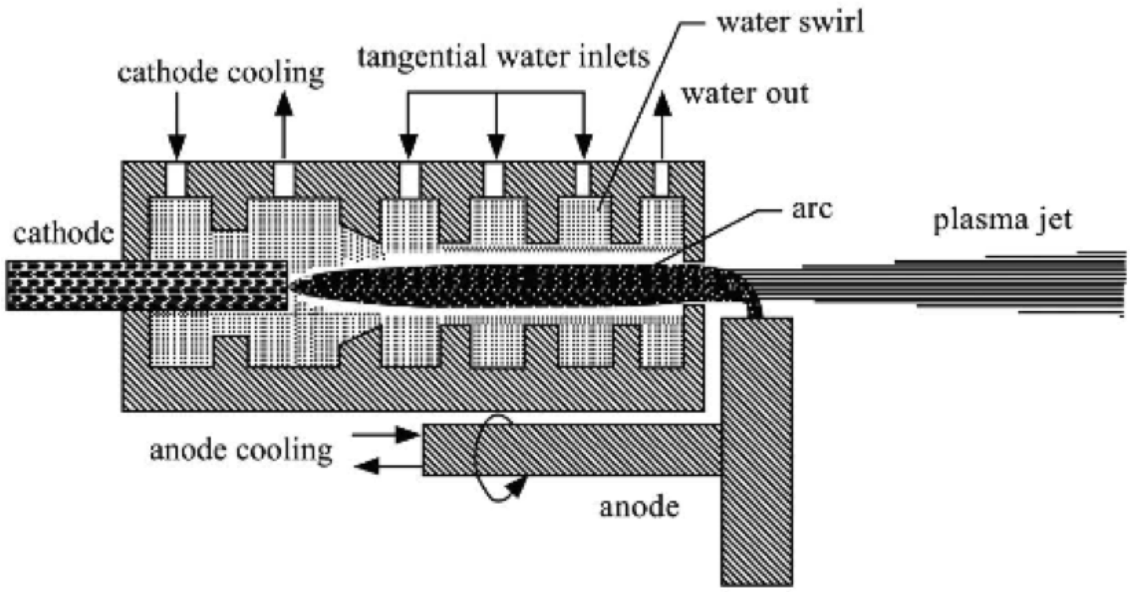

Figure 1.8: Schematic diagram of a water-stabilized plasma torch [17]

1.2.1.3 Hybrid plasma torch

The hybrid plasma torch, visible in figure 1.9, was developed at the IPP to fix problems with the lifetime and continuous movement of the cathode that was part of the water-stabilized plasma torch. This new plasma torch uses argon and water as a stabilization medium for plasma. Argon protects the cathode and reduces its degradation. Water provides the same effects as in the water-stabilized plasma torch and creates a vortex in three cylindrical segments with tangential water injection. [3, 12]

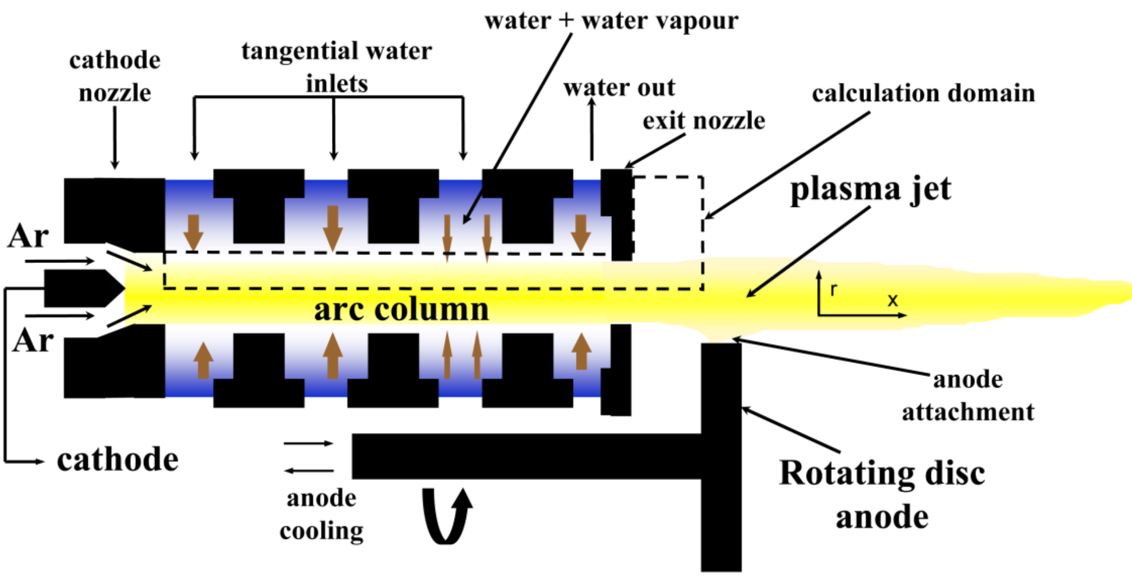

Figure 1.9: Schematic diagram of a hybrid plasma torch [18]

This configuration makes possible utilization of tungsten cathodes, which are resistant to oxidation as a result of flowing argon. This leads to a longer lifespan of cathodes. Tungsten cathodes are typically alloyed with trace amounts of lanthanum oxide or thorium oxide to improve emission and ignition properties. If the admixture is thorium oxide, handling and operation require greater caution for the compliance of work safety, since thorium is a radioactive element. Tungsten electrodes are typically axially edged to a point. [3]

The rotating anode copper disk design remained. Adding different alloys to improve attributes was for the case of the anode also tested. Currently, a disk with the admixture of 1 % silver is used, reducing anode wear and oxidation. This combination proved as a suitable compromise in terms of costs and anode lifespan, so it is still used today. Other tested alternative materials for anode disks were iron and nickel. These metals were not widely used after testing. [3]

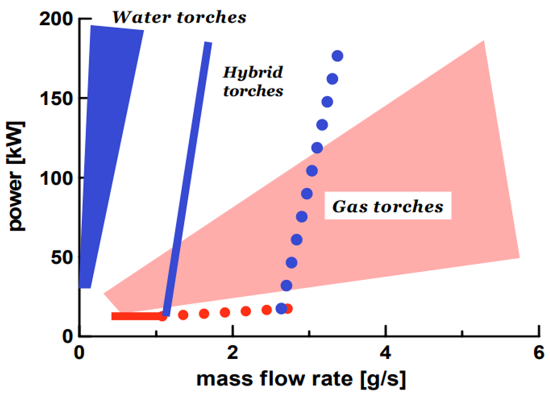

Figure 1.10: Operating modes of DC types of arc plasma torches [18]

Resolving the issue with the cathode part was only one of the advantages of the hybrid plasma torch. As shown in figure 1.10, in comparison to gas-stabilized torches, hybrid torches can achieve higher power with the same mass flow of stabilizing media and allow higher mass flows than water-stabilized torches. This means that the hybrid plasma torch can operate in a wider range of regimes, including those that are inaccessible to both gas and water-stabilized torches. [3]

1.2.2 Microwave plasma torch

Another principle for generating thermal plasma is the use of microwaves with the microwave plasma torch. It has been tested at IPP for over a year now. Because of the relatively short testing time of the microwave plasma torch compared to the hybrid arc plasma torch, only a limited number of experiments have been carried out so far. Nevertheless, part of this thesis will also be an effort to compare both types of plasma torches depending on measured experimental data and the results of related analyses. Hopefully, it will also be possible to assess both types of plasma torches from the perspective of their possibility of industrial use in some commercial facility for plasma material (waste) treatment.

Traditionally, the microwave discharge is required to be directly part of the microwave circuit. This condition limits the flexibility of the discharge and plasma parameters. In recent decades, microwave devices have been developed using electromagnetic surface waves or traveling wave discharges (TWDs) to stabilize plasmas. Operating frequency ranges from 1 MHz to 10 GHz and operating pressures from 10^{-3} Pa to several hundreds of kPa. The diameter of the discharge tube reaches dimensions between 0.5 and 150 mm. [2]

Similar to other types of torches, in a microwave plasma torch the discharge electrons primarily absorb the energy of the electric field. Again, sufficiently high pressures are desirable to achieve kinetic equilibrium, i.e. at least 10 kPa and more, which will also be considered in this work. [2]

First, the discharge needs to be induced by electrical breakdown, which is usually achieved by a high-frequency spark or some form of preionization. Subsequently, the surface wave moves along the interface between the discharge tube and the plasma and supplies energy to sustain the plasma flame. Therefore, the plasma and the wave are closely linked by their interaction. The wave is the energy source for the plasma, but without the plasma, the wave could not exist. These properties (including reflected power) are relatively stable in the steady state. [2]

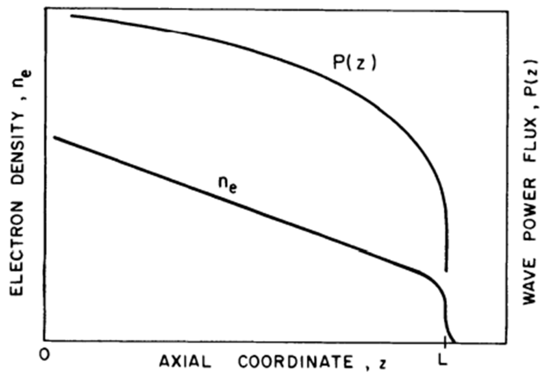

Figure 1.11: Power flux and electron density (schematically) in a TWD [2]

As a rule, the longer the waveguide, the less energy it is possible to deliver to the plasma. [2]

After reaching the critical length of the waveguide, the energy flow decreases to zero, as can be seen in figure 1.11, where together with the power (P (kW)) the qualitative relationship of the electron density (n_e (m^{-3})) depending on the distance from the discharge tube. [2]

A different method of plasma generation without the use of electrodes is the above-mentioned radio frequency induction coupled plasma. It is especially useful in applications where purity maintenance on a high level is necessary. However, the disadvantage is the required shielding and the low efficiency (approximately 40 %) of energy conversion, which decreases with increasing operation power. Therefore, this approach is inconceivable for applications like waste treatment. [19]

Replacing an arc plasma torch with a microwave plasma torch has two major operational advantages. Firstly, the time interval of the operating state of the system does not depend on the lifetime of the active parts of the arc torch, namely the electrodes. Consequently, the maximum lifetime is not limited to hundreds of hours, and the operating and maintenance costs are lowered. Secondly, due to the absence of an electric arc, the system using the microwave plasma torch is safer, and in the case of a steady working state, the torch can be also considered more stable (in some tested cases, the microwave plasma torch showed self-regulating behavior). [19]

Currently, microwave plasma technology is abundantly used in applications requiring low energy consumption and low flow rates of working media and stabilizers, for example, elemental analysis, atomic spectroscopy, chromatography, and material modifications like low-temperature etching or surface treatment. The technological scheme of the microwave plasma torch is captured in figure 1.12. [19, 20, 21, 22]

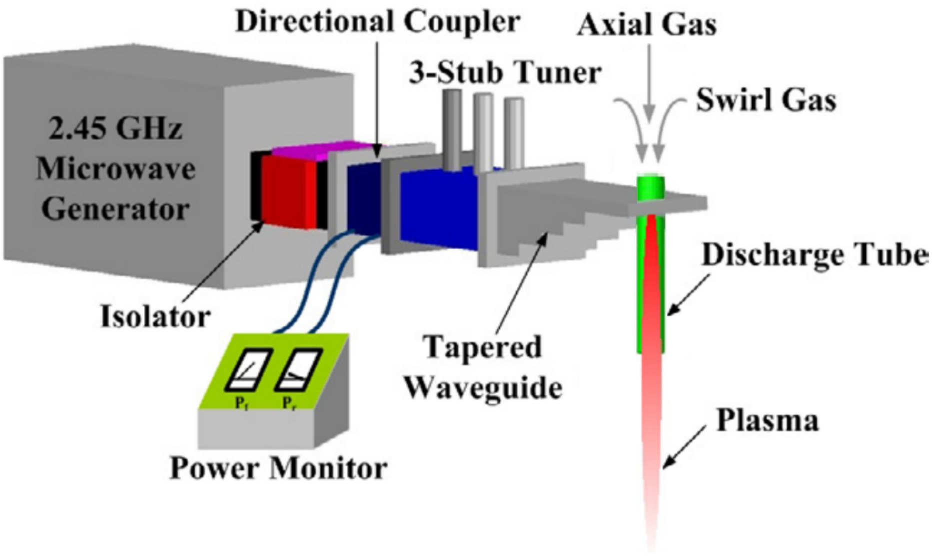

Figure 1.12: Schematic diagram of a microwave plasma torch - modified [19]

Considering the case of the Plasma Chemical Technologies Department of IPP, the microwave plasma generator can achieve higher power in comparison with the sources needed for instance for previously described applications (namely up to 100 kW). A larger power range is advantageous in wider possibilities of plasma torch usage, especially in more difficult applications like material processing or thermal decomposition of both organic and inorganic wastes.

The ignition of the plasma flame is performed by inserting a copper rod into the space designated for interaction between microwaves and the working gas. The copper rod triggers a reaction with the microwaves, causing the plasma to ignite, after which it is removed from the working area. Plasma is stabilized and maintained through tangential injection of working/stabilizing gas (air or argon), creating a swirling flow in the spiral shape.

Although the microwave coupling to the plasma is almost lossless, as the power of microwaves increases, reflected power (which is considered energy loss) may increase too. Therefore, the reflection of microwaves cannot be neglected. For the operating condition (both laboratory or commercial), it is optimal when the reflected power does not exceed 10 % of the generated power. An increase in microwave power also results in an increase in the size and temperature of the plasma flame. The increase in the flow of gas has a greater impact on the increase in electron density, as mentioned in [20].

Heat losses are especially more significant, but they are typical for all other types of plasma torches including arc torches. In addition, we cannot control these losses during operation remarkably, unlike reflection losses, which can be regulated by the geometry of the microwave generator or the waveguide.

Limiting factors for microwave plasma generation are most likely thermal stress, electrical field intensity, or both electric and dielectric features of materials. A comparison of the actual appearance of the generated plasmas from HPT and MWPT is (including a scale legend) visible in figure 1.13. [20]

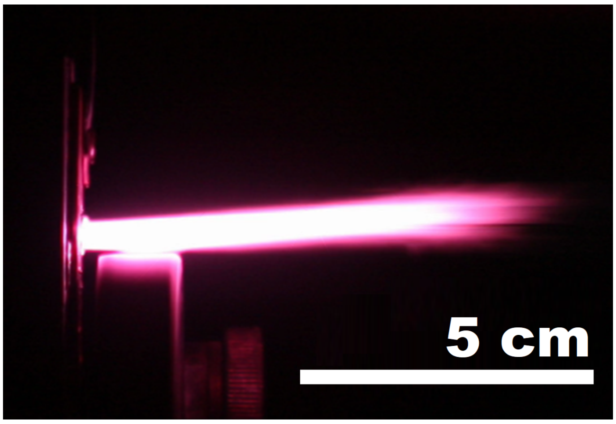

(a) HPT plasma jet

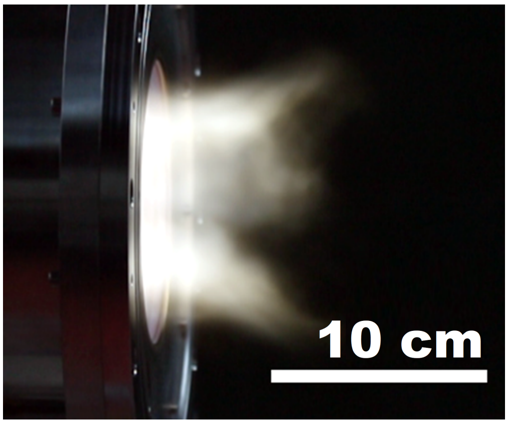

(b) MWPT plasma flame

Figure 1.13: Comparison of generated plasma by HPT and MWPT

1.3 Plasma reactor

Currently, there are many types of reactors for plasma material treatment. The most commonly used configurations of plasma reactors are for exampe descending fixed bed, ascending fixed bed, bubbling fluidized bed, circulating fluidized bed, entrained flow, rotary furnace or moving grate. (Some types are used in conventional pyrolysis without the use of plasma.) [13]

In overall material processing in a thermal plasma reactor, the dimensions of the processed material samples have a significant impact. The finer the sample, the higher temperatures it reaches on its surface when in contact with the plasma. [11]

The inner part of the processed piece of material is protected from heat transfer by a gas envelope evaporated from the outer layer of the material. Therefore, the larger the volume of the processed particle, the more difficult it is to process thermochemically in the reactor. [11]

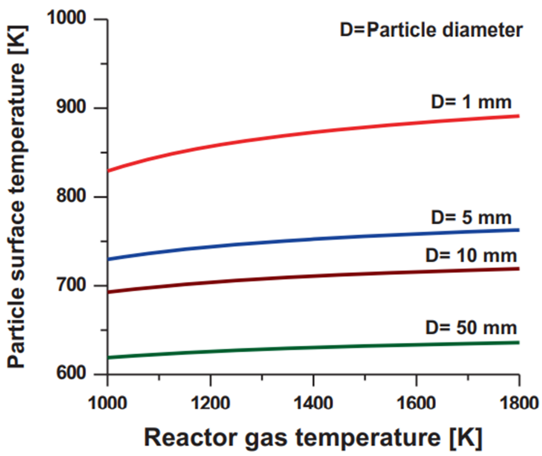

Figure 1.14: Surface temperature of wood particles depending on their diameter and reactor temperature [11]

This effect is shown in figure 1.14, where cases of processing wood particles of different diameter sizes have been modeled. It can be seen that the increasing dimensions of the particles of the material sample result in lower surface temperatures of these particles, which complicates their treatment. Depending on the size of the material sample pieces to be processed, it is appropriate to choose operating characteristics such as reactor dimensions, operating temperatures, and plasma torch power. [11]

1.3.1 PLASGAS

The plasma gasification reactor aggregate (PLASGAS) in the laboratory at the Department of Plasma Chemical Technologies of the IPP CAS is a complex semi-operational facility for processing waste materials and could potentially be considered as an updraft gasifier because the wastes are fed by the top of the reactor. The schematic diagram of PLASGAS is illustrated in figure 1.15, where arrangements and interconnections of the individual parts of the facility are visible.

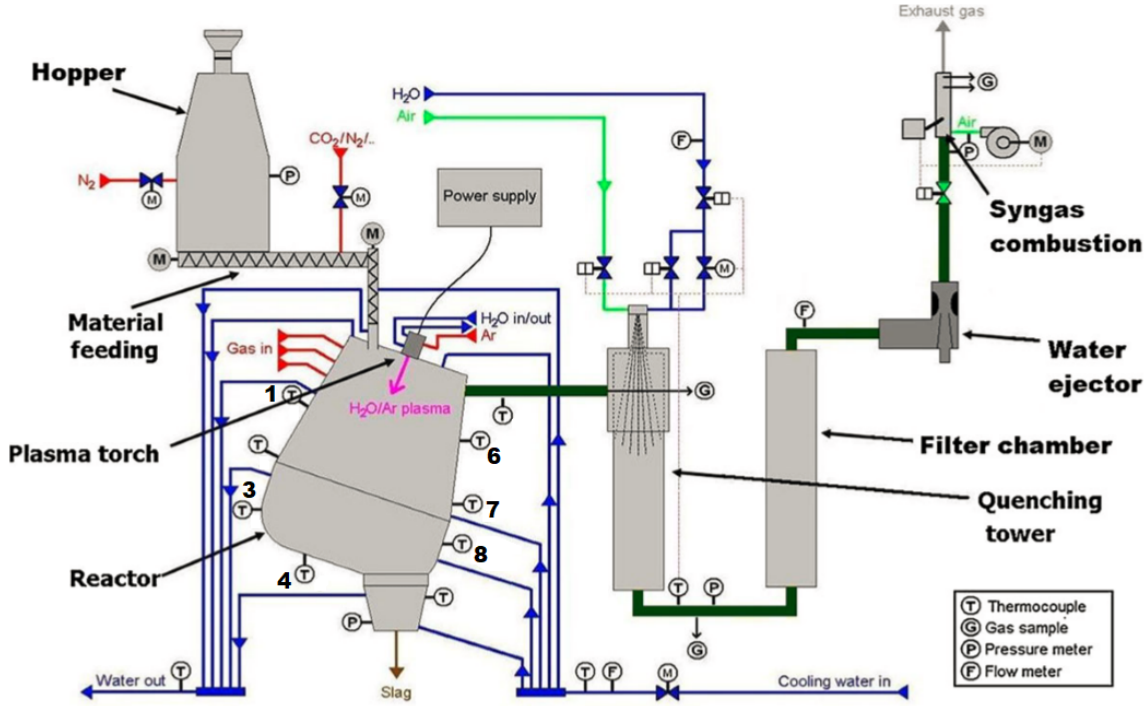

Figure 1.15: Schematic diagram of a plasma gasification reactor PLASGAS [23]

Figure 1.16: Plasma gasification reactor PLASGAS at IPP CAS

For this type of reactor, the oxidizing agent (air, oxygen, carbon dioxide, or steam) is usually fed through the bottom of the reactor. The gasification reaction takes place at the bottom of the reactor between the descending material and the ascending gas. The reaction temperatures are between 1000 and 1400 °C. The rise of hot gas starts the pyrolytic reaction of the material already at lower temperatures and dries it. The amount of tar can reach 10 to 20 % in the raw gas for complex input materials, which can complicate its subsequent purification and industrial application. [13]

However, for the PLASGAS at IPP CAS, the thermochemical reactions are secured by a plasma torch, which generates thermal plasma at the top of the reaction chamber. Furthermore, input gases are also supplied from the top, so they mix together with the processed material and the plasma and the mixture then continues either to the flue gas pipe as a synthesis gas or lands at the bottom of the reaction chamber, where it decomposes. Also, thanks to the thermal plasma in this configuration, tar production is suppressed during the process. The real look of the reactor can be seen in figure 1.16.

1.3.2 Technology description

In the upper flange (the lid) of the reactor, several orifices into the reactor chamber are necessary, namely for:

- plasma torch connection,
- feeding of processed material,
- dosing of any accompanying gases.

Material samples are delivered from the hopper through a horizontal pipe with an internal screw feeder (for a detailed view of a screw feeder see figure 1.17). At the end of the pipe, a T-junction is connected, which finally delivers the material into the reactor, where it is processed as a result of extreme thermochemical conditions attained by the plasma torch. In case of feeding complications, it is possible to install another screw feeder in the T-junction in the vertical direction. This prevents the material from getting clogged in the 90-degree bend. Inlet gases are dispensed simply with hoses connected to the lid.

The lining of the reactor walls is made of highly heat-resistant material (defined sequence of thick ceramic layers) that can withstand extreme temperatures. Despite the durability to high temperatures, the material is susceptible to rapid temperature changes, for instance as a result of geometry changes in the microscopic scale or drying of the layers.

Consequently to the high-temperature gradient the reactor walls may be damaged, which results in losing the insulating properties. For this reason, before the plasma torch is inserted and the ignition begins, the reactor temperature needs to be approximately the operating temperature.

On this scale, this process can take 24 hours. The temperature of 800-1000 °C is achieved by a heating element, while the working temperature in the reactor of

1000-1500 °C is already achieved by a plasma torch. The center of the plasma jet can reach temperatures of 6000-8000 °C.

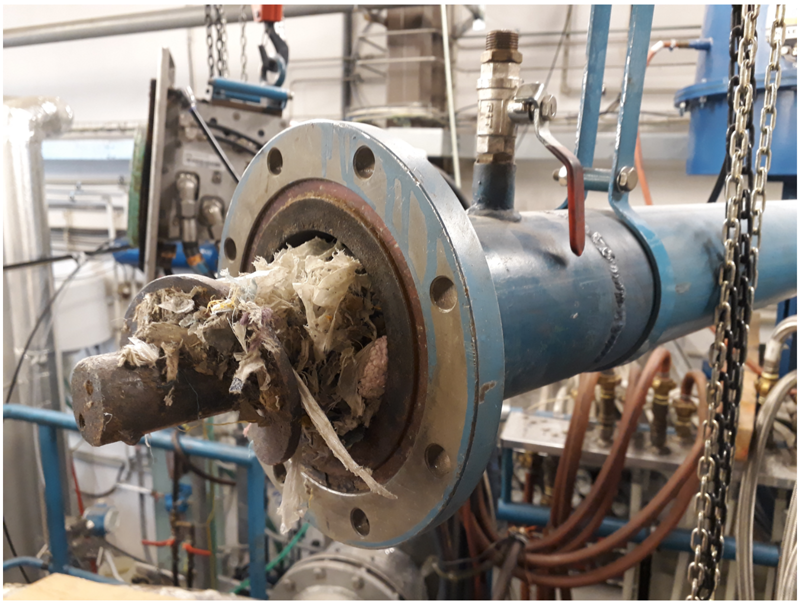

Figure 1.17: Detailed view of a screw feeder

The main functions of a plasma torch inside the plasma reactor are both a heat source and a chemical apparatus. Therefore, heat for thermochemical reactions is supplied to the system externally during operation (as mentioned above). These reactions cause difficulties in the reliable regulation of enthalpy in the reactor. Stabilization can be provided by means of electrical parameters, therefore total electrical energy supplied to the plasma torch.

On the contrary, the plasma is important for controlling the temperature in the reactor, for maintaining the process, and for its initiation. Moreover, these extreme conditions make it possible for materials to be decomposed into lesser molecules and atoms. This chemical mixture recombines into simpler compounds, which can be used as secondary raw materials (for example syngas, carbon black, or slag). The properties and behavior of the reaction and final compounds depend on operating conditions, for instance, the temperature, pressure, or residence time.

1.3.2.1 Chemical reactions

Simplified, the occurring reactions (or processes respectively) can vary from pyrolysis to plasma gasification, which can be considered as marginal. All other reactions are a form of a combination of these two. [3]

Pyrolysis is a process of thermal decomposition of substances without the presence of oxidants. Naturally, this is a chemical reaction that also occurs in the first seconds of the start of combustion. At 350-550 °C, the thermal decomposition of organic components in the biomass begins to occur. Rising up to temperatures of 700-800 °C, the long chains of carbon, hydrogen, and oxygen compounds of the biomass break down into smaller gas molecules, condensable vapors (oils and tars), and solid charcoal. In the presence of extreme temperatures during the gasification process, organic components (mainly containing chemically bound carbon, hydrogen, and oxygen) evaporate, and complex molecules dissociate. The mixture breaks down and reforms into synthesis gas (useful in the chemical synthesis industry or as a high-quality fuel). The processed inorganic materials melt and form a lava-like slag after cooling and solidification. Internal reactions determine the output products, the ratio of gas and solid components of the output products, maximum conversion efficiency is achieved if all the carbon is oxidized to carbon monoxide. [11]

Combustion (incineration respectively) is an extreme case of reaction in the plasma reactor chamber. It is undesirable and can take place when there is a deficiency in energy supplied by the plasma and a high amount of oxidizing agents is present. During the combustion of the material, it can be reduced by 70 % of mass and 90 % of volume. [6, 11]

However, in comparison to undesirable incineration, during gasification (or pyrolysis) of organic wastes, nitrogen oxides, sulfur oxides, products of incomplete combustion, and other hazardous emissions like chlorinated dibenzo-dioxins, dibenzofurans, and hydrochloric acid (depending on the composition of the fuel) are not produced. Furthermore, waste incineration does not offer a complete answer to the waste management issue for several reasons: [4, 11, 14]

- many wastes have a low calorific value,
- high flow rates of flue gases and waste gases,
- high production of residues containing hazardous materials and
- subsequent high costs of cleaning waste gases and leftover disposal.

In more detail, concerning chemistry, the first type of chemical reaction is the thermal cracking of complex molecules, causing them to dissociate into lighter molecules. These reactions are endothermic and form hydrocarbon gases and hydrogen. Secondly, partial oxidation creates combustible gases, essentially carbon monoxide. This also restraints the formation of water or carbon dioxide, which are undesirable compounds, as they are complete oxidation products and have a negative influence on the final heating value of the synthesis gas. Inorganic metals also undergo partial oxidation, but this is not crucial for the thesis, as the subject is the treatment of organic wastes in particular. The amount of delivered oxygen to the reactor (in all chemical forms) is one of the influencing factors of the resulting ratio between carbon monoxide and carbon dioxide. All partial oxidations are naturally exothermic. The third type is endothermic reforming reactions. These are convenient and have result of different reconfigurations of element atoms between molecules of different compounds. The high temperatures in the plasma reactor often suppress the production of higher hydrocarbons. Of course, the speed of the ongoing reactions and the state of their completion, also influence the formation of carbon monoxide and hydrogen, similar to the temperature in the reactor, for instance. A more detailed summary of some occurring organic chemical reactions is in table 1.3. Theoretically, with perfect knowledge of the composition of input and output products, the energy balance of chemical reaction processes could also be constructed on the basis of equations in table 1.3. [7, 11, 13, 16]

Reaction name	**Chemical reaction**	**Reaction enthalpy**
Methane partial oxidation	$CH_4 + 1/2\ O_2 \leftrightarrow CO + 2H_2$	- 35.66 kJ·mol^{-1}
Steam reforming	$CH_4 + H_2O \leftrightarrow CO + 3H_2$	+ 206.23 kJ·mol^{-1}
Dry reforming	$CH_4 + CO_2 \leftrightarrow 2CO + 2H_2$	+ 246.93 kJ·mol^{-1}
Methane oxidation	$CH_4 + 2O_2 \leftrightarrow CO_2 + 2H_2O$	- 802.29 kJ·mol^{-1}
Carbon oxidation	$C + O_2 \rightarrow CO_2$	- 393.65 kJ·mol^{-1}
Carbon partial oxidation	$C + 1/2\ O_2 \rightarrow CO$	- 110.56 kJ·mol^{-1}
Water–gas reaction	$C + H_2O \leftrightarrow CO + H_2$	+ 131.20 kJ·mol^{-1}
Boudouard reaction	$C + CO_2 \leftrightarrow 2CO$	+ 172.52 kJ·mol^{-1}
Hydrogasification	$C + 2H_2 \leftrightarrow CH_4$	- 74.87 kJ·mol^{-1}
Carbon monoxide oxidation	$CO + 1/2\ O_2 \rightarrow CO_2$	- 283.01 kJ·mol^{-1}
Hydrogen oxidation	$H_2 + 1/2\ H_2O \rightarrow H_2O$	- 241.09 kJ·mol^{-1}
Water–gas shift reaction	$CO + H_2O \leftrightarrow CO_2 + H_2$	- 41.18 kJ·mol^{-1}
Methanation	$CO + 3H_2 \leftrightarrow CH_4 + H_2O$	- 206.23 kJ·mol^{-1}

Table 1.3: Summary of some organic chemical reactions inside the reactor [11, 13]

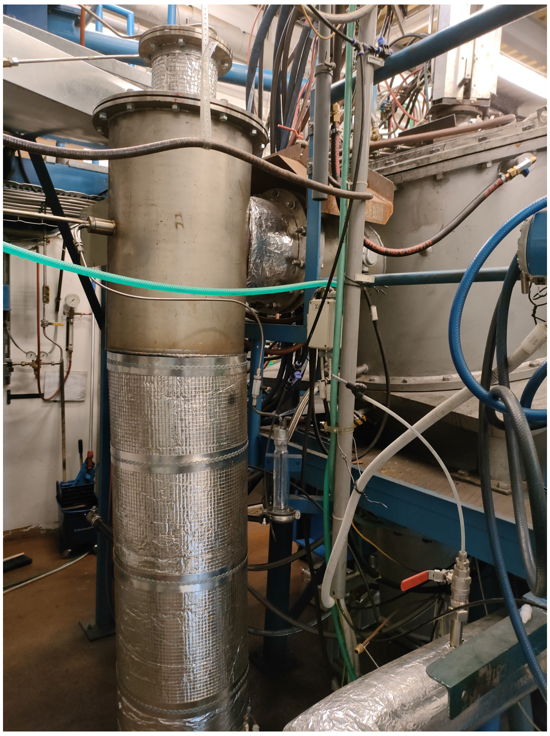

(a) Quenching tower

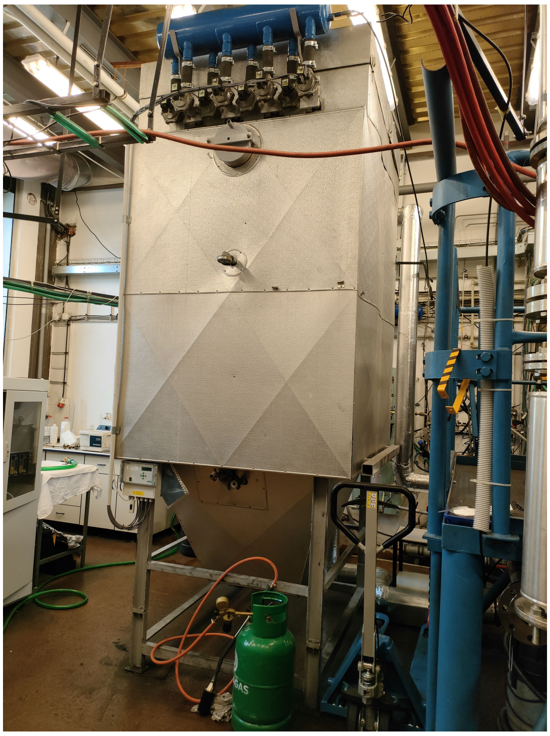

(b) Filter

Figure 1.18: Accompanying elements of the PLASGAS facility

1.3.2.2 Utilization of secondary raw materials

Secondary raw materials are transported through the flue gas pipe to the quenching tower (see figure 1.18a), where water droplets are cooling the gas. Temperature decrease suppresses other concomitant reactions and the composition of the gas remains preserved. The gas composition is measured using a mass spectrometer. The disadvantage is that carbon monoxide and nitrogen gas have practically identical molar masses, so these gases cannot be unequivocally distinguished with this method. Since no air (or nitrogen) is supplied to the reactor during the HPT experiments and the input material contains a practically negligible (trace) amount of nitrogen, the entire amount measured by the mass spectroscope will be considered carbon monoxide.

After cooling, the gas is passed through a filter, where solid parts are captured, especially carbon black particles. The filter is captured in the figure 1.18b. Another piece of equipment for further gas purification is currently being installed for testing, namely the desulfurization unit. The sorbents in the unit will be compounds like sodium carbonate, calcium hydroxide, and zinc oxide. In this consideration, synthesis gas cleaning is similar to flue gas cleaning in thermal power plants or W2E facilities.

The difference is that in power plants, flue gas cleaning takes place at approximately 90-150 °C or less, and it is often a wet scrubbing (milk of lime). In the case of gas cleaning from a plasma reactor, temperatures are around 300-600 °C and micro-ground calcium hydroxide sorbent is injected directly into the flue gas from the reactor during high-temperature cleaning. At these temperatures, it reacts with impurities in the flue gas and forms a filter pie.

In laboratory conditions, the obtained synthesis gas is burned by a combustion burner and not used for energy purposes. On a commercial or industrial scale, however, the synthesis gas could be accumulated in gas storage facilities or pressure cylinders, or further processed. This includes, for example, the production of hydrogen, motor fuels by Fischer-Tropsch synthesis, or other chemical compounds (for instance dimethyl ether, methanol, ethanol, or ammonia). Another option is energy utilization of the gas using a gas combustion turbine to generate alternating electrical energy. This configuration would require an intermediate segment to make a possible regulation independently of the reactions in the plasma reactor. Electrical energy generation together with the energy accumulation will be later discussed for the purposes of this thesis. Depending on the application, the different molar ratio of H_2/CO is suitable, for example, a ratio of 2 for Fischer-Tropsch synthesis applications or 0.5 for electricity generation using the internal combustion engine. [11]

For industrial applications using synthesis gas to generate electricity, a bottom draft fixed bed gasifier is generally preferable because the gas is produced at high temperatures and has a low percentage of tar and condensable content. On the other hand, in fluidized bed applications, the resulting ash is problematic together with the high alkali content, which leads to melting and the formation of clinker in the bed. [11]

Slag as a form of secondary raw material can be used for glass ceramics, road filler material, or building construction material. With thermal plasma pyrolysis or gasification, carbon nano-spheres or nano-tubes can be synthesized, too. By processing inorganic material like waste circuit boards, red mud, or galvanic sludge with thermal plasma, valuable metals can be recovered and refined, for instance, Ag, Au, Cu, Al, Fe, and Zn. [7]

Note: Some of the described characteristics discussed previously apply to the plasma reactor PLASGAS at IPP CAS. However, differences may take place depending on the producer and the actual operational application.

1.3.3 Configuration description

Depending on the type of plasma torch used, the overall configuration relating to the plasma reactor also differs in terms of the construction parts and their location. In the long term, the hybrid arc plasma torch with the entire apparatus was available and ready for conducting experiments (by approximately 2020/21).

Various orifices lead through the lid into the reaction chamber, for example for the placement of the plasma torch (as mentioned at the beginning of subsection *Technology description*). However, the microwave plasma torch has a much wider range of equipment necessary for operation. At the same time, the MWPT head has a completely different shape and dimensions than HPT.

The hybrid plasma torch is relatively small and it only requires a rectified electrical current supply and stabilization (cooling) media to operate. A microwave plasma torch is a much more complex device in terms of components and it works on a relatively different principle. Furthermore, the hybrid torch creates plasma using an electric arc flowing from a narrow exit nozzle. Output for plasma from the microwave torch is a wide cylindrical head with a large flange.

Modifying the existing reactor lid was practically impossible. For this fact, a completely new lid had to be manufactured that would be compatible with both the dimensions of the existing reactor and the MWPT outlet head. The openings for feeding the processed material and possible inlet gases were also necessary to keep in mind. This process took a long time and significantly delayed the planned microwave plasma torch experiments. Construction issues including this one are usually solved in cooperation with a team of institutional workers and technicians. After the installation of the new lid, the microwave plasma torch head was attached and bolted in an inclined vertical position, because of the horizontal orientation of the upper part of the reactor. For the reason of the large dimensions of the MWPT, its weight, and lack of working space, the laboratory crane was used for transportation.

Arrangement and assembly of the waveguide with the limited amount of its structural parts was another complication. For safety reasons (to protect the magnetron source), the waveguide had to include a circulator component at the same time. The circulator orients the internal microwaves in a defined manner and prevents the reflected power from returning to the magnetron. When the reflected power greatly increases, the sensors inside the circulator react and shut down the power supply. A major part of the microwave system is a powerful magnetron. The whole magnetron box weighs roughly 200 kg, yet it was necessary to place it as close as possible to the reactor lid in a suitable way to allow the waveguide to be assembled between the magnetron and the MWPT. For this purpose, an auxiliary elevated structure was assembled in the laboratory, on which the magnetron box was lifted, again with the help of a laboratory crane.

After the solution of these obstacles, it was clear that the design of the microwave plasma torch impeded the existing material transport system. In other words, it would not be possible to use the T-junction at the end of the screw feeder pipe, because the MWPT head was blocking it. Therefore a new part was made - the pipe elbow (see 1.19b). In this new MWPT configuration, using the pipe elbow, the material could not directly fall into the reactor vertically upon reaching the T-junction. The frictional forces between the material and the inclined inner wall of the pipe elbow need to be overcome earlier before the material gets clogged inside. However, the *Feeding calibration* section in the *Preparation of experiments* chapter is devoted to this issue. A comparison of the resulting configurations for 2 different types of plasma torches is shown in figure 1.19, where the key parts of both systems are numbered and described.

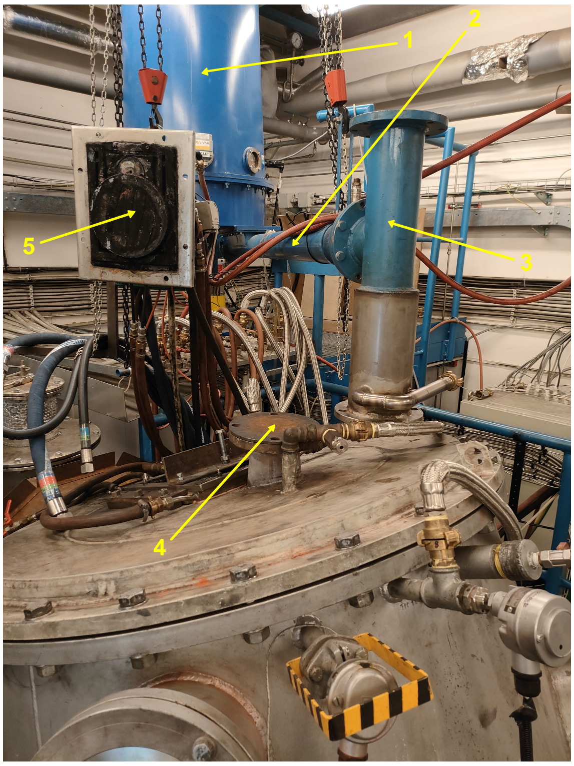

(a) Feeding for HPT configuration:
1 - hopper
2 - screw feeder pipe
3 - T-junction
4 - feeding hole
5 - HPT

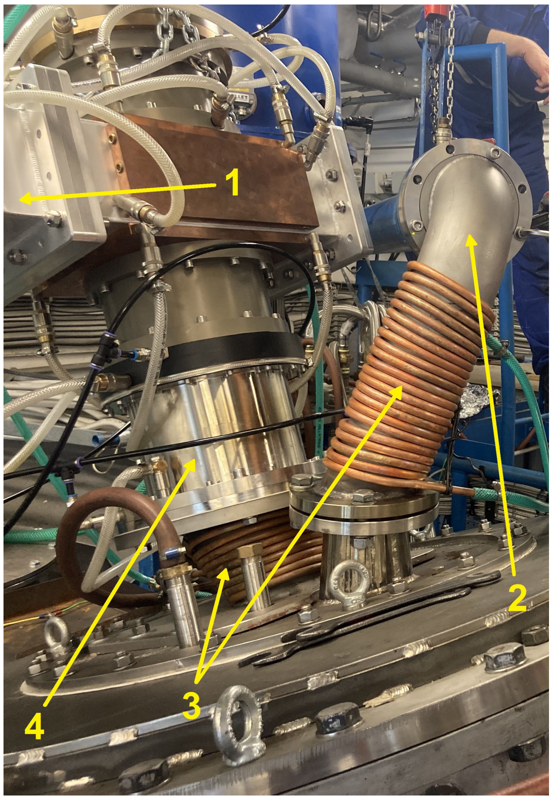

(b) Feeding for MWPT configuration
1 - end of the waveguide
2 - pipe-elbow
3 - improvised cooling
4 - MWPT unit

Figure 1.19: Comparison of two configurations for different plasma torches

Chapter 2

Preparation of experiments

This chapter will gradually summarize everything that needs to be secured and procured before the experiment itself. The provision of all requirements usually involves the cooperation of a team. The mechanical technical workers are most involved in construction matters. Electrical or scientific workers secure the control and power supply of the plasma torch, operate and maintain diagnostic and accompanying equipment, or supervise measurements. The resulting data is processed depending on its character. Chemical workers usually perform analyzes of the chemical composition of output products, for instance, the synthesis gas. More about these chemical analyses and the rest of the data obtained will be explained in the chapter *Experimental results*.

2.1 Plasma torches

Before the plasma torch is used inside the reactor, proper testing of its behavior and characteristics needs to be performed. This ensures the reliability of its operation during the actual experiment. In this thesis, two types of plasma torches are discussed in particular, namely the hybrid arc plasma torch and the microwave plasma torch.

2.1.1 Hybrid plasma torch (HPT)

Because the hybrid plasma torch was developed at IPP CAS many years ago as an improvement of the water-stabilized plasma torch, its properties, behavior, operating modes, and nominal parameters are already well known. Since that time, this torch was widely used for the purpose of plasma spraying of corundum powder (Al_2O_3) protective layers, for example. The principle of operation of the hybrid plasma torch is explained in the first chapter in subsection *Electric arc plasma torch*.

The ignition of a hybrid plasma torch is carried out by a capacitor circuit functioning as a voltage multiplier or charge pump. The design of the ignition circuit cannot be shared as a part of the content of this thesis. It is an intellectual property of IPP CAS. This method of ignition is necessary to ensure the electrical penetration of the stabilization medium, the formation of an electric arc, and the subsequent generation of a plasma jet. Because of the nature of the ignition, a voltage peak can always be noticed on the time course of the voltage on the plasma torch.

The peak reaches approximately 150-200 % of the plasma torch's working voltage. For more see (chapter *Experimental results*) section *Measured data*. The character of continuous electrical quantities is DC because they are measured after the rectifier. DC output power of the hybrid plasma torch ($P_{\mathrm{HPT_{OP}}}$) can therefore be simply expressed as the product of DC current and voltage of the hybrid plasma torch:

$$P_{\mathrm{HPT_{OP}}}(t) = U_{\mathrm{HPT}}(t) \cdot I_{\mathrm{HPT}}(t) \tag{2.1}$$

The efficiency of the rectifier (η_{rec}) should be more than 95 %. Because the η_{rec} may also change during time, it will not be considered, since the exact relation of $\eta_{\mathrm{rec}}(t)$ depending on the operating conditions is not know. Including the rectifier, the total input power ($P_{\mathrm{HPT_{IP}}}$) of the hybrid plasma torch is approximately:

$$P_{\mathrm{HPT_{IP}}}(t) = \frac{U_{\mathrm{HPT}}(t) \cdot I_{\mathrm{HPT}}(t)}{\eta_{\mathrm{rec}}(t)} \tag{2.2}$$

The total input electrical energy is then equal to the integral of the electrical input power as a function of time. The exact evaluation of electrical power by the measuring system is not known, so for the calculating purposes of energy balances, the average value of the measured power and the product of voltage and current will be considered as the input electrical power, as described in equation 2.3. (The resulting values are slightly different from each other and it is not possible to determine their accuracy compared to the real values).

$$P_{\mathrm{HPT}}(t) = \frac{P_{\mathrm{HPT_{IP}}}(t) + U_{\mathrm{HPT}}(t) \cdot I_{\mathrm{HPT}}(t)}{2} \tag{2.3}$$

The efficiency of the plasma torch itself can be further expressed as a fraction of the energy supplied for thermochemical reactions and total input power. This energy in the form of heat is the difference between total input power and the power taken away by a plasma torch cooling water during the observed time. Consequently:

$$\begin{gathered}\eta_{\mathrm{HPT}}(t) = \frac{Q_{\mathrm{HPT}}(t)}{P_{\mathrm{HPT_{IP}}}(t)} = \frac{P_{\mathrm{HPT_{OP}}}(t)}{P_{\mathrm{HPT_{IP}}}(t)} = \frac{P_{\mathrm{HPT_{IP}}}(t) - Q_{\mathrm{W_{HPT}}}(t)}{P_{\mathrm{HPT_{IP}}}(t)} \\ \eta_{\mathrm{HPT}}(t) = 1 - \frac{Q_{\mathrm{W_{HPT}}}(t)}{P_{\mathrm{HPT_{IP}}}(t)}\end{gathered} \tag{2.4}$$

More on electrical energy calculations related to the energy balance can be found in the *Energy balance* section, respectively the *Electrical energy* subsection.

2.1.2 Microwave plasma torch (MWPT)

The microwave plasma torch was not developed at IPP CAS, unlike the already mentioned hybrid arc plasma torch. It was supplied by an external company, MUEGGE. From this perspective, it is an unknown technology that needs to be examined through appropriate testing and the investigation of the documentation.

This is not a classic microwave plasma torch, as it has considerably higher power (up to 100 kW) compared to other available types. Secondly, the working frequency is different from the classically used frequency of 2.45 GHz (also typical for microwave ovens), namely about 916 MHz.

The existing continuous variable measurement system in the laboratory of IPP CAS was custom-designed many years ago for the needs and character of institutionally developed plasma torches. Consequently, it turned out not to be compatible with the MWPT and the measurement of its specific electrical parameters was not successful.

Though the MWPT system has its own user interface, only the required input power is adjustable and the data is not saved for later use. Accordingly, the $P_{\mathrm{MW}} = f(t)$ relation will be created by joining the subsequent intervals with constant values of the set power during the experiment.

The electrical efficiency (η_{GEN}) of the microwave generation is about 75 %. This means, for example, that 100 kW of power input corresponds to 75 kW of microwave power. Part of the microwave power is again reduced by the heat carried away by cooling water. Energy in the form of heat supplied for thermochemical reactions can be expressed as follows:

$$Q_{\mathrm{MWPT}}(t) = P_{\mathrm{MWPT_{IP}}}(t) \cdot \eta_{\mathrm{MW}} \tag{2.5}$$

where η_{MW} represents the efficiency of the entire system. However, part of the microwave power is always reflected, which is why the maximum operating power of the plasma (before transmitting energy to water) is around 70 kW.

Considering 7 % of the reflected power during steady state operation, the efficiency of the waveguide η_{WG} as the efficiency of transmission of microwave power to the MWPT head is stated to be 93 %. From the power supplied to the MWPT head, part of the energy is taken away by cooling water in the form of heat ($Q_{\mathrm{W_{MWPT}}}$). The total efficiency of the MWPT system is then:

$$\eta_{\mathrm{MWPT}}(t) = \frac{\eta_{\mathrm{GEN}}(t) \cdot \eta_{\mathrm{WG}}(t) \cdot P_{\mathrm{MWPT_{IP}}}(t) - Q_{\mathrm{W_{MWPT}}}(t)}{\eta_{\mathrm{GEN}}(t) \cdot \eta_{\mathrm{WG}}(t) \cdot P_{\mathrm{MWPT_{IP}}}(t)} \tag{2.6}$$

After adjusting the fraction:

$$\eta_{\mathrm{MWPT}}(t) = 1 - \frac{Q_{\mathrm{W_{MWPT}}}(t)}{\eta_{\mathrm{GEN}}(t) \cdot \eta_{\mathrm{WG}}(t) \cdot P_{\mathrm{MWPT_{IP}}}(t)} \tag{2.7}$$

The user interface for the microwave plasma torch is depicted in figure 2.14 in subsection *Diagnostic devices*, where the appropriate buttons for operation control are visible.

For the purpose of operating the new microwave plasma torch and to supply energy to the powerful magnetron, a new source from MUEGGE company was ordered. In contrast to the hybrid arc plasma torch, the microwave plasma torch cannot be ignited immediately. Before the ignition, it is necessary to wait for the ignition filament to heat up to prevent damage during the process. Shortly after, the magnetron can operate and start generating microwaves, which create a spiral stream of plasma after interacting with the stabilizing medium (in this case air). Before the experiment with the MWPT configuration, the plasma torch (together with the power source and all other components) had to be tried and tested. The components of the MWPT system before assembly into a sub-unit is captured by figure 2.1, where the individual parts are highlighted and described. The components are connected subsequently in the order in which they appear in the figure.

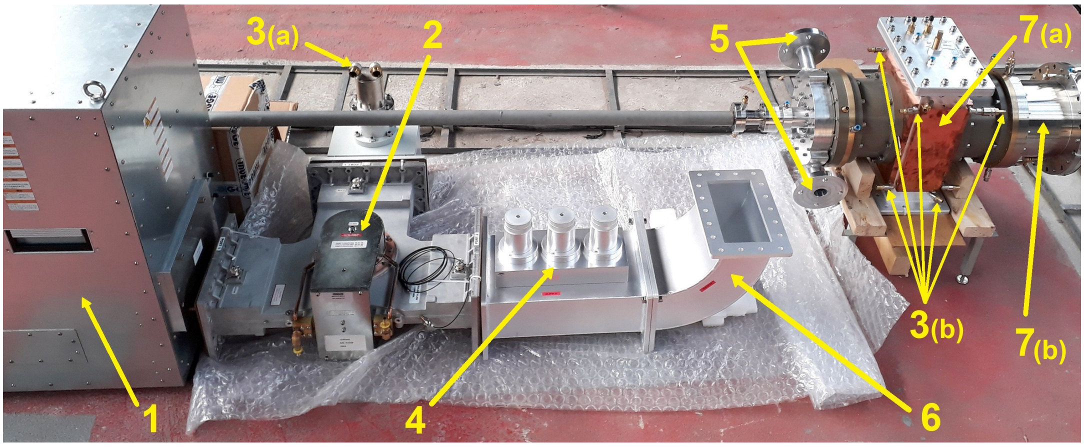

Figure 2.1: MWPT components before assembly

1 - magnetron, 2 - circulator, 3 - inlets for cooling (a - circulator, b - head), 4 - tuner, 5 - inlets for airflow, 6 - waveguide, 7 - MWPT head (a - reaction chamber, b - outlet nozzle)

The description of the overall function of the MWPT system is summarized as follows. The magnetron generates microwaves that travel through the circulator and the waveguide, where they are conveyed to the MWPT head chamber. In the chamber, microwaves react with the spiral stream of stabilizing medium to form a plasma that flows out the exit nozzle. The microwave plasma flame during the testing outside the reactor is shown in figure 2.2. In appearance, this flame resembles a classic flame of fire.

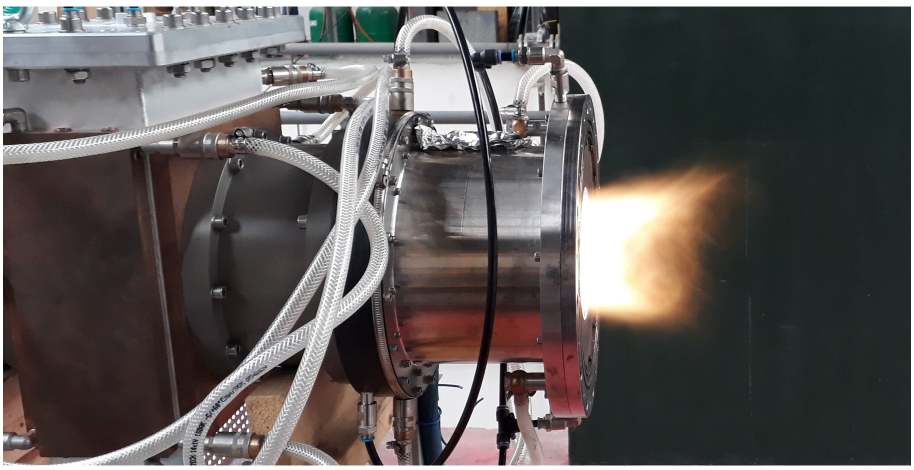

Figure 2.2: View of testing the MWPT outside the reactor before the experiments

The apparatus systems of individual plasma torches and their configuration were described in more detail in *Configuration description*.

2.2 Material samples

Almost any material can be processed using the thermal plasma generated by powerful plasma torches. Still, the testing material sample should be chosen with respect to the reasons for conducting the experiments.

For example, the energy of plasma can be utilized to process metals or steel materials in terms of cutting, welding, surface, or heat treatment. However, the objective of this thesis and the current efforts of the PCHT department of IPP CAS is the investigation of alternative methods of energy utilization of waste. Materials with a high energy value in chemical bonds (in the form of their calorific value) are usually of organic origin. Therefore, those types of wastes that have a high proportion of organic components in the overall material composition are attractive for related research. These can include biodegradable municipal waste, sorted waste, medical waste, or a large part of municipal solid waste.

2.2.1 RDF

From those wastes, which are highly contributed from materials with considerable calorific value, refuse-derived fuel (RDF) may be attractive for the experiments. RDF is a mixture made from the unsorted part of sorted waste, either in the form of chips or pellets. This mixture can be burned and used for energy purposes. However, for bigger commercial industrial applications, there is a need to adhere to set emission limits, which may complicate the potential use of RDF.

The reason why RDF is suitable for testing is its convenient composition, allowing it to be relatively easily transported into the plasma reactor using the screw feeder. Furthermore, according to the waste statistics, its production is constantly increasing, even if only the energy-usable part is taken into account. Table 2.1 includes data of EUW that was produced between the years 2015-2020 in the Czech Republic.

The last item (bulky waste) includes all municipal waste that cannot be placed in conventional containers or dustbins because of its large dimensions. Bulky waste includes both the energy-usable part (for instance furniture, carpets, cardboard, and plastic packaging), and the energy-unusable part (like sanitary ceramics, large electronics, glass and metal packaging). Because it is practically impossible to determine from this data what percentage of the bulky waste constitutes the energy-usable part, half of the total value of bulky waste will be taken for illustrative purposes.

The values of mixed waste are also shown in the last line for comparison. Mixed waste is not included in the total amount of energy-usable waste for illustrative purposes in figure 2.3. It definitely also contains a significant amount of energy-usable waste, but it is difficult to estimate how much could be efficiently sorted and used for energy purposes. Therefore, it will be neglected in figure 2.3 of the increase in the production of waste that can be used for energy (also, the trend of the curve is more important than the absolute values). It seems that the increase in waste has decreased in recent years and that it is heading towards stagnation, which is probably the effect of the provisions against Covid 19 that were implemented at that time. [24, 25]

Waste	**2015**	**2016**	**2017**	**2018**	**2019**	**2020**
Paper	30.4	32.4	33.6	33.4	32.5	28.5
Plastics	11.7	13.4	13.6	14.5	15.4	16.7
Biological	39.9	54.7	57.7	59.3	63.3	66.2
Wood	3.5	4.7	5.2	5.8	5.7	5.6
Textile	1.8	2.1	2.3	2.5	2.8	2.5
Bulky	32.7	36.0	38.0	40.7	45.1	48.8
(for heat)	16.4	18.0	19.0	20.4	22.6	24.4
Sum	**103.7**	**125.3**	**131.4**	**135.9**	**142.3**	**143.9**
Mixed	198.8	199.8	198.2	198.5	195.6	198.0

Table 2.1: The annual amount of EUW from municipalities and from citizens in the Czech Republic in kg per person [24]

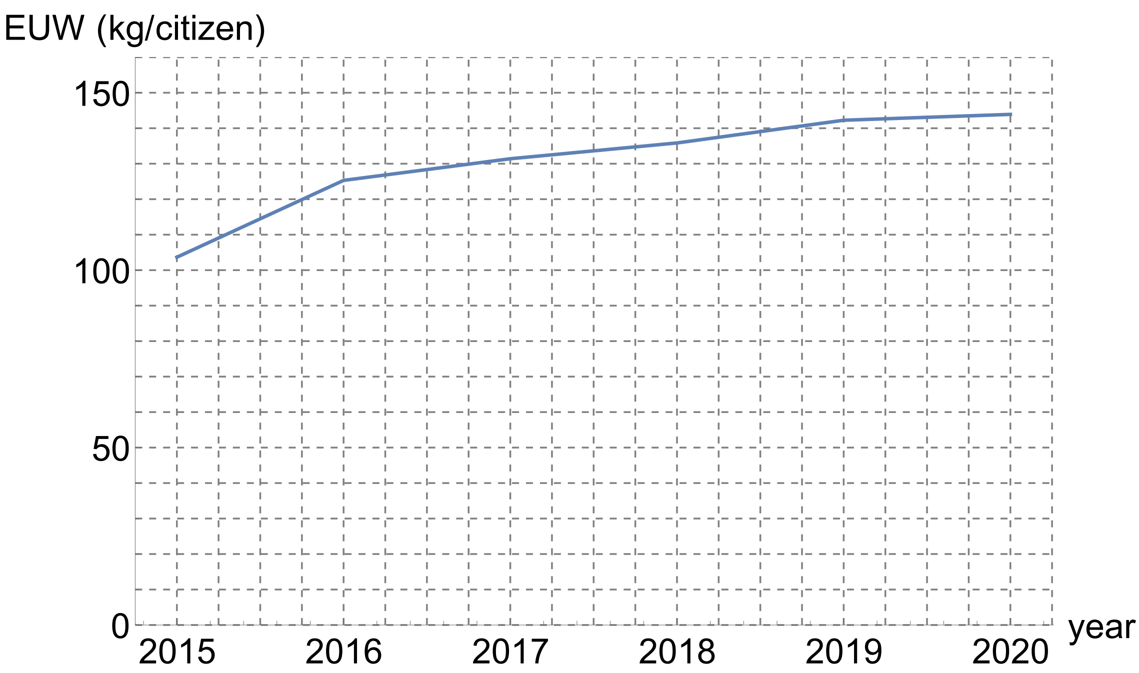

Figure 2.3: The annual amount of EUW from municipalities and citizens in the Czech Republic

RDF material sample was received directly from a real sorting line in Úholičky, which has been in operation since 2012. The line is equipped with a 50-ton continuous press and a sorting cabin with several automated boxes and is capable of receiving and processing approximately 15 thousand tons of transported sorted waste per year. Examples of RDF are shown in figure 2.4. [26]

(a) Ilustrative photo [27] **(b)** Actual sample

Figure 2.4: Images of RDF examples

2.2.2 SMW

Another type of waste that has a similar structure after processing and offers even greater potential for energy use is medical waste. However, it is very risky for testing in laboratory conditions, as it contains lots of dangerous parts, for example, chemicals or sharp objects like scalpel blades and needles, furthermore, potential infections and other biological threats that can enter the waste mixture in the form of body fluids or parts of patient organs, whether absorbed by medical pulp and textiles or on used medical devices. For this reason, waste from hospitals is non-recyclable and materially unusable. The only option for utilization of this waste is for energy purposes.

For experiments, the sample of simulated medical waste (SMW) was created. It was prepared by processing and crushing selected types of materials and mixed in the ratio defined by the pie chart in figure 2.8. The ratios in figure 2.8 are based on table 2.2, where all components of medical waste are included. Specific material components used for the SMW mixture is shown in figures 2.5, 2.6 and 2.7.

The liquids could be simulated in laboratory conditions by adding water, but this would have a minor effect on the experiment itself. On the contrary, the homogeneity of the sample would be worse, because the water would be absorbed by a small amount of the material sample. The ratio of inorganic salts and metals is negligible in the medical waste percentage representation. Secondly, these components are not usable for energy purposes, so these materials will also be neglected for the simulated medical waste sample.

(a) Cellulose wadding **(b)** Injection syringes

Figure 2.5: Biomass and plastics for SMW sample

Figure 2.6: Textiles for SMW sample - a surgical gown and a disposable sheet

(a) Silicone gloves **(b)** Technical cork

Figure 2.7: Rubber for SMW sample

Naturally, the material sample is not entirely homogeneous. During the operating conditions, the composition according to figure 2.8 may not always correspond, especially for smaller parts of the sample. Data regarding the percentage representation of medical waste are drawn from the source [28].

Material	Contribution
Biomass	57.7 %
Plastics	16.3 %
Textile	10.9 %
Rubber	6.9 %
Liquids	6.6 %
Inorganic salts	0.8 %
Metals	0.8 %

Table 2.2: Composition of medical waste

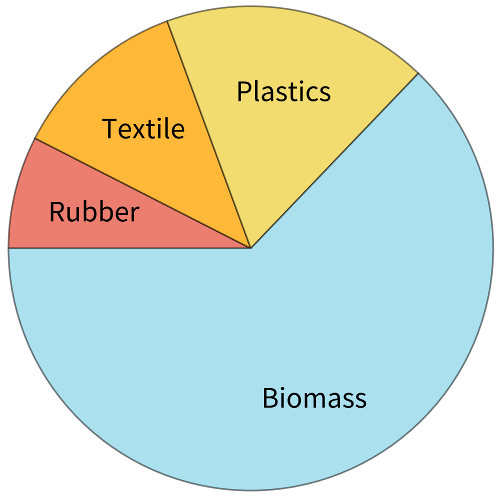

Figure 2.8: Composition of SMW

2.3 Feeding calibration

While operating, the system is hermetically sealed for safety reasons (hydrogen, which is explosive in the air at higher concentrations, could theoretically escape from the reactor into the hopper through the screw feeder pipe). For this reason, estimates regarding the amount of processed material during the experiment can only be made on the basis of the screw feeder velocity. The rotating velocity is set as a percentage of the maximum operating velocity of the screw feeder and is most often in the range of 10-20 % for most of the experiments. For different material samples, one particular velocity of a screw feeder corresponds to different mass flow rates. This includes fluctuations, which can be greater for more inhomogeneous or possibly compressible materials.

The reference material sample consists of polypropylene pellets. When measured correctly, there are practically minimal deviations from the experimentally measured relation between the mass flow rate and the rotation velocity of the screw feeder. For the reason of time savings, the mass flow rates in $kg \cdot h^{-1}$ are determined on the basis of ten-minute intervals. The measured amount of material fed is weighed and eventually multiplied by six. This increases the measurement error, but since this relation is linear, the trend of the curve is preserved. At the same time, specifying mass flow rates in kg per 10 minutes is unusual and impractical.

If more than ten measurements are completed, fairly good estimates can be expected. Apparently, performing more measurements does not bring much different outcome, because material feeding will always be a stochastic process. Even if the relationship between mass flow and screw feeder velocity may get more accurate with the increasing amount of measurements, the actual mass flow remains stochastic and cannot be anticipated precisely in future operations. Performing the right assessment is also complicated by the fact that the sample is a solid material, not a liquid or gas. A more extensive measurement would be suitable for a bigger facility before the actual commercial operation, for instance.

In addition, the material filled to the hopper before the experiment is weighed, similar to the leftovers in the hopper after the experiment. This provides the possibility of correcting the amount processed and eliminating discrepancies. Usually, the measured weights approximately match the predictions based on the screw feeder velocities during the experiment.

The calibration curve (of $\dot{m} = f(v_{\mathrm{rel}})$ relation) for the RDF feeding in the case of the HPT configuration coincided for both cases with and without the T-junction. The perpendicular angle of the pipe did not have a negative effect on the material feeding. However, in the *Configuration description* subsection, it is described that for the case of the MWPT, the end of the T-junction cannot be used. In this kind of configuration, a pipe elbow must be used for material sample feeding. Because in terms of operation, this component is yet unknown, the case of the feeding calibration with pipe elbow will be specified here. The rounded angle of the pipe elbow could possibly have a negative effect on the fluctuations in the mass flow of the material, or even worse, its complete clogging.

2.3.1 RDF

The first type of tested material sample was RDF. Although it is more inhomogenous than SMW, it is more suitable for feeding by screw feeder, because it is heavier, less compressible, and contains more solid parts.

v_{rel} (%)	$\dot{m}$ $(\frac{\mathrm{kg}}{10\ \mathrm{min}})$	$\dot{m}$ $(\frac{\mathrm{kg}}{\mathrm{h}})$
10	2.27	13.62
2	0.35	2.10
6	1.26	7.56
8	1.79	10.74
20	4.08	24.48
40	5.45	32.70
15	2.28	13.68
15	2.31	13.86
10	1.41	8.46
0.5	0.00	0.00
10	2.23	13.38
14	2.69	16.14

(a) First calibration

v_{rel} (%)	$\dot{m}$ $(\frac{\mathrm{kg}}{10\ \mathrm{min}})$	$\dot{m}$ $(\frac{\mathrm{kg}}{\mathrm{h}})$
2	0.29	1.74
10	2.11	12.66
10	1.85	11.10
10	2.15	12.90
60	9.01	54.06
40	4.99	29.94
10	1.51	9.06
10	1.43	8.58
10	1.85	11.10
10	1.63	9.78
10	2.11	12.66
10	1.71	10.26

(b) Second calibration

Table 2.3: Calibration of RDF feeding without pipe elbow

Before the experiment, it was, therefore, necessary to test the configuration with pipe elbow to see if any excessive complications during feeding occur, for instance causing the pipe to clog. In the beginning, the measurement was performed without the pipe elbow as a reference condition, and the calibration with the pipe elbow followed.

In the end, more than only one test without the pipe elbow was done. After the first calibration, it became clear that the subsequent feed rate did not depend only on the current rotation velocity of the screw feeder, but on some other factor. Table 2.3 summarizes the calibration results. The first guess was that it might be a defect in the converter that controls the rotation speed. This estimate was not confirmed, unlike subsequent consideration.

The velocity of the screw feeder influences not only the rotation itself but also the amount of material that can be dispensed into the pipeline directly from the hopper. At lower velocities, the screw feeder pipeline is better filled from the hopper, and therefore less space in the total volume of the pipeline is empty. (This is actually a desirable feature from the perspective of preventing the flow of gases from the reactor into the hopper.)

In a long-term steady state or during slow changes of operating conditions, this presents no serious issue. However, if the screw feeder velocity is changing dynamically, the mass flow of material may dramatically change from the predictions based on the relation $\dot{m} = f(v_{\mathrm{rel}})$. The deviation depends on whether the previous velocity states were lower or higher, thus if the velocity is continuously increasing or decreasing. This might be problematic for a potential commercial industrial operation.

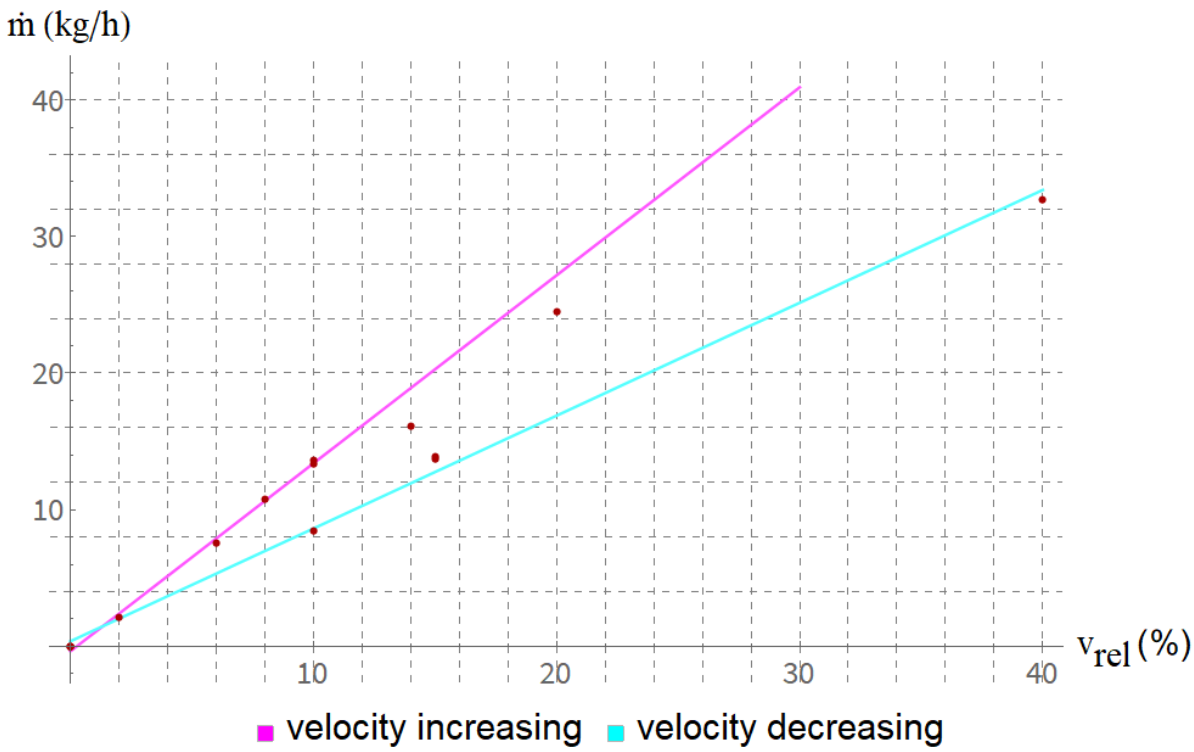

Figure 2.9: First calibration of RDF feeding without pipe elbow

This effect is captured by the graphical representation of the data from table 2.3 in figure 2.9. For reassurance regarding the dependence $\dot{m} = f(v_{\mathrm{rel}})$ and demonstration of its stochastic nature, another series of calibrations was carried out. Most of the independent values (velocities) now represented 10 %. Figure 2.10 shows a zoom of the measured data in the area $v_{\mathrm{rel}} \approx 10$ %, from which it is possible to see:

- the stochastic nature of the actual mass flow and
- the dependence on the velocity of the screw feeder in the previous state.

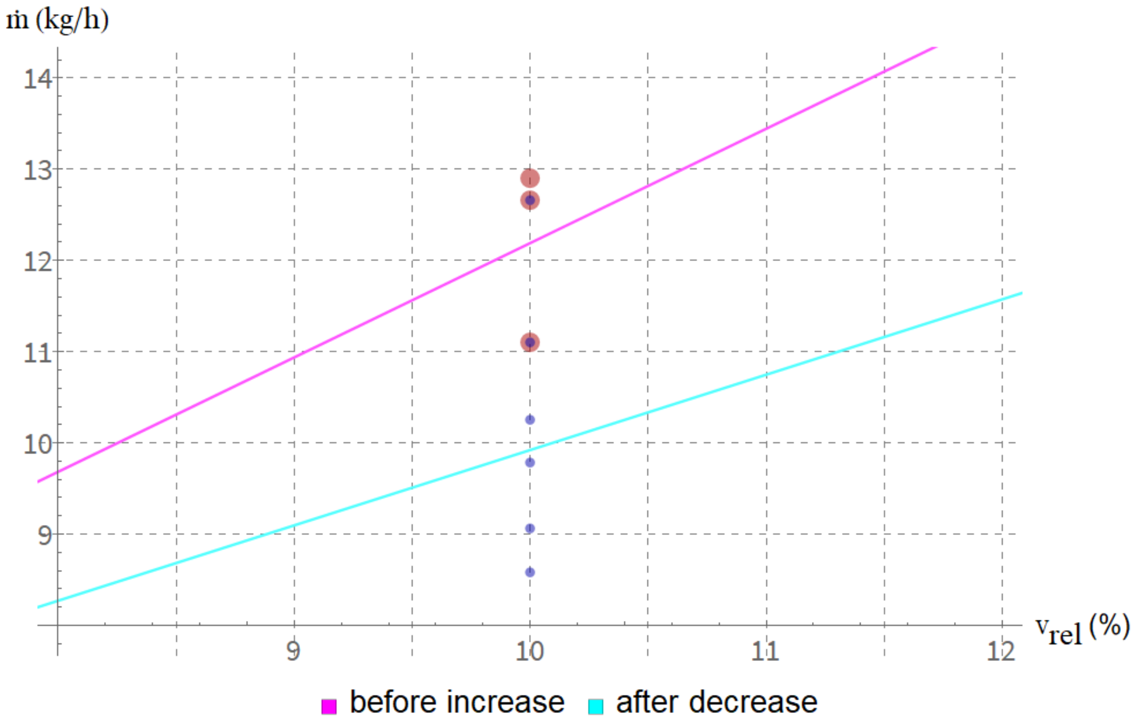

Figure 2.10: Second calibration of RDF feeding without pipe elbow

Initial calibration was followed by a calibration with a pipe elbow, listed in table 2.4. The tested velocities were deliberately chosen randomly, in order to suppress the effect of the continuous increase or decrease of the screw feeder velocity on subsequent mass flows of the material. The number of measurements was lower than without pipe elbow, because somewhere between $v_{\mathrm{rel}} \approx 30 \to 20$ %, the pipe elbow got clogged. This was manifested by the fact that the measured flow rate was significantly lower than expected already for $v_{\mathrm{rel}} = 30\%$. Given that, it can be assumed that the clogging began to occur already during this velocity. At $v_{\mathrm{rel}} = 20$ %, pieces of gradually compressed and slowly pushed RDF fell in the prepared bag at the end of the exit from the pipe elbow.

Based on this finding, the critical speed of the screw feeder in the MWPT configuration was estimated to be around 25 % for RDF. The pipe elbow was disassembled, cleaned, and refitted and the calibration was repeated, this time for lower velocities in the range of $v_{\mathrm{rel}} \in \langle 10, 15 \rangle$ %. These values correspond to velocities usually used during experimental operation.

An interpolation from the data (during clogging and subsequent final testing) situated to the reference graph (without pipe elbow) can be seen in figure 2.11. It is evident that at low speeds of around 10-15 %, the relation of $\dot{m} = f(v_{\text{rel}})$ correlates well with the original curve as the velocity was increased over time. Therefore this interpolation can be declared generally reliable for the subsequent determination of the mass flow rate. The coefficients of this first-order polynomial interpolation of the form of $(k_{\text{RDF}} \cdot v_{\text{rel}} + q_{\text{RDF}})$ can be stated. The q_{RDF} coefficient will be 0 because when the feeder is turned off, it cannot feed any mass flow. (Hence $\dot{m}_{\text{RDF}}(v_{\text{rel}} = 0) = 0$ was added to the data. The k_{RDF} coefficient was calculated by the computing software Wolfram Mathematica. The result is $k_{\text{RDF}} = 1.27$. Accordingly:

$$\dot{m}_{\text{RDF}} = 1.27 \cdot v_{\text{rel}} \tag{2.8}$$

v_{rel} (%)	$\dot{m}$ $\left(\frac{\text{kg}}{10\ \text{min}}\right)$	$\dot{m}$ $\left(\frac{\text{kg}}{\text{h}}\right)$
10	1.73	10.38
6	1.21	7.26
4	0.85	5.10
8	1.89	11.34
12	2.89	17.34
30	4.23	25.38
20	2.23	13.38

(a) First calibration

v_{rel} (%)	$\dot{m}$ $\left(\frac{\text{kg}}{10\ \text{min}}\right)$	$\dot{m}$ $\left(\frac{\text{kg}}{\text{h}}\right)$
10	2.17	13.02
11	2.31	13.86
12	2.36	14.16
13	3.09	18.54
14	2.93	17.58
15	3.29	19.74
16	3.25	19.50
10	1.85	11.10

(b) Second calibration

Table 2.4: Calibration of RDF feeding with pipe elbow

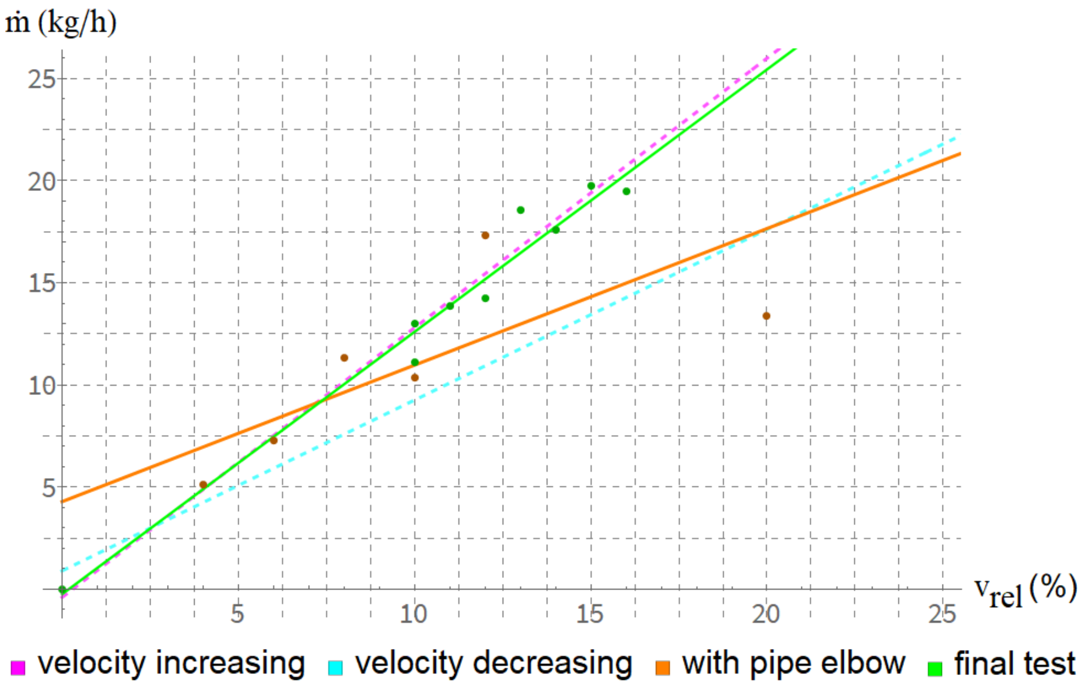

Figure 2.11: Calibration of RDF feeding with pipe elbow

2.3.2 SMW

Similarly to RDF, SMW also required proper calibration. This time, the measurements were not that detailed and did not take that long. The calibration consisted of six measurements without pipe elbow for the range of $v_{\mathrm{rel}} \in \langle 4, 12 \rangle$ % and nine measurements with pipe elbow for the range of $v_{\mathrm{rel}} \in \langle 8, 28 \rangle$ %. Once again, the point $\dot{m}_{\mathrm{SMW}}(v_{\mathrm{rel}} = 0) = 0$ was added to the interpolation. The feeding calibration results of SMW are summarized in tables 2.5 and shown in figure 2.12.

v_{rel} (%)	$\dot{m}$ $(\frac{\mathrm{kg}}{10\ \mathrm{min}})$	$\dot{m}$ $(\frac{\mathrm{kg}}{\mathrm{h}})$
10	1.57	9.42
4	0.62	3.72
4	0.63	3.78
8	1.25	7.50
6	0.98	5.88
12	1.83	10.98

(a) Without pipe elbow

v_{rel} (%)	$\dot{m}$ $(\frac{\mathrm{kg}}{10\ \mathrm{min}})$	$\dot{m}$ $(\frac{\mathrm{kg}}{\mathrm{h}})$
10	1.45	8.70
12	1.79	10.74
14	2.00	12.00
16	2.21	13.26
18	2.61	15.66
20	2.85	17.10
24	3.38	20.28
28	3.65	21.90
8	1.17	7.02

(b) With pipe elbow

Table 2.5: Calibration of SMW feeding

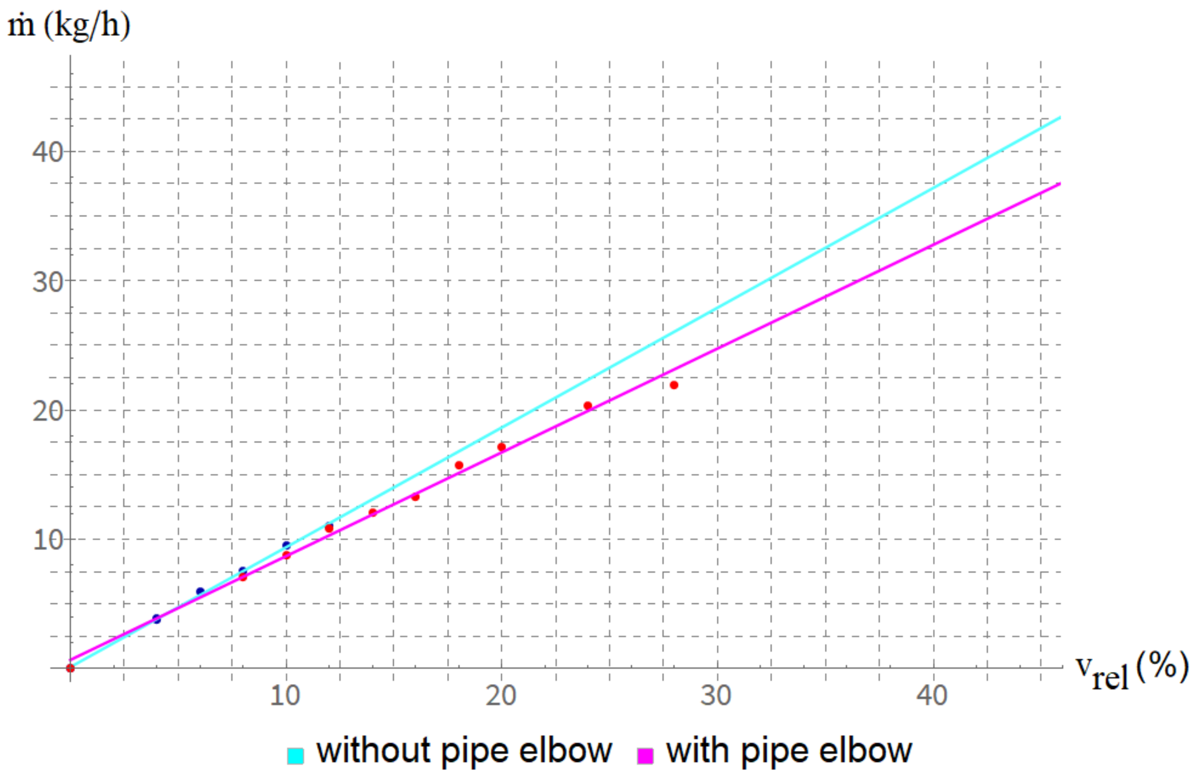

Figure 2.12: Calibration of SMW feeding

After fitting the data with a first-order polynomial, the k_{SMW} coefficient of $\dot{m}_{\mathrm{SMW}} = k_{\mathrm{SMW}} \cdot v_{\mathrm{rel}}$ was estimated 0.83. Therefore:

$$\dot{m}_{\mathrm{SMW}} = 0.83 \cdot v_{\mathrm{rel}} \tag{2.9}$$

It was expected that the k_{SMW} will be lower than k_{RDF} because SMW has a significantly lower density than RDF. Neglecting the compressibility of the material and considering roughly constant volume flow, the $\dot{m}_{\mathrm{SMW}}(v_{\mathrm{rel}}) < \dot{m}_{\mathrm{RDF}}(v_{\mathrm{rel}})$ inequality can be directly assumed. From the appointed relations $\dot{m}_{\mathrm{RDF}} = 1.27 \cdot v_{\mathrm{rel}}$ and $\dot{m}_{\mathrm{SMW}} = 0.83 \cdot v_{\mathrm{rel}}$, the necessary screw feeder velocity during the experiment for the required mass flow of the processed material will be estimated.

It is good to mention that the material feeding solution with a screw feeder at PCHT IPP CAS is far from optimal, considering the dimensions of the system and the low bulk mass of tested materials (SMW and RDF). In an industrial application, the feeding system would be optimized in terms of principles and dimensions for the specific type of material being processed. This should minimize feeding complications (which for instance occurred during the conducted experiments, as explained later). Different methods of material feeding or design are addressed, for example, in [29] or [30].

2.4 Reactor

Preparations of the reactor for the experiment mainly concerned of structural modifications, which are discussed in more detail in the *Configuration description* chapter. It involved replacing the top cover (lid) with a new one, which was supposed to be compatible with the needs and geometry of the newly tested source of thermal plasma, a microwave plasma torch. In connection with the disassembly of the original lid, it was possible to get into the inner chamber of the reactor to check the condition of the lining and to clean up the chamber from possible impurities.

Accompanying preparations related to the pipe elbow and its modification in the bend area, namely by the creation of an upper opening through which an anti-seize tool was placed for the possibility of cleaning the pipe elbow during operation. Similarly to most construction matters, the modification of the elbow and the manufacture of the anti-seize tool was realized by IPP CAS mechanical engineers and technicians. Connection of cooling water, thermocouples, and other measuring equipment can be also included in the preparations of the reactor. The following subsection *Diagnostic devices* is devoted to this topic.

2.4.1 Diagnostic devices

Continuous measurements of experimental variables and physical quantities are provided by the computing technology of the laboratory. On individual computers, the data is available in real-time in the various user interfaces. Values are gradually stored in data files, which can usually be converted into *.xlsx* files, from which the data can be processed for calculations or possible graphs.

The interface on the first computer is mainly used for monitoring the state of quantities directly related to the (hybrid arc) plasma torch. Most importantly the DC electrical current, voltage, and power, furthermore the flow rates and temperatures of the water or flow rates of argon supplied to the plasma torch. For the energy balance the argon and water mass losses are practically negligible (water consumption to stabilize plasma is about 2 liters per hour). The volume flows are controlled by the system through the relevant buttons. If the pipe hoses are connected appropriately, it is possible to use this interface system to cool even a microwave plasma torch (which can be also monitored, unlike electrical quantities of MWPT).

Quantities that are not relevant for the purposes of the work (for example for the energy balance) are not listed in the following figures or tables (similarly to the rest of the thesis and the appendices). On the contrary, important quantities are shown in the schematic in figure 2.13.

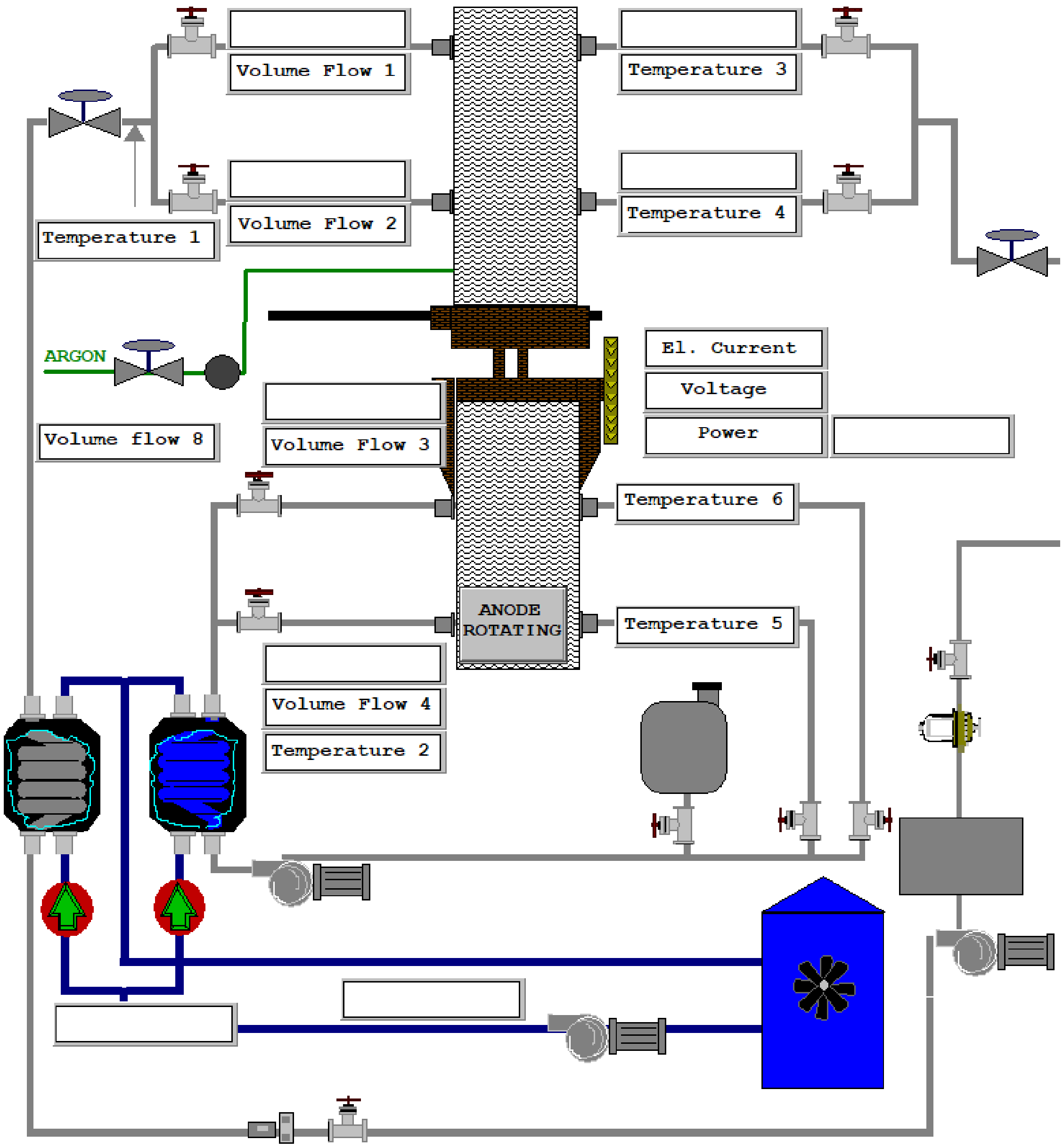

Figure 2.13: Hybrid plasma torch diagnostics interface scheme

Cooling water sub-circuits (on figure 2.13) 3 and 4 are separately divided, but sub-circuits 1 and 2 mix inside the chamber and it is not known exactly how many of the input flows correspond to the output flows. Therefore, the balance of flows 1 and 2 will be performed by summing the flows and averaging the water temperatures at the outlet. For MWPT experiments, all cooling water sub-circuits are separated. The temperature differences are quite similar, so the water properties will be averaged for the mean value of cooling water temperature.

As already mentioned, the current measuring system for the plasma torch is not compatible with the delivered microwave plasma torch from the perspective of electrical quantities monitoring.

However, the microwave plasma torch including the source has its own type of user interface available, which displays any warning, failure, or preparedness of the plasma torch, magnetron, or its filament.

It also displays cells for setting and displaying the required input power and offers the ability to monitor continuous quantities such as the mentioned delivered power or reflected power over time.

Unfortunately, data is not stored in time and only a short time interval is always visible. For this reason, information about input power was written on paper during the experiment. A view of the user interface is shown in figure 2.14.

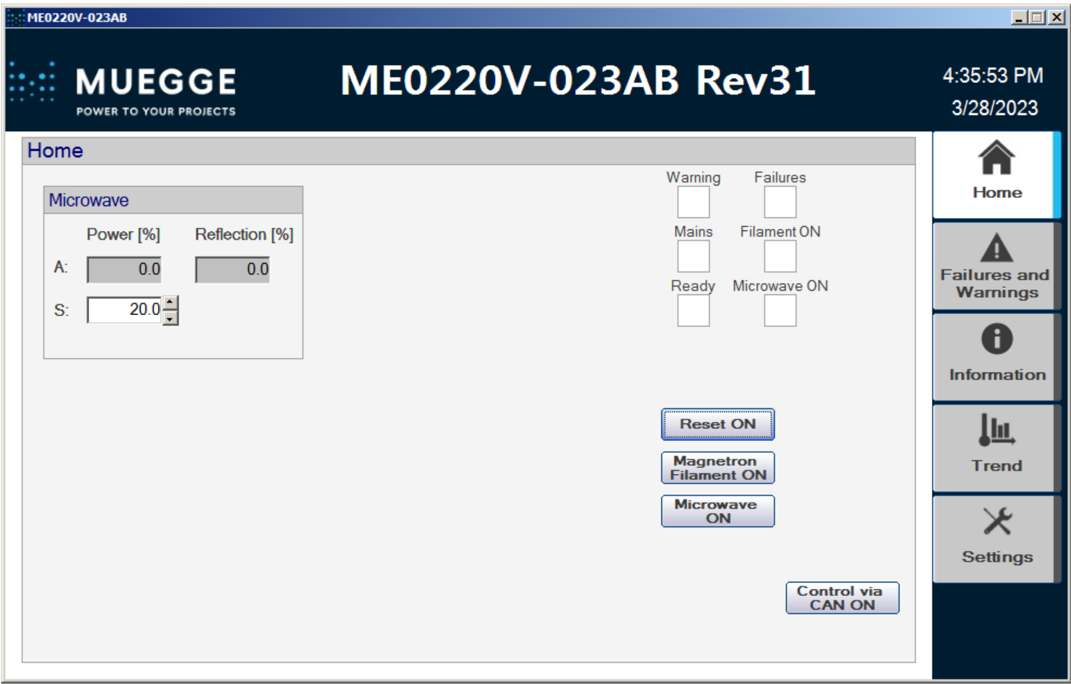

Figure 2.14: Microwave plasma torch user interface

It is clear from figure 2.15, that the value of the supplied power is very stable in the steady state, practically constant, so the simplification to declare the input power as constant is satisfactory.

Unfortunately, the power curve color (yellow) is set in the MWPT user interface by default and cannot be changed, so it is sometimes difficult to recognize.

Although the reflected power shows slight fluctuations, its course is also relatively stable in the steady state (less than 0.5 % deviation over time), as shown in figure 2.16.

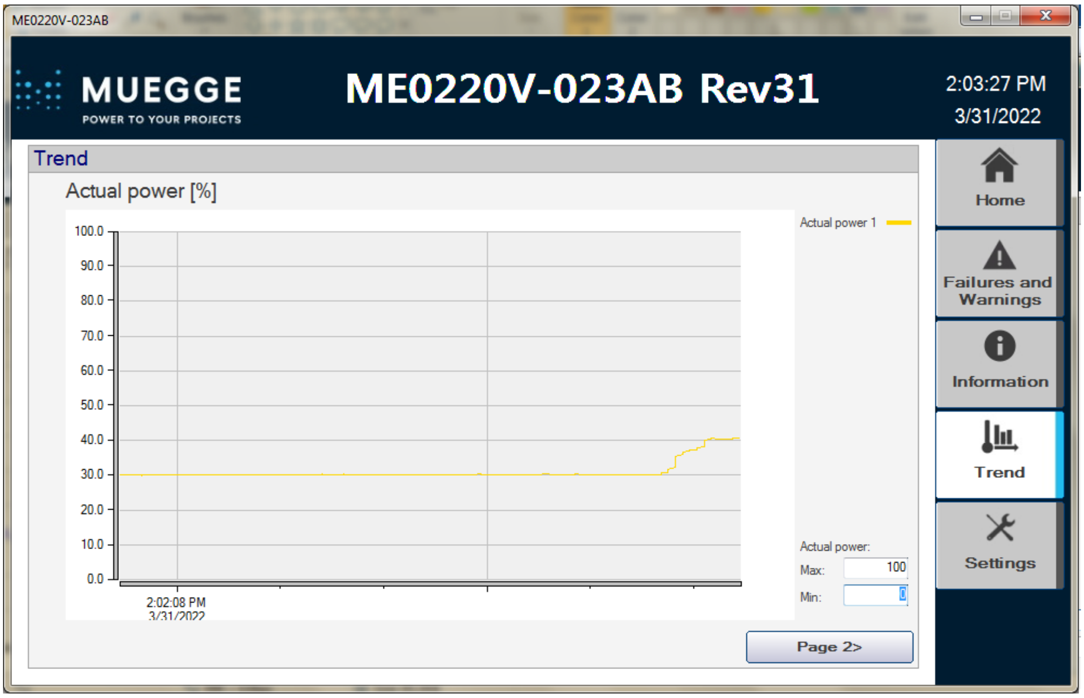

Figure 2.15: Example of microwave plasma torch power

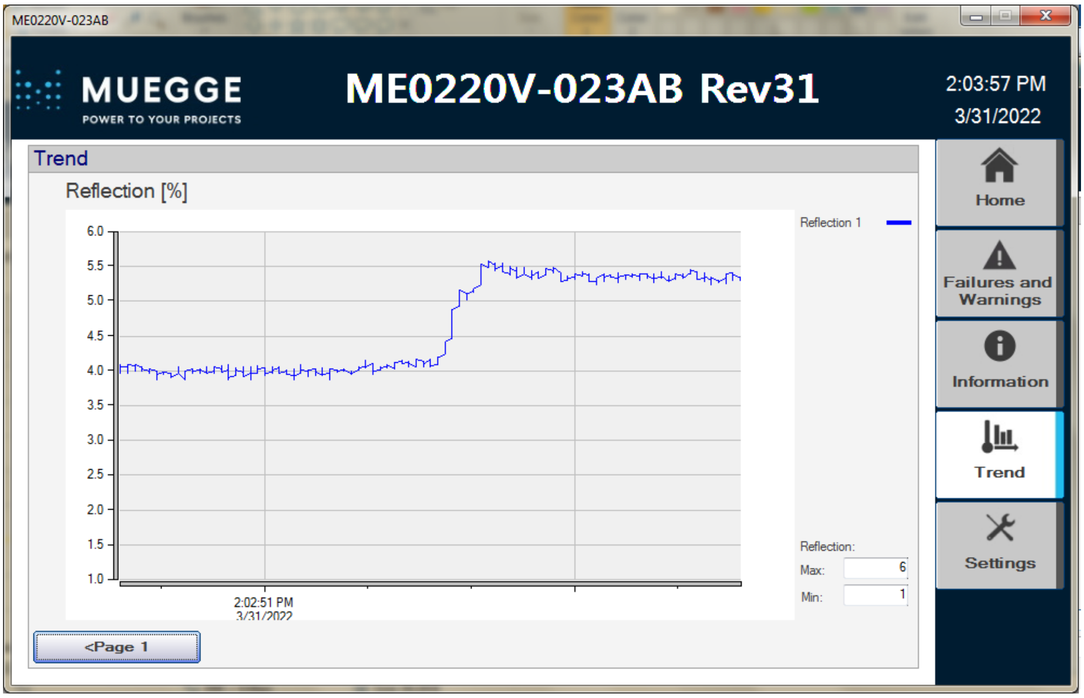

Figure 2.16: Example of microwave reflected power

For the technical use of the MWPT, the geometry of the waveguide needs to be tuned appropriately with the help of a tuner. This has a significant effect on the amount of reflected power and is optimal when it is in the range of 5-10 %, as mentioned in the *Microwave plasma torch* subsection. From the perspective of the reflected power regulation, this is the most sensitive part of the plasma torch burning process. If a certain reflected power limit is exceeded, the torch's safety system shuts down the plasma torch, practically immediately. This is a problem especially when the change is sudden, caused by impurity or some error, for example. This phenomenon caused great problems for the extension of the stabilizing medium (air) by water vapor. In the laboratory conditions at IPP CAS, saturated water steam from a Certuss steam boiler is used. Therefore, liquid droplets of water appear at the outlet of the steam pipe nozzle, which probably results in the sudden extinguishing of the plasma torch. In the nearest future, testing and tuning the MWPT for precise operation with water steam (outside the reactor) is planned. Water droplets will be removed by appropriate reheating and throttling regulation. The reason to continue research with water vapor as a stabilization medium is its very positive effect on the final composition of the synthesis gas, namely the substantial yield increase of hydrogen. For more see chapter *Experimental results*.

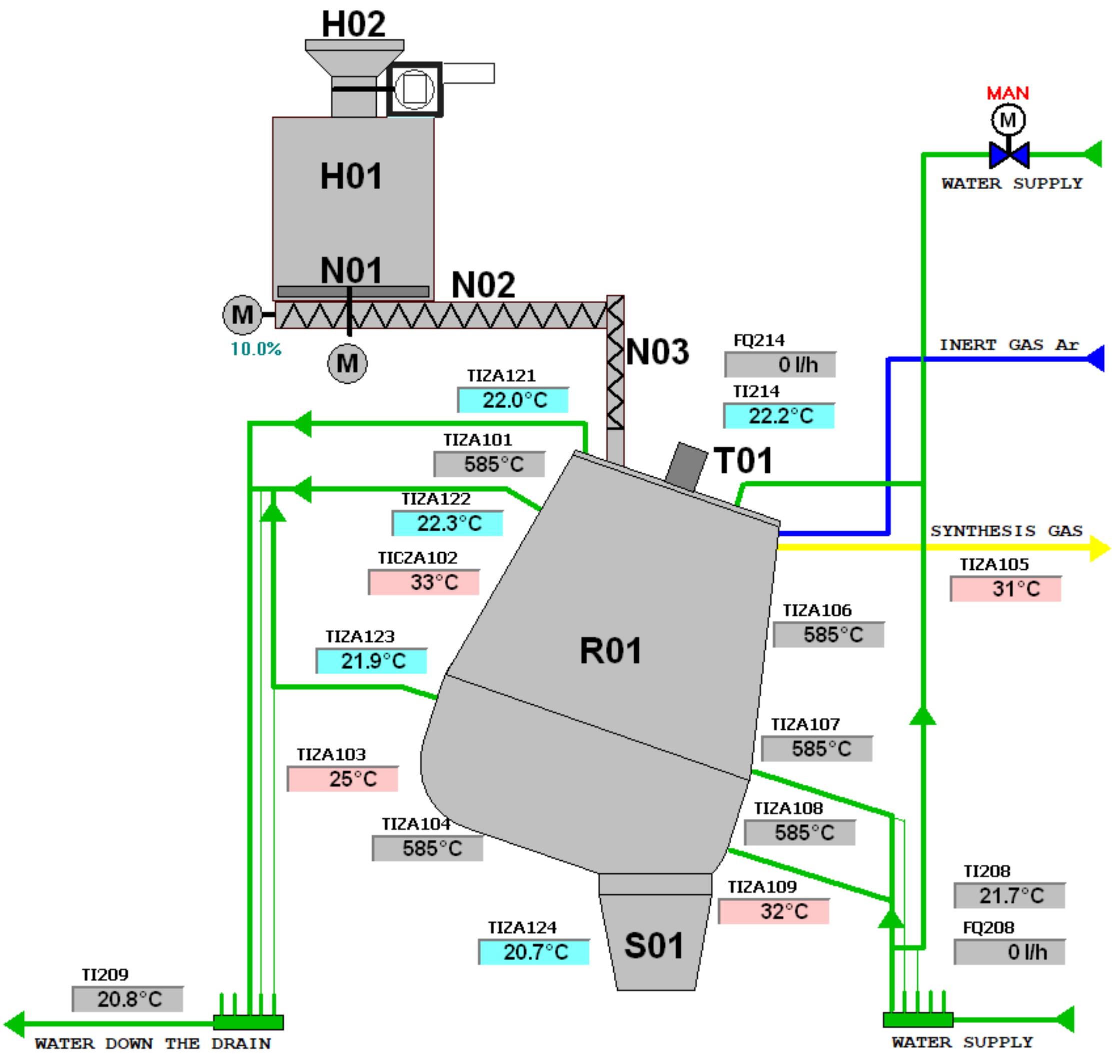

Figure 2.17: Reactor diagnostics interface scheme

Another part of the interface (shown in figure 2.17), located on another of the laboratory's computers consists of several parts, generally related to the reactor itself. The first one is mainly used to monitor temperatures in the reactor (thermocouples fit closely into the inner chamber) and the total volume flow rates of water and water temperatures. In this part of the interface, the rotation velocity of the screw feeder can be set (and monitored) and the corresponding motors can be switched on or off. Two main motors that are directly operated during operation are the screw feeder motor and the vault disruptor motor. The purpose of the vault disruptor is to mix the material in the hopper to ensure its delivery into the screw feeder pipe. The issue with the vault disruptor is that the material in the hopper sometimes tends to overload the vault disruptor, causing it to jam, overload and shut down. After this event, it is necessary to change the polarity of the motor rotation, which usually solves the problem.

The second important part of the reactor monitoring interface is only a more detailed view of partial cooling water circuits, including specific temperatures and flow rates (see figure 2.18). This part is important mainly for checking if there is no failure or overheating in any of the cooling sub-circuits. It can also be used for a more detailed calculation of the energy taken away by the cooling water in the form of heat, but the calculation would have to be much more precise, ideally performed by a simulation model. For energy balance purposes, the heat in cooling water will be calculated simply from data on the input and total output water (the circuit is made in such a way that the input water branches into sub-circuits and connects again after exiting the reactor). This may result even in a better estimate because the water combined from individual sub-circuits is well mixed, therefore the temperature measurement may be more accurate. The graphs, visible in the remaining part of the reactor interface, are part of the *Experimental results* chapter.

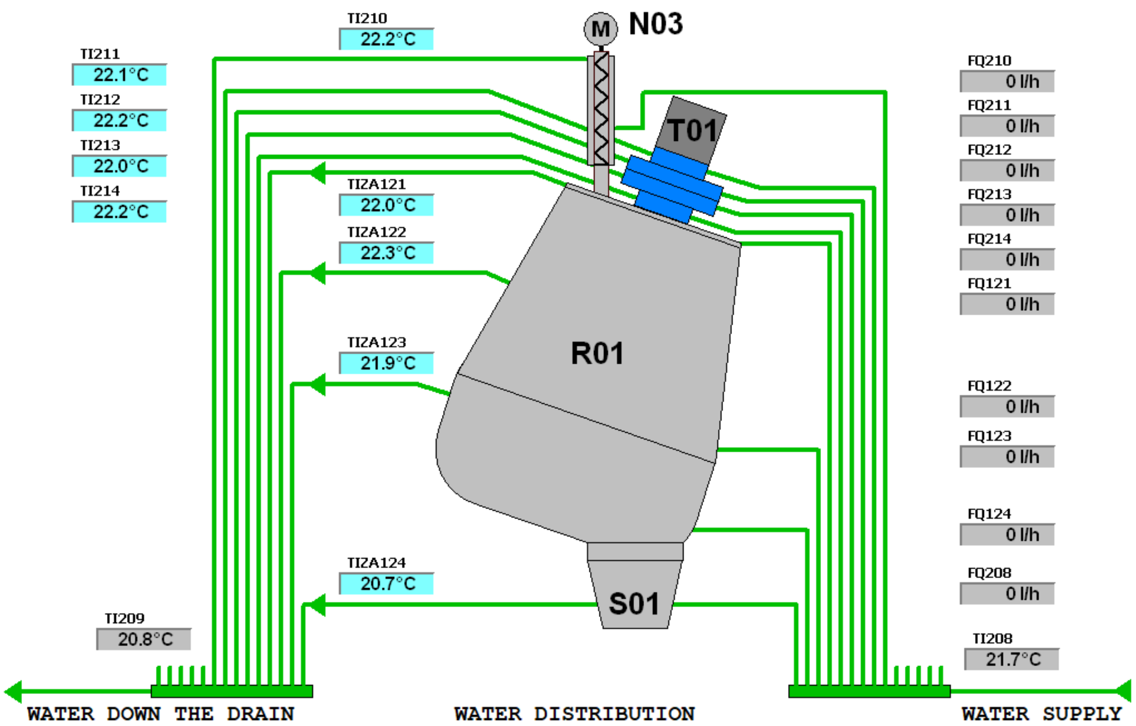

Figure 2.18: Reactor cooling interface scheme

The interface on the last important computer for the monitoring is the Data taker system, which measures other types of values and quantities, for example, inlet gas flows. It is always dependent, on how the flowmeters are connected to the distributions. It is necessary to note before the experiment which inputs correspond to the sub-columns of the data. Data can be extracted by selecting the day and time interval of the desired values after logging in to the individual address corresponding to the Data taker. The interface does not include any technological diagram, so it is not attached.

2.4.2 Preheating

As mentioned in the subsection *Technology description*, before performing the experiment at operating temperatures higher than 1000 °C, the reactor needs to be heated to at least 70 % of this temperature.

Preheating is started the day before the planned experiment and provided by a heating element inserted and sealed into the reactor. The heating element has a power in the range of 13-17 kW, usually at a supply voltage of 40-45 V and currents of around 300-400 A.

The heating parameters are slightly different each time. Considering the 24-hour preheating at an average power value of 15 kW, this is a consumption of 360 kWh even before the experiment itself. Since the energy balances of the process under different operating conditions will be assessed, energy consumed for preheating will not be taken into account. For commercial or industrial operations, the objective would be to maximize the use of the reactor over time, therefore to minimize the states when the reactor is not heated up, so the energy (and associated costs) of preheating would be less significant.

Keeping the reactor at high temperatures during potential operation is also desirable from the perspective of service life because the materials are primarily stressed by large temperature changes, not by high temperatures themselves.

Of course, the final discussion about the energy balances should acknowledge the temperature differences, especially for:

- the end of preheating & start of experiment or
- the end of the experiment (respectively the difference between the temperatures in the reactor at the beginning and the end of the experiment).

After replacing the heating element with the plasma torch, the reactor is still heated up by the plasma torch itself by more hundreds of °C. The start of the experimental process, however, is determined by the beginning of the feeding of input materials (not by a specific value of internal temperatures). Therefore, in the *Energy balances* section, the total energy supplied to the plasma torch will not be taken into account. Similarly, as electrical energy, all energy flows will be evaluated only during the considered experimental time interval.

Chapter 3

Experimental results

This extensive chapter is focused on the results of selected experimental processes carried out at the PCHT Department at the IPP CAS. At the beginning of the chapter, the selected experiments will be described, including a brief timeline diagram illustrating the key events of the experimental process.

A summary of graphical data representations of important measured quantities essential for the energy or material balance of the process follows. Some of the figures are accompanied by a short relevant commentary. Most quantities will appear similarly for all types of experiments. Tables of synthesis gas composition are also attached for individual time intervals, for which the chemical analyses were made. These intervals are also visible in figures 3.1, 3.2 and 3.3.

Subsequently, experimentally obtained data are processed in detail, specifically in the form of creating energy balances for individual processes. Unfortunately, during the calculations and creation of the energy balance models, it became clear that much of the input information and data were missing to create the balances (because it was not measured or could not be measured). For this reason, some of the input and output elements of the balance had to be estimated, which may result in more calculation errors.

Some of the elements of the energy balance are not crucial to the characterization of an individual process, so imprecise determination is not a great issue. Examples are heat-related quantities like losses Q_{loss} (by convection and radiation) or accumulated heat in the reactor Q_{accum} (for more see below).

On the contrary, other elements of the energy balance (for example input materials, output synthesis gas, or carbon black) are key for assessing the process. Because it is impossible to continuously measure some of the actual mass flows, the estimates regarding the material balance are only indicative, especially for the solid components of the process. Errors in the material balance will also adversely affect the resulting energy balance.

The topic of energy balance in this chapter is divided into 2 parts. The first part is theoretical, where calculations and thought procedures for creating energy balance models are declared and described. The second part summarizes the results obtained from energy balance models, which are part of the appendices of this thesis.

At the end of the chapter, the results of the balance models are discussed, especially considering the complications, inaccuracies, and discrepancies. The individual approaches are mostly compared in terms of the input material used or the plasma torch used.

3.1 Brief summary of experiments

For analysis purposes, experimental data from 3 experiments will be processed, differing in either the processed material or the plasma torch used. Namely, the combinations are as follows:

Number of experiment	Processed material	Used plasma torch
1.	SMW	HPT
2.	RDF	HPT
3.	RDF	MWPT

Table 3.1: Summary of experiments

The experiments with HPT are usually planned to be divided into 4 parts with different operating conditions. These conditions are mainly related to the inlet volumetric flow rate of carbon dioxide as an oxidizing agent (and the plasma torch power). In the beginning, the supply of carbon dioxide was supposed to be 110 % of the stoichiometric amount, followed by 80 %, 60 %, and finally 0 % (no carbon dioxide). The amount of input components (including gases) affects the requirements for input power. The decrease in carbon dioxide supply lowers the amount of energy needed for thermochemical reactions, therefore the input power of the plasma torch is reduced accordingly.

For the experiment with MWPT, the main objective was to test its functionality, including the configuration. The accompanying goal was to try to reach the gasification of the material (not combustion), to find out the required conditions for this process with the MWPT, and eventually compare it with the HPT. The various operating stoichiometric conditions in the HPT experiments, based on which the chemical analyses were performed, are summarized in Tables 3.2 and 3.3.

Part of experiment	1.	2.	3.	4.
Fuel ($kg \cdot h^{-1}$)	8	8	8	8
CO_2 (slm)	164	54	22	0
P_{elPT} (kW)	141	120	109	102
H_2O from PT ($g \cdot min^{-1}$)	27	27	27	27
Total Ar (slm)	135	135	135	135

Table 3.2: Presumed operating conditions of the SMW & HPT experiment

Part of experiment	**1.**	**2.**	**3.**	**4.**
Fuel ($kg \cdot h^{-1}$)	10	10	10	10
CO_2 (slm)	173	62	26	0
P_{elPT} (kW)	130	108	96	87
H_2O from PT ($g \cdot min^{-1}$)	27	27	27	27
Total Ar (slm)	55	55	55	55

Table 3.3: Presumed operating conditions of the RDF & HPT experiment

The water consumption of the plasma torch for the purpose of plasma jet stabilization is less than 2 liters per hour (as seen in the tables above). Therefore, this water loss will be neglected for the purposes of the material and energy balance.

The timelines of the experiments are illustrated by figures 3.1, 3.2, and 3.3. From these timelines, it is clear that the most smooth operation was for the first experiment with HPT and SMW. On the other hand, the most complications occurred during the experiment with MWPT. Related to these complications it is much more challenging to create a sufficient energy (and material) balance model. It is also evident from the timelines that sometimes the operating conditions did not directly correspond to the initial assumptions. However, this should not be a major problem, especially for the numerical evaluation of the given processes.

In the first experiment, the intervals of chemical analyzes are long enough (because a steady state was easily attainable) and the feeding of the material was consistent and continuous throughout the experiment.

In the second experiment, a decrease in the argon supply occurred shortly after the 3 p.m. It was necessary to pause the process and replace the pressure bomb with argon. It is noticeable that chemical analyses were performed for much shorter time intervals than in the previous case, which greatly complicates the situation. The processes inside the reactor have a certain inertia (for instance the residence time of the substances in the reactor). Therefore, the shorter the assessed interval from the energy balance perspective, the bigger computational errors can be made. For both experiments with RDF it is also difficult to achieve a steady state because the material is highly inhomogeneous (since the sample is made from real waste).

The last of the described experiments was very complicated throughout the whole experimental process. The material was constantly clogging up the pipe elbow and therefore it constantly needed to be removed. Simultaneously, the screw feeder was often switched off or operated at different speeds, so estimation of the real amount of material fed is the most complicated for this case. Chemical analyses, in this case, seem long enough, but usually in time intervals that can hardly be considered steady states. The formation of synthesis gas even during the nearly half-hour shutdown of the screw feeder proves the very long inertia of the thermochemical processes. Furthermore, complications with the gas calibration occasionally appeared, which could have been caused by large volume flows of the microwave stabilization medium.

3.1.1 Timelines

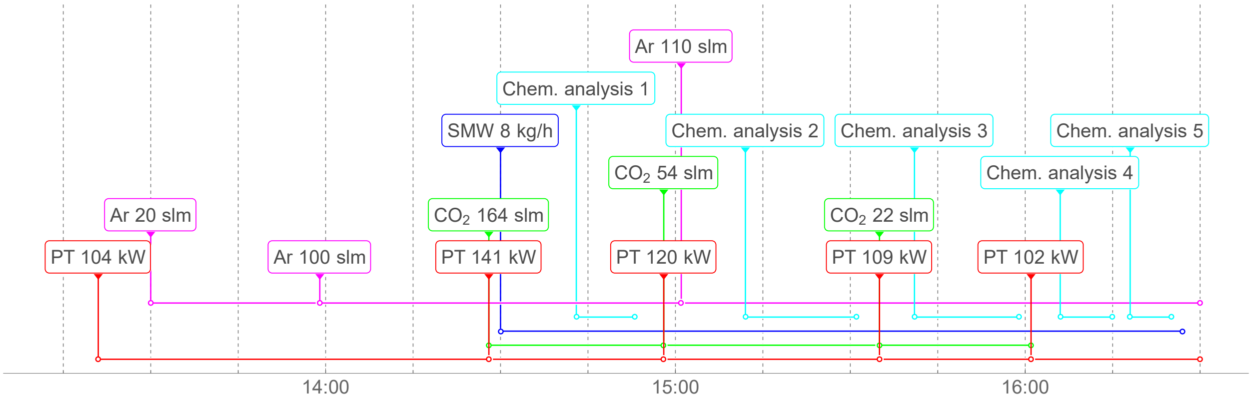

Figure 3.1: Summary of experiment with SMW & HPT

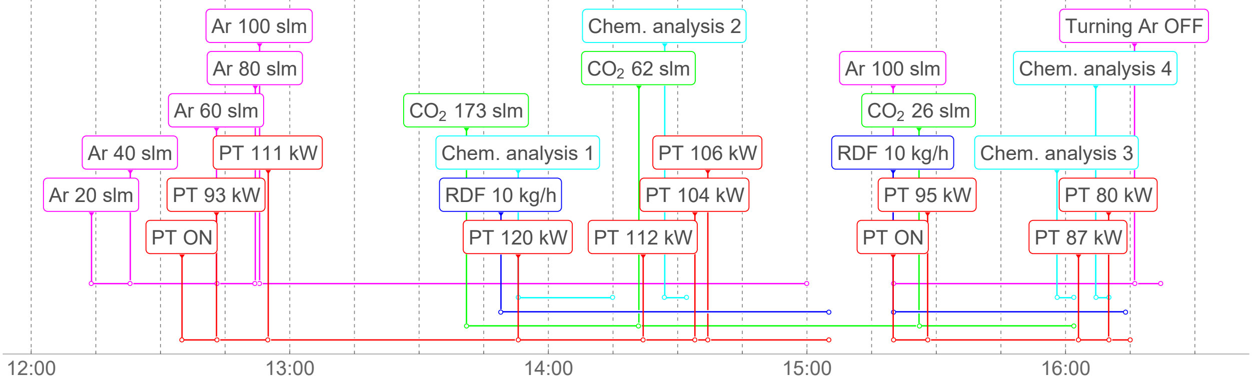

Figure 3.2: Summary of experiment with RDF & HPT

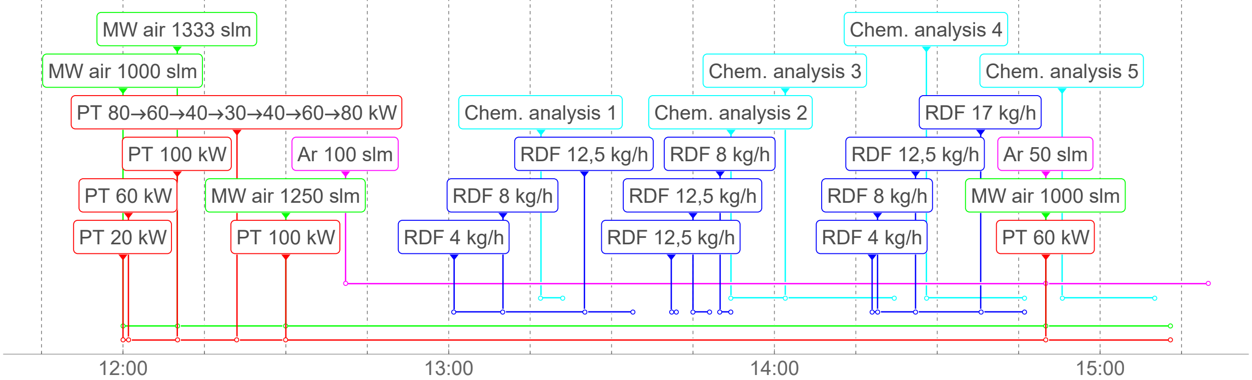

Figure 3.3: Summary of experiment with RDF & MWPT

Individual time intervals of chemical analyses shown in figures 3.1, 3.2 and 3.3 correspond to columns in the synthesis gas composition tables 3.4, 3.5 and 3.6.

3.2 Measured data

3.2.1 SMW & HPT

3.2.1.1 Electrical quantities

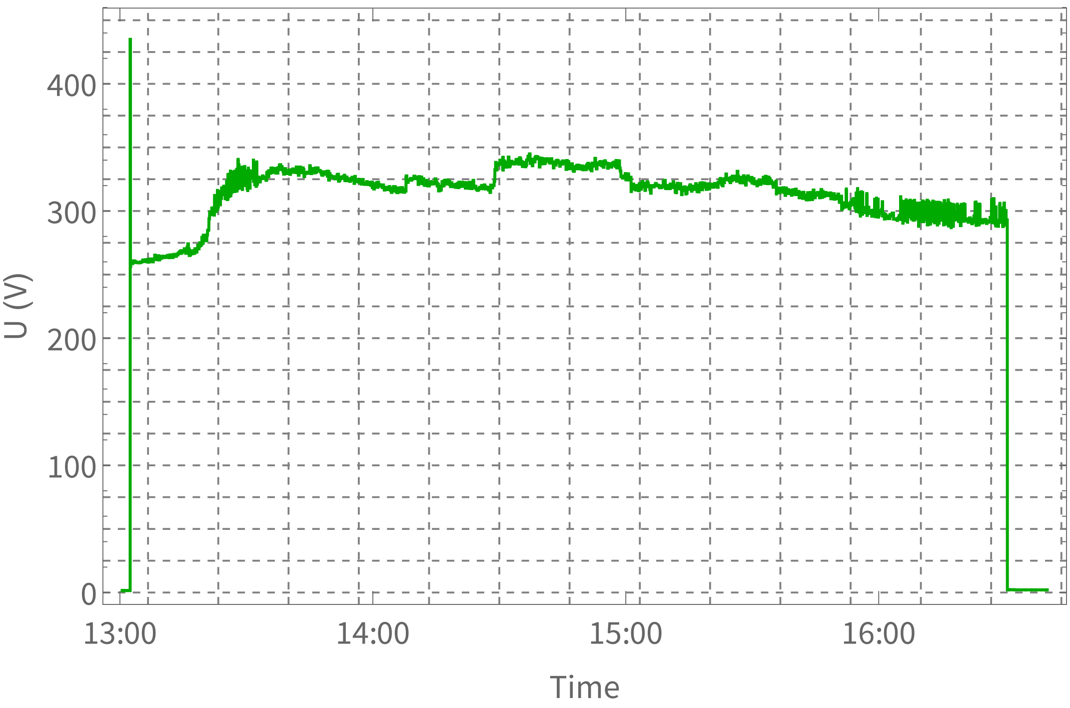

Figure 3.4: Voltage of the hybrid plasma torch

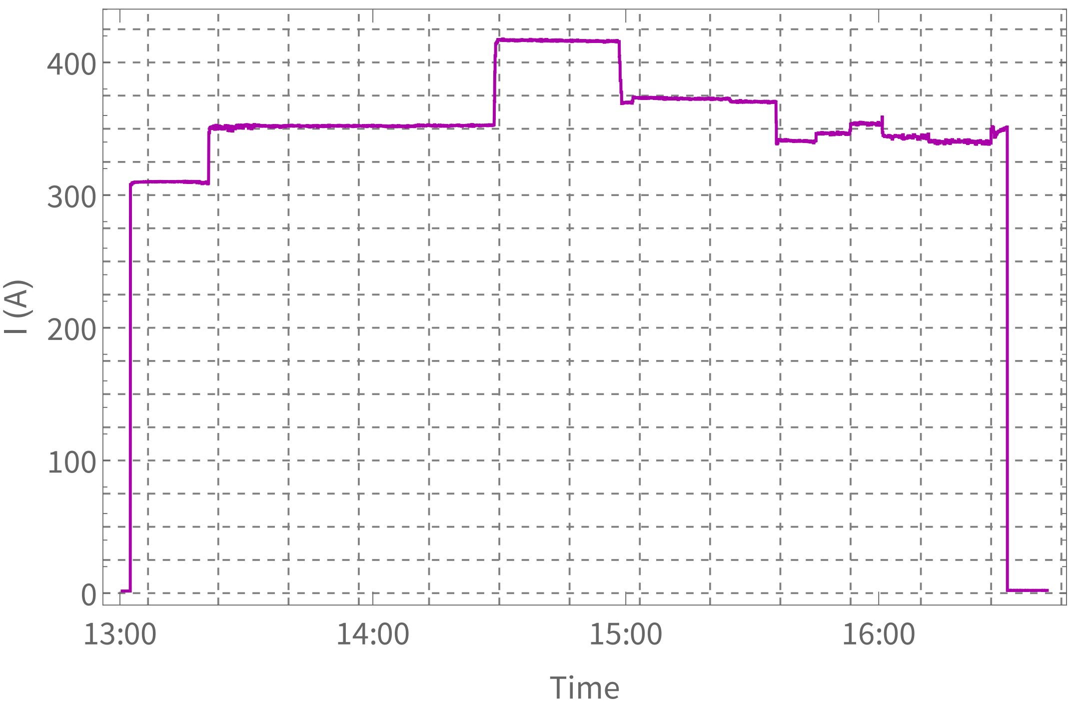

Figure 3.5: Electrical current of the hybrid plasma torch

Most of the electrical quantities time relations usually look very similar. The voltage curve of the HPT has a distinctive voltage peak, which is needed for the electrical breakthrough of the stabilization medium and the subsequent generation of the plasma jet. It is noticeable that the PT voltage fluctuates a little more than the current, which may be caused by the fouling of the burner with conductive carbon particles inside the reactor. At a steady state, the output power value is usually close to the mean power value for the monitored period. Electrical quantities are visible on the figures 3.4, 3.5 and 3.6.

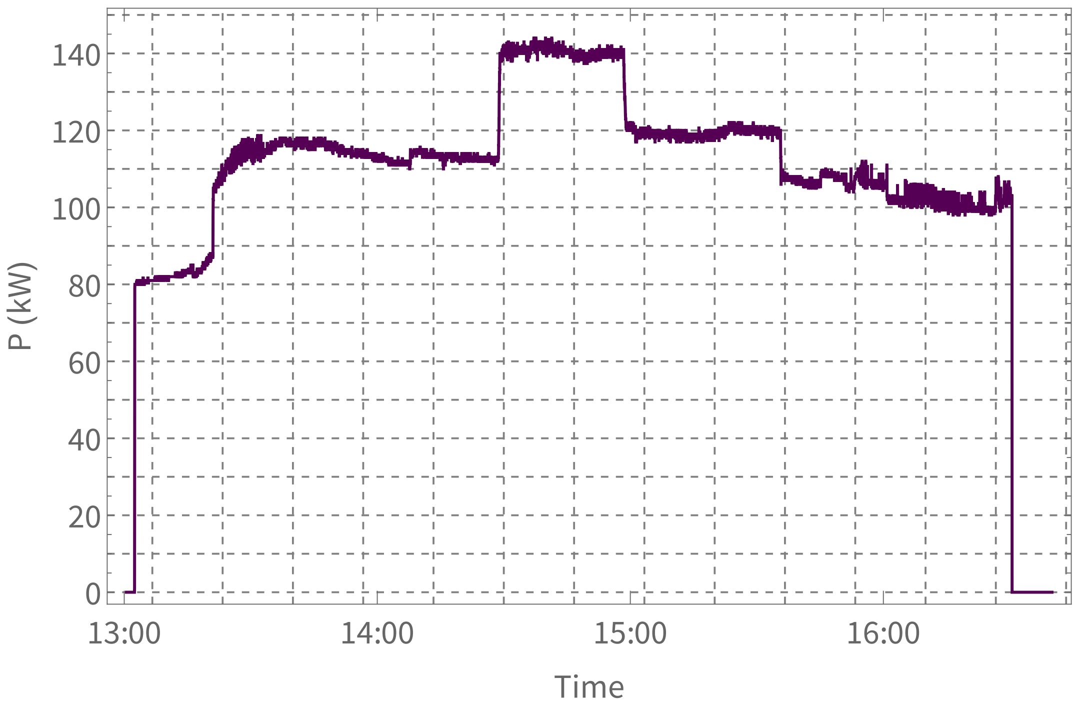

Figure 3.6: Power of the hybrid plasma torch

3.2.1.2 Temperatures in reactor

From the graph of temperatures inside the reactor in figure 3.7, the connection with the previous graphs can be clearly observed. After the plasma torch ignition, the reactor heats up to working temperatures of around 1400 °C.

The subsequent decrease in temperatures detects the start of the feeding of the processed material. In the temperature graphs, the curves belonging to individual thermocouples are marked by a number. The location of the thermocouples can be seen in figure 1.15. It is also visible that when the plasma torch is turned off, the temperatures drop exponentially.

The fluctuation in the temperature graph this time represents the unevenness of the process of the input material decomposition. During operation, the actual state of material feeding can be determined using the trend of temperatures. For example, if the temperatures start to rise rapidly, it means that the material has become blocked before the reactor in the T-junction or pipe elbow.

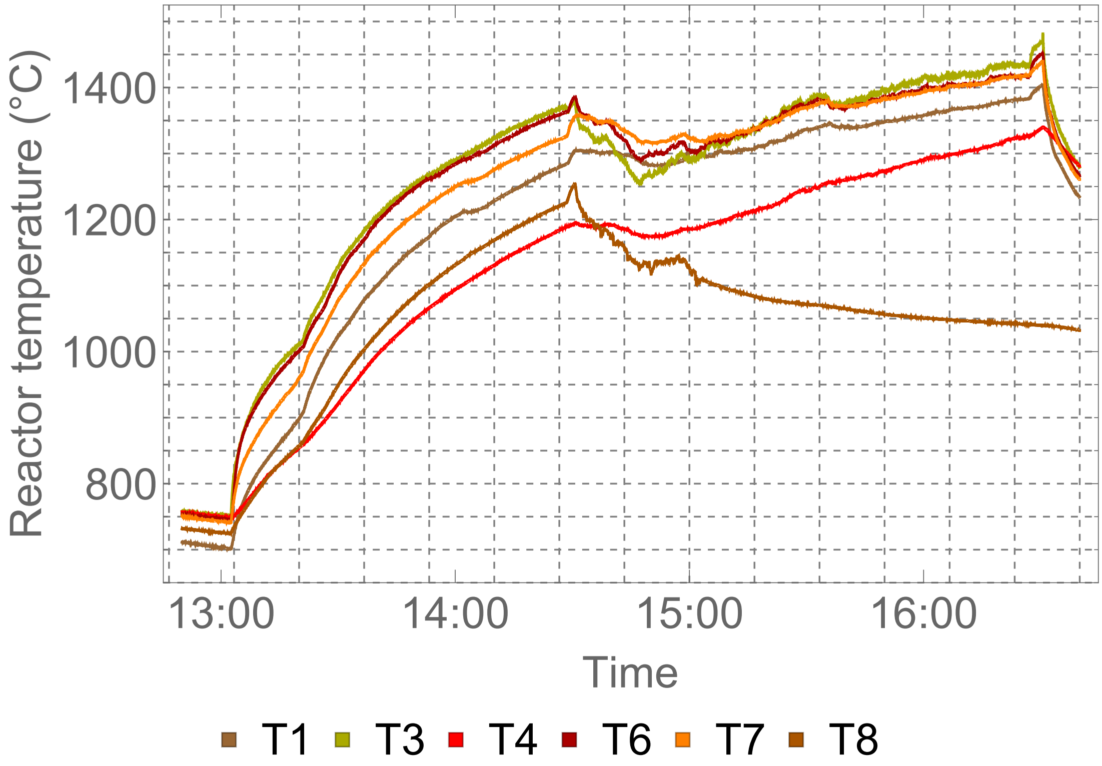

Figure 3.7: Temperatures measured inside the plasma reactor

3.2.1.3 Cooling water

Cooling water graphs are divided into 2 parts, reactor cooling water and plasma torch cooling water. It is evident that while the plasma torch is cooled by roughly constant water flow rates, the course of water temperatures is periodic. This corresponds to the periodic operation of the cooling unit.

In the case of the reactor, on the other hand, the cooling power gradually increases together with the volume flow of water, which correlates with the temperatures inside the reactor. (Unlike the PT, the reactor is cooled even before the experiment during the entire preheating process.)

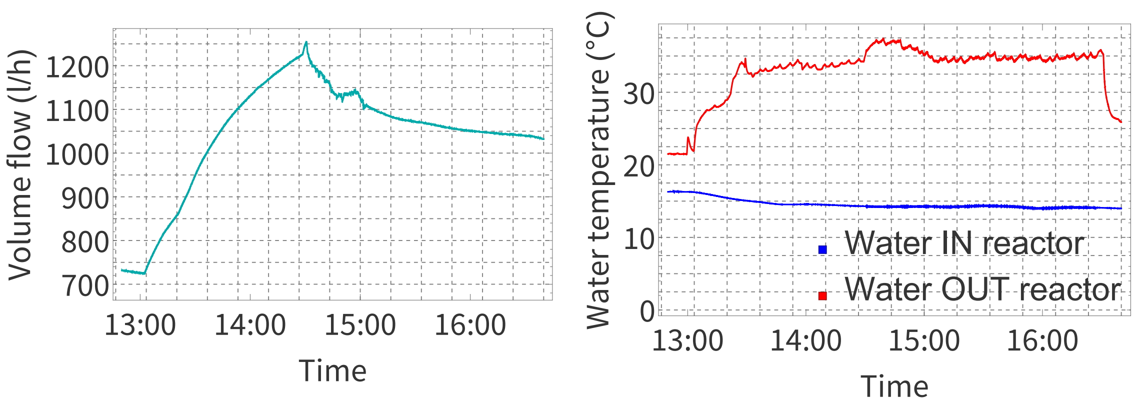

(a) Volume flow

(b) Temperatures

Figure 3.8: Cooling water into reactor

The temperature differences between the outlet and the inlet water remain quite similar throughout the overall experiment. The fluctuation of outlet water temperatures is most likely caused by the mixing of the water from all cooling circuits of the reactor into a common flow.

As already mentioned, the temperature values of the outlet cooling water of the first sub-circuit will be averaged and the flow rates summed up for the HPT case. These circuits are not separated and water from both inputs gets mixed inside. All cooling water volume flows and temperatures during the first experiment are in figures 3.8 and 3.9.

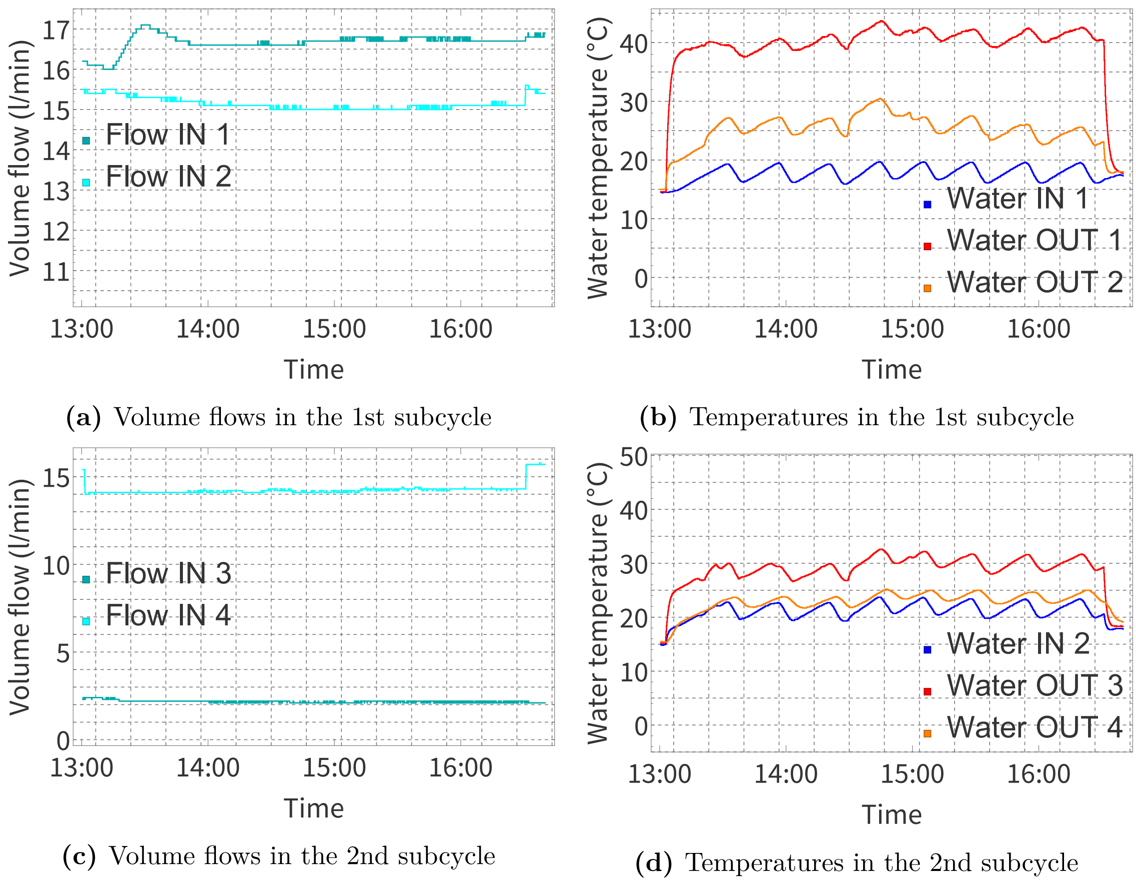

(a) Volume flows in the 1st subcycle

(b) Temperatures in the 1st subcycle

(c) Volume flows in the 2nd subcycle

(d) Temperatures in the 2nd subcycle

Figure 3.9: Cooling and stabilizing water into plasma torch

3.2.1.4 Input gases

In the case of experiments with HPT, the input gases are usually carbon dioxide (as an oxidizing agent) and calibration inert argon. It can be seen that argon is supplied even after the end of the experiment, namely for safety reasons, since extreme temperatures are still present in the reactor and synthesis gas can constantly be formed.

Figure 3.10 describes the supply of the input gases into the reactor in standard liters per minute. The measured negative value of carbon dioxide around 2:20 p.m. is most likely an error caused by handling or a sudden pressure difference.

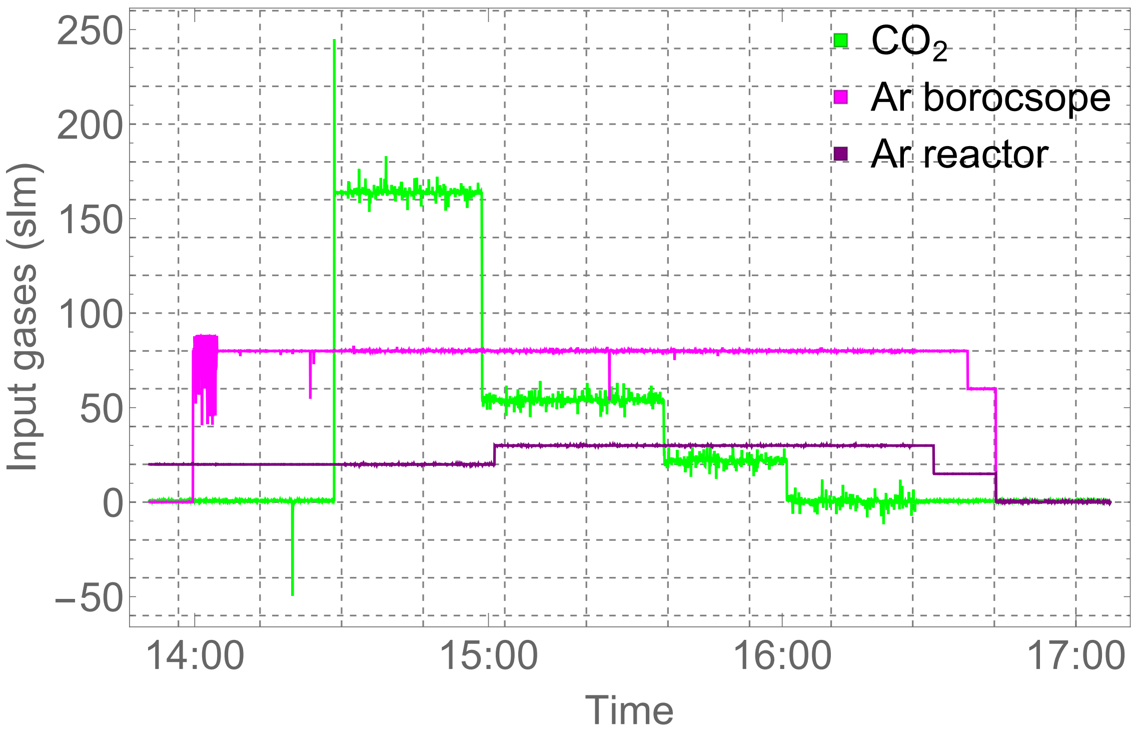

Figure 3.10: Input gases

3.2.1.5 Synthesis gas

The composition of the synthesis gas is determined as a uniform for the sub-evaluated time intervals, namely as the arithmetic mean of the measured values of the percentage representation for the given interval. For HPT experiments, the most significant output components will be hydrogen, carbon monoxide, and inert argon, as shown in table 3.4.

A smaller amount of carbon dioxide may appear in the output mixture as a leftover from the input carbon dioxide, as there was not enough energy in the reactor to process the whole amount supplied. This is expected especially from the beginning of the experiment because the supply of carbon dioxide is slightly over stoichiometric. Trace amounts of methane or oxygen may appear in the output mixture. Other trace elements reach even lower concentrations or are not recorded.

CHA	**1.**	**2.**	**3.**	**4.**	**5.**
H_2 (%)	32.77	33.99	33.55	35.18	32.76
CH_4 (%)	0.66	0.71	0.40	0.26	0.17
CO (%)	45.11	34.88	30.54	26.85	24.60
O_2 (%)	0.00	0.00	0.00	0.00	0.00
CO_2 (%)	6.05	3.59	2.37	0.85	1.01
Ar (%)	15.42	26.83	33.13	36.87	41.46

Table 3.4: Composition of synthesis gas

It is visible that the decrease in the carbon dioxide supply to the reactor for the duration of the experiment is reflected in the reduction of the yield of carbon monoxide in the output mixture. The gradual relative increase of the amount of output argon during its constant supply into the reactor can be interpreted as a decrease in the total synthesis gas yield (meant as energetically or materially usable gas). A lower amount of substances at the output is expected because of the lower amount of substances at the input (decrease in the supply of carbon dioxide). Although the concentration of hydrogen is similar for all parts of the experiment, its yield increases relative to the carbon monoxide compound.

One of the output forms of synthesis gas energy carried out of the process is the energy in the form of heat stored in the specific heat capacity of the gas mixture. Gas parameters, including temperature, are usually measured already in the flue gas pipe behind the reactor, where the synthesis gas still has a very high temperature, similar to the operating temperatures measured inside the reactor. Figure 3.11 shows the significant influence of the quenching tower, where the gas is rapidly cooled. After cooling, accompanying thermochemical reactions no longer occur in the gas, and the composition of the gas remains preserved.

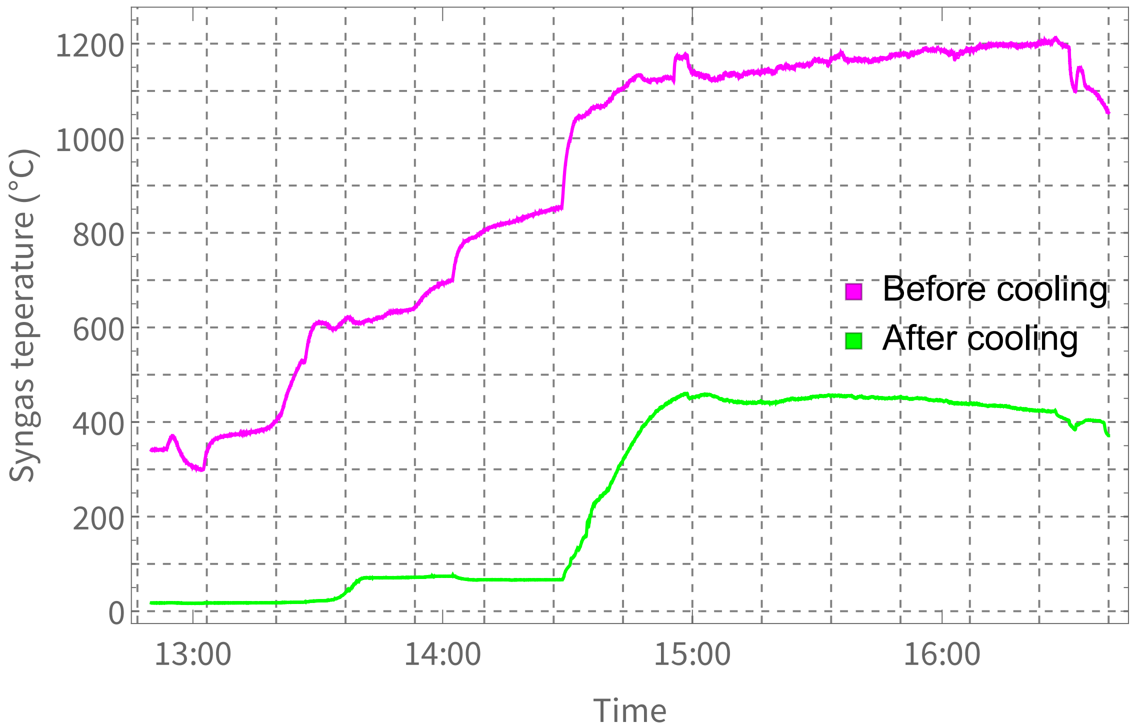

Figure 3.11: Temperatures of the synthesis gas on the output

3.2.2 RDF & HPT

3.2.2.1 Electrical quantities

Distinctively, the electrical parameters in this experiment are very similar to the previous one, because the same plasma torch was used. The main difference is the small pause, where the plasma torch was turned off during the experiment. This was caused by the need to replace the pressure bombs with argon inlet gas.

Another potential difference is that the electrical quantities, including the power, are in better rectangular shape and generally have slightly smaller fluctuations. Electrical parameters time relations from the experiment with RDF & HPT can be seen in figures 3.12, 3.13 and 3.14.

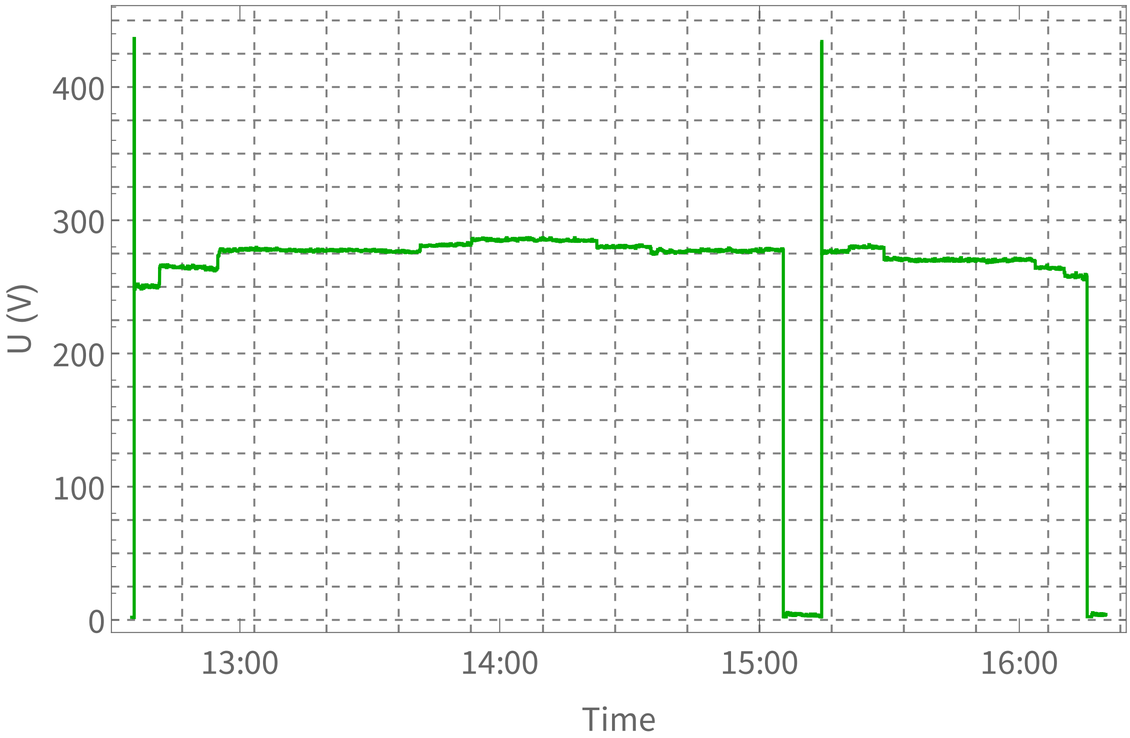

Figure 3.12: Voltage of the hybrid plasma torch

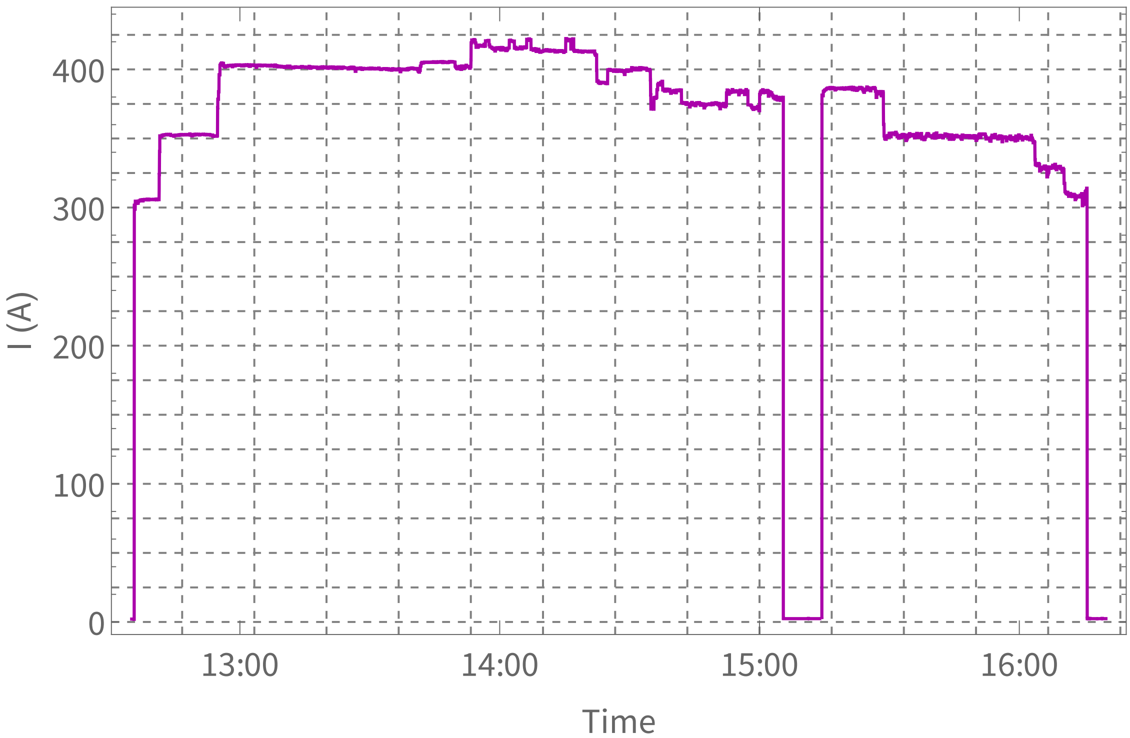

Figure 3.13: Electrical current of the hybrid plasma torch

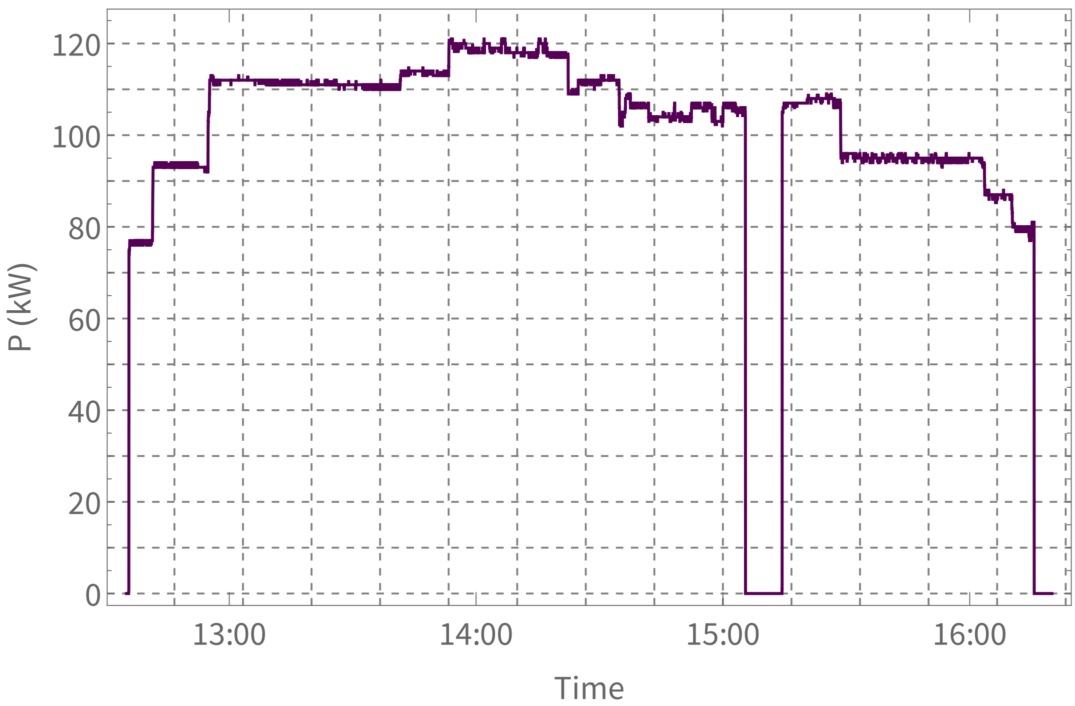

Figure 3.14: Power of the hybrid plasma torch

3.2.2.2 Temperatures in reactor

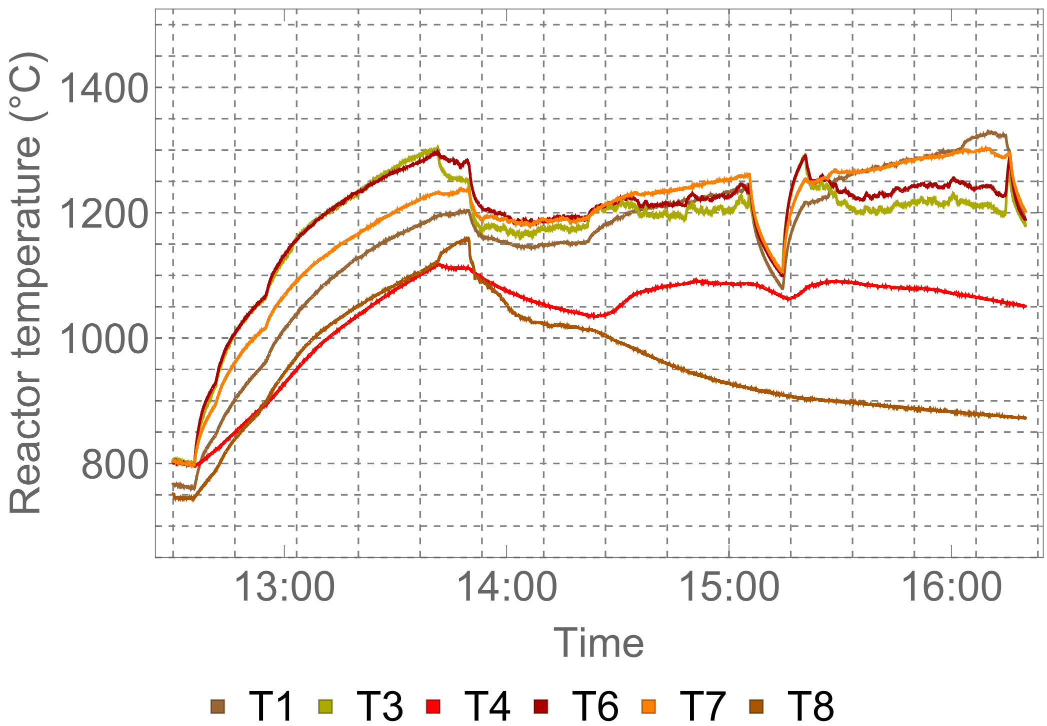

Figure 3.15: Temperatures measured inside the plasma reactor

From the graphs in figure 3.15 of the measured temperatures in the reactor during the experiment with HPT and RDF, it is visible that after the start of the material feeding into the reaction chamber, the temperatures practically do not reach the values before the start of the material feeding. This phenomenon can be caused by several factors.

First, the lower temperatures may be a consequence of the lower operating power of the plasma torch. However, it is conspicuous from the graphs of powers (or the timelines of the experiments) that (with a short exception) the powers are similar, namely between 100-120 kW for most of the duration of both experiments. In addition, during the first experiment, high-temperature increases occur only after 3 p.m., outside the interval when the plasma torch power was around 140 kW.

A reasonable explanation could be the fact that processing RDF requires more energy (heat) than processing SMW. The heat spent on thermochemical reactions can be expressed from the resulting balances by the difference between the internal energies of materials and substances at the output and the input. This idea can be confirmed or refuted by the results of energy balances.

The constant decrease in temperature at the bottom of the reaction chamber (measured by T8) can be caused by a build-up of material that keeps absorbing heat to form synthesis gas.

3.2.2.3 Cooling water

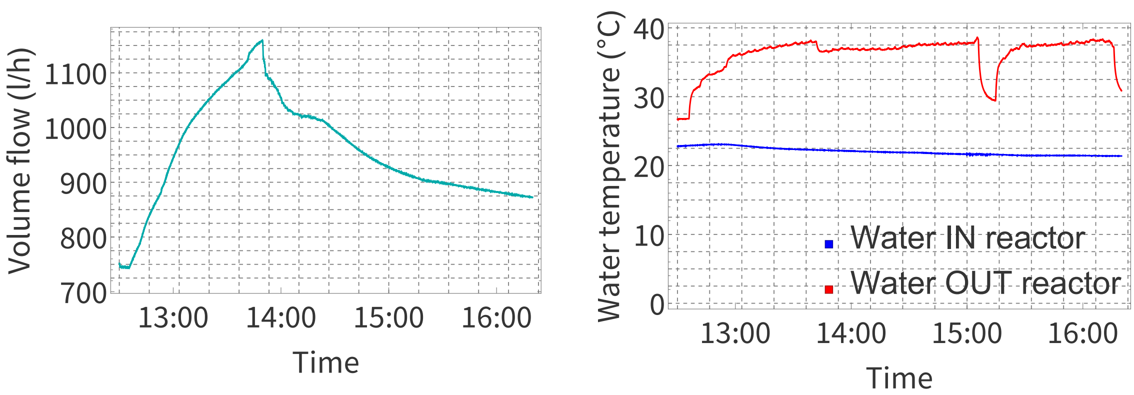

(a) Volume flow

(b) Temperatures

Figure 3.16: Cooling water into reactor

The trends of temperatures and volume flows of cooling water (in figures 3.16 and 3.17) in the second experiment are more or less similar to the trends in the first experiment. Here, once again, the pause of the operating process due to the exchange of pressure bombs with argon is visible.

The volume flow rates of water in the second sub-circuit of the plasma torch are roughly half compared to the first experiment, but the difference in water temperatures at the inlet and outlet is significantly higher. It is therefore not possible yet to say with certainty whether the cooling power of the plasma torch will be higher or lower. Considering the same characteristics of the torch and the nature of the process, however, it is expected to be roughly similar.

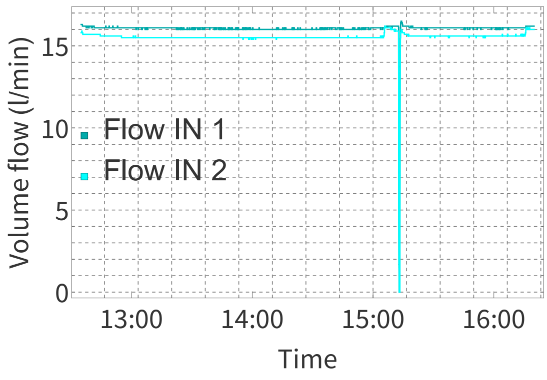

(a) Volume flows in the 1st subcycle

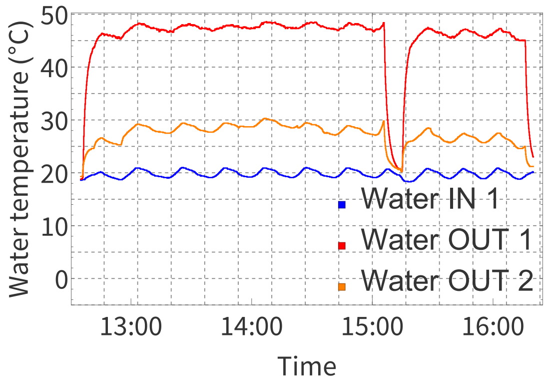

(b) Temperatures in the 1st subcycle

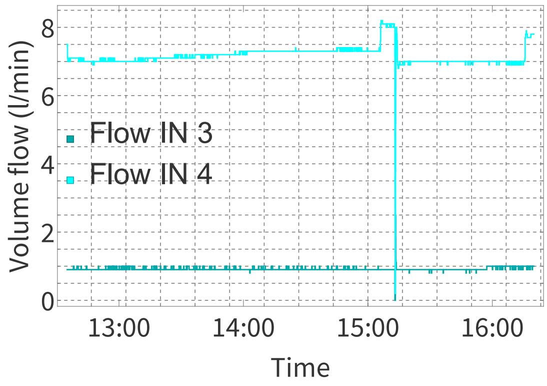

(c) Volume flows in the 2nd subcycle

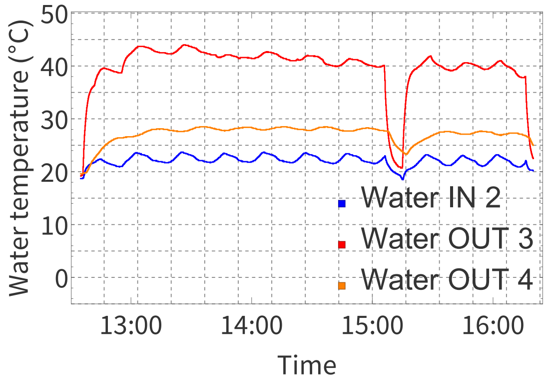

(d) Temperatures in the 2nd subcycle

Figure 3.17: Cooling and stabilizing water into plasma torch

3.2.2.4 Input gases

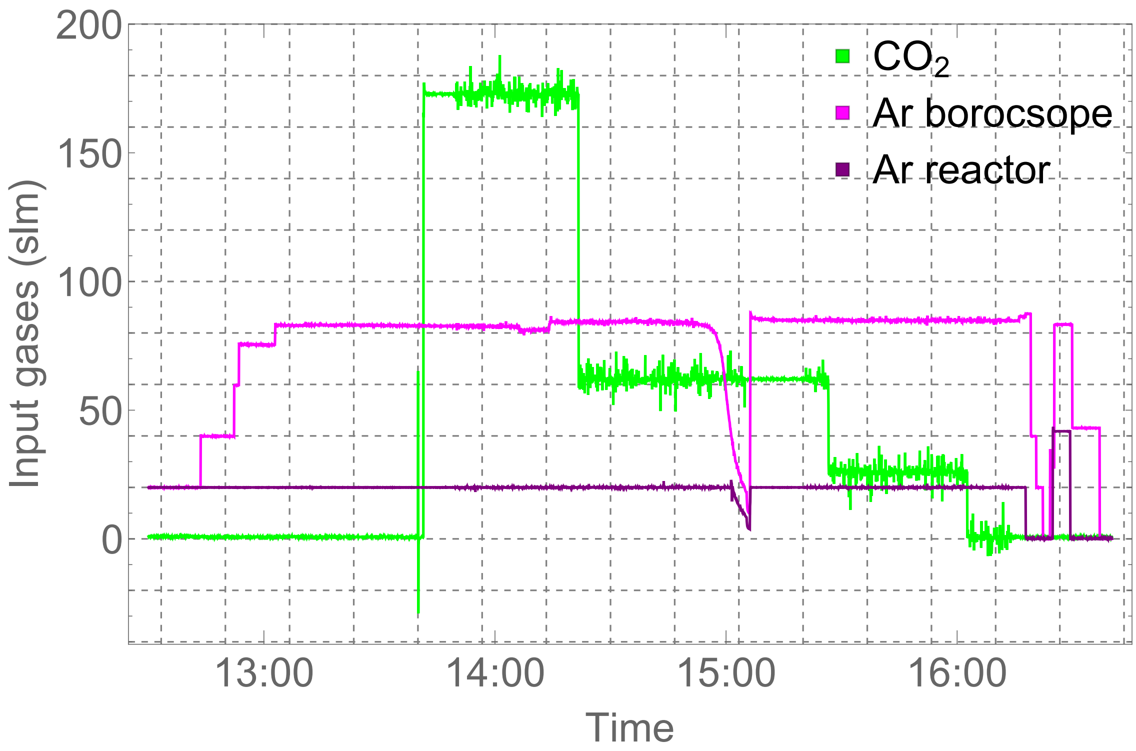

Figure 3.18: Input gases

The argon deficiency in pressure bombs is most noticeable in the figure 3.18 of the inlet gases volume flows. At first, a sudden drop in the argon flow is noticeable without manually changing the operating conditions. This event was identified as an argon shortage, whereupon the process was paused and the pressure bombs replaced.

3.2.2.5 Synthesis gas

CHA	1.	2.	3.	4.
H_2 (%)	26.09	36.62	40.67	44.91
CH_4 (%)	0.67	0.98	0.85	0.88
CO (%)	48.06	38.35	29.99	20.61
O_2 (%)	0.09	0.19	0.12	0.05
CO_2 (%)	7.45	1.65	0.41	0.24
Ar (%)	17.62	22.21	27.96	33.31

Table 3.5: Composition of synthesis gas

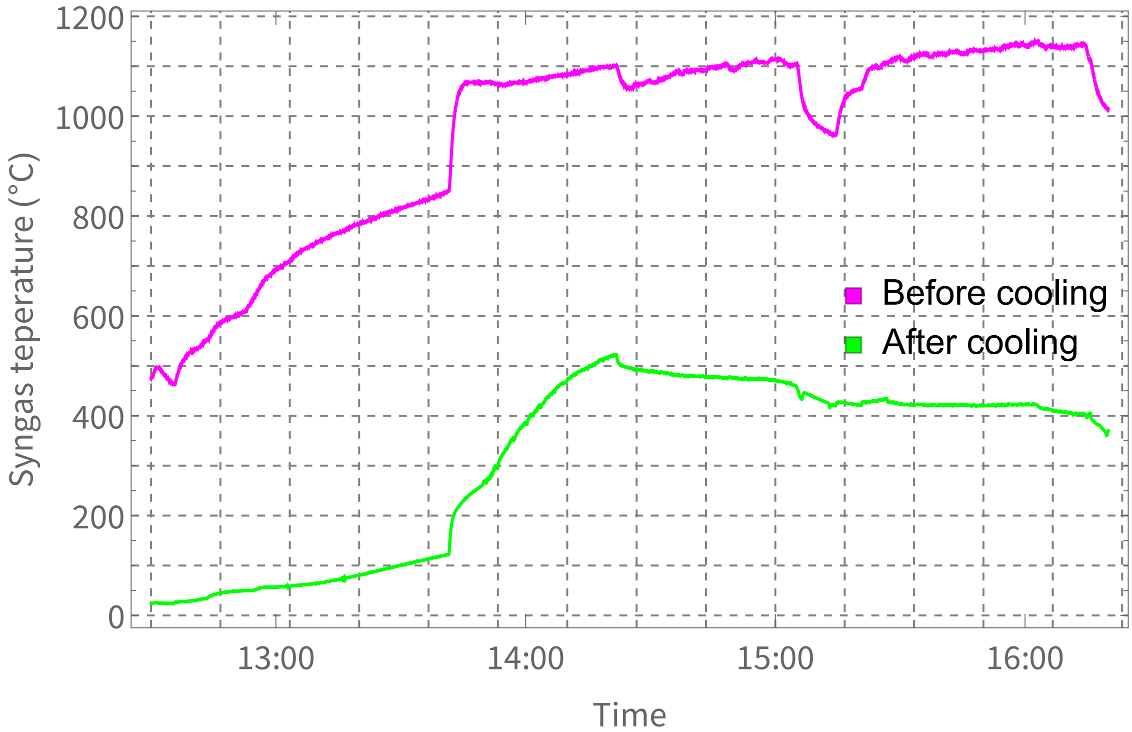

Figure 3.19: Temperatures of the synthesis gas on the output

Similarly to the first experiment, there is also a noticeable decrease in the yield of carbon monoxide with a decreasing supply of the oxidizing agent. Synthesis gas production is now generally higher than in the case of the first experiment, which is caused by a higher supply of input carbon dioxide and RDF material.

It is evident that the (relative) increase of hydrogen representation in the output mixture is very significant, namely from 26 % in the first part of the experiment to almost 45 % in the final part of the experiment (see table 3.5). The temperatures needed to calculate the accumulated heat in the gas in the form of specific heat capacity before (and after) cooling are shown in figure 3.19.

3.2.3 RDF & MWPT

3.2.3.1 Electrical quantities

In the case of MWPT, which was delivered from an external company, the control was carried out through the interface compatible with this specific plasma torch. Therefore, the power of the plasma torch was continuously monitored (and changed when needed), but information about power is based on handwritten notes. Figure 2.15, however, proves the good stability of the MWPT power, as was discussed earlier. For this reason, the power can be replaced with sufficient accuracy by constant power curves for individual intervals as shown in figure 3.20.

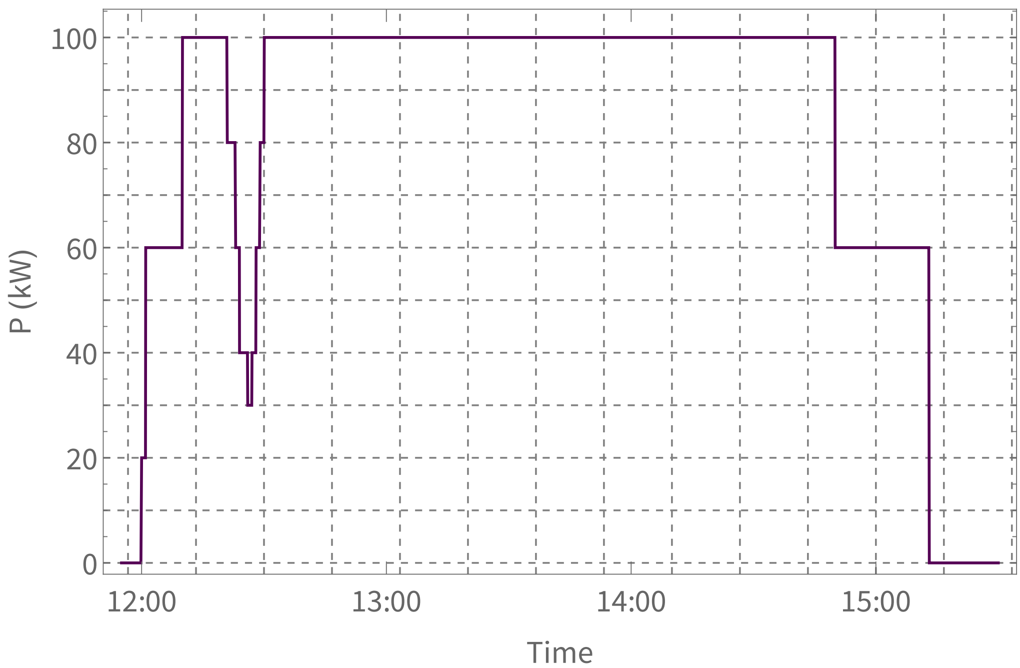

Figure 3.20: Power of the microwave plasma torch

3.2.3.2 Temperatures in reactor

The behavior of temperatures inside the reactor seems more turbulent than in the case of HPT experiments (see figure 3.21). One of the big differences between these two plasma torches is the character of the generated plasma, which greatly affects the measured temperatures in the reactor.

The hybrid arc torch creates a narrow and small jet of plasma that has an extreme temperature in the center using a relatively low volume flow rate of the stabilization medium. This jet then serves as a local source of heat, which gradually spreads into the reactor space and subsequently into the surrounding walls.

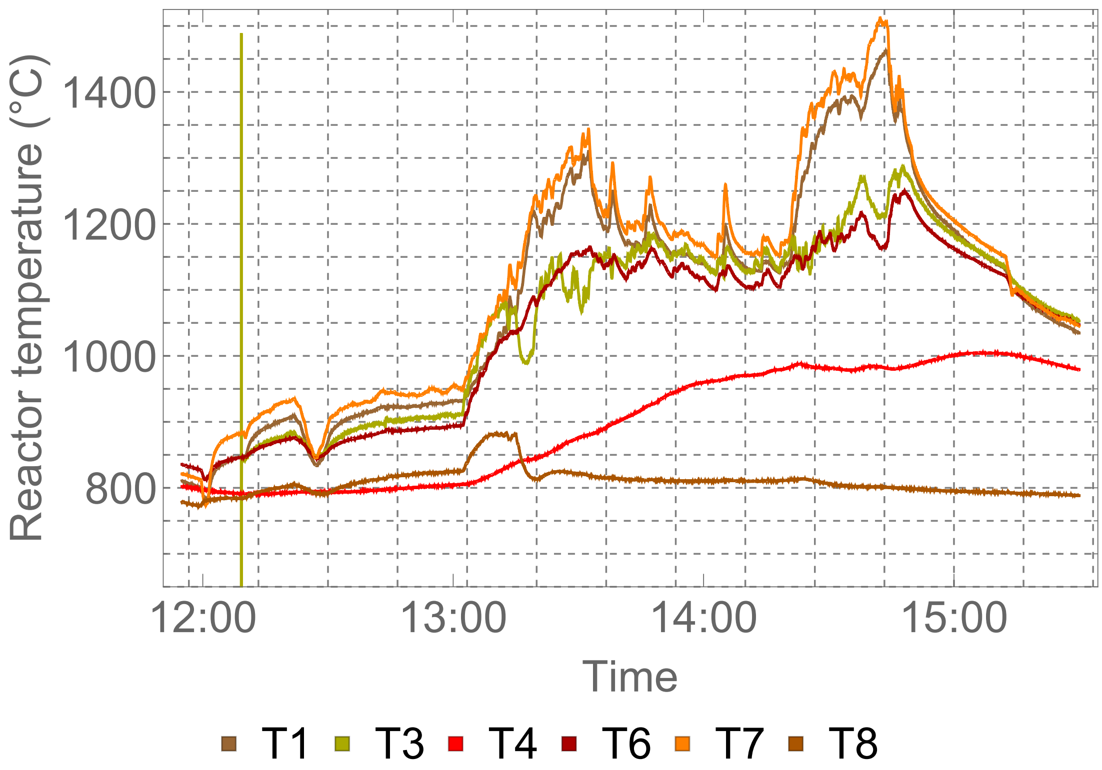

Figure 3.21: Temperatures measured inside the plasma reactor

On the contrary, the microwave plasma torch has much larger flow rates of the stabilizing medium and the dimensions of the flame. This creates much more active conditions in terms of heat transfer at the regions of gas flow, even when the plasma flame itself has lower temperatures in general.

For this reason, the heat is also not effectively distributed evenly to the surrounding walls of the reactor, and there are much larger differences in the temperature curves. While the upper part of the inner walls around the hot synthesis gas outlet is heated very intensively, the lower part stays at a practically constant temperature of 800 °C and the middle part barely reaches the limit of 1000 °C towards the end of the experiment.

For reason of the high inertia of the processes, these large and rapid temperature fluctuations can greatly complicate the estimation of accumulated heat during the short time intervals determined by chemical analyses. Another issue in the area of the accumulated heat computation is that the mean value of the inner wall of the reactor will be determined as the average of the measured temperatures of the inner wall. In this case, however, the temperature differences are much bigger and a simple averaging can already cause a larger deviation because there are more thermocouples in the upper part of the reactor (where the temperatures are higher) than in the lower part of the reactor (where the temperatures are lower).

The calculations of accumulated heat will not be different for the MWPT experiment, but this needs to be considered in the final discussion evaluating the results of the models.

3.2.3.3 Cooling water

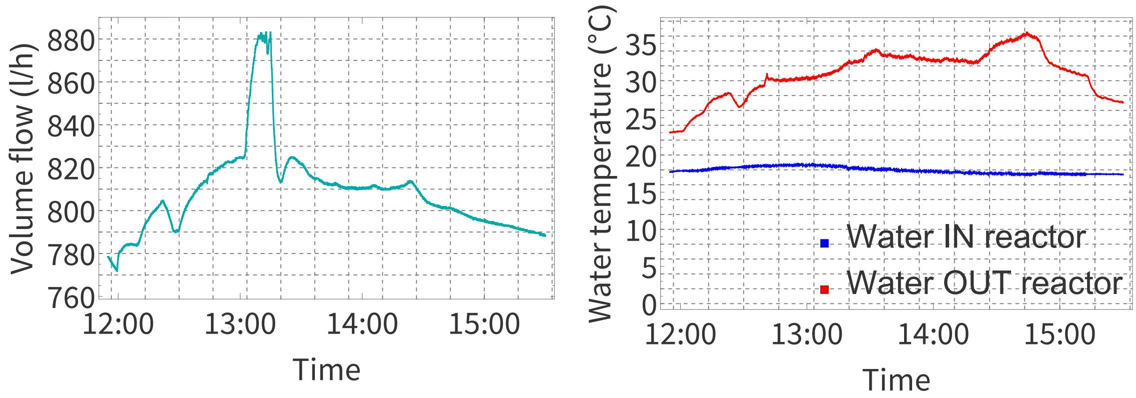

(a) Volume flow **(b)** Temperatures

Figure 3.22: Cooling water into reactor

The curves of the cooling water of the reactor flow (and temperatures) during the experiment with MWPT are distinctively different from the curves with HPT. First of all, the volume flow of the cooling water was regulated much more steeply, in both cases of increasing or decreasing the volume flow. As seen in figure 3.22, the temperature differences of the inlet and outlet cooling water of the reactor are similar in order to the previous experiments, but the volume flow rates are significantly lower, so a lower cooling power of the reactor can be expected.

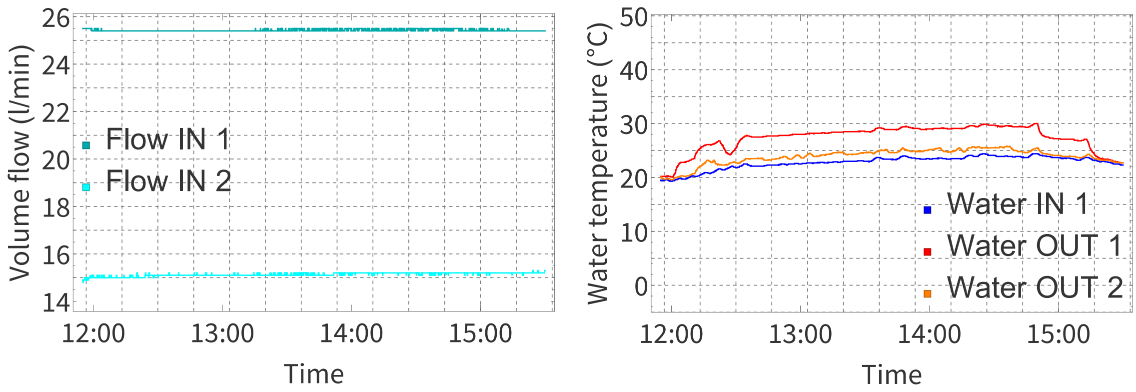

(a) Volume flows in the 1st subcycle **(b)** Temperatures in the 1st subcycle

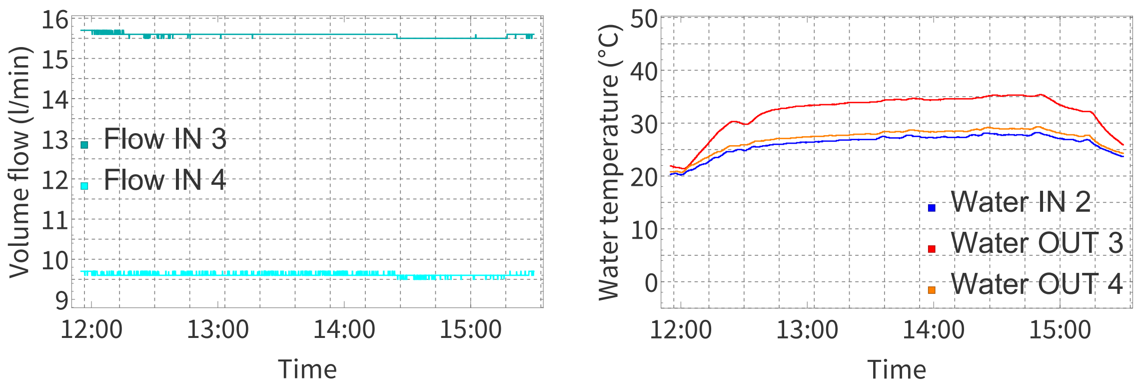

(c) Volume flows in the 2nd subcycle **(d)** Temperatures in the 2nd subcycle

Figure 3.23: Cooling and stabilizing water into plasma torch

Cooling power of the microwave plasma torch unit will probably be significantly lower, since the temperature differences of the water at the inlet and outlet are minimal in this experiment, as shown in figure 3.23.

3.2.3.4 Input gases

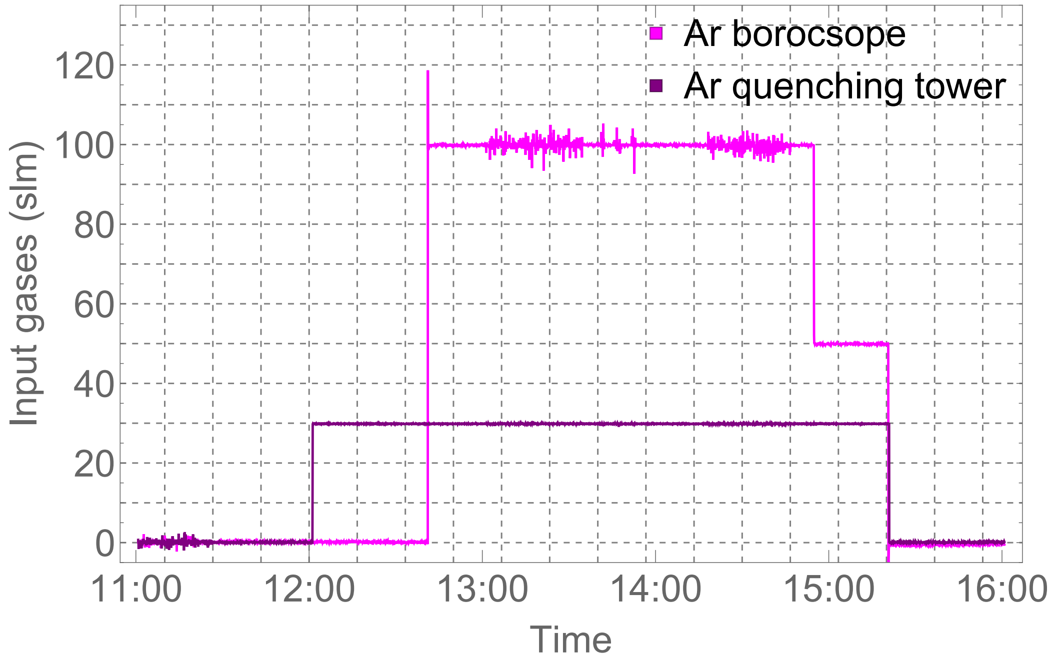

Figure 3.24: Input gases

In this experiment, no oxidizing agent was added to the reactor, because the air (made of about 21 % oxygen) represents the function of an oxidizing agent even as the plasma stabilization medium. For this reason, the inlet gas is only argon, as seen in figure 3.24. Airflow was then recorded by an external interface and written manually in notes. Unfortunately, in the course of the experiment, it turned out that the calibration is unreliable because the measured data showed unrealistic values in the case of argon. However, from the knowledge of the airflow and the simplified determination of its composition in the table 3.15, the calibration can be made using nitrogen, provided that there is a negligible amount of nitrogen in the input material (less than 1 %). Thanks to nitrogen calibration, reasonable values for the material (mass) balance have already been obtained. It is good to emphasize that in the case of MWPT, the volume flow rates of the stabilization medium are significantly higher than in the case of HPT, namely between 1000 and 1300 slm, as can also be seen in the timeline figure 3.3.

3.2.3.5 Synthesis gas

It is clear from table 3.6 that most of the output consists of gases from the inlet air supplied to the plasma. Of the considered 78 % of nitrogen at the input, there is roughly between 72 and 77 % at the output. The higher the proportion of nitrogen in the output mixture, the less energy-usable synthesis gas was produced. *(Note: Nitrogen oxides must also be included in the output nitrogen.)*

CHA	1.	2.	3.	4.	5.
H_2 (%)	1.90	0.00	0.00	1.44	<0.01
CH_4 (%)	0.09	0.00	0.00	0.03	0.00
CO (%)	0.01	0.01	<0.01	2.20	0.02
N_2 (%)	76.87	73.78	73.53	74.20	72.20
NO/NO_2 (%)	0.34	0.78	0.85	0.36	0.63
O_2 (%)	0.08	15.81	16.18	0.03	15.22
CO_2 (%)	12.60	1.34	1.03	13.63	1.55
Ar (%)	8.12	8.29	8.41	8.11	10.38

Table 3.6: Composition of synthesis gas

In some time intervals, the yield of energy components was so low that (for illustrative purposes) it can practically be considered as zero. However, calculations in the models are performed with all available decimal places.

From table 3.6 (and the yield of hydrogen or carbon monoxide) it is also evident that partial gasification was achieved only in some periods. By the comparison of oxygen and carbon dioxide representation, it can be ascertained that during the 1st and 4th interval the input material (RDF) was combusted, because the oxygen from the input air was used for exothermic reactions while producing carbon dioxide. For the remaining time intervals, it is not possible to determine whether the combustion was suppressed because of the absence of fuel or the velocity of the gas flow exiting the reactor was too high (in other words, the residence time to combust the fuel completely was not long enough).

Because of the combustion reaction (also occurring more often than gasification in this experiment), ash is produced during the process (or the material does not have enough time to burn and a solid residue remains in the reactor). Its amount further depends on the stoichiometry of the process, which is considered quite poor for this particular experiment. Large volume flows of the gaseous medium and the problems with feeding of the material made the situation even worse. For these reasons, ash (and other solid residues) needs to be included in the material balance. Under specific conditions and assumptions of this experiment, however, it is not realistically possible to determine the ratio between produced ash and carbon black, especially not for previously selected short time intervals.

A balance correction could be made if the experiment was assessed as a whole and the output carbon black and ash were removed from the reactor (and filter and other components) and weighed after the experiment. Another possibility is a detailed elemental analysis, which would be based on the results of some experiments carried out with a reference type of fuel. This analysis is not available, and the composition of RDF is (similarly to the mass flow of RDF during feeding) stochastic. More detailed chemical calculations of the process are not the subject or competence of this thesis. Equal formation of carbon black and ash will be considered for the determination of the output carbon black weight. Therefore, the weight of the output carbon black will correspond to the weight of the produced ash. This is an incorrect approach to the material balance, but unfortunately, a more accurate estimate is simply not available at the moment.

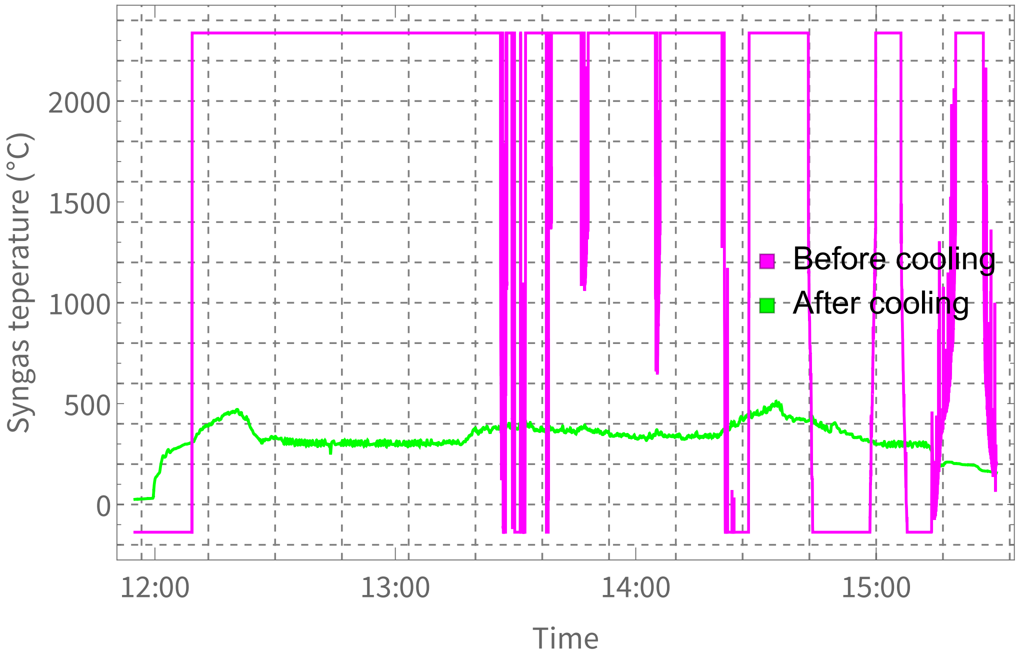

Figure 3.25: Temperatures of the synthesis gas on the output

Unfortunately, during the MWPT experiment it became evident (from Figure 3.25) that the thermocouple in the flue gas pipe, where the synthesis gas samples are analyzed, was damaged. For this reason, the accumulated heat in the gas will be calculated based on the knowledge of the temperatures behind the exit from the quenching tower. This adds 2 more elements to the energy balance, namely the heat (convection and radiation) losses of the quenching tower and the heat supplied to warm and evaporates the water into overheated steam (as explained later).

3.3 Energy balances - theory

One of the most important parts of this thesis is the analysis of the measured data and their appropriate evaluation, including the resulting conclusion statements. For the possibility of a qualitative assessment of the operation, a convenient methodology is necessary. The entire process of plasma gasification of waste is, even on the laboratory scale, very energetically, technologically, and logistically demanding.

For a detailed evaluation and comparison of experiments in terms of the yield of secondary raw materials, energy consumption and generation, or efficiency of energy conversion, it is necessary to design a calculation model for the energy balance, which will, if possible, include all inputs and outputs of the process. The structure of this model is captured by figure 3.26 below. The meaning of the quantities is described below the default energy balance equation 3.1.

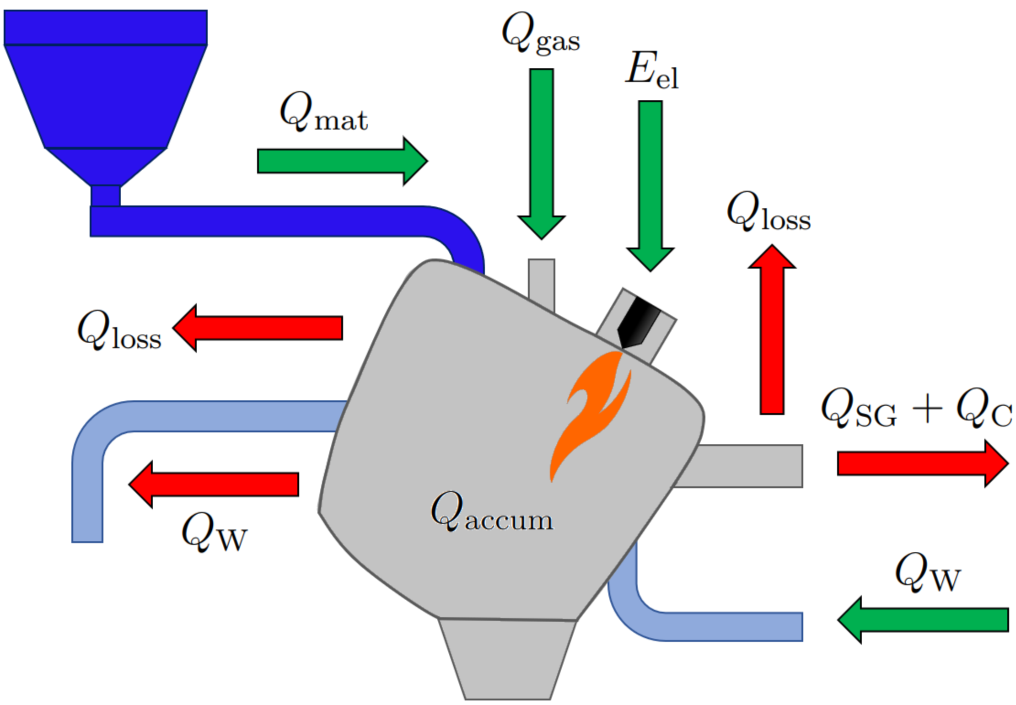

Figure 3.26: Energy balance scheme

It is evident that the plasma gasification process is very complex and complicated from an analytical point of view and constructing a computational model is quite challenging, as it requires not only knowledge of electrical engineering and heat transfer but also chemical engineering or material engineering. All energy quantities are dynamic over time, similar to state quantities, which are mostly in relation to operating conditions. For this case, the most common relation is to temperature. An equation describing the energy balance can be expressed by a non-linear differential equation (or set of equations) that could be solved by appropriate numerical calculation methods if all sufficient data were available. This case is limited by the availability of only some data from the process and many parameters and quantities need to be determined either by estimation or performing averages, respectively weighted averages, for instance for gas mixture properties. In order to draw appropriate conclusions, this form of the equation will henceforward not be used.

The following necessities are crucial for the specific model solution design:

- effort and time to make the model,
- knowledge in the given areas of the issue,
- software to perform calculations,
- initial experimental data.

Unfortunately, for the scale of this thesis, a more complex data or analytical model will be excluded. The data needed for its construction, and detailed knowledge of thermochemical processes under extreme conditions in the reactor are not yet available. Similarly, the time for model development, testing, and debugging is very limited.

Instead of describing the specific processes over time using the power model, the experiments will be divided into time intervals that will be assessed by the overall energy inputs and outputs. The final form of the equation, including the amount of energy of partial balance elements in absolute numbers, is described by equation 3.1. The basic unit of this equation a kWh is chosen, as the basic unit in the electrical power engineering sector.

$$E_{\mathrm{el}} + Q_{\mathrm{mat}} + Q_{\mathrm{gas}} = Q_{\mathrm{accum}} + Q_{\mathrm{W}} + Q_{\mathrm{SG}} + Q_{\mathrm{C}} + Q_{\mathrm{loss}} \tag{3.1}$$

E_{el} is electrical energy consumed during the experiment, Q_{mat} is energy usable from the input material, Q_{gas} is energy carried by the input gas, Q_{accum} is energy accumulated in the reactor, Q_{W} is energy carried away by cooling water, Q_{SG} is energy in synthesis gas, Q_{C} is energy in carbon black and Q_{loss} are the losses, particularly in the form of heat. The energy value of slag is negligible, as explained further.

Quantitative evaluation of the specific energy inputs and outputs will make it possible to examine various factors characteristic for the specific process. These factors include the efficiency of the energy conversion process, the amount of energy needed for thermochemical processes, or the amount of waste heat that could theoretically be further used on an industrial or commercial scale, for instance.

3.3.1 Electrical energy

The first element in the balance sheet, the amount of electrical energy consumed, is relatively simple to calculate. Electrical quantities of both plasma torches needed for the calculation (electrical input power and efficiencies of the components in particular) are well known during the experiment. For the hybrid arc plasma torch, voltage and electrical current time relations are also available.

The input power of the plasma torch (PT) per time unit expresses the amount of electrical energy consumed. If the input power over time could be expressed continuously as an analytic function, the energy consumption of the plasma torch would be expressed using the following integral:

$$E_{\mathrm{el_{PT}}} = \tau_{\mathrm{h}} \cdot \int_{t_{\mathrm{min}}}^{t_{\mathrm{max}}} P_{\mathrm{el}}(t)\, dt = \tau_{\mathrm{h}} \cdot \int_{t_{\mathrm{min}}}^{t_{\mathrm{max}}} U(t) \cdot I(t)\, dt \tag{3.2}$$

where $E_{\mathrm{el_{PT}}}$ (kWh) is the energy supplied to the PT, t (s) is time, t_{min} (s) and t_{max} (s) are the start and end of the experiment, P_{el} (kW) is the electrical input power, U (V) is the voltage and I (A) is the electrical current. τ_h $(-)$ is the conversion factor from seconds to hours and is equal to $1/3600$. It is attached only for completeness and to indicate the unit conversion necessity. For clarity, it will be omitted in the following equations and all the time units will therefore be considered in hours.

Since the measurement of all quantities is inherently discrete, the calculation cannot be performed analytically, but numerically. The previous integral is thus replaced with the sum, more specifically using the numerical integration by the trapezoidal method approximation. The time step difference of the data is not constant, however, on average varies between 1-2 seconds. Experiments usually take several hours, so good calculation accuracy can be assumed. The equation 3.3 shows the replacement form of equation 3.2:

$$E_{\mathrm{el_{PT}}} \approx \sum_{i=0}^{N} \left(\frac{P_{i+1} + P_i}{2} \right) \cdot \Delta t_i = \sum_{i=0}^{N} \left(\frac{U_{i+1} \cdot I_{i+1} + U_i \cdot I_i}{2} \right) \cdot (t_{i+1} - t_i) \tag{3.3}$$

This energy will be included in the final balance. Correctly, the efficiency of the semiconductor converter (the controlled rectifier) η_{REC} should also be included in the evaluation accordingly by the following formula:

$$E_{\mathrm{el_{PTtotal}}} \approx \frac{E_{\mathrm{el_{PT}}}}{\eta_{\mathrm{REC}}} \tag{3.4}$$

This efficiency is not exactly known but is considered relatively high (more than 95 %). For this reason, the calculations will not be further complicated by the efficiency of the rectifier. However, only a part of the total input energy reaches the reactor in the form of heat.

For the possible discussion about the energy efficiency of the process, the energy used for thermochemical reactions can be calculated from the energy supplied to the plasma torch reduced by the heat taken away by the plasma torch cooling water (which is closer addressed in the following subsection *Water*). This may bring a better view of the efficiency of the energy conversion process inside the reactor. Nevertheless, the supplied energy should not be reduced by this heat for balance purposes, because the plasma torch cannot operate safely without cooling during the process. The ratio between the heat delivered into the reactor and total energy supplied (heat into reactor and heat into cooling water) expresses the efficiency of the plasma torch itself, given by the formula 2.4 in the Chapter **2**.

For the microwave plasma torch respectively, both the efficiency of the energy conversion to microwaves and the efficiency of the waveguide (transmission of microwaves to plasma torch head) have to be considered, as given in 2.7 formula in the 2.1.2 subsection. For the determination of total consumption of electrical energy by a MWPT, the calculation by a product of electrical power and the unit of time is sufficient, similarly to the case of the HPT.

Device motor	**Input power P_{el_i} (kW)**
Screw feeder	2.2
Vault disruptor	2.2
Cooling water management	10.0
Water pump	10.0
Rotating anode	0.2
Secondary cooling unit	4.0
Others	0.8
Main power source losses	10.0
SUM	39.3

Table 3.7: Input power of accompanying devices

The energy consumed by the plasma torch cannot be yet declared as the total electrical energy consumed during the process. There are many accompanying devices to the system consuming electrical energy, without which the experiment could not take place. Individually, the power consumption of each piece of equipment is almost negligible, but in total, this represents an increase in the input power by almost 40 kW. The list of accompanying equipment is summarized in table 3.7. In addition to the device inputs, the table also includes the power losses of the main source.

Despite not all of the equipment listed in table 3.7 is in operation for the entire duration of the experimental process, the power consumption will be stated as a constant sum of all the mentioned input powers (and losses). The error is practically negligible for the result because the intervals out of service of some devices are only occasional and very short. Therefore, the total electrical energy consumption of HPT for the duration of the experiment will be:

$$E_{\mathrm{el}} = E_{\mathrm{el}_{\mathrm{PTtotal}}} + \sum_{i=1}^{\mathrm{n}} E_{\mathrm{el}_i} = \sum_{i=0}^{N} \left(\frac{P_{i+1} + P_i}{2} \right) \cdot \Delta t_i + \sum_{i=1}^{\mathrm{n}} P_{\mathrm{el}_i} \cdot (t_{\max} - t_{\min}) \tag{3.5}$$

where N $(-)$ is the amount of time intervals of PT electrical parameters measurement and n $(-)$ is number of accompanying devices. The other quantities have already been described. For MWPT, the equation is less complicated:

$$E_{\mathrm{el}} = E_{\mathrm{el}_{\mathrm{PTtotal}}} + \sum_{i=1}^{\mathrm{n}} E_{\mathrm{el}_i} = \sum_{i=0}^{N} P_i \cdot \Delta t_i + \sum_{i=1}^{\mathrm{n}} P_{\mathrm{el}_i} \cdot (t_{\max} - t_{\min}) \tag{3.6}$$

3.3.2 Water

The heat taken away by cooling water as another element of the energy balance has also great importance. In this regard, both the reactor and the plasma torch cooling water will be included for the heat evaluation. As discussed in the previous subsection 3.3.1, both the reactor and the plasma torch have to be cooled for safety and material lifetime purposes.

Although from the procedural perspective, this heat energy presents losses (which are primarily undesirable), in a potential industrial facility this energy could be recuperated with a suitable waste heat utilization. The limits for the use of this heat are determined by thermodynamic laws and a more detailed discussion is beyond the extent of this thesis. Equivalently to the introductory equation representing the electrical energy consumption, thermal energy in water can be analytically written using the integral equation:

$$Q_{\mathrm{W}} = \int_{t_{\min}}^{t_{\max}} \dot{Q}_{\mathrm{W}}(t)\, dt = \int_{t_{\min}}^{t_{\max}} \left(\dot{Q}_{\mathrm{W_{RE}}}(t) + \dot{Q}_{\mathrm{W_{PT}}}(t) \right) dt \tag{3.7}$$

where Q_{W} (kWh) is the total energy carried away by the cooling water, $\dot{Q}_{\mathrm{W}}$ (kW) is the drained thermal power (cooling power respectively), of which $\dot{Q}_{\mathrm{W_{RE}}}$ (kW) is the reactor cooling power and $\dot{Q}_{\mathrm{W_{PT}}}$ (kW) is the plasma torch cooling power. For convenience and clarity $\dot{Q}_{\mathrm{W_{RE}}}(t) + \dot{Q}_{\mathrm{W_{PT}}}(t)$ will be further replaced by $\dot{Q}_{\mathrm{W}}(t)$.

$$\dot{Q}_{\mathrm{W}}(t) = \dot{m}_{\mathrm{W}}(t) \cdot c_{p_{\mathrm{W}}}(T) \cdot \Delta T_{\mathrm{W}}(t) \tag{3.8}$$

$\dot{m}_{\mathrm{W}}$ ($\mathrm{kg \cdot s^{-1}}$) is the mass flow of the water, $c_{p_{\mathrm{W}}}$ ($\mathrm{kJ \cdot kg^{-1} \cdot K^{-1}}$) is the specific heat of water and ΔT_{W} (K) is the water temperature difference between input and output. This presents only a general equation, for both cases of the reactor and the plasma torch, all quantities need to be determined separately.

Since the water flow is measured in liters per hour, it is necessary to convert the flow into $\mathrm{m^3}$ per second and multiply by the water density. Final form of the 3.7 equation will be:

$$Q_{\mathrm{W}} = Q_{\mathrm{W_{RE}}} + Q_{\mathrm{W_{PT}}} \tag{3.9}$$

where:

$$\begin{aligned} Q_{\mathrm{W_{RE}}} &= \int_{t_{\min}}^{t_{\max}} \rho_{\mathrm{W_{RE}}}(T) \cdot \dot{V}_{\mathrm{W_{RE}}}(t) \cdot c_{p_{\mathrm{W_{RE}}}}(T) \cdot \Delta T_{\mathrm{W_{RE}}}(t)\, dt \\ Q_{\mathrm{W_{PT}}} &= \int_{t_{\min}}^{t_{\max}} \rho_{\mathrm{W_{PT}}}(T) \cdot \dot{V}_{\mathrm{W_{PT}}}(t) \cdot c_{p_{\mathrm{W_{PT}}}}(T) \cdot \Delta T_{\mathrm{W_{PT}}}(t)\, dt \end{aligned} \tag{3.10}$$

Because the data of the water flow and water temperatures are also discrete, the integrals will be substituted by sums again. As estimates, the specific heat (capacity) of water and the density of water will be considered constant, namely for the mean value of the temperature of inlet water and the temperature of the outlet water. Therefore in general:

$$\begin{aligned} Q_{\mathrm{W_{RE}}} &\approx \sum_{i=0}^{M} \Delta Q_{\mathrm{W}i_{\mathrm{RE}}} = \sum_{i=0}^{M} \rho_{\mathrm{W_{RE}}} \cdot \dot{V}_{\mathrm{W}i_{\mathrm{RE}}}(t) \cdot c_{p_{\mathrm{W_{RE}}}} \cdot (T_{\mathrm{W_{OUT}}i\mathrm{RE}} - T_{\mathrm{W_{IN}}_{i\mathrm{RE}}}) \\ Q_{\mathrm{W_{PT}}} &\approx \sum_{i=0}^{N} \Delta Q_{\mathrm{W}i_{\mathrm{PT}}} = \sum_{i=0}^{N} \rho_{\mathrm{W_{PT}}} \cdot \dot{V}_{\mathrm{W}i_{\mathrm{PT}}}(t) \cdot c_{p_{\mathrm{W_{PT}}}} \cdot (T_{\mathrm{W_{OUT}}i\mathrm{PT}} - T_{\mathrm{W_{IN}}_{i\mathrm{PT}}}) \end{aligned} \tag{3.11}$$

The situation is complicated by the different properties of water at different temperatures, especially the density and specific heat capacity. If a detailed analytical model were to be compiled, these physical quantities would be defined by subsequent interpolations based on tables from [31, 32]. Interpolation functions of the physical properties of water are shown in figure 3.27.

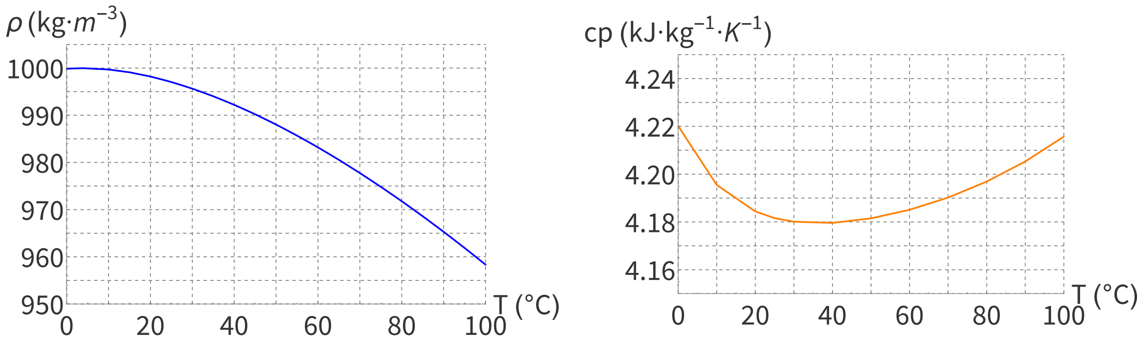

(a) Density **(b)** Specific heat

Figure 3.27: Physical properties of water in relation to temperature

The temperature differences between input and output cooling water are yet relatively low, so heat evaluation can be significantly simplified by estimating the specific heat capacity and density values as constant, namely to the arithmetic mean temperature of all measured temperatures. These water properties will then be determined separately for individual experiments. This simplification should have a minimal effect for the purposes of the model and the final result.

3.3.2.1 Evaporation

For the experiment with MWPT, another element of the energy balance related to water needs to be quantified. Because the temperatures inside the flue gas pipe were not measured because of thermocouple failure, only the temperatures after the quenching tower are available. Synthesis gas gets cooled in two ways inside the flue gas pipe:

- by the heat losses (calculated in 3.3.4.5) and
- by reacting with water droplets inside the quenching tower.

Because this water gets evaporated, the usual equation for removed heat cannot be used. Instead, the energy has to be calculated using the volume flow and both difference of enthalpies and temperatures. Enthalpy of water at reference state (before entering the quenching tower) considering atmospheric pressure and 20 °C is about 83.91 $\text{kJ} \cdot \text{kg}^{-1}$.

The temperature of the water vapor (at the outlet of QT) will be considered as the temperature of the synthesis gas at the outlet of the QT, from which it is possible to determine the amount of energy required for the state and temperature change of the cooling water droplets. Unfortunately, the water flow measuring device in QT is not precisely calibrated, so it is not possible to determine the total water volume exactly. However, the values (measured in counts) between 10-15 thousand roughly correspond to a volume flow of 1 $\text{l} \cdot \text{min}^{-1}$. The measurement of water flow to QT is captured by figure 3.28. In the interval where the values are between 10-15 thousand counts, the volume flow will be considered 1 $\text{l} \cdot \text{min}^{-1}$ and in the short interval where the counts reach 20 thousand, the flow will be considered 1.5 $\text{l} \cdot \text{min}^{-1}$. Because of the inaccuracy of the calibration, trying for greater accuracy is meaningless.

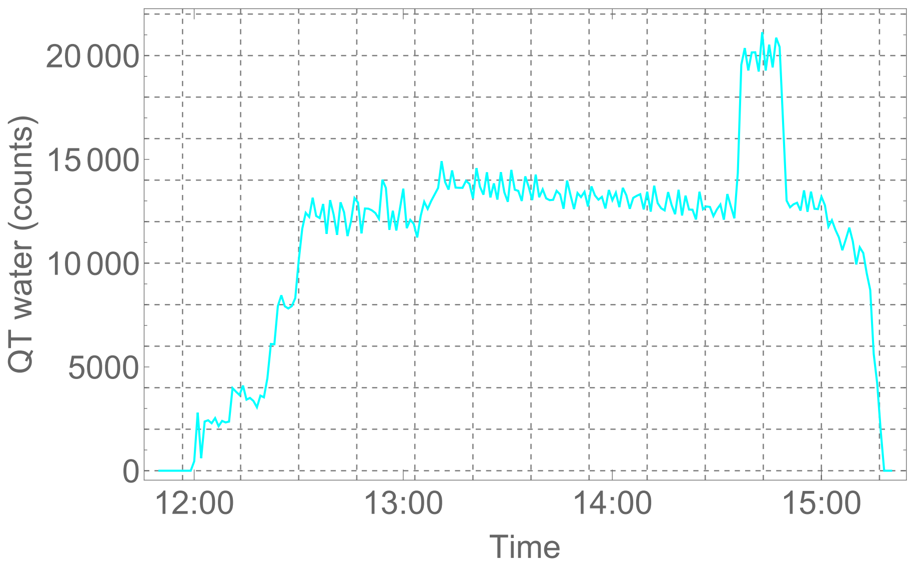

Figure 3.28: Water to quenching tower during the MWPT experiment

The enthalpy difference of water before entering and after exiting the QT:

$$\Delta H_{\mathrm{W}} = (h_{\mathrm{W}}(T_{\mathrm{SG}}) - h_{\mathrm{W}}(20°\mathrm{C})) \cdot m_{\mathrm{W}} = (h_{\mathrm{W}}(T_{\mathrm{SG}}) - h_{\mathrm{W}}(20°\mathrm{C})) \cdot \rho_{\mathrm{W}} \cdot \dot{V}_{\mathrm{W}} \cdot \Delta t \quad (3.12)$$

where ΔH_{W} (kJ) is the difference in the energy content (enthalpy) of water, $h_{\mathrm{W}}(T_{\mathrm{SG}})$ ($\mathrm{kJ \cdot kg^{-1}}$) is specific enthalpy of overheated steam of atmospheric pressure and temperature T_{SG}, $h_{\mathrm{W}}(20°\mathrm{C})$ ($\mathrm{kJ \cdot kg^{-1}}$) is specific enthalpy of water at atmospheric pressure and reference temperature of 20 °C, m_{W} (kg) is the total weight of water supplied to the quenching tower.

3.3.3 Input gases & input material

Other elements of the energy balance are the input gases and the processed material (specifically RDF and SMW). Energetic values of the inputs will be determined on estimated mass/volume flows and calorific values of these inputs. It should be noted that the energy of the output and input materials does not differ only based on the determined masses and calorific values. The components at the output have significantly increased energy by reason of their high temperatures (around 1000 °C). Based on this, the reference temperature level will be set at 20 °C.

The input gases are important as oxidizing or calibrating agents. Nitrogen and argon are from the energy balance perspective only heated during the process, while carbon dioxide, (water) steam, or other input gas components are decomposed and heated. For the microwave plasma torch operation, the air is also the input component as a plasma stabilizing medium. In all cases, these are endothermic reactions, and therefore the entire element Q_{gas} can be neglected.

Unlike gases, solid input materials are feasible for energetic utilization by burning to obtain heat. As a result, the energetic value of this potential fuel can be specified by the estimation of the processed amount and an average calorific value. Accurate estimation is difficult because the material is inhomogeneous and the composition or the mean calorific values are not known exactly. Accordingly, the calorific values of RDF and SMW will be estimated based on the following paragraphs.

Calorific value distincts on the higher heating value (HHV, also called gross heating value) and the lower heating value (LHV, also called net heating value). LHV will be considered as a reference calorific value because LHV is energetically usable (without further chemical reactions and with neglect of heat losses). For various waste materials, the calorific values often reach around 10-30 $\mathrm{MJ \cdot kg^{-1}}$, depending on the composition. The more inhomogeneous the material (waste), the more its calorific value can change for smaller samples. With increasing inhomogeneity, the accurate estimation of the mean calorific value of the material is more complicated.

The calorific value of RDF can be around 20 $\mathrm{MJ \cdot kg^{-1}}$, some sources even state up to 36 $\mathrm{MJ \cdot kg^{-1}}$ for parts of RDF composed of materials with high energy value. A chemical analysis of the composition and calorific value of HHV and LHV was performed for part of the sample used in the laboratory. Table 3.8 summarizes the results of these measurements. The calorific value of RDF fuel for experimental purposes will be chosen as LHV for the raw sample of RDF, namely 24 $\mathrm{MJ \cdot kg^{-1}}$.

RDF parameter	Raw	Dry	Dry & Ash-free
HHV ($MJ \cdot kg^{-1}$)	26.05	26.44	29.15
LHV ($MJ \cdot kg^{-1}$)	**24.24**	24.64	27.16
C content (%)	62.2	63.1	69.6
H content (%)	8.1	8.2	9.0
N content (%)	0.6	0.6	0.6
O content (%)	18.5	18.8	20.7
S content (%)	< 0.1	< 0.1	< 0.1

Table 3.8: Chemical analysis of the RDF sample used for experiment

The situation is similar for medical waste. Again, it depends on the specific composition of the material sample or, for example, on the moisture content (when the moisture content is too high, synthesis gas can be diluted with carbon dioxide and water). Because of similarities in the composition of SMW and RDF, the calorific values of these materials will be similar. For example, in the W2H facility in UHHK the calorific value of 17-18 $MJ \cdot kg^{-1}$ for the medical waste is expected. The book resource [33] gives calorific values between 9-12 $MJ \cdot kg^{-1}$ and, for instance, the web resource [34] states values in the range of 19-24 $MJ \cdot kg^{-1}$. In the author's bachelor thesis [3], the calorific value was set at nearly 21 $MJ \cdot kg^{-1}$, and the evaluation of the chemical analysis showed a calorific value very close to the RDF sample, specifically around 26 $MJ \cdot kg^{-1}$. [11]

For all types of substances, when determining the internal energy, the energy carried by the specific heat (capacity) of the substance will be included, and, if it is possible, potential energy in the form of calorific value. The potential energy of gravitational forces and kinetic energy will be neglected. All operating pressures are close to atmospheric pressure. Synthesis gas velocities from the reactor are low, and because of the compressibility of the gas, this is an acceptable simplification.

Carbon dioxide as an oxidizing agent and inert argon for the means of calibration are the gases on the input of the reactor. Carbon dioxide is supplied depending on stoichiometric quantity requirements, so the volume flow may change during the course of the experiment. In contrast, argon (as an inert gas) is supplied throughout most of the experiment at a constant volumetric flow rate. Depending on its percentage representation in the output mixture of synthesis gas, it is possible to determine the yield of synthesis gas and the particular weight of partial components of the gas mixture.

The volumetric flow rates of the input gases are adjustable, therefore their total volume can be easily calculated by the product of the flow rate and the time for which they are supplied to the reactor. These products will always be performed for time intervals where the flow rates are considered constant. Consequently

$$V_{\mathrm{CO_2}} = \int_{t_{\min}}^{t_{\max}} \dot{V}_{\mathrm{CO_2}}(t)\, dt \approx \dot{V}_{\mathrm{CO_2}} \cdot \Delta t = \dot{V}_{\mathrm{CO_2}} \cdot (t_{\max} - t_{\min}) \tag{3.13}$$

In order for later correction using the law of conservation of mass, a conversion from volume to mass will be performed using the equation of state for an ideal gas. (Thus, the gases will be considered ideal gases. Considering the gases as ideal gases is another significant simplification of the model for the consecutive calculations.) The mass of the gas will always be calculated by converting the volume into substance quantities and then by multiplying it with the molar mass of the given gas. Using the equations below

$$p \cdot V = n \cdot \mathrm{R} \cdot T, \qquad m = n \cdot M \tag{3.14}$$

where p (Pa) is the pressure, V (m^3) the volume, n (mol) the amount of substance, R ($\mathrm{J \cdot K^{-1} \cdot mol^{-1}}$) the gas constant, T (K) the thermodynamic temperature, m (kg) the mass and M ($\mathrm{kg \cdot mol^{-1}}$) the molar mass. The final conversion equation can be written:

$$m = \frac{p \cdot V}{\mathrm{R} \cdot T} \cdot M \tag{3.15}$$

Carbon dioxide and argon are not energetically valuable gases. Theoretically, the energy of these gases is in the form of kinetic energy of specific heat capacity. The temperature of the input gases is equal (or very similar) to the reference temperature and the kinetic energy is practically insignificant. This is only stated for completeness, the inlet gas balance is necessary for the mass conservation balance, not the energy conservation balance. As already mentioned, the energy of input gases will therefore be:

$$Q_{\mathrm{gas}} \approx 0 \text{ kWh} \tag{3.16}$$

The energy of the solid input material is expressed using the product of the weight of the processed amount m_{mat} and the calorific value H_{mat}. Processed weights of material will be estimated from the feeding calibration and calorific values based on considerations in the previous paragraphs. Consequently:

$$Q_{\mathrm{mat}} = m_{\mathrm{mat}} \cdot H_{\mathrm{mat}} \approx \dot{m}_{\mathrm{mat}} \cdot H_{\mathrm{mat}} \cdot \Delta t = \dot{m}_{\mathrm{mat}} \cdot H_{\mathrm{mat}} \cdot (t_{\mathrm{max}} - t_{\mathrm{min}}) \tag{3.17}$$

where:

$$\begin{gathered} H_{\mathrm{mat}} = H_{\mathrm{RDF}} \quad \text{or} \quad H_{\mathrm{mat}} = H_{\mathrm{SMW}}, \\ H_{\mathrm{RDF}} \approx 24 \text{ MJ} \cdot \mathrm{kg}^{-1} = 6.67 \text{ kWh} \cdot \mathrm{kg}^{-1} \\ H_{\mathrm{SMW}} \approx 26 \text{ MJ} \cdot \mathrm{kg}^{-1} = 7.22 \text{ kWh} \cdot \mathrm{kg}^{-1} \end{gathered} \tag{3.18}$$

This element of the energy balance is the first, that can already contain a bigger error. As already stated, neither of the product values can be determined precisely, because the initial assumptions are based on the estimation of feeding mass flow (addressed in the section 2.3) or material composition, which are both stochastic.

3.3.4 Heat losses

Heat losses together with heat accumulation are the biggest issues of the entire energy balance model because heat transfer is a complicated topic and is all based on empirical models, using for example the theory of similarity, which evaluates only some special simple cases. Furthermore, the dimensions and geometry of the entire laboratory facility are distinctive and complex, most of the inputs for the calculation of heat losses are practically unknown, the actual airflow and accompanying quantities are not defined and a correct procedure would require countless effort, ideally with the help of a mechanical engineer. The goal to determine the heat losses in this thesis is to not neglect them from the perspective of the overall energy balance. On behalf of this fact, an approximate estimate is acceptable.

The error will probably be even bigger than for the element of the input material Q_{mat}, but the heat calculations will not be accurate under any circumstances when the required data for computation are missing. Furthermore, heat losses will be estimated only once for one specific experiment and used in all energy balances, for the following reasons:

- missing data of the surface temperatures of the outer walls from experiments that were already carried out,
- the calculation is long and complicated,
- heat losses are not a significant element in the overall energy balance and
- the calculation is only indicative, even with precise knowledge of the inputs.

Most of the heat losses are provided by cooling water, as mentioned in subsection 3.3.2. Considering the correlation between the heat losses and the heat carried away by water from the reactor, the calculation could be a little more precise, but this correction will not be implemented, because it is practically insignificant.

Heat losses can be calculated using the basics of heat transfer. The case presents a compound of heat transfer by radiation, convection, and conduction, with convection having the greatest effect. Radiation is not considered significant, yet it will be expressed with a short calculation for completeness. Conduction will apply inside the reactor walls, exhaust pipe walls, and cooler walls, while convection on the boundary layers inside and outside the walls. Each of the parts (reactor, pipeline, and cooler) will be assessed individually. Heat transfer from an energy point of view represents the major part of the losses during operation, that cannot be utilized even in the form of waste heat using the cooling water, which is the main reason for the estimation of heat losses. Heat losses from the quenching tower will no longer be included in the final energy balances with HPT since the synthesis gas sample (including its temperature parameter) is already taken in the flue gas pipe.

Starting with the reactor, because of its geometry and spatial location, it needs to be divided into 3 parts, namely the lid (cover), the shell, and the bottom. The reason is that the lid has a thinner layer of insulation, which makes it less resistant to heat transfer, and the surface of the cover has distinctly higher temperatures than the rest of the reactor surface. At the same time, a slag container is placed at the bottom of the reactor, which complicates the calculation due to different insulating layers and a more distinct geometry. This geometry will be for the reason of simplification also reduced to an inclined horizontal plate, similar to the upper lid. The difference between these plates is that the lid is cooled from the upside while the bottom is from the bottom side.

Heat comes from the inside of the reactor to the outside in all directions. From the perspective of consideration of dividing the reactor into parts for the cause of calculation, this represents a parallel combination of the thermal resistances of cover, shall, and bottom. For the computation, the analogy of the electrical circuit model can be introduced. Individual electrical parameters correspond to thermal parameters, as shown in the table 3.9. Similarly, an analogy can be made to Ohm's law, as in equation 3.19.

Thermal quantity, symbol, unit	**Electrical quantity, symbol, unit**
Temperature, T (K or °C)	Voltage, U (V)
Heat flow, $\dot{Q}$ (W)	Electrical current, I (A)
Thermal resistance, R_{th} ($\mathrm{K{\cdot}W^{-1}}$)	Electrical resistance, R (Ω)

Table 3.9: Analogy between thermal and electrical circuits

$$\Delta U = R \cdot I \quad \rightarrow \quad \Delta T = R_{\mathrm{th}} \cdot \dot{Q} \tag{3.19}$$

Using the proportions of the reactor, the thermal conductivities of the internal layers and the electrical circuit analogy, the heat flow balance for the element of time could be potentially drawn up.

The issue is that the structure and geometry, including cooling and possible openings for thermocouples or borescopes, are already much more complex, and the calculation would require a 3D computational model and exact knowledge of wall temperatures. Only the temperatures inside the reactor are measured. It cannot be stated, whether the average of these temperatures is equal to the average temperature of the inner walls.

However, the fact of common heat flow both for conduction through the walls and for convection on the surface can be used (of course in the limiting case of neglecting the decrease of heat flow considering the heat capacity of the material). In this case, the estimation of losses based only on the calculation of convection is satisfactory. Since the reactor can be divided into 3 parts, the heat flux losses will be divided into 5 separate equations 3.20, where the first equation with index i covers all three reactor equations. Index $i = 1$ stands for the lid, $i = 2$ stands for the shell, and $i = 3$ stands for the bottom of the reactor. The resulting heat loss flux will be the sum of the heat fluxes from 3 reactor parts and flue gas pipe losses (index FGP). The quenching tower losses will be calculated for visualized comparison. Because of thermocouple failure during the experiment with MWPT, these will be included only in the final energy balance for MWPT, as stated in the equations 3.21:

$$\begin{aligned} \dot{Q}_{\mathrm{loss}_i} &= \alpha_i \cdot A_i \cdot \Delta T_i \\ \dot{Q}_{\mathrm{loss_{FGP}}} &= \alpha_{\mathrm{FGP}} \cdot A_{\mathrm{FGP}} \cdot \Delta T_{\mathrm{FGP}} \\ \dot{Q}_{\mathrm{loss_{QT}}} &= \alpha_{\mathrm{QT}} \cdot A_{\mathrm{QT}} \cdot \Delta T_{\mathrm{QT}} \end{aligned} \tag{3.20}$$

$$\begin{aligned} \dot{Q}_{\mathrm{lossHPT}} &= \sum_{i=1}^{3} \dot{Q}_{\mathrm{loss}_i} + \dot{Q}_{\mathrm{loss_{FGP}}} \\ \dot{Q}_{\mathrm{lossMWPT}} &= \sum_{i=1}^{3} \dot{Q}_{\mathrm{loss}_i} + \dot{Q}_{\mathrm{loss_{FGP}}} + \dot{Q}_{\mathrm{loss_{QT}}} \end{aligned} \tag{3.21}$$

A (m^2) elements represent the areas of individual heat exchange surfaces. These surfaces will be determined by a simplified calculation using a reduction to basic geometric shapes - cylinders. For the case of bevelling or narrowing of the cylinder in the dimension of height or length, the mean value will be used for the calculation. The dimensions of the individual components of the facility are described in figure 3.29 and summarized in table 3.10 in the basic units.

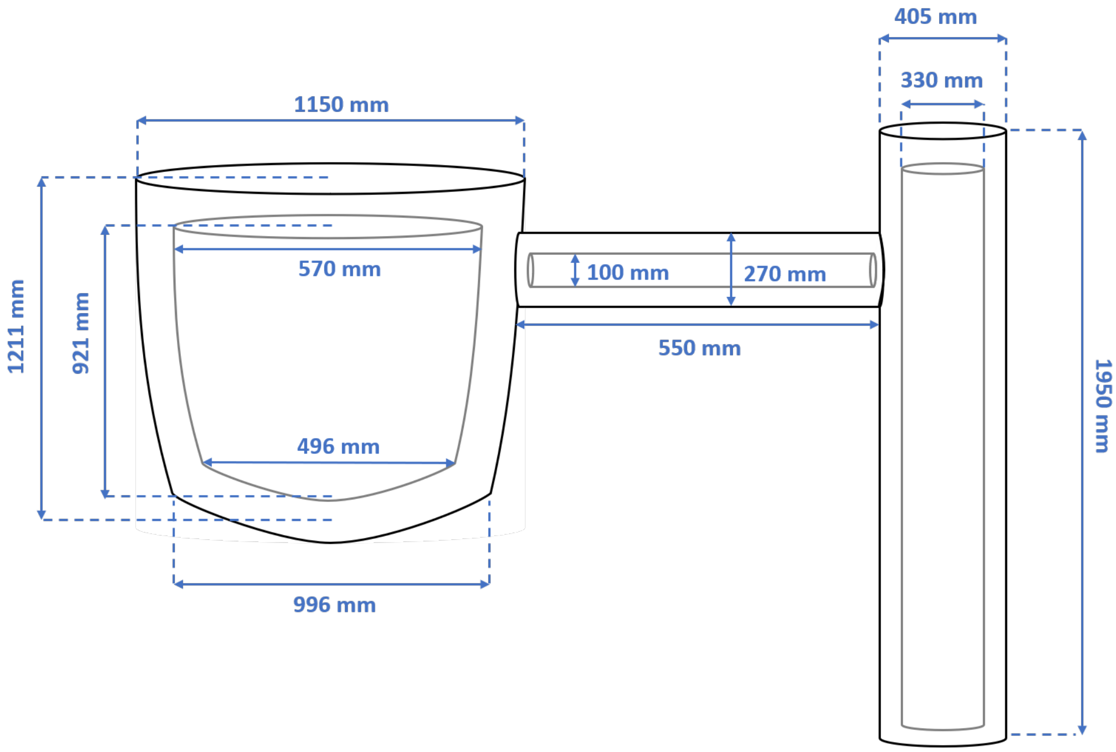

Figure 3.29: Dimensions of reactor components scheme (from left: RE, FGP, QT)

Dimension	Reactor	Flue gas pipe	Quench. tower
d_{OUTmax} (m)	1.150	0.270	0.405
d_{OUTmin} (m)	0.996	0.270	0.405
d_{OUTavg} (m)	1.073	0.270	0.405
d_{INmax} (m)	0.570	0.100	0.390
d_{INmin} (m)	0.496	0.100	0.270
d_{INavg} (m)	0.533	0.100	0.330
h_{max} (m)	1.211	-	1.950
h_{min} (m)	0.921	-	1.950
Δh (m)	0.29	-	-
l (m)	-	0.550	-

Table 3.10: Dimensions of reactor components

Conceptually, the entire reactor can be replaced by an inclined vertical cylinder. The lid (upper cover) will be considered as a horizontal plane inclined by the angle $\delta = 20°$. The temperature difference between the lid and the air will be higher than the temperature difference between the rest of the reactor and the air. The reactor shell will be considered as a cylinder shell and the bottom will be again considered as a horizontal plane inclined by the angle $\delta = 20°$.

The incline of the shell will be neglected because the sum of the incline angles around the perimeter of the cylinder is zero. Specifically from the perspective of heat transfer conditions, the incline angle at each point of the shell is compensated by the complementary angle on the opposite side of the reactor shell. This simplification is feasible thanks to the small incline of the reactor. For bigger angles (for example $\delta = 45°$) it would be appropriate to average the conditions between the vertical and horizontal cylinder. The temperature of the reactor shell and the bottom surface is lower compared to the upper lid. The flue gas pipe will be simplified to a horizontal cylinder and the quenching tower will be simplified to a vertical cylinder.

For both HPT experiments, losses in the quenching tower (which follows after the flue gas pipe) will no longer be part of the energy balance, because synthesis gas parameters (respectively the samples and their temperatures) are measured inside the flue gas pipe. For the flue gas pipe and quenching tower, the surface temperature depends on the state of the experiment. Before the material feeding and synthesis gas formation, the surface temperature is about the room temperature, and during the operational steady state, surface temperatures can get even higher than the reactor lid (because the flue gas pipe and the quenching tower are not cooled by water).

First, the surface areas A of the mentioned parts will be specified:

$$
\begin{aligned}
A_1 &= \pi \cdot \left(\frac{d_{\mathrm{RE_{OUTmax}}}}{2}\right)^2 = \pi \cdot \left(\frac{1.15}{2}\right)^2 = 1.04\ \mathrm{m}^2 \\
A_2 &= 2 \cdot \pi \cdot \left(\frac{d_{\mathrm{RE_{OUTavg}}}}{2}\right) \cdot h_{\mathrm{RE}} = 2 \cdot \pi \cdot \left(\frac{1.073}{2}\right) \cdot 1.211 = 4.08\ \mathrm{m}^2 \\
A_3 &= \pi \cdot \left(\frac{d_{\mathrm{RE_{OUTmin}}}}{2}\right)^2 = \pi \cdot \left(\frac{0.996}{2}\right)^2 = 0.78\ \mathrm{m}^2 \\
A_{\mathrm{FGP}} &= 2 \cdot \pi \cdot \left(\frac{d_{\mathrm{FGP_{OUT}}}}{2}\right) \cdot l_{\mathrm{FGP}} = 2 \cdot \pi \cdot \left(\frac{0.27}{2}\right) \cdot 0.55 = 0.47\ \mathrm{m}^2 \\
A_{\mathrm{QT}} &= 2 \cdot \pi \cdot \left(\frac{d_{\mathrm{QT_{OUT}}}}{2}\right) \cdot \left(h_{\mathrm{QT}} + \frac{d_{\mathrm{QT_{OUT}}}}{2}\right) = \\
&= 2 \cdot \pi \cdot \left(\frac{0.405}{2}\right) \cdot \left(1.950 + \frac{0.405}{2}\right) = 2.74\ \mathrm{m}^2
\end{aligned}
\tag{3.22}
$$

The temperatures of individual surfaces were determined experimentally by measuring different parts of the system components at several places along the entire perimeter and length, specifically with a digital thermocouple (TM-902C) and a laser infrared non-contact thermometer (VA6530). The measured temperature values of both thermometers correlated quite well.

The resulting values of average surface temperatures are summarized in table 3.11. The temperatures were measured from the end of preheating until the end of the experiment. If the experiment was to continue, the temperatures could probably rise further. Heat losses will be calculated for the steady state. Therefore, the last state of measurement will be considered as a steady state. The purpose is to simulate commercial industrial operation as closely as possible, where operating times could last for days. However, temperature values will not be extrapolated for this case. At the same time, the measured temperatures vary greatly depending on the specific measurement location. Unfortunately, there was no thermal camera available, but with the help of a laser thermometer, most of the surface area could be examined relatively well, even in places that were hard to reach with thermocouple. Surface temperatures changed continuously in the measured interval and reached extreme values only in small sections. For this reason, the average value of the interval will be taken as the surface temperature, and the air parameters in the boundary layer (BL) will be determined for the average temperature of the wall surface and the surrounding air. Temperature averages, including surface and boundary layer temperature averages, are summarized in table 3.12.

Time	**Lid (°C)**	**Shell (°C)**	**Bot. (°C)**	**FGP (°C)**	**QT (°C)**
Preheating	$\in (35, 55)$	≈ 20	$\in (20, 60)$	$\in (30, 35)$	$\in (20, 30)$
PT ON	$\in (35, 55)$	≈ 20	$\in (20, 60)$	$\in (30, 35)$	$\in (20, 30)$
After 2 h	$\in (40, 80)$	$\in (20, 30)$	$\in (25, 60)$	$\in (20, 85)$	$\in (25, 45)$
After 3 h	$\in (40, 95)$	$\in (20, 30)$	$\in (25, 70)$	$\in (25, 120)$	$\in (35, 200)$
After 4 h	$\in (50, 100)$	$\in (20, 30)$	$\in (25, 70)$	$\in (30, 140)$	$\in (50, 250)$
After 5 h	$\in (55, 120)$	$\in (25, 40)$	$\in (30, 80)$	$\in (40, 200)$	$\in (70, 260)$
PT OFF	$\in (55, 120)$	$\in (25, 40)$	$\in (30, 80)$	$\in (40, 200)$	$\in (70, 260)$

Table 3.11: Intervals of measured temperature values of the reactor parts surfaces

Now, the heat transfer coefficients α $(\mathrm{W \cdot m^{-2} \cdot K^{-1}})$ are necessary to specify. Since in the general theory of heat transfer, α depends on countless quantities, in this thesis, similarly to other practical technical calculations, α will be determined using the Nusselt similarity number Nu, which indicates the ratio between convective and conductive heat transfer at a boundary in a fluid. Nu is defined by: [35]

$$\mathrm{Nu} = \alpha \cdot \frac{D_{\mathrm{char}}}{\lambda} \qquad \rightarrow \qquad \alpha = \mathrm{Nu} \cdot \frac{\lambda}{D_{\mathrm{char}}} \tag{3.23}$$

where Nu $(-)$ is the Nusselt number, λ $(\mathrm{W \cdot m^{-1} \cdot K^{-1}})$ is thermal conductivity of a fluid and D_{char} (m) is the characteristic length. Usually, the characteristic length is determined as the ratio between volume and surface for 3D objects. For 2D object analysis, it is often stated as the ratio between the area and the perimeter, or for some cases, also as the square root of the area, for instance. For upcoming calculations in this thesis, D_{char} for flat surfaces will be the ratio between area and perimeter, for vertical cylinders it will be the height, and for horizontal cylinders the diameter. [36]

Depending on the state of the airflow, the following relationships apply:

- $\mathrm{Nu} = f(\mathrm{Pr}, \mathrm{Gr})$ for free convection and
- $\mathrm{Nu} = f(\mathrm{Pr}, \mathrm{Re})$ for forced convection.

Because of different geometries and temperatures, the Nusselt number (and the heat transfer coefficient accordingly) is necessary to determine individually for each part of the facility.

Pr (−) is the Prandtl number defined as the ratio of momentum diffusivity to thermal diffusivity, Gr (−) is the Grashof number representing the estimate of the ratio of the buoyancy to viscous forces acting on a fluid and Re (−) is the Reynolds number, describing the ratio between inertial and viscous forces. The number Ra (−), which often occurs in empirical model formulas (especially for natural convection), is the Rayleigh number, defined as the product of the numbers Pr and Gr. Written in the equations: [35]

$$\mathrm{Pr} = \frac{\mu \cdot c_p}{\lambda} \tag{3.24}$$

$$\mathrm{Gr} = \frac{g \cdot \beta \cdot (T_s - T_{\mathrm{air}}) \cdot D_{\mathrm{char}}^3}{\nu^2} \tag{3.25}$$

$$\mathrm{Re} = \frac{u \cdot D_{\mathrm{char}}}{\nu} = \frac{\rho \cdot u \cdot D_{\mathrm{char}}}{\mu} \tag{3.26}$$

$$\mathrm{Ra} = \mathrm{Pr} \cdot \mathrm{Gr} \tag{3.27}$$

where μ ($\mathrm{N \cdot s \cdot m^{-2}}$) is dynamic viscosity, c_p ($\mathrm{J \cdot kg^{-1} \cdot K^{-1}}$) is specific heat (of the fluid), λ ($\mathrm{W \cdot m^{-1} \cdot K^{-1}}$) is thermal conductivity, g ($\mathrm{m \cdot s^{-2}}$) is gravitational acceleration (in respect to Earth), β ($\mathrm{K^{-1}}$) is coefficient of thermal volume expansion, T_s (K) and T_{air} (K) are the temperature of the surface and bulk (air) temperature, D_{char} (m) is characteristic length, ν ($\mathrm{m^2 \cdot s^{-1}}$) is kinematic viscosity, u ($\mathrm{m \cdot s^{-1}}$) is the velocity of the fluid and finally ρ ($\mathrm{kg \cdot m^{-3}}$) is the density of the fluid.

For the purposes of heat losses computation, the convection will be limited to free (natural) convection, especially also because of the:

- location of individual components,
- overall layout of the laboratory
- unavailability of specific information necessary for calculation like:
  - temperatures of the wall surfaces during the analyzed experiments
  - knowledge of air flows and temperatures

Note: Forced convection can briefly occur as a consequence of the movement of people nearby the reactor or the flow of air caused by open windows. Despite the open windows, the main draft of air would lead towards the door of the laboratory and not towards the reactor or the rest of the facility. Moreover, the components are relatively close to each other and most of the equipment is shaded from windows by a large-volume filter, which blocks the airflow with its size.

In the following calculations of the similarity numbers introduced by equations 3.23 - 3.27, thermodynamic properties of air take an important place. All these properties will be assessed in relation to temperature, specifically:

- density ρ ($\mathrm{kg \cdot m^{-3}}$) and thermal volume expansion β ($\mathrm{K^{-1}}$),
- dynamic viscosity μ ($\mathrm{kg \cdot m^{-1} \cdot s^{-1}}$) and kinematic viscosity ν ($\mathrm{m^2 \cdot s^{-1}}$),
- specific heat c_p ($\mathrm{kJ \cdot kg^{-1} \cdot K^{-1}}$) and thermal conductivity λ ($\mathrm{W \cdot m^{-1} \cdot K^{-1}}$).

Because the surface temperature of the wall is different for each part of the reactor, air properties will be assessed individually for each computed part of the reactor, respectively for the similarity numbers calculated for specific cases of heat transfer. In general, the temperature of the air (or the fluid respectively) in the boundary layer T_{BL} is considered as the mean value of the temperature of the wall surface and the ambient air (or the fluid respectively):

$$T_{\mathrm{BL}_X} = \frac{T_{\mathrm{surface}_X} + T_{\mathrm{air}}}{2} \tag{3.28}$$

For simplicity, T_{air} will be taken as constant. T_{surface_X} will be substituted by average value of T_{lid}, T_{shell}, T_{bottom}, T_{FGP} or T_{QT} for individual cases. Surface temperature averages and boundary layer temperature averages are summarized in table 3.12.

T_X	**Lid (°C)**	**Shell (°C)**	**Bot. (°C)**	**FGP (°C)**	**QT (°C)**
T_{avg_X}	88	33	55	120	165
T_{air_X}	20	20	20	20	20
T_{BL_X}	54	26	38	70	93

Table 3.12: Temperature averages of the surfaces and boundary layers (BL)

For clarity and space-saving, numerical values of the mentioned air physical quantities will not be inserted in repeated calculations (value differences are minor for individual cases). The specific values were obtained from the interpolation functions shown on graphs in figure 3.30, which were plotted based on the tables of air properties in relation to temperature from [37, 38, 39, 40].

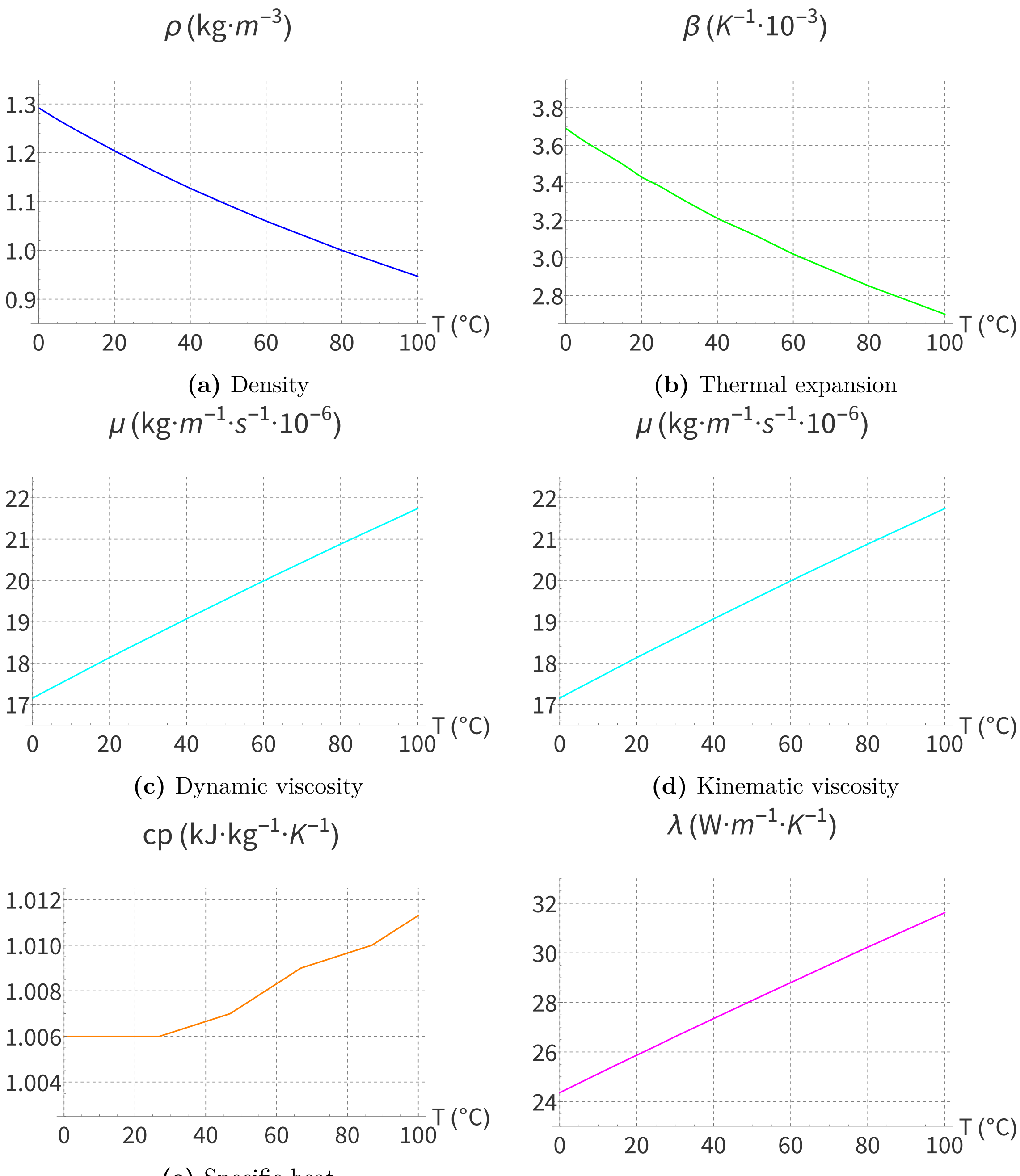

(a) Density **(b)** Thermal expansion **(c)** Dynamic viscosity **(d)** Kinematic viscosity **(e)** Specific heat **(f)** Thermal conductivity

Figure 3.30: Properties of air in relation to temperature

3.3.4.1 Lid

From now on, the calculations will be divided into further subsections depending on the part of the system for the purposes of better orientation. Beginning with the lid, this represents a horizontal plane inclined by $\delta = 20°$. According to the table 3.12, the average lid temperature during the experiment was measured at about 88 °C. The heat loss through the lid during the experiment will be expressed as the sum of convective heat losses and radiation heat losses, which also applies to thermal powers of these losses:

$$\begin{aligned} Q_{\text{lid}} &= Q_{\text{lid}_\text{R}} + Q_{\text{lid}_\text{C}} \\ \dot{Q}_{\text{lid}} &= \dot{Q}_{\text{lid}_\text{R}} + \dot{Q}_{\text{lid}_\text{C}} \end{aligned} \tag{3.29}$$

For radiation:

$$Q_{\text{lid}_\text{R}} = \dot{Q}_{\text{lid}_\text{R}} \cdot \Delta t \tag{3.30}$$

where:

$$\dot{Q}_{\text{lid}_\text{R}} = \sigma \cdot \varepsilon_{\text{RE}} \cdot A_1 \cdot ((T_{\text{lid}} + 273)^4 - (T_{\text{air}} + 273)^4) \tag{3.31}$$

where σ ($\text{W} \cdot \text{m}^{-2} \cdot \text{K}^{-4}$) is Stefan–Boltzmann constant and ε ($-$) is the emissivity of the surface. Since the temperatures are stated in °C, it is necessary to convert them into K. Most of the reactor and flue gas pipe surface is made of heat-resistant steel, most often type P265GH non-alloy steel. The majority of the quenching tower shell (about 2/3) then consists of a smooth, shiny aluminum sheet with mesh (the remaining part of the quenching tower surface is similar to the reactor surface). The exact emissivity values of these materials are not known. The estimation of the aluminum part is quite simple. Emissivity ranges from 0.05 for a polished sheet to 0.25 for oxidized aluminum. Since the aluminum casing around the cooling tower is polished, but also partially oxidized with the appearance of occasional impurities (and at the same time it is bent into the shape of a cylinder), the emissivity of aluminum for the calculation of radiation losses will be determined as the average of these values, therefore $\varepsilon_{\text{Al}} = 0.15$. Estimation of the emissivity value for unalloyed steel is a little more challenging. Polished steel sheets can have an emissivity similar to aluminum, about 0.1-0.2. If the steel has a rough surface, it can have an emissivity from around 0.7 to 0.9. Oxidation of the surface also greatly increases the emissivity, heavily oxidized steel can have an emissivity of up to 0.96. Since the surface of the reactor is matte in most places (therefore probably also oxidized), the emissivity value will be selected from the interval (0.70, 0.96). The average of marginal values of the interval will be used for the calculation, therefore $\varepsilon_{\text{RE}} = 0.83$. A better estimate is probably not possible. (QT will be discussed in more detail in 3.3.4.5.) Because $\sigma \approx 5.67 \cdot 10^{-8}$, radiation heat losses of the lid are approximately: [41, 42, 43]

$$\dot{Q}_{\text{lid}_\text{R}} = 5.67 \cdot 10^{-8} \cdot 0.83 \cdot 1.04 \cdot ((88 + 273)^4 - (20 + 273)^4) = 469.93 \text{ W} \tag{3.32}$$

Convective heat losses calculation is a little more complicated, because of the heat transfer coefficient α:

$$Q_{\text{lid}_\text{C}} = \dot{Q}_{\text{lid}_\text{C}} \cdot \Delta t = \dot{q} \cdot A_1 \cdot \Delta t = \alpha \cdot (T_{\text{lid}} - T_{\text{air}}) \cdot A_1 \cdot \Delta t \tag{3.33}$$

To determine the heat transfer coefficient at the boundary layer of the lid to the 3.33 formula above, it is necessary to find the values of similarity numbers starting with Pr and Gr. (For clarity, surface indexes will not follow after the BL index, individual BL temperatures are unambiguous thanks to the calculation division.)

$$\text{Pr}_1(T_{\text{BL}}) = \frac{\mu(T_{\text{BL}}) \cdot c_p(T_{\text{BL}})}{\lambda(T_{\text{BL}})} = \frac{19.7 \cdot 10^{-6} \cdot 1.01 \cdot 10^3}{28.37 \cdot 10^{-3}} = 0.700 \tag{3.34}$$

$$\begin{aligned} \text{Gr}_1(T_{\text{BL}}) &= \frac{g \cdot \beta(T_{\text{BL}}) \cdot (T_{\text{lid}} - T_{\text{air}}) \cdot D_{\text{char}}^3}{\nu(T_{\text{BL}})^2} = \\ &= \frac{9.81 \cdot 3.08 \cdot 10^{-3} \cdot (88 - 20) \cdot 0.29^3}{(18.27 \cdot 10^{-6})^2} = 1.46 \cdot 10^8 \end{aligned} \tag{3.35}$$

where:

$$D_{\text{char}} = D_{\text{char}_\text{lid}} = \frac{\pi \cdot r_{\text{lid}}^2}{2 \cdot \pi \cdot r_{\text{lid}}} \tag{3.36}$$

The inclination of the surface by $\delta = 20°$ can be included in the computation by modifying the Rayleigh number as follows: [35]

$$\mathrm{Ra}_{\delta 1} = \mathrm{Ra}_1 \cdot \cos(\delta) = \mathrm{Pr}_1 \cdot \mathrm{Gr}_1 \cdot \cos(\alpha) = 0.70 \cdot 1.46 \cdot 10^8 \cdot \cos(20°) = 9.62 \cdot 10^7 \quad (3.37)$$

Nusselt number for the horizontal plane: [44]

$$\mathrm{Nu}_1 = 0.15 \cdot \mathrm{Ra}_\delta^{1/3} = 0.15 \cdot (9.62 \cdot 10^7)^{1/3} = 68.74 \quad \text{for } \mathrm{Ra}_\delta \in (10^7, 10^{11}) \quad (3.38)$$

From the above relations, it is possible to substitute into the equation of $\mathrm{Nu} = f(\mathrm{Pr}, \mathrm{Gr}, ...)$ and express the heat transfer coefficient alpha from the default relation $\alpha = f(\mathrm{Nu})$ from the beginning of the chapter:

$$\alpha_1 = \mathrm{Nu} \cdot \frac{\lambda(T_{\mathrm{BL}})}{D_{\mathrm{char1}}} = 68.74 \cdot \frac{28.39 \cdot 10^{-3}}{0.29} = 6.73 \text{ W} \cdot \text{m}^{-2} \cdot \text{K}^{-1} \quad (3.39)$$

The convective heat loss power through the lid:

$$\dot{Q}_{\mathrm{lid_C}} = \alpha_1 \cdot A_1 \cdot (T_{\mathrm{lid}} - T_{\mathrm{air}}) = 6.73 \cdot 1.04 \cdot (88 - 20) = 479.06 \text{ W} \quad (3.40)$$

For both heat power losses:

$$\dot{Q}_{\mathrm{lid}} = 469.93 + 479.06 = 948.99 \text{ W} \quad (3.41)$$

Since each experiment takes a different time, the total losses will only be determined by substituting the total heat loss power into the following equation:

$$Q_{\mathrm{lid}} = \dot{Q}_{\mathrm{lid}} \cdot \Delta t = \dot{Q}_{\mathrm{lid}} \cdot (t_{\max} - t_{\min}) \quad (3.42)$$

Or in general for remaining surfaces:

$$Q_X = \dot{Q}_X \cdot \Delta t = \dot{Q}_X \cdot (t_{\max} - t_{\min}) \quad (3.43)$$

For reasons of savings, calculation of all similarity numbers Pr, Gr, and Ra (or Ra_δ) for the following surfaces will not take place, because the calculations are analogical. The summary of the resulting similarity numbers for the individual surfaces of the entire system is summarized in table 3.13.

Surface	**Pr**	**Gr**	**Ra**	**Ra$_\delta$**
Lid	0.700	$1.46 \cdot 10^8$	$1.02 \cdot 10^8$	$9.62 \cdot 10^7$
Shell	0.704	$3.11 \cdot 10^9$	$2.19 \cdot 10^9$	-
Bottom	0.702	$6.16 \cdot 10^7$	$4.33 \cdot 10^7$	$4.07 \cdot 10^7$
FGP	0.699	$1.44 \cdot 10^8$	$1.00 \cdot 10^8$	-
QT	0.696	$5.29 \cdot 10^8$	$3.68 \cdot 10^8$	-

Table 3.13: Similarity numbers for different surfaces

3.3.4.2 Shell

Heat power losses through the reactor shell:

$$\dot{Q}_{\text{shell}} = \dot{Q}_{\text{shell}_\text{R}} + \dot{Q}_{\text{shell}_\text{C}} \tag{3.44}$$

Radiation is defined by an identical equation for all parts of the reactor, therefore the following computation of radiation losses will always be performed at the beginning.

$$\begin{aligned}\dot{Q}_{\text{shell}_\text{R}} &= \sigma \cdot \varepsilon_{\text{RE}} \cdot A_2 \cdot ((T_{\text{shell}} + 273)^4 - (T_{\text{air}} + 273)^4) = \\ &= 5.67 \cdot 10^{-8} \cdot 0.83 \cdot 4.08 \cdot ((33 + 273)^4 - (20 + 273)^4) = 268.51 \text{ W}\end{aligned} \tag{3.45}$$

Similarly, as with the rest of the similarity numbers, the Nusselt number is necessary to compute individually for each part of the system. Moreover, the Nu will be based on a different empirical formula, because the subject of the calculation has a different geometric shape (and temperature).

Subject to the following limit: [45]

$$\frac{d}{h} = \frac{1.073}{1.211} = 0.89 \geq \frac{35}{\text{Gr}^{1/4}} = \frac{35}{(3.11 \cdot 10^9)^{1/4}} = 0.15 \tag{3.46}$$

the Nu for a vertical cylinder can be stated: [45]

$$\begin{aligned}\text{Nu}_2 &= \frac{4}{3} \cdot \left(\frac{7 \cdot \text{Gr} \cdot \text{Pr}^2}{5 \cdot (20 + 21 \cdot \text{Pr})}\right)^{1/4} + \frac{4 \cdot (272 + 315 \cdot \text{Pr}) \cdot h}{35 \cdot (64 + 63 \cdot \text{Pr}) \cdot d} = \\ &= \frac{4}{3} \cdot \left(\frac{7 \cdot 3.11 \cdot 10^9 \cdot (0.704)^2}{5 \cdot (20 + 21 \cdot 0.704)}\right)^{1/4} + \frac{4 \cdot (272 + 315 \cdot 0.704) \cdot 1.211}{35 \cdot (64 + 63 \cdot 0.704) \cdot 1.073} = \\ &= 118.87\end{aligned} \tag{3.47}$$

The relation for the heat transfer coefficient of the convective heat loss of the reactor cylindrical shell can be written again:

$$\alpha_2 = \text{Nu}_2 \cdot \frac{\lambda(T_{\text{BL}})}{D_{\text{char2}}} = 118.87 \cdot \frac{26.35 \cdot 10^{-3}}{1.211} = 2.59 \text{ W} \cdot \text{m}^{-2} \cdot \text{K}^{-1} \tag{3.48}$$

Convective heat losses of the shell:

$$\dot{Q}_{\text{shell}_\text{C}} = \alpha_2 \cdot A_2 \cdot (T_{\text{shell}} - T_{\text{air}}) = 2.59 \cdot 4.08 \cdot (33 - 20) = 137.28 \text{ W} \tag{3.49}$$

Total heat power losses of the shell are then:

$$\dot{Q}_{\text{shell}} = 268.51 + 137.28 = 405.79 \text{ W} \tag{3.50}$$

3.3.4.3 Bottom

Heat power losses through the bottom of the reactor:

$$\dot{Q}_{\text{bottom}} = \dot{Q}_{\text{bottom}_\text{R}} + \dot{Q}_{\text{bottom}_\text{C}} \tag{3.51}$$

where again:

$$\begin{aligned}\dot{Q}_{\text{bottom}_\text{R}} &= \sigma \cdot \varepsilon_{\text{RE}} \cdot A_3 \cdot ((T_{\text{bottom}} + 273)^4 - (T_{\text{air}} + 273)^4) = \\ &= 5.67 \cdot 10^{-8} \cdot 0.83 \cdot 0.78 \cdot ((55 + 273)^4 - (20 + 273)^4) = 154.16 \text{ W}\end{aligned} \tag{3.52}$$

Similar to the top lid, the bottom of the reactor can be considered an inclined plane, neglecting the presence of the slag container. (The slag container further complicates the overall geometry of the entire system, but the result of the total heat loss calculation should not differ greatly.) From the computational point of view in comparison to the lid, the difference is the direction of the surface normal to the cooler ambiance. While the lid is cooled from above, the bottom is cooled from below. The computational empirical formula is similar but has different coefficients.

Again to account for the effect of incline angle: [35]

$$\text{Ra}_{\delta 3} = \text{Ra}_3 \cdot \cos(\delta) = \text{Pr}_3 \cdot \text{Gr}_3 \cdot \cos(\delta) = 0.702 \cdot 6.16 \cdot 10^7 \cdot \cos(20°) = 4.07 \cdot 10^7 \tag{3.53}$$

The following relation can be written according to [44]:

$$\text{Nu}_3 = 0.52 \cdot \text{Ra}_\delta^{1/5} = 0.52 \cdot \left(4.07 \cdot 10^7\right)^{1/5} = 17.29 \tag{3.54}$$

Heat transfer coefficient for the bottom of the reactor:

$$\alpha_3 = \text{Nu}_3 \cdot \frac{\lambda(T_{\text{BL}})}{D_{\text{char3}}} = 17.29 \cdot \frac{27.17 \cdot 10^{-3}}{0.25} = 1.89 \text{ W} \cdot \text{m}^{-2} \cdot \text{K}^{-1} \tag{3.55}$$

where again:

$$D_{\text{char}} = D_{\text{char}_\text{bottom}} = \frac{\pi \cdot r_{\text{bottom}}^2}{2 \cdot \pi \cdot r_{\text{bottom}}} \tag{3.56}$$

Convective heat losses through the bottom of the reactor:

$$\dot{Q}_{\text{bottom}_\text{C}} = \alpha_3 \cdot A_3 \cdot (T_{\text{bottom}} - T_{\text{air}}) = 1.89 \cdot 0.78 \cdot (55 - 20) = 51.45 \text{ W} \tag{3.57}$$

Total heat loss through the bottom of the reactor:

$$\dot{Q}_{\text{bottom}} = 154.16 + 51.45 = 205.61 \text{ W} \tag{3.58}$$

3.3.4.4 Flue gas pipe

For flue gas pipe heat losses:

$$\dot{Q}_{\text{FGP}} = \dot{Q}_{\text{FGP}_\text{R}} + \dot{Q}_{\text{FGP}_\text{C}} \tag{3.59}$$

Again for radiation:

$$\begin{aligned}\dot{Q}_{\text{FGP}_\text{R}} &= \sigma \cdot \varepsilon_{\text{RE}} \cdot A_{\text{FGP}} \cdot ((T_{\text{FGP}} + 273)^4 - (T_{\text{air}} + 273)^4) = \\ &= 5.67 \cdot 10^{-8} \cdot 0.83 \cdot 0.47 \cdot ((120 + 273)^4 - (20 + 273)^4) = 361.92 \text{ W}\end{aligned} \tag{3.60}$$

From a geometric point of view, the flue gas pipe is a horizontal cylinder. For horizontal cylinders based on [46] applies:

$$\text{Nu}_{\text{FGP}} = \left(0.6 + \frac{0.387 \cdot \text{Ra}^{1/6}}{\left(1 + \left(\frac{0.559}{\text{Pr}}\right)^{9/16}\right)^{8/27}}\right)^2 = \left(0.6 + \frac{0.387 \cdot (1 \cdot 10^8)^{1/6}}{\left(1 + \left(\frac{0.559}{0.699}\right)^{9/16}\right)^{8/27}}\right)^2 = 56.50 \tag{3.61}$$

Heat transfer coefficient and convective heat losses for flue gas pipe:

$$\alpha_{\mathrm{FGP}} = \mathrm{Nu}_{\mathrm{FGP}} \cdot \frac{\lambda(T_{\mathrm{BL}})}{D_{\mathrm{charFGP}}} = 56.50 \cdot \frac{29.52 \cdot 10^{-3}}{0.27} = 6.18\ \mathrm{W} \cdot \mathrm{m}^{-2} \cdot \mathrm{K}^{-1} \tag{3.62}$$

$$\dot{Q}_{\mathrm{FGP_C}} = \alpha_{\mathrm{FGP}} \cdot A_{\mathrm{FGP}} \cdot (T_{\mathrm{FGP}} - T_{\mathrm{air}}) = 6.18 \cdot 0.47 \cdot (120 - 20) = 288.12\ \mathrm{W} \tag{3.63}$$

Heat loss of the flue gas pipe:

$$\dot{Q}_{\mathrm{FGP}} = 361.92 + 288.12 = 650.04\ \mathrm{W} \tag{3.64}$$

3.3.4.5 Quenching tower

Heat power losses of the quenching tower:

$$\dot{Q}_{\mathrm{QT}} = \dot{Q}_{\mathrm{QT_R}} + \dot{Q}_{\mathrm{QT_C}} \tag{3.65}$$

For radiation from the quenching tower, the surface will be divided into 2 parts differing by the material of the cover. Top $1/3$ of the surface has about the same emissivity as the rest of the facility $\varepsilon_{\mathrm{RE}}$, but the bottom $2/3$ of the surface is covered in aluminum with emissivity $\varepsilon_{\mathrm{Al}} \approx 0.15$. Consequently

$$\dot{Q}_{\mathrm{QT_R}} = \sigma \cdot \left(\frac{1}{3} \cdot \varepsilon_{\mathrm{RE}} + \frac{2}{3} \cdot \varepsilon_{\mathrm{Al}}\right) \cdot A_{\mathrm{QT}} \cdot ((T_{\mathrm{QT}} + 273)^4 - (T_{\mathrm{air}} + 273)^4) =$$
$$= 5.67 \cdot 10^{-8} \cdot (\frac{1}{3} \cdot 0.83 + \frac{2}{3} \cdot 0.15) \cdot 2.74 \cdot ((165 + 273)^4 - (20 + 273)^4) = 1721.63\ \mathrm{W} \tag{3.66}$$

Calculations of heat losses for the quenching tower will be concluded only for the case of energy balance from the RDF + MWPT experiment. It is evident from figure 3.25, that the thermocouple measuring the synthesis gas temperature in the flue gas pipe was not functional during the experiment. Therefore, it is necessary to work with the gas parameters after the exit from the quenching tower. This gets further complicated by the fact that part of the energy of the synthesis gas (in the form of heat) is transferred to the sprayed water inside the quenching tower, which must be included in the balance. However, an inaccurate calculation will not affect the calculation of the energy value of the gas in the form of calorific value, but rather the amount of energy in the form of heat that could be used as waste heat. For this reason, it is probably not necessary to calculate the energy balances in this manner for the other two experiments.

For the calculations of the quenching tower convective heat losses, similarly to the reactor shell, the object will be replaced by a simple geometric structure – a vertical cylinder. The following inequality limit for the calculation formula utilization does closely not apply: [45]

$$\frac{d}{h} = \frac{0.405}{1.950} = 0.21 \ngeq \frac{35}{\mathrm{Gr}^{1/4}} = \frac{35}{(5.29 \cdot 10^8)^{1/4}} = 0.23 \tag{3.67}$$

However, if the coefficient ξ defined by the following formula 3.68 is within interval $(0, 5)$ and Pr is within $(0.01, 100)$, the 3.69 equation can be used to calculate Nu. [45]

$$\xi = \frac{4 \cdot h}{d} \cdot \left(\frac{\mathrm{Gr}}{4}\right)^{-1/4} = \frac{4 \cdot 1.950}{0.405} \cdot \left(\frac{5.29 \cdot 10^8}{4}\right)^{-1/4} = 0.18 \tag{3.68}$$

$$\begin{aligned}
\mathrm{Nu_{QT}} &= \left(1+0.3\cdot\left(32^{1/2}\cdot \mathrm{Gr}^{-1/4}\cdot\frac{h}{d}\right)^{0.909}\right)\cdot\left(0.68+\frac{0.67\cdot \mathrm{Ra}^{1/4}}{\left(1+\left(\frac{0.492}{\mathrm{Pr}}\right)^{9/16}\right)^{4/9}}\right)=\\
&=\left(1+0.3\cdot\left(32^{1/2}\cdot\left(5.29\cdot 10^{8}\right)^{-1/4}\cdot\frac{1.950}{0.405}\right)^{0.909}\right)\cdot\left(0.68+\frac{0.67\cdot\left(3.68\cdot 10^{8}\right)^{1/4}}{\left(1+\left(\frac{0.492}{0.696}\right)^{9/16}\right)^{4/9}}\right)=\\
&=76.28
\end{aligned} \tag{3.69}$$

Therefore, the heat transfer coefficient and convective heat losses for the quenching tower:

$$\alpha_{\mathrm{QT}}=\mathrm{Nu_{QT}}\cdot\frac{\lambda(T_{\mathrm{BL}})}{D_{\mathrm{charQT}}}=76.28\cdot\frac{31.10\cdot 10^{-3}}{1.950}=1.23\ \mathrm{W\cdot m^{-2}\cdot K^{-1}} \tag{3.70}$$

$$\dot{Q}_{\mathrm{QT_C}}=\alpha_{\mathrm{QT}}\cdot A_{\mathrm{QT}}\cdot(T_{\mathrm{QT}}-T_{\mathrm{air}})=1.23\cdot 2.74\cdot(165-20)=483.08\ \mathrm{W} \tag{3.71}$$

And heat power losses of the quenching tower:

$$\dot{Q}_{\mathrm{QT}}=1721.63+483.08=2204.71\ W \tag{3.72}$$

It is interesting to notice that the losses of the quenching tower itself are similar to the losses of the rest of the apparatus. In summary, total heat losses for the energy balance of HPT experiments and MWPT experiment will be stated:

$$\begin{aligned}
\dot{Q}_{\mathrm{loss_{HPT}}} &= \dot{Q}_{\mathrm{lid}}+\dot{Q}_{\mathrm{shell}}+\dot{Q}_{\mathrm{bottom}}+\dot{Q}_{\mathrm{FGP}}=2.21\ \mathrm{kW}\\
\dot{Q}_{\mathrm{loss_{MWPT}}} &= \dot{Q}_{\mathrm{lid}}+\dot{Q}_{\mathrm{shell}}+\dot{Q}_{\mathrm{bottom}}+\dot{Q}_{\mathrm{FGP}}+\dot{Q}_{\mathrm{QT}}=4.42\ \mathrm{kW}
\end{aligned} \tag{3.73}$$

3.3.5 Heat accumulation

The exact determination of the accumulated heat in the reactor during the experiment is practically impossible, similar to the heat losses. Again, a 3D computational model of the reactor using for instance the finite element method and knowledge of the temperatures of the partial sections of the reactor could be used for a closer estimate. This would require considerable effort and calculation of that level is not necessary for the purposes of the thesis.

Although the temperatures in the reactor (respectively the walls of the reactor) are approximately known, given the following facts it is sufficient to simplify this case:

- most of the temperatures show a similar trend,
- the reactor is relatively symmetrical (in terms of layers and materials used),
- most of the accumulated heat will be in the inner part of the ceramic wall lining,
- individual specific heat capacities of the lining parts are not known.

However, in order to resolve the accumulated heat, the total specific heat capacity of the reactor must be known according to the following formula.

$$Q_{\text{accum}} = m_{\text{RE}} \cdot c_{p\text{RE}} \cdot \Delta T_{\text{RE}} \tag{3.74}$$

where $\Delta T_{\text{RE}} = (T_{\text{RE}}(t_{\max}) - T_{\text{RE}}(t_{\min}))$ is the difference of reactor temperatures at the beginning and the end of the experiment. Index RE represents the reactor.

The specific heat capacities of some materials were available in the reactor documentation. Specifically, for material JM30, the heat capacity at 1000 °C is $c_{p_{\text{JM30}}} = 1.1\ \text{kJ} \cdot \text{kg}^{-1} \cdot \text{K}^{-1}$. The lowest value found for other lining layers was $c_{p_{\min}} = 1.05\ \text{kJ} \cdot \text{kg}^{-1} \cdot \text{K}^{-1}$ and the highest $c_{p_{\max}} = 1.13\ \text{kJ} \cdot \text{kg}^{-1} \cdot \text{K}^{-1}$, this time without specifying the temperature. For some materials, specific heat capacity values were not available in the reactor documentation, but based on their name and type, the specific heat capacity can be found in technical sheets and documentation on selected websites. For instance, $c_{p_{\text{ALS}}} \in (1.04, 1.14)\ \text{kJ} \cdot \text{kg}^{-1} \cdot \text{K}^{-1}$ for ALSIFEX material and $c_{p_{\text{PROM}}} \in (0.86, 1.08)\ \text{kJ} \cdot \text{kg}^{-1} \cdot \text{K}^{-1}$ for PROMALIGHT material for $T \in (200,\ 800)$ °C. For the NOVOBET SPI-TAB material, only information about thermal conductivity was found. It was not possible to find relevant information about the rest of the materials, so it would be appropriate to try to verify the chosen value of the specific heat capacity of the reactor by calculation. [47, 48, 49]

For the case of heat accumulation, one common temperature of the reactor lining will be considered, which will be calculated using the following assumptions:

- temperature of the outer wall surfaces remains the same,
- (convective) heat losses remain the same,
- temperature of the inner wall will be taken as an average of the measured temperatures,
- the radial profile of the reactor will be considered homogeneous (important for the shape of the temperature curve),
- the resulting mean value of the reactor temperature will be calculated using the weighted temperature average (based on knowledge of the temperature curve shape, the inner and outer wall surface temperatures, and the total body volume)

For the average temperature of the reactor $T_{\text{RE}} = T_{\text{RE}_{\text{avg}}}$ as a whole applies $T_{\text{RE}_{\text{avg}}} \in (T_{\text{RE}_{\text{OUT}}}, T_{\text{RE}_{\text{IN}}})$. The outer wall temperature $T_{\text{surface}_{\text{OUT}}}$ will be determined as a weighted average of the outer temperatures of the parts and the proportional quantity will be the area. The inner wall temperature $T_{\text{RE}_{\text{IN}}}$ will be determined as a mean value of inner temperatures that are measured. Finally, the total average temperature of the reactor lining $T_{\text{RE}_{\text{avg}}}$ will be assessed based on the volume of the reactor lining as a proportional quantity. For the outer reactor wall surface:

$$\begin{aligned} T_{\text{RE}_{\text{OUT}}} &= \frac{T_{\text{lid}} \cdot A_1 + T_{\text{shell}} \cdot A_2 + T_{\text{bottom}} \cdot A_3}{\sum\limits_{i=1}^{3} A_i} = \\ &= \frac{88 \cdot 1.04 + 33 \cdot 4.08 + 55 \cdot 0.78}{5.9} = 45.6\ ^\circ\text{C} \end{aligned} \tag{3.75}$$

The temperature of the inner wall will be the average of the temperatures measured by 5 thermocouples and will be plotted discretely in time (for more, see the cooling curves in figures 3.31 and 3.32):

$$T_{\mathrm{RE_{IN}}}(t) = \frac{\sum_{i=1}^{5} T_{\mathrm{RE_{IN}}i}(t)}{5} \tag{3.76}$$

In order to estimate the average temperature of the reactor, it is necessary to assume that the lining is homogeneous. This assumption allows using the formula for the temperature curve through the cylindrical wall, knowing the boundary conditions - the temperatures of the walls inside ($T_{\mathrm{RE_{IN}}}$) and outside ($T_{\mathrm{RE_{OUT}}}$). For the temperature inside the homogenous cylindrical wall in the radius of r_x: [50]

$$T_x = T_{\mathrm{RE_{IN}}} - \frac{T_{\mathrm{RE_{IN}}} - T_{\mathrm{RE_{OUT}}}}{\ln\left(\frac{r_2}{r_1}\right)} \cdot \ln\left(\frac{r_x}{r_1}\right) \tag{3.77}$$

When using volume as a proportional quantity, the following equation should apply:

$$T_{\mathrm{RE_{avg}}} \cdot V_{\mathrm{RE}} = \int_{V_{\mathrm{REmin}}}^{V_{\mathrm{REmax}}} T_x \, dV_{\mathrm{RE}} \tag{3.78}$$

where V_{REmin} corresponds to the lowest radius r_{min} and the V_{REmax} corresponds to the highest radius r_{max}. For possible substitution of r_x for $V_{\mathrm{RE}x}$, the elementary volume increment of the cylinder needs to be expressed. According to the derivation of the volume substitution formula:

$$\frac{dV_{\mathrm{RE}}}{dr_x} = 2 \cdot \pi \cdot r_x \cdot h \quad \rightarrow \quad dV_{\mathrm{RE}} = 2 \cdot \pi \cdot r_x \cdot h \cdot dr_x \tag{3.79}$$

After expressing the $T_{\mathrm{RE_{avg}}}$ from the 3.78 equation, rewriting the limits, substituting for T_x and substituting for dV_{RE}:

$$T_{\mathrm{RE_{avg}}} = \frac{\displaystyle\int_{r_{\mathrm{min}}}^{r_{\mathrm{max}}} \left(\left(T_{\mathrm{RE_{IN}}} - \frac{T_{\mathrm{RE_{IN}}} - T_{\mathrm{RE_{OUT}}}}{\ln\left(\frac{r_2}{r_1}\right)} \cdot \ln\left(\frac{r_x}{r_1}\right) \right) \cdot 2 \cdot \pi \cdot r_x \cdot h \right) dr_x}{V_{\mathrm{RE}}} \tag{3.80}$$

Equation 3.80 is crucial for calculations of the reactor specific heat in the following subsection parts 3.3.5.1 and 3.3.5.2. Another complication is that the inner part of the bottom of the reactor is not empty, but there is also a wall lining. Therefore, the temperature relation will not only depend on the radius but also on the height. This would significantly complicate all the calculations. The height of the bottom lining is $\Delta h = h_{\mathrm{max}} - h_{\mathrm{min}} = 0.29$ m.

This is less than a quarter of the total height of the reactor. The supplementary volume of the inner part of the lining V_{sup} for $r_x < r_{\mathrm{min}}$ is:

$$V_{\mathrm{sup}} = \pi \cdot r_{\mathrm{min}}^2 \cdot \Delta h = \pi \cdot \left(\frac{0.533}{2}\right)^2 \cdot 0.29 = 0.065 \text{ m}^3 \tag{3.81}$$

The rest of the volume of the reactor is equal to:

$$V_{\mathrm{RE}} = \pi \cdot h \cdot (r_{\mathrm{max}}^2 - r_{\mathrm{min}}^2) = \pi \cdot 1.211 \cdot \left(\left(\frac{1.073}{2}\right)^2 - \left(\frac{0.533}{2}\right)^2\right) = 0.825 \text{ m}^3 \quad (3.82)$$

Total volume is:

$$\begin{aligned} V_{\mathrm{RE_{TOT}}} &= V_{\mathrm{RE}} + V_{\mathrm{sup}} = 0.825 + 0.065 = 0.890 \text{ m}^3 \\ &\rightarrow V_{\mathrm{RE}} = 0.927 \cdot V_{\mathrm{RE_{TOT}}} \\ &\rightarrow V_{\mathrm{sup}} = 0.073 \cdot V_{\mathrm{RE_{TOT}}} \end{aligned} \quad (3.83)$$

This means, that the V_{sup} is about 7 % of the total reactor volume $V_{\mathrm{RE_{TOT}}}$. Neglecting the change in the dependence of the reactor wall temperature on the radius in the area of the lower part of the lining will of course affect the overall calculation, but it will probably not cause a fatal deviation. In order for correct calculations in 3.78, 3.79 and 3.80, it is necessary that the volumes on both sides of the equation are equal. For this reason, the reactor volume V_{RE} will be used for further computation instead of $V_{\mathrm{RE_{TOT}}}$. This is another simplification which according to the 3.83 equation is acceptable. The volume of the reaction chamber is then:

$$V_{\mathrm{RE_{IN}}} = \pi \cdot r_{\mathrm{min}}^2 \cdot h_{\mathrm{min}} = \pi \cdot \left(\frac{0.533}{2}\right)^2 \cdot 0.921 = 0.21 \text{ m}^3 \quad (3.84)$$

3.3.5.1 Regular phase method

The specific heat capacity of a body can be estimated using the cooling curve, visible in figures 3.31 or 3.32. The cooling curve for the case of the reactor is the part of the temperature graph after the experiment, when the plasma torch is turned off, material or input gases to the reactor are no longer supplied, and reactions producing secondary raw materials, like synthesis gas, no longer occur. The theory of the solid body cooling process is described in [50] by the regular phase method under the following conditions:

- ambient temperature T_{air} & heat transfer coefficient α do not change over time,
- there are no internal heat sources in the body.

The cooling process can be divided into 3 parts:

  - state of disorderly march,
  - state of the regular phase and
  - state of thermal equilibrium.

The first state is a transient event depending on the initial temperature state. It generally has a random character, independent of the cooling conditions. The second state occurs after the passing of the transient initial state. The influence of the initial temperature state disappears and the law of the temperature change acquires a simple form of equation 3.85. The third state theoretically occurs in infinite time, practically in the case of balance between the temperatures of the body and the ambient fluid.

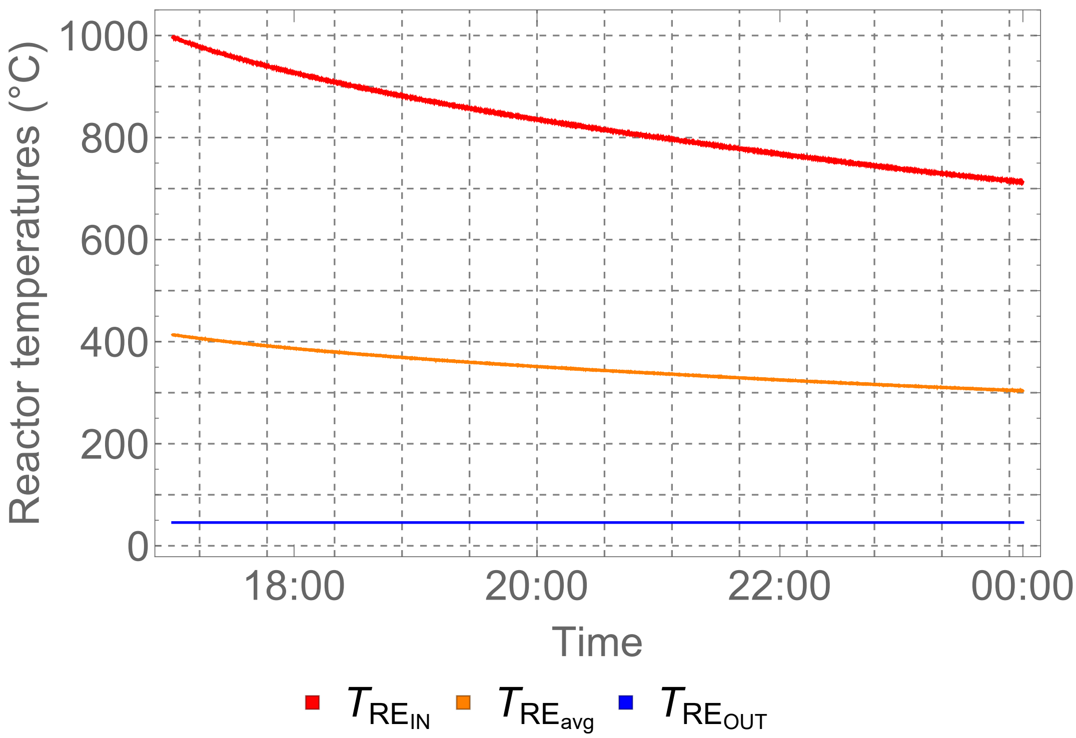

Figure 3.31: Temperatures of the reactor during regular phase method

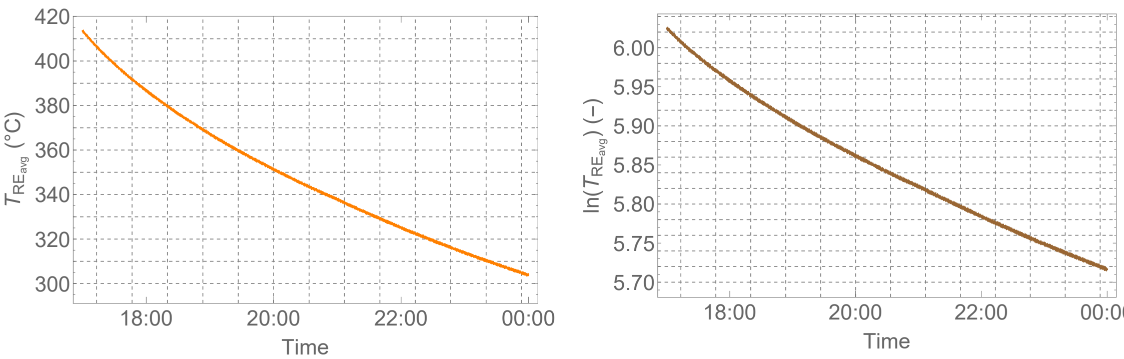

(a) $T_{\mathrm{RE_{avg}}}$

(b) $\ln\left(T_{\mathrm{RE_{avg}}}\right)$

Figure 3.32: Cooling curves of the $T_{\mathrm{RE_{avg}}}$ and $\ln\left(\mathrm{T_{RE_{avg}}}\right)$

During the regular phase, the excess temperature (T_{EX}) of the body changes according to the exponential law. Therefore the natural logarithm of the excess temperature changes linearly. Excess temperature means the difference between the temperature of the body (the mean value of the body temperature $T_{\mathrm{RE_{avg}}}$ will be considered) and the ambient air temperature. [50]

$$\ln\left(T_{\mathrm{EX}}(t)\right) = \ln\left(T_{\mathrm{RE_{avg}}}(t) - T_{\mathrm{air}}\right) = -\zeta \cdot t + \mathrm{C} \tag{3.85}$$

The temperature of the reactor is so high compared to the ambient temperature that it can simply be considered an excessive temperature for the beginning of the regular phase. Similarly for the logarithms.

$$T_{\mathrm{EX}}(t) \approx T_{\mathrm{RE_{avg}}}(t) \quad \& \quad \ln\left(T_{\mathrm{EX}}(t)\right) \approx \ln\left(T_{\mathrm{RE_{avg}}}(t)\right) \tag{3.86}$$

The number ζ (s^{-1} or h^{-1}) is a positive number characterizing the cooling rate and it is independent of the initial state of the temperature field. In essence, it is sufficient to know the course of temperatures (or the logarithm of excess temperatures) in the reactor during the cooling period, long enough after the end of the experiment. By deriving with respect to time, the 3.85 equation takes the following form:

$$\frac{\partial \ln \left(T_{\mathrm{EX}}(t)\right)}{\partial t} = -\zeta \tag{3.87}$$

Applying this relation to two-time instants (cooling curves), it is possible to find out the number ζ. It is important to follow the unit convention in the calculations. The minus sign corresponds to a decrease in body temperature.

From the general theory of solving the regular phase method of G. M. Kondratěv, the analytical relationship between the physical dependencies for the quantity ζ is based, from which the unknown variable - heat capacity of the body (the reactor) - can be directly expressed: [50]

$$\zeta = \psi \cdot A_{\mathrm{RE}} \cdot \frac{\alpha}{\left(c_{\mathrm{RE}}(T) \cdot m_{\mathrm{RE}}\right)} \tag{3.88}$$

The quantity ψ is dimensionless and physically indicates the degree of non-uniformity of the temperature field in the observed body. This quantity changes over time if the temperature of the wall is considered constant (theoretically limited from 0 to 1; 0 – the temperature of the wall surface is the same as the ambient temperature, 1 – a perfectly uniform distribution of temperatures). In order to simplify the calculation, the average value of the non-uniformity ψ_{avg} could be considered:

$$\psi_{\mathrm{avg}} = \frac{\left(\dfrac{T_{\mathrm{RE}_{\mathrm{OUT}}}}{T_{\mathrm{RE}_{\mathrm{avg}}}(t_1)} + \dfrac{T_{\mathrm{RE}_{\mathrm{OUT}}}}{T_{\mathrm{RE}_{\mathrm{avg}}}(t_2)}\right)}{2} \tag{3.89}$$

The quantity A_{RE} (m^2) in 3.88 then represents the surface of the outer wall of the cooled body, α ($W \cdot m^{-2} \cdot K^{-1}$) coefficient of heat transfer at the interface of the outer wall and the environment, m_{RE} (kg) the mass of the body and $c_{p\mathrm{RE}}$ ($kJ \cdot kg^{-1} \cdot K^{-1}$) the seeked specific heat capacity of the body. After rearrangement and substitution from the 3.88 equation, the specific heat capacity $c_{p\mathrm{RE}}$ can be expressed subsequently:

$$c_{\mathrm{RE}}(T) = \frac{\psi \cdot A_{\mathrm{RE}} \cdot \alpha}{m_{\mathrm{RE}} \cdot \dfrac{\partial \ln \left(T_{\mathrm{RE}_{\mathrm{avg}}}\right)}{\partial t}} \tag{3.90}$$

This differential equation can be adjusted by separating the variables and numerically solved based on the knowledge of the other independent quantities.

However, here comes a big issue. For safety reasons, the reactor is actively cooled with cooling water even after the end of the experiment, practically until the reactor nearly reaches the state of thermal equilibrium. Although the cooling power is smaller because of the lower flow rates of cooling water (and lower water temperature differences), it is not negligible from the perspective of the specific heat capacity of the reactor determination. Since the regular phase method assumes spontaneous cooling of the body, this method cannot be fully utilized (in addition, the influence of the cooling water layer significantly deforms the radial temperature profile in the region of the outer surface layer).

The inclusion of the cooling power into equation 3.90 is questionable. The situation is complicated by the logarithm of the ratio between the temperatures, which removes the temperature unit from the equation. Using apporpriate adjustments, the $\mathrm{W} \cdot \mathrm{K}^{-1}$ (or $\mathrm{W} \cdot {}^{\circ}\mathrm{C}^{-1}$) dimension can be achieved. In order to include the cooling power in the equation, it must be divided by some temperature, or the remaining elements of the equation must be multiplied by the temperature. Which temperature to choose (and under which conditions or assumptions) is ambiguous. Therefore, the computation of the specific heat capacity will be simplified by the following linearization.

3.3.5.2 Linearization

It is clear from figure 3.32, that the trend of the relations $T_{\mathrm{RE}_{\mathrm{avg}}} = f(t)$ and $\ln\left(T_{\mathrm{RE}_{\mathrm{avg}}}\right) = f(t)$ is practically identical, aspecially for a smaller scale. The linearization of temperatures on short time intervals can be done based on this similarity. This adjustment adds the temperature dimension to the 3.90 equation, which makes it possible to include the active cooling power.

Using the method of linearization, the cooling curve can be used to estimate the replacement total specific heat capacity. For reminder and explanation, the cooling curve is a part of the temperature graph after the experiment, when the plasma torch is turned off, material or input gases to the reactor are no longer supplied, and reactions producing secondary raw materials, like synthesis gas, no longer occur in the reactor. The only other way in which energy is drained away is by means of cooling water. Both temperature difference and volume flow of cooling water are measured and well known.

In this case, the only source of energy is the accumulated heat. This energy flows out of the reactor in two ways, namely as heat losses and waste heat carried away by cooling water. This state is described by the equation:

$$\dot{Q}_{\mathrm{OUT}} = \sum_{i=1}^{3} \dot{Q}_{\mathrm{loss}_i} + \dot{Q}_{\mathrm{W}} \tag{3.91}$$

where again, index $i = 1$ stands for the cover, $i = 2$ stands for the shell and $i = 3$ stands for the bottom of the reactor. (Indexes for other physical quantities in the following calculations are identical.) The sum can be rewritten into individual heat flows in the same way as in equations 3.20.

Note that this time the flue gas pipe and quenching tower are no longer part of a computation. Considering the size and weight of the reactor relative to the rest of the system, both the flue gas pipe and the quenching tower are neglected for the heat accumulation calculation. This, of course, makes a bigger computation deviation, but the component parameters, for example, temperatures, are not continuously measured. Furthermore, neither the flue gas pipe nor the quenching tower is cooled by water, so the accuracy of the calculation is completely dependent on the heat transfer calculations. For this reason, the calculation of the thermal capacities of flue gas pipe or quenching tower is practically impossible (and probably not that important).

From the inside perspective of the reactor balance during cooling down, the heat flow relation can also be expressed as:

$$\dot{Q}_{\mathrm{OUT}} = -m_{\mathrm{RE}} \cdot c_{p\mathrm{RE}}(T) \cdot \frac{dT}{dt} \tag{3.92}$$

The opposite sign indicates a decrease of the temperature of the reactor, accompanied by a decrease in accumulated energy. Moreover, the specific heat capacity of the reactor is important to find out only for a shorter temperature interval. With small temperature changes, thermal capacity change is not that significant. For simplification of equations and calculation, the specific heat capacity will be considered constant for now. Together:

$$-\, m_{\mathrm{RE}} \cdot c_{p\mathrm{RE}} \cdot \frac{dT}{dt} = \sum_{i=1}^{3} \dot{Q}_{\mathrm{loss}_i} + \dot{Q}_{\mathrm{W}} \tag{3.93}$$

Also, the heat can be accumulated in the inner chamber of the reactor, specifically in the air inside. Considering that the air has the same temperature as the inner walls during the regular phase method, the excess energy in this air in the form of heat at the beginning of the stabilized cooling will be:

$$\Delta Q_{\mathrm{RE_{air}}} = m_{\mathrm{RE_{air}}} \cdot c_{p_{\mathrm{air}}} \cdot (T_{\mathrm{RE_{IN}}} - T_{\mathrm{air}}) \tag{3.94}$$

$m_{\mathrm{RE_{air}}}$ (kg) is the mass of the air in the reactor, which can be calculated from the ideal gas equation of state by 3.14 and 3.15. Specific heat capacity $c_{p_{\mathrm{air}}}$ ($\mathrm{kJ \cdot kg^{-1} \cdot K^{-1}}$) will be determined as the average specific heat capacities for marginal temperatures and $(T_{\mathrm{RE_{IN}}} - T_{\mathrm{air}})$ (K or °C) is the temperature difference of the air inside and the air outside.

$$m_{\mathrm{RE_{air}}} = \frac{p \cdot V_{\mathrm{RE_{IN}}}}{\mathrm{R} \cdot T} \cdot \frac{M_{\mathrm{air}}}{1000} \tag{3.95}$$

Pressure p (Pa) will be atmospheric, $V_{\mathrm{RE_{IN}}} = 0.29\ \mathrm{m^3}$ according to 3.84, $\mathrm{R} = 8.314\ \mathrm{m^3 \cdot Pa \cdot K^{-1} \cdot mol^{-1}}$, T (K) will be taken as average of: [51]

- temperature at the beginning of the regular phase (996 °C, or 1269 K) and
- temperature at the theoretical thermal equilibrium (20 °C, or 293 K).

and $M_{\mathrm{air}} = 28.96\ \mathrm{g \cdot mol^{-1}}$ is the molar weight of air, thousand in the denominator is for the conversion g → kg. [52] Therefore:

$$m_{\mathrm{RE_{air}}} = \frac{10^5 \cdot 0.21}{8.314 \cdot 781} \cdot \frac{28.96}{1000} = 0.094\ \mathrm{m^3} \tag{3.96}$$

Mean value of $c_{p_{\mathrm{air}}}$ for marginal temperatures is about $1.083\ \mathrm{kJ \cdot kg^{-1} \cdot K^{-1}}$. Consequently:

$$\Delta Q_{\mathrm{RE_{air}}} \approx 0.094 \cdot 1.083 \cdot (996 - 20) = 99\ \mathrm{kJ} \approx 0.028\ \mathrm{kWh} \tag{3.97}$$

Although the calculation was simplified again by averaging the values of the physical quantities of air, it is noticeable that the inner part of the reaction chamber will almost have no influence on the total thermal capacity of the reactor.

The alleged excess energy inside the air in the reactor is less than 0,03 kWh, which is negligible both for the energy balance and for calculating the heat capacity of the reactor.

Under simplifying assumptions, equation 3.93 is a simple first-order linear differential equation and can be solved using, for example, the method of separation of variables. For simplicity, the independent variable (t) is not shown for quantities.

$$\int_{T(t_{\min})}^{T(t_{\max})} -m_{\mathrm{RE}} \cdot c_{p\mathrm{RE}}\, dT = \int_{t_{\min}}^{t_{\max}} \left(\sum_{i=1}^{3} \dot{Q}_{\mathrm{loss}_i} + \dot{Q}_{\mathrm{W}} \right) dt \tag{3.98}$$

Assuming that the specific heat capacity of the reactor does not change excessively in relation to temperature (which is comparably achieved for a solid ceramic lining), the equation can be further adjusted:

$$- m_{\mathrm{RE}} \cdot c_{p\mathrm{RE}} \int_{T(t_{\min})}^{T(t_{\max})} dT = \int_{t_{\min}}^{t_{\max}} \left(\sum_{i=1}^{3} \dot{Q}_{\mathrm{loss}_i} + \dot{Q}_{\mathrm{W}} \right) dt \tag{3.99}$$

The unknown here is the replacement specific heat capacity of the reactor. The following equation is obtained after the (numerical) integration:

$$c_{p\mathrm{RE}} = \frac{\sum_{j=1}^{\mathrm{N}} \left(\left(\sum_{i=1}^{3} \dot{Q}_{\mathrm{loss}_{ij}} + \dot{Q}_{\mathrm{W}_j} \right) \cdot \Delta t_j \right)}{m_{\mathrm{RE}} \cdot (T(t_{\min}) - T(t_{\max}))} \tag{3.100}$$

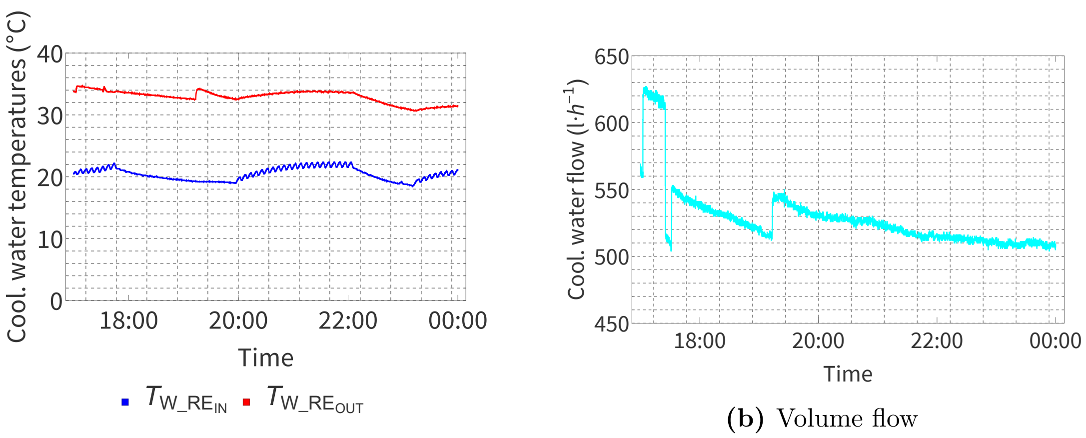

(a) Temperatures

(b) Volume flow

Figure 3.33: Cooling water during the regular phase

For even better linearization, the entire interval will be divided into subintervals of 1 hour, for which $c_{p\mathrm{RE}}$ will be determined separately. If the intervals were small enough, a relatively continuous relation of $c_{p\mathrm{RE}}(T)$ could be obtained, but it would be necessary to know exactly the convective (and radiation) heat losses, cooling power of water, and all the temperatures.

Because the overall heat losses will remain very similar (also because of the simplified estimation) for the course of the cooling, the resulting specific heat capacities of the reactor obtained by the calculation will be probably higher for lower temperatures of the reactor. This is caused by the smaller temperature differences of the reactor on the interval marginals over time. For this reason, the biggest accuracy of the calculation is estimated for the first interval, where the temperatures are closest to the operating temperatures. Practically, high-temperature ceramics usually have lower specific heat capacity for lower temperatures, as discussed earlier.

Figure 3.33 shows the temperatures and flow rate of the reactor cooling water during the regular cooling phase. Based on these courses, it can be assumed that the cooling capacity of the reactor is approximately constant (with the exception of the first interval, where the flow of cooling water was significantly higher).

The results of calculations of total losses (to the surroundings and to the water), average temperatures of the reactor including the temperature differences, and the final specific heat capacities are summarized in table 3.14 below.

Interval (h)	$T_{\mathrm{RE_{avg}}}(t_{\min})$ (°C)	$T_{\mathrm{RE_{avg}}}(t_{\max})$ (°C)	$\Delta T_{\mathrm{RE_{avg}}}$ (°C)	$Q_{\mathrm{loss}} + Q_{\mathrm{W}}$ (kWh)	$c_{p\mathrm{RE}}$ ($^{\mathrm{kJ}}/_{\mathrm{kg \cdot K}}$)
17 - 18	413.6	386.7	26.8	10.10	**1.13**
18 - 19	386.7	367.0	19.7	9.60	1.46
19 - 20	367.0	351.3	15.7	10.15	1.94
20 - 21	351.3	337.7	13.6	9.16	2.02
21 - 22	337.7	325.1	12.7	8.66	2.05
22 - 23	325.1	313.8	11.3	8.82	2.34
23 - 00	313.8	303.7	10.0	8.20	2.45

Table 3.14: Results of computation of the ΔT_{avg}, removed heat $Q_{\mathrm{loss}} + Q_{\mathrm{W}}$ and specific heat $c_{p\mathrm{RE}}$ for time intervals

It is evident from table 3.14 that the inaccuracy of the calculation really resulted in higher specific heat capacity of the reactor for lower temperatures. Consequently, the resulting value of the specific heat capacity of the reactor for the calculation of heat accumulation will be determined based on the value from the first interval. This also correlates well with the information obtained in the available documentation and websites.

Because the reactor temperatures during the experiment are a still little higher than during cooling down, the resulting specific heat capacity will be computed from an average of found values and the calculated value. Found values are for temperatures $T > 800$ °C in the interval (1.04, 1.14), where 1.09 is the mean value. Better accuracy of the $c_{p\mathrm{RE_{avg}}}$ estimation is probably not achievable at the moment. Therefore:

$$c_{p\mathrm{RE}_{\mathrm{avg}}} := \frac{1.09 + 1.13}{2} = 1.11\ \mathrm{kJ} \cdot \mathrm{kg}^{-1} \cdot \mathrm{K}^{-1} \tag{3.101}$$

3.3.6 Synthesis gas & carbon black (& slag)

Unlike the input gases, the output synthesis gas has already a high energy value. Ultimately, for this energy value, it is an effort to produce synthesis gas and optimize its composition. Practically, the output materials as the elements of energy balance are the most important and interesting part of the overall balance for the purposes of this thesis, specifically the synthesis gas energy - Q_{SG}. Moreover, there are elements like solid carbon (Q_{C}) and slag.

The calculation of the output material elements of the energy balance equation, unlike the heat-related elements, needs to be performed as accurately as possible, because a quality estimate is the basis for the final evaluation, for example of the energy conversion efficiency of the process or the competitiveness of this technology.

The energy of the slag element would appear in the default energy balance equation if the input processed material contained a significant part of the inorganic component. Although the slag cannot be further used energetically, it would be a non-zero output energy component because of its temperature (much higher than room temperature). This would be caused by absorbing part of the heat energy supplied by the plasma torch. This leaves less energy for the remaining thermochemical reactions, for instance for synthesis gas formation.

If the slag was being formed during the process, the output energy of the slag would be determined based on its quantity, temperature, and specific heat capacity. None of these quantities are known and under laboratory conditions, the slag part is practically not formed, therefore the slag can be neglected as a member of the energy balance.

Most often, solid carbon comes out of the process in the form of soot called carbon black. The energy of the output carbon black will be given by the sum of the internal energies of the carbon in both forms of chemical and thermal energy. Thus, knowing the weight of the soot produced:

$$Q_{\mathrm{C}} = m_{\mathrm{C}} \cdot H_{\mathrm{C}} + m_{\mathrm{C}} \cdot cp_{\mathrm{C}} \cdot \Delta T_{\mathrm{C}} \tag{3.102}$$

Since carbon black is practically homogenous from the energetic perspective, assessment of the energy value by equation 3.102 is quite sufficient. Based on the knowledge of the properties of carbon as a function of temperature, similar to the case of water, these parameters can be considered as constant, namely for the arithmetic mean of the temperature of the carbon at the outlet and the room temperature.

Specifying the temperature of the carbon at the outlet is remaining. Since most of the carbon black passes through the pipe system together with the gas mixture, it can be stated that the temperature of the carbon corresponds approximately to the temperature of the synthesis gas.

Considering the small amount of carbon black produced, both its calorific value and specific heat capacity will be considered as constant, namely $H_\mathrm{C} = 32.9\ \mathrm{MJ \cdot kg^{-1}}$ and $c_{p\mathrm{C}} = 0.71\ \mathrm{kJ \cdot kg^{-1} \cdot K^{-1}}$. [53, 54]

Because the weight of produced carbon black cannot be measured continuously during the experiment, it will be determined for each time interval from the law of conservation of mass:

$$m_\mathrm{C} = m_\mathrm{gas} + m_\mathrm{mat} - m_\mathrm{SG} \tag{3.103}$$

The most complicated output in terms of substances is the synthesis gas. In order to calculate the output energy of the synthesis gas, it is necessary to determine its composition. If it was homogeneous and consisted exclusively of one compound, the energy of the output gas could be expressed similarly to the case of solid carbon, consequently:

$$Q_\mathrm{SG} = m_\mathrm{SG} \cdot H_\mathrm{SG} + m_\mathrm{SG} \cdot c_{p\mathrm{SG}} \cdot \Delta T_\mathrm{SG} \tag{3.104}$$

However, synthesis gas is a mixture of gases. The concentration of the mixture changes during the experiment, same as its temperature (which both have significant effects on the resulting properties and the energy content). Not only will it be necessary to estimate its physical properties based on chemical analyses of its specific composition, but for each analyzed interval these properties must be estimated separately.

This complicated issue will be simplified by appropriate averaging of both the composition values for the considered interval and by averaging the gas temperature from the temperatures measured during the monitored interval. Generally for the energy of synthesis gas and for its individual components:

$$\begin{gathered} Q_\mathrm{SG} = \sum_{X=1}^{N} Q_X \\ Q_X = m_X \cdot H_X + m_X \cdot c_{pX} \left(\frac{T_\mathrm{SG} + T_\mathrm{ref}}{2} \right) \cdot (T_\mathrm{SG} - T_\mathrm{ref}) \end{gathered} \tag{3.105}$$

where T_SG (°C) is the average temperature of the synthesis gas and T_ref (°C) is reference temperature - the room temperature (20 °C).

To determine the component percentage representation of gases and compounds in the output synthesis gas mixture, a mass spectroscope is used. The chemical analyses of the gas samples are usually performed by chemical researchers at the IPP CAS.

Usually, the ambition during the experiment is to test several types of operating conditions, basically for the purposes of chemical analyses. Therefore, after the operating conditions change, a steady state is waited for. After a short period, the operating conditions are changed again. For this reason, information about the synthesis gas composition is only available for relatively short time intervals during which the process of gas formation (including its composition) can be considered as a steady state.

The gas composition cannot be extrapolated beyond the examined intervals of chemical analysis for energy balance purposes. Therefore, the resulting balances have to be quantified for specific time intervals of performed chemical analyses. This fact complicates the situation greatly. The entire facility of the plasma reactor is relatively extensive and the inertia of the processes (for example residence time of the material or gas in the reactor) can take a long time, usually even longer than the length of the evaluated intervals. As the length of the quantified interval decreases, the risk of bigger errors in the final balance greatly increases. The energy balance compiled for the entire duration of the experimental process is ideal. Unfortunately, this is not achievable because of the aforementioned impossibility of extrapolation.

In addition to the composition of the gas, it is also necessary to quantify the physical and chemical properties of the gas. For energy balance purposes, each of the synthesis gas components will be assessed separately and the result for the whole mixture will be given as the sum of the obtained values, specifically the energy value in the form of calorific value or heat stored in the specific heat capacity of the gas. This is an acceptable simplification.

The volume yield of the synthesis gas will be determined from the supplied calibration gas - inert argon. For the experiment with MWPT (stabilized by air), it is necessary to include argon supplied from the air. In general, the air composition will be simplified according to the table 3.15. [55]

Air component	**Nitrogen**	**Oxygen**	**Argon**
Representation	78 %	21 %	1 %

Table 3.15: Simplified air composition for balance calculations

The volume flow of the output synthesis gas after the calculation is available in standard liters per minute (slm). It is necessary to convert the slm to the real output volume flow, given by the difference in gas temperatures at the inlet and outlet. With the simplified assumption of an ideal gas, the conversion will be based on the equation of state as follows:

$$V_{\mathrm{OUT}} = V_2 = V_1 \cdot \frac{T_2}{T_1} = V_{\mathrm{IN}} \cdot \frac{T_{\mathrm{OUT}}}{T_{\mathrm{IN}}} \tag{3.106}$$

To determine the energy content of the synthesis gas, the weight of the gas will be used. The total weight of individual gas components will be expressed by the product of its substance quantity and molar mass. The substance quantity will be expressed from the equation of state. To quantify the energy of the individual gas components, knowledge of calorific value and specific heat capacity is necessary. The calculation of the mass of the partial components of the synthesis gas is expressed by the equation 3.107. Summary of the values of molar masses and calorific values of occurring gases is summarized in table 3.16. [56, 57]

$$m_X = n_X \cdot M_X = \frac{p \cdot V_{\mathrm{OUT}_X}}{\mathrm{R} \cdot T_{\mathrm{OUT}}} \cdot M_X = \frac{p \cdot V_{\mathrm{IN}_X} \cdot \dfrac{T_{\mathrm{OUT}}}{T_{\mathrm{IN}}}}{\mathrm{R} \cdot T_{\mathrm{OUT}}} \cdot M_X = \frac{p \cdot V_{\mathrm{IN}_X}}{\mathrm{R} \cdot T_{\mathrm{IN}_X}} \cdot M_X \tag{3.107}$$

Note: By reason of trace amount of nitrogen oxides in the synthesis gas mixture during the MWPT experiment and not distinguishing these components in the chemical analysis, the average of the values of the chemical properties of both nitrogen oxides will be taken as their common chemical parameter.

Gas	H_2	CH_4	CO	N_2	NO	NO_2	O_2	CO_2	Ar
M $(\mathrm{g \cdot mol^{-1}})$	2.02	16.04	28.01	28.01	30.01	46.01	32.00	44.01	39.95
H $(\mathrm{MJ \cdot kg^{-1}})$	120.09	49.85	10.16	-	-	-	-	-	-

Table 3.16: Molar masses M_X and calorific values H_X of gases

The specific heat capacity of gases is highly dependent on their temperature, therefore it will be determined for the mean value of the gas temperature for the given analyzed time interval (for each interval of chemical analysis individually). This is an acceptable simplification because, within the range of the intervals, the temperature changes of the output gas are not that significant. The specific heat capacity values will be determined on the basis of interpolations visible in figures 3.34, which have been plotted on the basis of tabular data. [58, 59, 60, 61, 62, 63, 64, 65, 66].

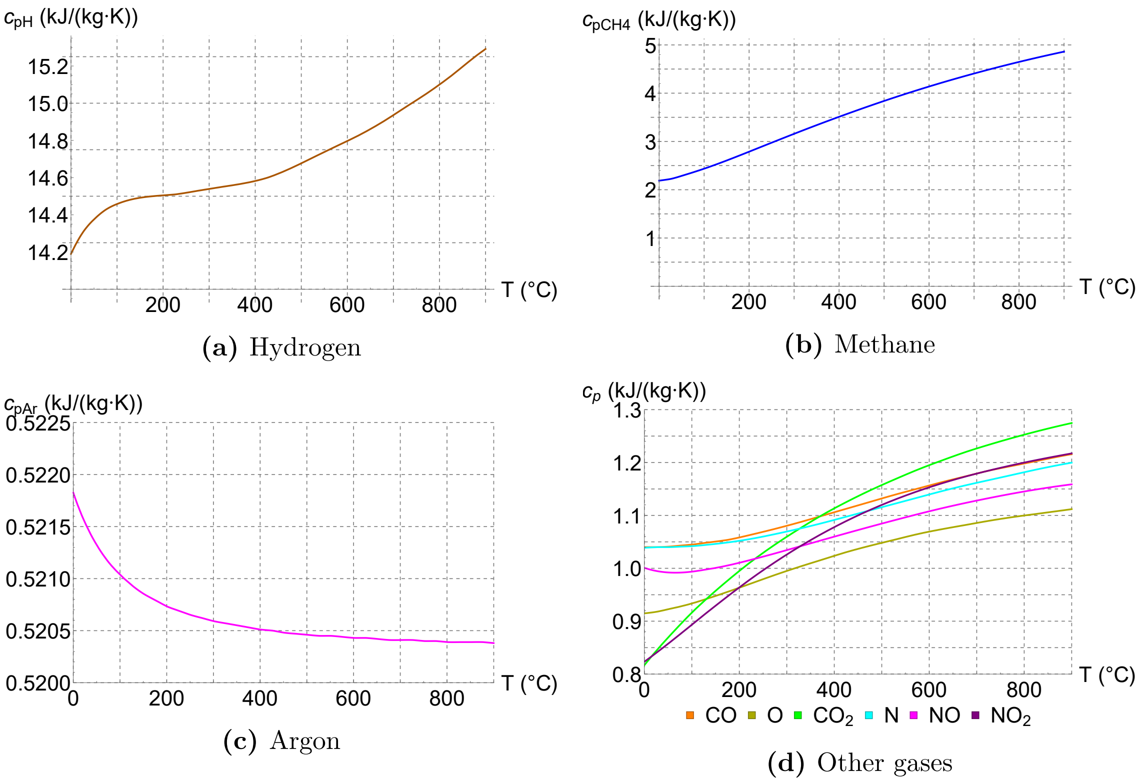

Figure 3.34: Interpolating functions for specific heat capacities of gases

3.4 Energy balances - results

3.4.1 SMW & HPT

Analysis number	**1.**	**2.**	**3.**	**4.**	**5.**
Interval duration	10 min	19 min	18 min	9 min	7 min
E_{el} (kWh)	29.85	50.32	43.99	21.31	16.26
Q_{mat} (kWh)	9.63	18.30	17.33	8.67	6.74
Q_{IN} SUM (kWh)	39.48	68.62	61.32	29.98	23.00
$Q_{\mathrm{W_{RE}}}$ (kWh)	4.47	7.75	7.43	3.77	2.95
$Q_{\mathrm{W_{PT}}}$ (kWh)	7.25	12.04	10.88	5.46	4.37
Q_{accum} (kWh)	-2.58	4.40	2.53	0.80	0.61
Q_{loss} (kWh)	0.37	0.70	0.66	0.33	0.26
Q_{SG} (kWh)	15.96	16.85	11.83	5.08	3.23
Q_{SG} (spec. heat) (kWh)	2.57	2.91	2.15	0.94	0.64
Q_{C} (kWh)	3.15	7.92	18.11	3.25	3.72
Q_{C} (spec. heat) (kWh)	0.07	0.19	0.45	0.08	0.09
Q_{OUT} SUM (kWh)	31.25	52.77	54.06	19.71	15.88
En. balance diff. (kWh)	8.23	15.85	7.26	10.27	7.13
Q for TCHR (kWh)	12.11	9.58	15.21	0.68	0.95
Energy utilization (%)	55.07	40.62	53.07	31.17	33.43
Conversion efficiency (%)	48.39	36.10	48.83	27.76	30.24
$(Q_{\mathrm{SG}} + Q_{\mathrm{C}})/Q_{\mathrm{mat}}$ (−)	1.98	1.35	1.73	0.96	1.03
Usable waste heat (kWh)	14.36	22.89	20.92	10.25	8.05
Usable waste heat (%)	36.37	33.36	34.12	34.18	35.02

Table 3.17: Summary of energy balance results for experiment with SMW & HPT

3.4.2 RDF & HPT

Analysis number	**1.**	**2.**	**3.**	**4.**
Interval duration	22 min	5 min	4 min	3 min
E_{el} (kWh)	57.98	12.65	8.99	6.35
Q_{mat} (kWh)	24.44	5.56	4.44	3.33
Q_{IN} SUM (kWh)	82.42	18.20	13.44	9.68
$Q_{\mathrm{W_{RE}}}$ (kWh)	7.66	1.81	1.52	1.16
$Q_{\mathrm{W_{PT}}}$ (kWh)	16.45	3.61	2.67	2.02
Q_{accum} (kWh)	-3.47	1.15	0.25	0.07
Q_{loss} (kWh)	0.81	0.18	0.15	0.11
Q_{SG} (kWh)	31.68	5.72	3.54	2.03
Q_{SG} (spec. heat) (kWh)	5.07	0.86	0.56	0.34
Q_{C} (kWh)	16.10	2.40	2.26	2.04
Q_{C} (spec. heat) (kWh)	0.37	0.05	0.05	0.05
Q_{OUT} SUM (kWh)	74.28	15.75	10.94	7.78
En. balance diff. (kWh)	8.14	2.46	2.50	1.90
Q for TCHR (kWh)	28.77	3.48	1.97	1.13
Energy utilization (%)	64.56	49.66	47.71	46.09
Conversion efficiency (%)	57.96	44.63	43.16	42.06
$(Q_{\mathrm{SG}} + Q_{\mathrm{C}})/Q_{\mathrm{mat}}$ $(-)$	1.95	1.46	1.30	1.22
Usable waste heat (kWh)	29.54	6.34	4.79	3.57
Usable waste heat (%)	35.84	34.81	35.69	36.90

Table 3.18: Summary of energy balance results for experiment with RDF & HPT

3.4.3 RDF & MWPT

Analysis number	**1.**	**2.**	**3.**	**4.**	**5.**
Interval duration	4 min	10 min	20 min	18 min	17 min
E_{el} (kWh)	9.41	23.24	46.79	41.73	32.14
Q_{mat} (kWh)	3.56	11.11	8.89	25.00	15.11
Q_{IN} SUM (kWh)	12.96	34.35	55.68	66.73	47.25
$Q_{\mathrm{W_{RE}}}$ (kWh)	1.07	2.84	5.68	6.08	4.54
$Q_{\mathrm{W_{PT}}}$ (kWh)	1.34	3.31	6.72	6.05	3.98
$Q_{\mathrm{W_{QT}}}$ (kWh)	3.42	8.54	17.06	20.89	14.22
Q_{accum} (kWh)	6.14	-1.71	6.57	3.85	-8.09
Q_{loss} (kWh)	0.29	0.74	1.47	1.33	1.25
Q_{SG} (kWh)	0.31	0.00	0.00	2.71	0.01
Q_{SG} (spec. heat) (kWh)	0.58	1.43	2.87	2.71	1.98
Q_{C} (kWh)	5.94	15.27	21.13	26.91	13.36
Q_{C} (spec. heat) (kWh)	0.04	0.11	0.15	0.25	0.08
Q_{OUT} SUM (kWh)	19.09	30.43	61.65	70.77	31.34
En. balance diff. (kWh)	-6.12	3.92	-5.97	-4.04	15.91
Q for TCHR (kWh)	3.31	5.70	15.26	7.57	0.33
Energy utilization (%)	52.97	48.95	43.37	48.81	32.68
Conversion efficiency (%)	48.18	44.47	37.96	44.38	28.31
$(Q_{\mathrm{SG}} + Q_{\mathrm{C}})/Q_{\mathrm{mat}}$ $(-)$	1.76	1.37	2.38	1.18	0.89
Usable waste heat (kWh)	3.03	7.68	15.41	15.09	10.59
Usable waste heat (%)	23.37	22.37	27.68	22.61	22.40

Table 3.19: Summary of energy balance results for experiment with RDF & MWPT

3.5 Discussion on models

In this section, the results summarized in 3.17, 3.18 and 3.19 in previous section *Energy balances - results* will be discussed. The summary also includes other parameters and quantities resulting from the constructed energy balances. These characterizations can provide a good qualitative evaluation of the given process. For clarity, all quantities occurring in the summary will be reminded or explained with a short description.

3.5.1 Definitions

E_{el} represents the electrical energy consumption by the plasma torch and accompanying devices, Q_{mat} is an estimate of the input material energy in the form of calorific value, $Q_{\mathrm{W_{RE}}}$ and $Q_{\mathrm{W_{PT}}}$ (or $Q_{\mathrm{W_{QT}}}$) is the heat absorbed by water from the reactor or plasma torch (or in the quenching tower), Q_{accum} is the accumulated heat inside the reactor, Q_{loss} are the convective and radiative heat losses, and Q_{SG} and Q_{C} represent the energies of synthesis gas and carbon black (primarily in the form of calorific value, secondarily in the form of specific heat capacity). *En. balance diff.* is the absolute difference between the input and output energy of the balance model.

Q for TCHR is the heat required for thermochemical reactions, calculated as the difference between the energy of the output (including the accumulated heat in the specific heat capacity) and the input substances:

$$Q_{\mathrm{TCHR}} = \sum Q_{\mathrm{SG}} + \sum Q_{\mathrm{C}} - Q_{\mathrm{mat}} \tag{3.108}$$

This simplified calculation does not include the energy of the input gases, since gases with no energy value at a reference temperature are fed into the reactor. The kinetic and potential energies of the gases are neglected.

Parameters *Energy utilization* and *Conversion efficiency* are very similar, namely representing the ratios between the energy of the output products (synthesis gas and carbon) and the total energy consumed during the process (electrical energy and solid material fuel). *Energy utilization* then considers all the energy components of the output products, and *Conversion efficiency* considers only its calorific value.

$$\begin{aligned} Energy\ utilization &= \frac{\sum Q_{\mathrm{SG}} + \sum Q_{\mathrm{C}}}{E_{\mathrm{el}} + Q_{\mathrm{mat}}} \cdot 100\ \% \\ Conversion\ efficiency &= \frac{Q_{\mathrm{SG}} + Q_{\mathrm{C}}}{E_{\mathrm{el}} + Q_{\mathrm{mat}}} \cdot 100\ \% \end{aligned} \tag{3.109}$$

The following parameter $(Q_{\mathrm{SG}} + Q_{\mathrm{C}})/Q_{\mathrm{mat}}$ represents the ratio between the energy values between the materials at the output and the input, specifically in the form of products of the masses and the calorific values.

Usable waste heat is the waste heat that can potentially be used technologically by various methods of low-potential heat utilization. Of course, it depends on the maximal temperature of the heat-carrying medium. A higher amount of waste heat does not necessarily mean its higher usability. Because the aspect of the heat removal in the way of cooling is similar for all experiments, this element serves as a good comparative parameter. As a percentage is the *Usable waste heat* expressed by the ratio between the absolute amount of *Usable waste heat* to the total amount of input energy.

$$\begin{aligned} Usable\ waste\ heat\ (\mathrm{kWh}) &= Q_{\mathrm{W_{RE}}} + Q_{\mathrm{W_{PT}}} + Q_{\mathrm{SG_{spec.heat}}} + Q_{\mathrm{C_{spec.heat}}} \\ Usable\ waste\ heat\ (\%) &= \frac{Usable\ waste\ heat\ (\mathrm{kWh})}{E_{\mathrm{el}} + Q_{\mathrm{mat}}} \cdot 100\ \% \end{aligned} \tag{3.110}$$

3.5.2 Deficiencies

Regarding the energy and material balance elements, it is appropriate to emphasize that most of them were determined by a rough estimate. Good accuracy of the calculation can only be assumed for the case of electrical energy, and eventually also for the energy in the form of heat removed by cooling water. From the perspective of consumed electrical energy, the the efficiency of energy conversion is affected by the different nominal powers of the individual plasma torches, since the power of the accompanying devices was assumed to be the same. For this reason, the relative consumption of the plasma torch in relation to the total consumption of electricity is lower in the case of MWPT, which can negatively affect the efficiency of energy conversion for this experiment.

However, key elements of the balance Q_{mat}, Q_{SG}, and Q_{C} are difficult to quantify exactly, mainly because:

- the input material is considerably inhomogeneous (either from the perspective of the mass flow or the composition),
- the actual weight of output carbon black extracted from the interior of the facility components cannot be measured exactly for individual time intervals and
- gases, including the output synthesis gas, are not ideal gases, which were considered in the models.

Thermodynamic calculations for plasma (respectively plasma gas) could be made more precise by one of the correction methods, for example, Debye correction or Virial correction. Thanks to the Debye correction, pressure changes caused by Coulomb forces would then be considered, and the effect of this correction would increase with the density of charged particles (in most cases, however, the difference in the results is around 2-3 %). The Virial correction makes it possible to take into account the repulsive interaction potentials of approaching atoms and generally is also negligible for thermal plasmas in most cases. [2]

The entire issue of plasma gasification of material is very comprehensive and requires extensive knowledge of energetics, the technology of materials, chemistry, and thermodynamics. All kinetic and potential energies of the flowing media have been neglected in the models, which will also reflect in the exclusion of energy dissipation in the process. Moreover, all pressures in the process were considered atmospheric, although they may differ slightly in various places.

Furthermore, because of the absence of the necessary data and the equipment for relevant measurements, thermal quantities like Q_{loss} and Q_{accum} were estimated only provisionally, specifically from data obtained during one specific experiment, which was not even from the experiments analyzed in this thesis.

As the power of the plasma torch and consequently reactor wall temperature increases, so does the absolute power loss, as evidenced by the measurements in [16]. In the energy balance, the bigger heat loss of the torch itself is reflected in the balance element of the cooling water, but the calculation of the convective and radiative heat loss of the reactor is not corrected. The experimental relations of individual thermal powers depending on the wall temperatures investigated in [16] are captured in figure 3.35. However, from the results of the calculation estimates of the thermal quantities, it can be concluded that Q_{loss} and Q_{accum} do not have such a fundamental role for short-term time intervals.

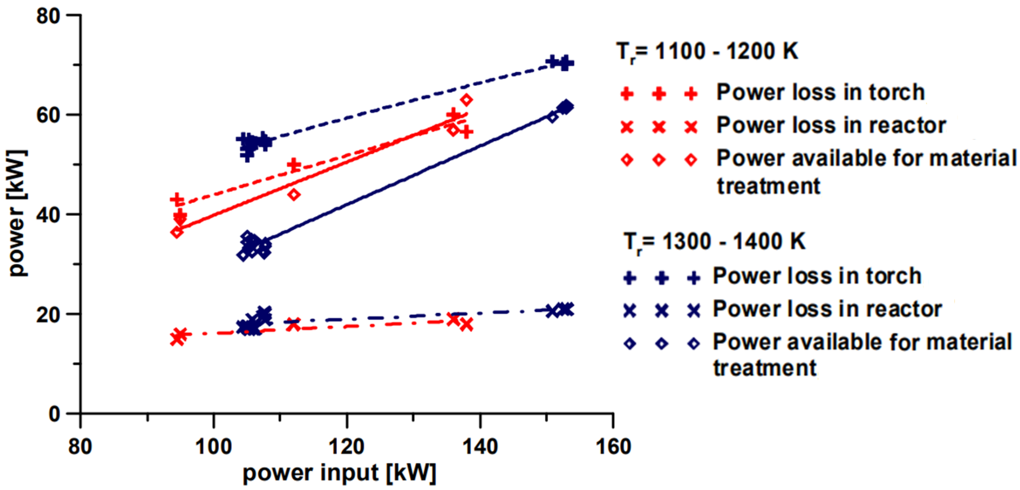

Figure 3.35: Power balance of the reactor for two temperatures of the inner wall - modified [16]

The lids (top covers) for particular plasma torch configurations are also different, which results in slightly different thermal properties and conditions, hence the heat losses through this reactor part. The reasons for the considerable effort devoted to the Q_{loss} and Q_{accum} elements are:

- the minimum amount of data and knowledge regarding these balance elements,
- the original assumption that the evaluated part of the process will be much longer than the time intervals based on chemical analyses (this applies mainly to the Q_{accum} element, which becomes significant and more accurate for longer time intervals when the temperature difference is higher and the influence of big time constants of the process is partially suppressed),
- the facility is extremely complicated from the geometric and the material perspective and thermal quantities are very difficult to measure accurately, especially under associated conditions and the dimensions of the entire equipment.

From the results of the energy balances, it appears that the thermal quantities Q_{loss} and Q_{accum} are minor elements of the whole balance. Therefore, it is probably not necessary to calculate them more precisely for the purposes of this thesis. However, the design of a real commercial aggregate would require a more detailed computational model.

Based on the observation of the resulting data, it can be concluded that the thermal convective and radiation losses might probably be higher than they were determined. This is most likely caused by simplifying the geometry of the reactor parts and averaging the measured surface temperatures.

For higher accuracy of the calculations, it would be necessary to monitor the entire facility with a thermal camera during each individual experiment, including the recording of atmospheric conditions. The mean value of the surface temperature would then be determined by numerical integration from the temperature values measured and areas on the given surfaces.

Another option for measuring heat losses is using plane wattmeters, specially designed to calculate thermal power from measuring the heat flow with the knowledge of sensor dimensions. However, these wattmeters would need to be evenly distributed over the entire surface of the reactor parts, which is also financially and operationally demanding.

The temperature distribution in the PLASGAS reactor is addressed, for example, in Ivan Hirka's doctoral thesis, where a 3D model describing the operating conditions is created in the ANSYS Fluent program. The simulation calculation model of the distribution of temperatures inside the walls of the reaction chamber is shown in figure 3.36. It is evident from figure 3.36, that the issue of heat transfer is highly non-linear in the case of a plasma reactor, and from the perspective of this thesis, this represents a too extensive issue. Because of the absence of this calculation model, the thermal calculations were significantly simplified. [67]

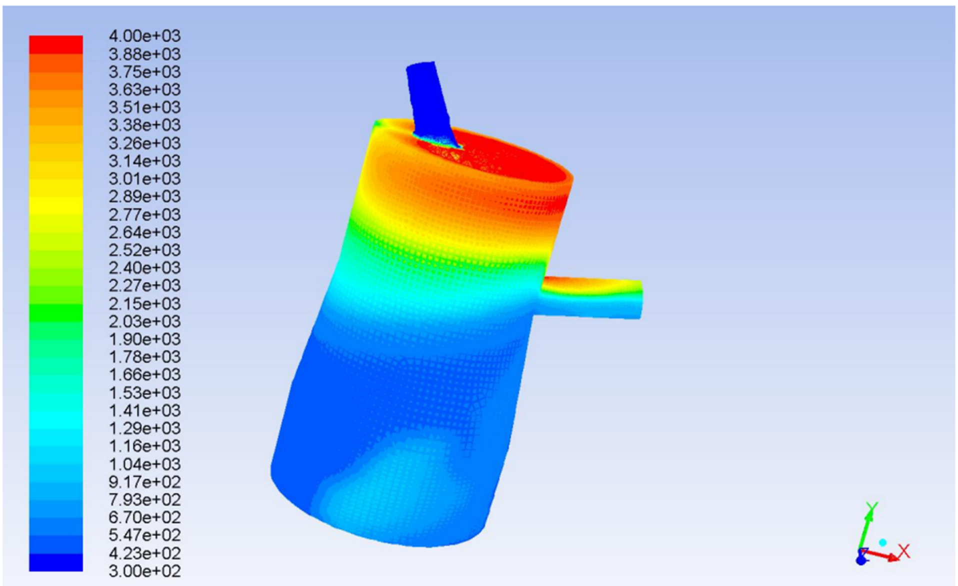

Figure 3.36: Simulated temperature distribution inside the reactor chamber performed in [67] - modified

One of the crucial challenges is the limited possibilities of the verification of the measured and calculated values. Because of dividing the experiment into several time intervals for chemical analysis purposes, it is not possible to continuously check some of the important quantities. In addition, the experiment with MWPT was one of the first of its kind, and therefore it was greatly affected by operational complications, which made it even more difficult to quantify the individual elements of the balance.

Another deficiency of the model is its discrete character based on the measured experimental data. A better solution for the energy balance would be to compile a time-reliant power balance in one of the simulation programs. The ideal approach to solve this issue would be to build both data and analytical models of the process, which would then be combined, optimized, and tested during further experiments. This would require a team of experts and weeks (maybe months) of work and development, which unfortunately was not in the capacity of this thesis.

3.5.3 Processed materials

In the case of MWPT, practically none of the analyzed intervals can be considered as a steady state from the perspective of input material feeding. The pipe elbow required constant cleaning with the anti-seize tool and the screw feeder was constantly being turned off and on with different velocities. For this reason, the estimates of RDF mass flow rates in this experiment were probably the most imprecise. For individual consecutive intervals, the mass flow rates were determined by the set $\{8, 10, 4, 12.5, 8\}$ $kg \cdot h^{-1}$. Considering this issue and the results of the energy balances, the following outcomes will be stated based on the comparison of the experiments with HPT.

Firstly, the assumption (based on the graphs of the measured temperatures in the reactor) that the processing of RDF generally requires more energy than the processing of SMW was confirmed.

The situation would probably not be that different if the SMW was replaced by real medical waste, because the tested sample does not contain energetically unusable components and especially the moisture (this would result in a lower calorific value of the input fuel, which, on the contrary, could improve the characteristic parameters of the process).

Comparing the conversion efficiencies of materials (based on the experiments with HPT), plasma waste processing of the RDF seems more efficient than of SMW. In general, this is probably caused by more effective utilization of the input energy for material treatment purposes, which may associate with more energy required for TCHR while processing the RDF.

Apparently, for real medical waste can be expected better results than for SMW. In comparison with SMW, the calorific value of the real medical waste is lower and the proportion of hydrogen higher (because of moisture). This hydrogen would be separated and formed into the component of the synthesis gas mixture (meaning that the yield of hydrogen would increase).

The amount of heat for TCHR yet relates to more aspects. As it increases, the better the resulting parameters and the more amount of energy is converted into the chemical bonds of the output substances. This converted energy in another form represents accumulated energy (also called P2G, for instance).

A more accurate assessment of individual fuel samples (also applies to plasma torches) from the perspective of material processing requires a wider range of conducted experiments. More measurements and energy model results would lead to more precise conclusions.

The number of experiments is however limited by time and technology. For each individual experiment, a lot of effort and the cooperation of many people is necessary. Consequently, specific experiments are chosen and planned carefully. The frequency of experiments is not bigger than 1 experiment per month on average (usually even less).

Also, the amount of processed material is another factor affecting greatly the resulting efficiency of the energy conversion. In general, the components at the output have a higher energy value than at the input. This means that the more material can be processed, the higher the conversion efficiency.

The main influence on the gas composition is neither the power of the plasma torch nor the velocity of material feeding, but the ratio between the input carbon and hydrogen, as also mentioned in the first chapter *Plasma aggregate*. The increase in synthesis gas yield relation to higher feeding rates of input material is captured by figure 3.37 from the source [16]. This means, that in reality, efficiency would be bigger because probably even more material could be processed than during the conducted experiments.

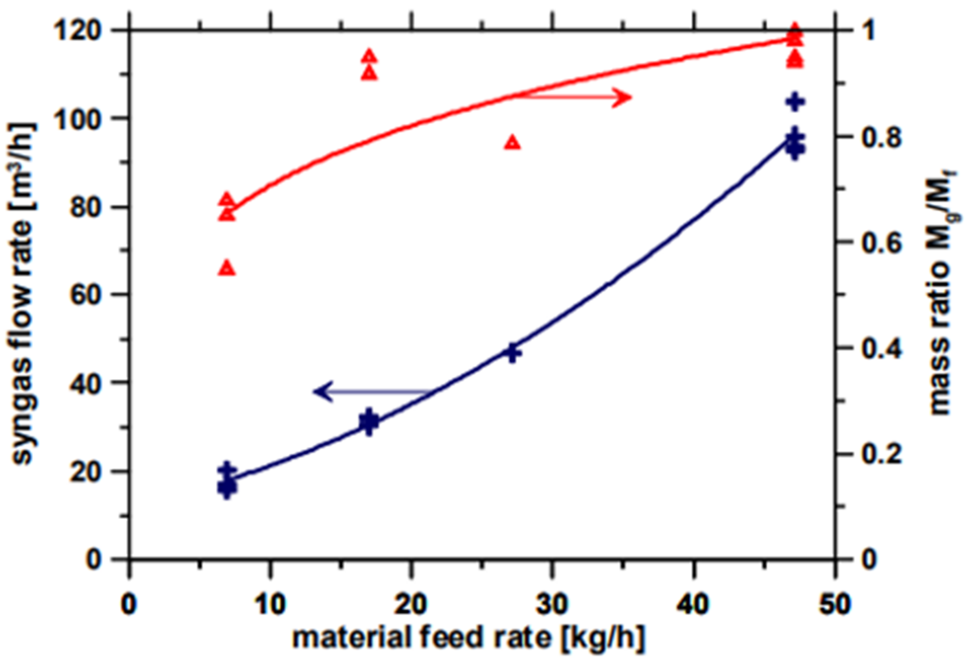

Figure 3.37: Flow rate of synthesis gas and the ratio of synthesis gas mass flow rate to material feed rate in relation to material feed rate [16]

Figure 3.37 shows the real potential of increasing the amount of processed material. Unfortunately, because of the complications during the experiments that are part of this thesis, it was not possible to feed the material with larger mass flow rates. A large amount of material mass flow is also problematic for the semi-operational experimental mode for the reason of the material residues at the bottom of the reactor. If the temperature at the bottom of the reactor is not sufficient, the material will not be gasified.

It can also be seen that it was possible to increase the energy value of the material at the input by up to 75 % (during the experiment with HPT and RDF). This energy value can allegedly be even more than doubled. The experiment with MWPT fared the worst in the case of increasing the energy value of the material, where an increase of 35 % still seems somewhat optimistic given the complications in the experiment and subsequent calculations. [16]

Also worth noting is the fact that one of the reasons why SMW generally required less energy for TCHR than RDF may be due to the significantly smaller particle size of the material sample (as discussed in the first chapter and shown in figure 1.14). While the SMW parts are very small (a mix of materials finely processed by a shearing mill), some pieces of the RDF sample can reach several centimeters.

3.5.4 Plasma torches

The real differences in possibilities of plasma waste treatment using either hybrid arc or microwave plasma torch are a little questionable. During the experiment with MWPT, there were so many complications, that it is not possible to draw appropriate conclusions with sufficient certainty.

Only for some intervals of the MWPT experiment, the output energy of the energy balance came out bigger than the input energy (namely for 3 out of total 14 time intervals). The biggest impact on this outcome has:

- the rapid temperature changes measured in the upper part of the reactor,
- the inaccuracies of the material balance caused by the poor stoichiometry of the process, and
- the absence of knowledge about the ratio between the output carbon black and ash.

Consequently, the high temperature in the upper part of the reactor may imply that the current geometry of the reactor is not suitable for the MWPT, in contrast to HPT. For example, better results could be achieved in the case of MWPT, if the reactor and reaction chamber were larger. This would increase both the residence time and the uniform heating of the reactor.

Another possibility for improvement could be the placement of the MWPT from the bottom of the reaction chamber and the exhaustion of the synthesis gas and flue gas at the top.

Specifying the carbon black and ash production as equal is rather optimistic. From the results of energy balances and their comparison (from the perspective of ratios between outputs and inputs), it is more likely that the carbon black yield was even lower.

Accordingly, this would also result in Q for TCHR coming out negative in some cases. This would correspond to a situation where the input material has a higher energy value than the output material, indicating the occurrence of exothermic combustion instead of endothermic gasification. Unfortunately, the actual material balance is unknown.

Actually, it is conspicuous, that combustion could practically be the dominant reaction during the last (fifth) time interval of the MWPT experiment. In the second and fourth time interval, endothermic reactions could already prevail and in the first and third time interval, gasification was most likely the governing reaction.

The release of heat by the material combustion can then help to subsequently gasify the material, after which the energy inside the reactor again decreases and the combustion occurs again. This cycle was perhaps repeated multiple times during the MWPT experiment.

There are many differences between MWPT and HPT from both technological and operational points of view. The first thing to mention is the design and the different principles of plasma generation, including the character of the plasma jet/flame. The dimensions and properties of individual types of plasma (and plasma torches) have already been explained.

When comparing the plasma torches in terms of efficiency of the energy conversion for plasma generation in general, the MWPT with an efficiency of around 70-75 % appears better than the HPT with an efficiency of between 45-65 %. From the associated results of the thesis experiments (see table 3.22 below), it follows that the MWPT efficiencies mostly corresponded to the mentioned interval, namely most often in the range of 71-72 % (in one extreme case only around 67 %). For the HPT, the values were surprisingly better than expected, namely approximately in the interval of values (54,69) %.

The lower efficiency of HPT results from bigger heat losses, namely by active cooling (which is evident from a comparison of the $Q_{\mathrm{W_{PT}}}$ between HPT and MWPT experiments). The higher heating intensity of HPT is also caused by much lower volume flows of the stabilization medium compared to the MWPT.

3.5.5 Optimal conditions

In order to easily compare the experiments, all the energy balance interval values will be added up and converted to an experiment length of 1 hour. For example of the first experiment, the analyzed parts lasted 63 minutes in total.

The sum of the balance values will therefore be multiplied by the coefficient $^{60}/_{63} = 0.952$ (analogously for the remaining 2 experiments). The remaining 6 parameters characterizing the process will be determined afterward from the results of balance summations and conversions.

Experiment	HPT & SMW	HPT & RDF	MWPT & RDF
Equivalent interval duration	1 h	1 h	1 h
E_{el} (kWh)	154.03	151.71	133.31
Q_{mat} (kWh)	57.78	66.67	55.36
Q_{IN} SUM (kWh)	211.81	218.37	188.68
$Q_{\mathrm{W_{RE}}}$ (kWh)	25.11	21.44	17.57
$Q_{\mathrm{W_{PT}}}$ (kWh)	38.10	43.66	18.61
$Q_{\mathrm{W_{QT}}}$ (kWh)	-	-	55.77
Q_{accum} (kWh)	5.49	-3.53	5.89
Q_{loss} (kWh)	2.21	2.21	4.42
Q_{SG} (kWh)	50.42	75.83	2.64
Q_{SG} (spec. heat) (kWh)	8.77	12.05	8.32
Q_{C} (kWh)	34.43	40.23	71.84
Q_{C} (spec. heat) (kWh)	0.85	0.93	0.54
Q_{OUT} SUM (kWh)	165.39	191.90	185.46
En. balance diff. (kWh)	46.42	26.48	3.21
Q for TCHR (kWh)	36.70	62.38	27.97
Energy utilization (%)	44.60	59.09	44.17
Conversion efficiency (%)	40.06	53.15	39.47
$(Q_{\mathrm{SG}} + Q_{\mathrm{C}})/Q_{\mathrm{mat}}$ $(-)$	1.47	1.74	1.35
Usable waste heat (kWh)	72.84	78.08	45.04
Usable waste heat (%)	34.39	35.75	23.87

Table 3.20: Summary of results of energy balances for all experiments

The resulting table 3.20 comparing the experiments shows that the most effective from the perspective of energy conversion was the experiment with HPT and RDF, having the conversion efficiency of over 53 %. In commercial or industrial operations, overall efficiency would be lower than this, because it is necessary to consider the discontinuous operation of the facility, which would result in more significant overall heat losses relative to a unit of time.

On the other hand, a commercial industrial plasma gasification aggregate would likely have larger dimensions and optimized thermal insulation, so losses would likely be lower relative to a reactor volume unit.

In comparison, if plasma gasification unit or aggregate was able to achieve operational reliability, it would reasonably compete with other types of accumulation technologies, at least from the perspective of the energy conversion efficiency and the fact that the primary material sources are (alongside with the electrical energy) wastes or gases with no energy value. These commodities usually have very low or even negative costs. This feature may soon become even more prominent and might happen especially as a consequence of the more strict landfilling limits (and more expensive payments and fees associated with landfilling), which is also probably only a matter of the near future.

The following task related to energy storage by plasma waste treatment is now to find out the efficiency of the reverse conversion back to the electrical energy from the obtained synthesis gas (if it is even possible).

From the comparison of all individual experimental intervals, it is noticeable that depending on the requirements of the process, different operating conditions appear to be attractive. Since the operating conditions were purposely changed only in the experiments with HPT, this comparison is not illustrative in the case of the experiment with MWPT.

Table 3.21 shows the H_2/CO ratios and, as a reminder, summarizes the energy conversion efficiency of the synthesis gas η_{CE} for individual intervals of the HPT experiments. It is evident that with the decreasing supply of carbon dioxide (in the case of HPT), although the efficiency of energy conversion decreases, the ratio between output hydrogen and carbon dioxide increases.

Experiment	**CHA**	**1.**	**2.**	**3.**	**4.**	**5.**
HPT + SMW	H_2/CO (-)	0.73	0.97	1.10	1.31	1.33
	η_{CE} (%)	48.39	36.10	48.83	27.76	30.24
HPT + RDF	H_2/CO (-)	0.54	0.95	1.36	2.18	-
	η_{CE} (%)	57.96	44.63	43.16	42.06	-
MWPT + RDF	H_2/CO (-)	329.23	0.00	0.00	0.65	0.06
	η_{CE} (%)	48.18	44.47	37.96	44.38	28.31

Table 3.21: Synthesis gas H_2/CO ratios and energy conversion efficiencies for all experimental intervals

If the requirement is to maximize the yield of hydrogen, pyrolysis (decomposition of the material without the presence of an oxidizing agent in the form of carbon dioxide) will be a more suitable process (in the case of water or steam as an accompanying input medium, the results could be different). If the requirement is to maximize the efficiency of the energy conversion, the gasification of the mixture of material and input oxidizing gases appears to be more appropriate. Analogously as in the case of different solid materials at the input (SMW or RDF), the efficiency of energy conversion is higher in the case where more energy needs to be supplied for thermochemical reactions.

Another option (mainly for comparison and contemplation) is to assess the efficiency of the energy conversion based only on the energy supplied by the plasma itself. This calculation will reveal the efficiency of energy use right inside the reaction chamber. This efficiency will be referred to as the efficiency of the thermochemical reactions η_{TCHR} and will be determined as follows:

$$\eta_{\mathrm{TCHR}} = \frac{Q_{\mathrm{SG}} + Q_{\mathrm{C}}}{Q_{\mathrm{mat}} + E_{\mathrm{elPT}} \cdot \eta_{\mathrm{PT}}} \tag{3.111}$$

where η_{PT} represents the efficiency of energy conversion to plasma. Therefore, for the case of the HPT experiment, the plasma generation efficiency is $\eta_{\mathrm{PT}} = \eta_{\mathrm{HPT}}$ and for the case of MWPT experiment the plasma generation efficiency is $\eta_{\mathrm{PT}} = \eta_{\mathrm{MWPT}}$. These efficiencies are expressed by the equations 2.4 and 2.7 in the section *Plasma torches* of the chapter *Preparation of experiments*.

For completeness, in table 3.22, in addition to the efficiencies of thermochemical reactions η_{TCHR}, the efficiencies of energy conversion to plasma are also summarized. It is conspicuous that the claim of higher efficiency of MWPT in contrast to HPT has been confirmed. As already mentioned, the calculated efficiency of HPT ranges between 54 % and 69 %. In the case of MWPT, it is around 67 % to 72 %. In these specific experiments, the maximum difference between the achieved efficiencies of the plasma torches is close to 18 %. On average, the difference in the efficiencies of the plasma torches is about half, namely around 9 %.

Experiment	**CHA**	**1.**	**2.**	**3.**	**4.**	**5.**
HPT + SMW	η_{HPT} (%)	68.89	68.21	66.20	64.60	62.54
	η_{TCHR} (%)	74.38	56.14	77.47	44.68	49.53
HPT + RDF	η_{HPT} (%)	62.26	61.50	58.16	53.92	-
	η_{TCHR} (%)	92.64	71.77	71.15	71.49	-
MWPT + RDF	η_{MWPT} (%)	71.69	71.57	71.41	71.03	66.58
	η_{TCHR} (%)	74.16	66.26	64.15	64.01	50.51

Table 3.22: Efficiencies of plasma generation η_{PT} and TCHR η_{TCHR}

It is worth noting that in one extreme case at the beginning of the second experiment, the efficiency of the thermochemical reactions reached over 92 %. In general, it can be stated that the η_{TCHR} ranged between 50-75 % in the case of MWPT and between 45-75 % in the case of HPT. It can be seen that the η_{TCHR} efficiency correlates well with the total heat supplied for thermochemical reactions Q_{TCHR}.

The type of the heat source, stipulating the nature of the plasma, also indicates the amount of waste heat that can be further used technologically. The hybrid arc plasma torch creates a small, but high-temperature heat source. Therefore, the heat is more evenly distributed within the reaction chamber and subsequently into the surrounding reactor walls. For this reason, practically a third of the input energy can be used in the form of waste heat.

The large amount of gas flow through the plasma torch unit in the case of MWPT creates a draught outward from the reaction chamber through the flue gas pipe, which quickly carries away and dissipates the heat. This reduces the possibility of MWPT utilizing waste heat to around a fifth or quarter of the input energy.

One of the main advantages of the air-stabilized MWPT is the lower energy consumption per unit weight of processed material. If the economics of the operation was built exclusively around waste processing, the use of this type of plasma torch could be considered. Additionally, its operation would be cheaper and easier also in terms of maintenance, since the MWPT has no active electrodes that would wear out during operation.

For industrial applications of a microwave plasma torch, there are several ambitions and opportunities. The operation of the MWPT is relatively simple and the regulated power is stable over a wide range. There is also a possibility to replace the stabilizing medium of air with water vapor. Short tests, during which it succeeded to operate the torch with a mixture of air and steam, showed that water vapor significantly increases the yield of hydrogen as a component of synthesis gas. The representation of nitrogen (and nitrogen oxides) in the output mixture naturally decreases with lower relative airflow.

However, attempts to completely replace the air with steam failed, because the MWPT was repeatedly shut down. This was caused by protection in the waveguide circulator that detects reflected microwave power. Inside the microwave unit, where the plasma is created, water droplets were probably condensating, which significantly changed the dispersion of the environment and as a result led to a high reflectivity of microwaves back from the plasma unit.

MWPT testing with water vapor is currently under research at IPP CAS and results for this operating mode are not yet available. If it turns out that it is possible to switch completely to water vapor as a stabilizing medium, this could mean a significant increase in the yield of hydrogen in the output synthesis gas mixture, which can have the consequence of better competitiveness of the MWPT.

This also means, that if the goal would be to maximize hydrogen production, a MWPT with steam could theoretically be a more suitable option than HPT. Water vapor as a stabilizing medium also has the advantage of higher heat capacity compared to air, which can result in more efficient use of energy and easier temperature regulation inside the reactor. Another advantage of using water vapor in a microwave plasma torch compared to a hybrid arc plasma torch is that the microwave plasma torch does not have active electrodes that would erode because of the oxidizing environment created by the water vapor.

The experiment with HPT & RDF appears to be the best option according to all qualitative indicators. It would be interesting to compare the results of the experiment with SMW with real medical waste as a material sample, but this cannot be achieved in laboratory conditions considering the dispositions of the used semi-operational gasification device.

3.5.6 Comparison with the project report

For comparison with the outcomes of this thesis, here are some of the project report results on *Plasma gasification of hazardous waste*, on which IPP CAS cooperates together with the Institute of Physics of the CAS and HVM PLASMA, spol. s.r.o.

Comparing the plasma torches, this paper states that the HPT is capable of producing approximately twice the amount of energy-usable synthesis gas than the MWPT per unit of fuel processed.

As for the advantages of HPT, it is mentioned that 80-90 % of the output gas mixture when using HPT is energy-usable products, in contrast to air stabilized MWPT, when it is a maximum of 30-40 %. Another advantage of HPT is the possibility of supplying and decomposing carbon dioxide, which ultimately improves the process parameters in terms of the balance of inputs and outputs.

Regarding the advantages of MWPT, it is declared that up to 2-3 times more fuel per unit of time can be processed with MWPT than with HPT.

Furthermore, under suitable operating conditions, the microwave plasma torch requires up to 4 times less energy to process a unit of fuel (also assuming partial combustion and partial gasification). Because of the experimental complications with the feeding (during MWPT experiment), this parameter (similarly to Q_{mat}) cannot be determined objectively from the received results, therefore it is no longer a part of this discussion.

Chapter 4

Electricity market

In this chapter, focus on the issue of commercialization of plasma waste gasification technology is initiated. The main research points of this chapter will be the energy market, legislation, energy mix, economics of operation or system, and support services. All of these domains relate to the potential plasma gasification facility project accordingly in terms of implementation or operation. Therefore, the following text is devoted to this concern.

4.1 Energy commerce

The main activities of energy commerce are to ensure the services provided by the transmission system operator (TSO), specifically system and transmission services, and to procure TSO services, namely supporting services and electricity supply for covering transmission losses.

Further activities of energy commerce include reporting data for deviation evaluation, daily operations through an electronic trading portal, and the development of energy markets for system and transmission services.

The inseparable factor of the market is the price of electricity, composed of several parts primarily dividable into regulated and unregulated parts. Power electricity is the most significant component of the unregulated part of the price. The regulated part of the price consists mainly of the transmission charge, the distribution charge, the system services charge, the support for renewable energy sources, CHP, and secondary sources. To be more specific, the tax or charge to the energy market operator (EMO) can also be mentioned.

4.2 Tariff structure

For the regulated part of the price for electrical energy the Energy Regulatory Office (ERO) is responsible, respectively for the tariff amounts - the individual parts of the regulated component of electricity. Additionally, ERO provides licenses to new subjects in the electricity market (or in the energy sector in general).

This is very important for two reasons. First, according to the latest reports, the entire tariff structure in the coming years will be changed, on behalf of the expected transformation (not only) of the local power grid infrastructure and energy market. The main motivators for these changes are: [68]

- decarbonization of the energy sector,
- development of renewable energy sources (RES),
- development of decentralization & the emergence of energy communities,
- introduction of Automated Meter Management (AMM) system,
- development of electromobility and charging infrastructure.

Second, tariff structure may be an important aspect in determining the profitability, commercial viability, and economic self-sufficiency of the technology.

In the document *Concept of the interconnection of the new design of the electricity market with the requirements for changes in regulated prices and tariffs* the concern of the tariff structure is explained. Mainly, motivation to assess the customers accordingly to the characteristics of the consumption is stated. The tariffs will be adjusted appropriately to the rate of help or load of the network by the customer. [68, 69]

At the beginning of the document, the main current problems of the existing tariff structure are introduced: [68]

- the inefficiency of the two-tariff system in a dynamic environment (changes in consumption or appliances may benefit or disadvantage some consumers over time),
- problematic allocation of costs (spill-over of costs between customers, therefore someone is paying more than is necessary and someone less than is needed),
- oversized RP – inefficient strengthening of system capacities (increased costs transferred to consumer), furthermore, dependency on the size of the circuit breaker can constitute a problem for individual consumers.

Note: Reserved power (RP) at low voltage (LV) level refers to the value of input electrical power agreed with the distribution company for a given consumption point at the nominal current value of the main circuit breaker placed before the measuring device. At high voltage (HV) or very high voltage (VHV) level, it is the value of the average quarter-hour electrical load that cannot be exceeded during consumption. Exceeding the reserved input power at the consumption point can threaten the reliability of electrical energy distribution for other customers (for exceeding the limit at HV and VHV levels penalties are imposed). Therefore, if the existing RP is no longer sufficient for the demands of the consumer, it is necessary to request an increase. [70]

As mentioned earlier, the development of energy storage and renewable energy, an increase in the number of decentralized sources, sharing of generated electricity, and an increase in the number of electric vehicles and charging stations are considered the essential expected changes. This will have a certain impact on the capacity dimensioning of the systems. Consequently, greater flexibility in the energy systems and mutual interconnection and cooperation between industries will be necessary to ensure. This relates to the power engineering, gas, and heating industry. The introduction of AMM system serves also as an example. [68]

4.2.1 Goals and principles of innovation in the area of regulated prices

The basic principles of the new tariff structure consist of simplicity and simple applicability (suppressed by the current tariff structure, as a result of a wide range of distribution rates for the customer at the LV level right now). Furthermore, non-discrimination, accessibility, transparency, and safety are fundamental. The main objectives in the area of regulated prices are: [68]

- appropriate price for customers,
- long-term predictability of the tariff system,
- higher utilization and efficiency of system operation and development.

Moreover, the network tariff should also be designed respectively to:

- motivation of market participants to effectively use the systems and their purposeful development
- RP assessment and impact on effective use of systems
- the influence of the shape and volume of the customer's consumption diagram on the effective use of systems or the provision of flexibility (SuS, PBS)

Embracing the possibilities of self-generated energy production and eliminating possible obstructions has a high priority (particularly in the context of small rooftop photovoltaic systems). From the point of TSO, this can appear as a lower electricity consumption and therefore a lower load on the grid, resulting in lower demands on the system and lower losses. This will consecutively lead to lower operating costs of the system and lower costs associated with connecting energy sources to the grid, additionally resulting in the reduction of costs for end consumers. In summary, the more efficient the way of the utilization of the grid by the end-user, the more favorable the tariff will be. [68]

4.2.2 Automated Meter Management (AMM)

Another factor affecting the operation of power systems will be the gradual implementation of AMM, namely in the steps: [68]

- a preparatory phase (to June 30, 2024),
- equipping all points of common coupling (PCC) with consumption above 6 MWh/year (to June 30, 2027),
- and then equipping all remaining consumption points.

According to this, for the case of plasma aggregate construction implementation the AMM system as an associate system can be assumed. In relation to the installation of AMM to PCC, a gradual transfer of consumption from high-demand to low-demand times is expected, which is desirable. [68]

Some of the emerging trends that will impact grid network operators can be applied immediately, individually: [68]

- enabling limited sharing of electricity in an apartment building,
- increasing the motivation of customers to optimize the RP at VHV and HV levels or
- faster adjustment of the charging system for non-compliance with the consumption power factor (thus the supply/consumption of unsolicited reactive energy).

The last point may be crucial for a potential plasma aggregate, specifically in the case of the system using arc plasma torch technology, as the electric arc impedance changes over time during the process. This significantly affects the power factor, therefore the delivery (or consumption) of reactive energy. In consideration of this case, an appropriate filtering-compensation station should be equipped as a part of the aggregation block. [68]

Another aspect of the concept document, as one of the basic perspectives in setting the tariff system, is technological neutrality. Welcoming new services and optimized processes is the aim while increasing stability and security. Assessing the customers based on measurable quantities (shape and character of power consumption, capacity load of the grid), unlike the purpose of electricity consumption is intended. The ambition is to prevent negative impacts on the grid that could affect the energy supply and its quality for other consumers. Depending on the operating conditions, these provisions can either be advantageous or disadvantageous for the project of plasma aggregate integration. [68]

The current penalty system for reactive energy includes charges for: [68]

- non-compliance with the power factor and
- unsolicited supply/consumption of reactive power during electrical energy consumption.

The charges are stated using a complicated calculation. Briefly, a bigger exceeding of prescribed parameters determines the rate of price surcharge. The evaluation period of this method will be adjusted from monthly to 15-minute intervals, charging for reactive energy in all four quadrants. The objective is to increase the requirements for the electrical system's functionality to improve reactive energy management. Safe and reliable operation of the electrical system cannot be carried out without important mechanisms like non-frequency SuS. At the same time, the full potential of smaller providers of SuS should be involved accordingly to the tariff system. [68]

The basic trend of the tariff system adjustment in the area of SuS will allow provisions of these types of services to a wider range of potential customers, including active customers with low consumption. Active customers can fully provide flexibility after the installation of AMM. [68]

In the future use of AMM, system operators will have more accurate information about the grid load and overall demands. This will be useful in the future tariff structure setting. AMM will also make it easier to recognize if the customer meets the relevant tariff conditions. From the perspective of the possible new tariff structure setting, the data from ongoing monitoring can be utilized to create a new method for determining the individual components of the tariff. In addition to specifying tariffs, AMM can also be used for the efficient provision of non-frequency SuS. That may also include small providers, assuming it is not economically inefficient and technically impossible. [68]

4.3 Legislation

The European Parliament and Council Regulation (EU) 2019/943 of June 5th, 2019 on the internal market for electricity, linked with the directive, sets out the principles for tariff formation and rules for trading. These regulations will soon be legislatively followed by implementing regulations from the European Commission, specifically the Network Code on Flexibility and the Implementing Act on Data Interoperability. [68]

One of the central documents for the transformation of the power sector and energy markets is the *Fit for 55* package. This also includes a proposal for the regulation of alternative fuel infrastructure (LNG or CNG). Fit for 55 declares that *DSOs should cost-effectively integrate new electricity generation, particularly from renewable sources along with new appliances like heat pumps or electric vehicles. The efficient level of integration of decentralized generation and consumption should be defined to avoid waste of investment funds.* [68]

The most important provisions of the stated legal regulations are: [68]

- *the creation of civil energy communities with guaranteed non-discriminatory access to all electricity markets and the possibility to share the electricity produced inside and outside the community,*
- *more active involvement of customers in the electricity market through decentralized RES, accumulation, aggregation or energy communities,*
- *market approach to the purchase of SuS, flexibility services also as redispatching,*
- *the development of energy storage, including energy conversion (P2X systems, for example P2G),*
- *further development of smart grids associated with an increase in decentralized RES, electromobility, active customers, and aggregation.*

In relation to the NAP for Smart Grids, tariff innovations in the following area appear to be crucial for the plasma aggregate project: [68]

- use of aggregation, flexibility for electricity systems (decentralized energy sources, consumption) and accumulation,

possibly also:

- decentralized energy sources (integration and utilization for the operation of the electricity system) or
- harnessing the potential of AMM.

The fundamental attributes are safety, competitiveness, and sustainability. The strategic goals of the updated NAP are: [68]

- *to create conditions for higher penetration of decentralized, especially renewable, sources of electrical energy, storage, and electromobility in accordance with the NAP for Smart Grids and their integration into the coordination and management of the energy system, and*
- *to increase the reliability, quality, and safety of electrical energy supplies. Ensure lower levels of supply interruptions and higher quality of electrical energy defined mainly by the stability of frequency and voltage, similarly as a high ability to restore supply after an outage and resilience of power grids to external conditions (terrorism, climate events, and cybersecurity).*

Regarding to rules for energy storage (in any form), its implementation should be carried out by adopting a new energy law or by appropriate amendment of the existing law. In behalf of the development of decentralized generation and renewable energy sources (and therefore the related need to store this energy), the creation of new services that improve the flexibility of the energy system or services that will contribute to the interconnection of individual energy sectors can be expected. [68]

According to the statement in the Analytical Part of the concept, renewable gases (e.g. products of Power-to-gas technology) are suitable tools for achieving EU goals in reducing greenhouse gas emissions (i.e. decarbonization). Because of the requirements of Directive 2019/944, a new activity of energy storage needs to be included in the Czech legal framework. By the following definition, the term energy storage refers to both accumulation and conversion: *The Directive 2019/944 defines energy storage in the electrical system as deferring the consumption of electricity for a later moment than it was produced, or converting electricity into a form that can be stored. Storing the energy, and then converting it back into electricity or using it as another energy carrier.* [68]

This activity should only be permitted to be carried out commercially on the basis of receiving a license for supply into the system. In some cases, accumulation and return supply to the grid do not differ. In the case of aFRR, the impact may be more negative than for power plants. Given that the concept of accumulation is not yet included in Czech legislation, it is regarded as a supplementary element of existing or new sources from the perspective of the DSO and TSO. [68]

The crucial tool for integrating decentralized and intermittent renewable energy sources is considered to be flexibility, which allegedly cannot be fully utilized without reliable and efficient aggregation. The future form of the tariff structure will be defined based on the source of funding for flexibility and will consider various forms of discounts and surcharges. A discount signifies that another individual or entity assumes a portion of the expenses and provides financial support to a foreign entity, with a particular emphasis on the tariffs imposed on the distribution network. A surcharge is a form of allocating induced expenses and can be utilized not only for financing the enhancement of system capacity but also for purchasing flexible services. This model could be probably used for higher voltage levels. [68]

4.4 Energy mix

Another relevant aspect worth considering is the energy mix of the investigated part of the system (Czech Republic or Europe, for instance), within which the plasma aggregate would be associated. One of the crucial issues of this technology is its energy demandingness. This can be beneficial in the increasing capacity of RES or nuclear power blocks scenarios, opposingly, shortage and high costs of energy as a consequence of power grid development and transformation stagnation is a threat in relation to the energy consumption characteristic of the plasma aggregate.

4.4.1 Core & coal

According to CEZ and the article *Czech Energy in the 21st Century*, the installed capacity of coal-fired power plants in the Czech Republic energy mix should change (decrease) according to the following points: [71]

- 2022: around 10800 MW (approximately 53.0 %),
- 2035: an estimate of 6400 MW (31.5 %),
- 2040: an estimate of 2600 MW (12.7 %),
- 2050: carbon neutrality,

and around 2040, the shutdown of the Dukovany power plant blocks is anticipated. A further decrease in installed capacity of 2040 MW will result. In total, the deficit of installed capacity by 2040 of more than 10 GW (namely 10240 MW, based on the review above) can be expected. This presents quite a problem, especially as long as the Czech Republic has limited options for RES development and usage, either because of natural limitations, environmental protection requirements, or legislation. Simultaneously, a greater demand for energy supplies in the interest of increasing the importance of electromobility and consumption itself is expected. For these reasons, nuclear energy will remain the major element of the Czech energy mix in the upcoming decades. [71]

Nuclear power plants are important for the safe operation of the energy system, representing the stable sources essential for grid management, as they ensure reliable energy supplies, even when other sources cannot. The Czech Republic, as a member of the EU, has committed to contribute to the achievement of carbon neutrality by 2050, which the European Commission has declared as the main strategy for protecting the environment and reducing the impacts of climate change in the European Union. (The estimated emission savings from 60 years of a nuclear power plant operation are roughly 1 billion tons of CO_2 compared to a coal-fired plant and about 500 million tons of CO_2 compared to a gas-fired plant in comparison per unit of power output.) [71]

Building new nuclear power plants in the Czech Republic is in accordance with the state plan to achieve these goals. If the power (installed power respectively) of nuclear power plants (theoretically) exceeds the basic load of the system along with other sources, energy can be purchased at a lower cost during low consumption periods. For any plasma aggregate that is not SuS or PBS, a low tariff in a multi-tariff regime can be also considered in this scenario. [71]

The precedences of nuclear energy include low emissions and low land usage (per unit of energy). This is why the promotion of nuclear energy in the Czech Republic is expected as it is a relatively small country, limited by the amount of space for construction. In the field of nuclear energy, the growth of small modular reactors is also prospective, which are easier and faster to build compared to conventional large nuclear reactors. The first one will allegedly be completed in Temelín between 2032 and 2035. With respect to the construction of another conventional nuclear block, the start is planned for 2029, and the commissioning is for 2036. [72]

Theoretically, coal-fired power plants could be preserved by the CCS technology. Nevertheless is this not sustainable in the long-term period because it increases fuel consumption (and emissions) and permanent tightness of underground storage facilities cannot be ensured (estimated only for about 50 to 100 years). Additionally, there is a risk of inefficient draining funds instead of appropriately investing in energy savings and renewable sources. CCS technology is reportedly causing more harm than good and is also very expensive. It is also estimated that water consumption for energy production would roughly double. If it is possible to reduce the carbon footprint, long-term storage of carbon dioxide is ensured by natural processes. According to some appraisals, it would be necessary for anthropogenic emissions to be eliminated by 2100 and replaced by anthropogenic storage of roughly 10 gigatons of carbon dioxide per year in order to achieve the limit of 1.5 °C warming. [73, 74, 75]

4.4.2 Gas

In May 2019, the Commission approved a targeted revision of the 2009 Gas Directive (Directive (EU) 2019/692). This revision would grant the immediate applicability of basic provisions of the Gas Directive to cross-border pipelines shared with third countries, respectively those parts located in the EU domain. This would help to ensure that no existing, planned, or future gas infrastructure project between a Member State and a third country would disrupt the single energy market or impair the security of supply in the EU. [76]

In September 2020, the Commission announced that a new regulatory framework for competitive decarbonized gas markets will be developed in 2021. To this end, the Commission launched a public consultation on February 10, 2021. This initiative was a response to the decarbonization challenge of gas networks and proposes a revision of EU rules for gas with an effort to facilitate the entry of renewable and low-carbon gases into the market and remove any unjustified regulatory barriers. [76]

With regards to the relationship between gas and coal-fired power plants to the timeline for their closure, the deadline cannot be established without certainty of a suitable replacement in time. Currently, almost no accurate completion date (and thus increase in installed capacity) of any particular energy source can be stated. It is appropriate to add a note that the argument for closing the coal sources is the reduction of emissions (greenhouse gasses) and conventional gas sources are not low-emission. Taking methane leakages during its mining and subsequent transport into account, gas does not appear much better compared to coal in terms of emissions footprint. From the point of this perspective, synthesis gas is a more suitable and practical option, for the reason that it is not mined but produced and will not be necessarily transported over distances that long. In the long-term, closing the conventional gas power plants or replacing natural gas with synthesis gas can be considered, similar to coal-fired power plants in the present and near future. [77]

4.4.3 RES

4.4.3.1 Wind

By the opinion of David Hanslian from the Institute of Atmospheric Physics of the CAS, the weather conditions for wind power plants in the Czech Republic are similar to those in southern Germany, particularly the occurrence of wind, its speed, and the character of the landscape and its relief. Nevertheless, the use of wind power plants in the Czech Republic is still far lower than in Germany. [78]

As reported in David Hanslian's study for the Czech Wind Energy Association and the Renewable Energy Branch Council, wind power plants in the Czech Republic could indeed cover less than a third of the current electrical energy consumption in the Czech Republic by 2040, being aware of all the limitations and practical problems associated with their implementation. [78]

Stephan Chalupa, Chairman of the Chamber of Renewable Energy Sources, points to the fact that the argument about increasing energy prices in cause of RES and their support is no longer valid. Not only are RES one of the cheapest energy sources, but according to the law, costs for their development and support shall have no impact on the final price of electricity. The comment, that *The state can pay for the construction of wind farms from the sales of EU (emission) allowances or from billions of CZK available from the European funds through the Green Deal.* accompanies the statement. [79]

The Czech Republic's annual electricity consumption in 2019 was 61.1 TWh, while wind power plants produced 0.7 TWh, which corresponds to one percent of consumption. In the countries of the European Union, wind power plants provided an average of 15 % of consumption that year. Inland Austria covers 13 % of its consumption with wind power plants, for instance. [79]

The Sokolovská uhelná group, one of the leading coal miners and producers of electrical energy through coal-fired power plants can bring a good opportunity for RES in the Czech Republic. The company is completing initial and preparatory arrangements for large green projects, getting ready for the shift to clean energy. So far, the group has developed and submitted eleven RES projects, four of which are wind and seven photovoltaic. The group wants to build RES with an installed capacity of 250 MW within 10 years. The amount of the investment is expected to be around 10 billion CZK and construction of the first power plants is expected to begin this year. [80]

4.4.3.2 Solar

CEZ group, the largest producer of electrical energy in the Czech Republic, aspirates to significantly improve the company image among investors by focusing on the production of energy from RES in the future. The plan is to shut down or convert most of the owned coal-fired power plants and heating plants to burn other fuels and heavily invest in RES, photovoltaics in particular. By 2030, the construction of photovoltaic sources with a total capacity of 6 GW (and worth approximately 90 billion CZK) is prepared. Part of it, namely of 1.5 GW installed capacity, should be completed by 2025. Considering the scale of the projects, CEZ will not invest in wind parks, as administrative management and lack of public support become significant obstacles for projects of these proportions. [81]

Battery storage with a capacity of around 300 MW is also included in the plan for 2030. An already operating battery storage located near the Tušimice power plant was proven to be functional and effective. Currently, the Czech Republic has installed power capacity in photovoltaics of 2.2 GW (about 10 % of total installed power in the country). The Ministry of the Environment concludes that by the end of 2030, this capacity could increase to 7-14 GW. [81, 82]

Of course, a case study of energy mix development scenarios would require much broader research. This is a very short list of found interesting ideas related to the topic, considering only the development of the energy mix in the Czech Republic.

4.5 Economics of operation

Industrial applications of plasma waste treatment processes strongly depend not only on legislative but also on economic factors. The biggest issue of plasma material treatment is, in addition to the technological complexity and high initial installation investments, also the high level of electrical energy consumption during operation, especially considering the current transformation of the energy market and the increase of energy prices, including electricity. [4, 7]

A preliminary analysis in the study [4] showed that processing waste rubber with this approach has economic potential under the following considerations:

- capital investment for a plant processing rubber waste 300 $kg \cdot h^{-1}$ is 1.5 million USD,
- specific energy consumption is 1 $kWh \cdot kg^{-1}$ rubber feed,
- electricity price for the industrial sector is \$0.05 per kWh,
- carbon black recovery is 23 % of rubber feed; market price for semi-reinforcing carbon black is $\$500 \cdot ton^{-1}$,
- gate fee for receiving rubber waste is $\$30 \cdot ton^{-1}$,
- gas yield is 3 $Nm^3 \cdot kg^{-1}$ rubber feed, and with a calorific value of 9 $MJ \cdot Nm^{-3}$,
- the gas is combusted in a boiler or gas engine for power generation at an efficiency of 26 %.

If a subject operating a plasma aggregate connected to the grid was only an energy consumer, the economics of operation would need to be based on these services provisions:

- waste collection and disposal and
- production of secondary raw materials, namely:
  - functional carbon black (active carbon, nanoparticles),
  - vitrified slag (building and base material),
  - synthesis gas (similar to coal gas or natural gas).

By definition, most of the wastes usually have a negative value. If some process adds value to these wastes, it should logically reduce the cost of its disposal. This is naturally related to government regulations, which tend to be stricter for hazardous waste. Of course, landfilling, for instance, may not only be limited by legislation, but also by space and the environment. [14]

For the energy sector, synthesis gas as a secondary raw material is the most relevant output. This is strongly amplified considering the current geopolitical situation, the dependence on natural gas imports, and the effort to use gas as a transitional primary medium for electricity generation.

In this scenario, the most decisive aspect of the project is to determine if the operating costs in the form of energy (or maintenance) will not exceed the revenues generated from providing the given materials.

In general, as the size and capacity of the facility increases, its efficiency increases (by extension using reheating, recuperation, external overheating or higher pressures), and the specific cost per unit of product (be it energy or secondary material) decreases. [6]

The general conclusion about the influence of the potentially higher efficiency of energy conversion by plasma gasification on the economy of operation compared to conventional processes is not yet strictly unambiguous. The competitiveness of plasma gasification technology is supported by a wide list of advantages, which I would summarize in the subsection *Advantages of plasma gasification* in the chapter *Plasma aggregate*. [14]

A 2020 study [6] comparing waste treatment using conventional incineration and thermal plasma gasification states that, in theory, the cost of processing a ton of plasma plant waste could be less than €2. The lowest price for landfilling a ton of MSW in the EU is €3 (usually between €6 and €15), which means that this technology can theoretically be competitive and self-sufficient. Even if the cost of MSW treatment using plasma technology would be several times higher, with the appropriate legislation, this could still represent the cheapest method of waste processing. In comparison, the most expensive fee for landfilling one ton of waste is in France, specifically €150. It is therefore evident that the country in which the potential plasma plant is located has a significant influence on the overall economy and competitiveness. In addition to France, countries like Finland or Ireland can be also included in the list of most attractive countries for the construction of a waste processing plasma gasification facility. The study concludes that the electricity sales price and indeed also the landfill fee have the greatest impact on the economics of operation. Factors like the discount rate, the sales price of secondary raw materials, and the initial investment are also influential, but yet far smaller than the former ones. [6]

The more difficult but economically more interesting solution might be changing the role in the energy market from a mere consumer to a provider of some system services or becoming a combined producer and consumer (prosumer). Especially for this case, the (upcoming) diverse distribution tariffs from ERO may be considered. Synthesis gas may be used to produce peak energy using a gas engine, turbine, or combined heat and power generation (CHP).

Some quantitative indicators for the economic comparison of different projects include, for example, net present value (NPV), internal rate of return (IRR), or payback period (PBP). These are mainly used to describe the potential profitability or return of individual projects. Determining these parameters requires extensive research and detailed economic models. The robustness of the mentioned qualitative economical indicators can be estimated using sensitivity analyses. [11]

According to [11], an economic model was created depending on the size of the processing capacity of the plasma gasification installation for subsequent electricity generation. The input material is considered RDF with considered ash content of 5 % and the moisture content of 10 %. The price of electricity was considered to be 0.12 USD per kWh and the process heat sold was 50 % of the electricity cost. Table 4.1 summarizes the results for the processing capacity range from 1 ton per day to 100 tons per day for factors like total plant costs, variable costs, fixed costs, IRR, NPV, and PBP. Other economic parameters will not be given further attention in this thesis. More research and commentary are devoted to these parameters, for example in [6] or [11]. [7]

Plant capacity ($^{\text{tons}}/_{\text{day}}$)	**1**	**10**	**20**	**50**	**100**
Plant cost (millions of $)	1	2.8	4	11	18
Variable costs ($ per year)	310	3.9k	8k	21k	118k
Fixed costs ($ per year)	104k	890k	890k	890k	996k
IRR (%)	1.6	14	38	47	58
NPV (millions of $)	0	4	19	72	158
PBP (years)	19	6.9	2.8	2.3	1.2

Table 4.1: Economic viability model results [11]

Furthermore, in the model from which table 4.1 is based, the payback period was set at 5 years. If one of the project requirements was a low (or medium) risk factor, it should generally apply that IRR > 20 %. Under these assumptions, it can be concluded that a processing capacity from 1 to 10 tons per day for RDF is not suitable and that only installations with a daily capacity of 20 tons (and more) reach favorable values. [11]

4.6 System services (SyS)

System Services (SyS) are activities performed by CEPS, which ensure the quality and reliability of electrical energy supply at the level of power systems. CEPS also fulfills international commitments and conditions for the interconnection of the Czech Republic's power system. The quality of electricity corresponds mainly to frequency and voltage. Reliability is related to the continuity of power supply at transmission system supply points. [83]

System services include:

- maintaining the quality of electrical energy,
- maintaining real-time power balance,
- restoring operation,
- dispatching control.

4.7 Support Services (SuS)

Supporting Services (SuS) are means of ensuring System Services (SyS). SuS are the activities of physical or legal entities ensuring the operation of the Power System, and the quality and reliability of the power supply. Through SuS, the difference between production and consumption can be regulated. This regulation is mediated by a change in consumption or power production. Subjects connected to the Power

System have the opportunity to offer SuS if they match the technical and commercial conditions set by the TSO. SuS can be divided into Power balancing services (PBS) and other SuS. According to the Transmission System Codex, these categories can be further divided to: [83]

- Power balancing services:
  - FCR - Frequency Containment Reserve,
  - aFRR - Automatic Frequency Restoration Reserve,
  - mFRR - Manual Frequency Restoration Reserve,
  - RR - Restoration Reserve.
- Other Support Services:
  - SRUQ - Secondary Regulation of U/Q,
  - OG - Off-Grid Operation,
  - BS - Black Start.

The following text in this section and further section *Conditions* is mostly inspired by [83] and [84].

4.7.1 Power balancing services

PBS are used to ensure the balance between production and consumption.

4.7.1.1 Frequency Containment Reserve

FCR is a local automatic function. Using a proportional regulator, a precisely defined change in unit output occurs depending on the deviation of frequency from the set value. FCR must occur within 30 seconds of the power imbalance appearance. The minimum power of one FCR unit is 1 MW, the maximum is 10 MW.

4.7.1.2 Automatic Frequency Restoration Reserve

aFRR is mediated by the change in power output of the regulated unit according to the requests from the CEPS Dispatch Center by the frequency and balance regulator of transferred powers. The regulating unit must provide the entire aFRR within 7.5 minutes from the CEPS Dispatch Center request. The minimum power of per unit providing aFRR is 1 MW, and the maximum is 99 MW. The reserve is divided into positive aFRR+ and negative aFRR-.

4.7.1.3 Manual Frequency Restoration Reserve

These reserves are mediated by a change in power output in response to requests from the CEPS Dispatch Center. The entire mFRR must take place within 12.5 minutes from the request. The minimum power of per mFRR providing unit is 1 MW and the maximum is 99 MW. The reserve is divided into positive mFRR+ and negative mFRR-.

4.7.1.4 Manual Frequency Restoration Reserve within 5 minutes

The entire mFRR5 reserve must be provided within 5 minutes of the request and there must be a guarantee of providing this reserve for a minimum of 4 hours per day. This reserve is only provided as positive. The minimum amount of mFRR5 is 1 MW, and the maximum amount is based on an agreement between CEPS and the SuS provider, the exact value is not specified.

4.7.1.5 Restoration Reserve

This is a reserve of active power available for cases of restoration or support of the required level of PBS, which is prepared for the upcoming system deviations. These reserves are performed by activating the regulation reserve RR+ or RR- and must be done within 30 minutes from the CEPS Dispatch Center request. In this case, there is no reservation fee for RR, only regulation energy is charged. The minimum amount of RR power is 1 MW and the maximum is 99 MW.

4.7.2 Other support services

Other support services, also known as non-frequency services, are used for voltage quality assurance and operation of the power system.

4.7.2.1 Secondary Regulation of U/Q

SRUQ refers to the automatic regulation of voltage and reactive power. The regulation uses the full contracted regulatory range of reactive power of blocks to maintain the requested voltage level in the power system within the prescribed tolerance. Additionally, this regulation must be able to cooperate with the tertiary regulation of reactive voltages and powers.

4.7.2.2 Off-Grid Operation

This SuS specifies the ability of a power plant block to operate in the off-grid mode, or within an isolated part of the system. The off-grid operation has strict requirements for the regulatory capability of the block and is essential for preventing and resolving emergency situations. The requirements for the block's capabilities are

- transition to the off-grid mode,
- off-gird mode,
- reconnection, and
- availability of the service at the necessary moment.

4.7.2.3 Black Start

BS denotes to the potential of the power plant block to start up without support from an external voltage source. The specified voltage and reconnection to the network must be achieved. The capability of OG operation of the block is needed too. The safe return of the state of operation in the affected part of the grid in the required time after a failure is the objective.

4.8 Conditions

Any participant in the electricity market who meets all the conditions for the specific SuS set out in the Transmission System Codex (Part II.) can be a provider of the SuS. These conditions are summarized as follows: The provider must have either a PBS Agreement or an Agreement on the conditions for purchasing and providing PBS, or a valid contract for providing other SuS except the PBS, before starting to offer SuS. Furthermore, certification for providing SuS in the commercial portal is necessary, and the approved certificate must be submitted to the DSO. Opinions from the DSO regarding the conditions for outputting active power for providing PBS to the CEPS through the DS are also required. The prerequisite for issuing this opinion is the assessment of the possibilities and conditions for providing PBS from the perspective of the DS to which the Provider is connected. As already mentioned, the following text in this chapter is largely inspired by [83, 84].

4.8.1 Aggregation

The growing number of decentralized sources of electrical energy in the Czech Republic opens up the possibility for the electricity system to utilize this energy. There is also the possibility of providing energy from small sources to the power system. However, if the service was defined by the providers and the time it fits them the best, it would be problematic to regulate the power grid. The prediction of a bigger number of sources for production and consumption would be very difficult, and deliveries could not be relied upon. Random moments of energy delivery to the grid also set up troubles for its regulation.

If someone is interested in providing electrical energy from their own sources, certain requirements and procedures set by the DS or TS must be complied. This also applies to the case of providing SuS. The energy-providing source should be flexible, which means the ability to turn on/off if necessary. The development of technologies (decentralized production, accumulation, electromobility, and others) increases the potential for flexibility and aggregation in the energy sector. Flexibility is a change in the amount of electricity taken/delivered by a market participant from/to the TS or DS during a given time interval compared to the agreed or expected schedule of consumption or delivery in response to price signals or commands.

Aggregation in the energy sector refers to an activity realized by a physical or legal entity that combines the electrical energy generated or consumed (including energy stored) from multiple customers for the purpose of selling, purchasing, or auctioning on any electricity market. These customers must be equipped with continuous or smart metering. Aggregation can also be described as sharing of electrical energy by market participants. These participants form certain energy communities that work with electrical energy within a defined energy system.

In the energy sector, an aggregate is a device capable of generating electrical energy or heat. Aggregates can include renewable energy sources, biogas stations, diesel generators, or plasma generators, after appropriate adjustments. Currently, the amount of these lesser power sources is increasing compared to conventional power plants (coal, nuclear). As long as the technical and commercial conditions set by the TSO are complied with, these entities have the right to provide SuS in the case of interest. The Transmission System Codex (Part II.) describes these conditions in detail.

There is no need for these small aggregates to meet the minimum power requirements for providing SuS. At the same time, a wide range of sources would be more difficult to control. Despite that, these aggregates together can form larger entities, called aggregation blocks, fulfilling the minimum power requirements.

4.8.2 Conditions for creating, changing and operating aggregation blocks

When the provider of SuS has a large number of energy facilities, that can be difficult to manage, there is the option to create aggregation blocks (ABs) that would simplify their overall remote control. The second option for creating AB is when the facilities of the SuS provider separately do not meet the requirements for providing PBS individually, for example in terms of minimal power. Reserve provision would then be facilitated through one terminal unit controlling the entire group of devices in one AB. To create ABs or to introduce a new Provider, certain criteria, precisely defined in the Transmission System Codex (related to administration and technical requirements for the given SuS), must be attained.

Before submitting a written request to CEPS, it is necessary to first have a SuS Provider Study, prepared by a Certifier. These documents are then submitted. If changes of the AB are made (expansion of AB or permanent removal of a device from AB) by June 30, 2023, recertification is not necessary. From July 1, 2023, AB will need to be recertified for some PBS, after the changes.

An aggregation block can provide one or a combination of PBS, or it can provide FCR to CEPS. If CEPS approves the study of the SuS provider, the provider is granted the identification number for the AB along with the approval.

4.8.2.1 The process of introducing a new provider, a new unit

The prospective provider of SuS or the implementation of a new unit must undergo a process, specified in the Transmission System Codex (Part II). In summary, it consists of the following processes:

- The prospective provider contacts CEPS regarding the intention of providing SuS, and submits a *Study of the Provider of CEPS*, which is prepared by a Certifier.
- As of July 1st, the study must include the identification code of the energy facility providing SuS.
- CEPS will approve the materials submitted by the Provider in a positive case scenario.

- Upon approval, tests and trials will take place in cooperation with CEPS.
- The prospective provider will then submit the DSO statements.
- The prospective provider will conclude a PBS Agreement or an agreement for the provision of other SuS with CEPS.

4.8.2.2 Conditions for the operation of aggregation blocks

AB can provide any of the PBS individually or as a combination of PBSs. It can also provide FCR for CEPS. If CEPS approves the Study of Provider of SuS, the Provider obtains the approval and the identification number of AB.

AB must be composed of energy facilities operated by one provider. In the case of a billing rate change at the energy facility providing SuS within the AB, the Provider must inform CEPS and submit consent from the new billing entity. The AB must be metered and the appropriate measured quantities need to be transmitted to the CEPS unified dispatch control system. When providing PBS with input/output installed power over 1.5 MW, the actual power must be conveyed separately.

4.8.2.3 Energy equipment

The Transmission System Codex (Part II) distinguishes energy facilities in terms of the way energy is transformed. This work examines energy facilities falling into the category of gas and combustion power plants.

4.8.2.4 Register of energy equipment

The energy facility register contains a list of energy facilities that can provide SuS. The register is part of the commercial portal. Energy facilities are recorded in the register based on the Provider Study of SuS or the values established by the Certifier. The register contains the following information:

- manufacturer of the energy equipment,
- type (typical designation by the manufacturer of the energy equipment),
- kind of energy equipment,
- primary energy source,
- serial number, label photo, EAN,
- GPS coordinates of the energy equipment, including closer location (floor and room number),
- DSO's statement in case of connection to DS,
- nominal power (P_n), minimal power (P_min), and maximal power (P_max) of the equipment,
- size of the potential value of reserves for each PBS that can be provided using the energy equipment,
- category of the energy equipment: I/II.

Chapter 5

Pilot projects, studies, and proposals

This chapter will describe some of the pilot projects or studies concerning the issue of the commercial and industrial implementation of the technology of plasma gasification of waste. In the second part, proposals for some types of potentially attractive projects to be implemented will be indicated, including a discussion about their possible competitiveness.

Plasma waste treatment reactors require a significant amount of energy, which makes their operation quite expensive. If the secondary products of the process are used and recycled in terms of energy or material, the process can be self-sufficient. This waste management approach has already been implemented in places where there are strict environmental regulations and very high landfill costs. [4]

The energy required to process a ton of waste can range from 665 to 5000 kWh. It always depends on the specific type of waste, the treatment process and its thoroughness. [7]

5.1 Studies

Many authors have addressed the issue of the economics of plasma gasification facilities theoretically and come to conclusions about whether such a project can be reasonable, competitive, and self-sufficient. Assumptions and conditions under which operation is expected have been established, which is the basis for following drawn conclusions.

Mustoe and co-authors reviewed various operating cost factors for plasma vitrification plants assuming full-time (24-hour) operation for 300 days per year and a lifetime of 8 years with the cost of \$0.06 per kWh. By using the energy of flue gas, the specific costs per unit of energy can be reduced, and a capacity of over 100 tons per day would appear to be sufficient. From a purely financial point, with current energy prices, the situation is quite different. Since the internal structure of the model is not known, it is impossible to say with certainty how much the conditions for profitable operation would change. [7]

Jun Li and other researchers investigated the economic process of operating a plant for plasma gasification of MSW combined with energy generation. In this case, a daily processing capacity of 600 tons, an electricity price of $0.097 per kWh, and approximately 350 kWh per ton of processed material were sold. The annual production of secondary raw materials was 100 thousand tons and the total initial investment was nearly 100 million USD. [7]

In total, annual profits from the sale of electricity, secondary raw materials, and subsidies are said to be around $28.8 million. In comparison, the revenues of conventional combustion thermal power plants do not exceed 9.5 million USD annually. Considering similar investment sizes, this would mean a roughly three times faster payback time for a project with an integrated plasma gasification system than in the case of ordinary incinerators. [7]

E. N. Kalogirou discusses the tools and business models of various W2E technologies and tentatively designs equipment and sets an indicative range of initial capital expenditure (CAPEX) for construction at $450-900 per ton of processing capacity per year. For instance, included parameters are energy properties of processed materials, local socio-financial conditions, gross domestic product (GDP), or climatic conditions. Annual Operating Expenses (OPEX) depend on many aspects, but as a first estimate can be determined as 2-3 % of the capital investment. [7]

To give a real example, South Korea's installation of a W2E plasma gasification facility with a capacity of 10 tons of MSW per day (3.3 thousand tons per year) had a CAPEX of 3 million USD. [7]

5.2 Real operating facilities

This section will summarize some of the world's existing pilot projects and existing functioning W2E facilities, using thermal plasma waste treatment technology.

Commission of one of the first plasma pyrolysis plants for the processing of fly ash with a daily capacity of 200 tons dates back to 1983 in Sweden. In 1985, a facility with a daily capacity of 24 tons was opened in Alabama, and in 1991 in Canada for 50 tons per day of aluminum scrap, and in Asia the first plasma processing plant MSW also with a capacity of 50 tons per day was opened in 1995. At the turn of the millennium, plants in France and Norway followed, namely for the processing of MSW ash, asbestos, and tannery all with daily capacities between 10-20 tons. [6]

In Japan, where landfilling is strictly controlled, 70 % of MSW has already been incinerated 15 years ago. About a third of the mass is then collected as bottom ash or fly ash. These residues can be reduced by 50 % with the use of plasma pyrolysis technology, while toxic heavy metals are encapsulated in a non-leachable slag. The safety parameters of this slag are significantly better than required by any regulation. This is one of the most widespread uses of thermal plasma technology for material treatment. [14]

For example, in the Japanese city of Utashinai, there is a large operating power plant designed by Hitachi Metals Corp. since 2002. mainly for automotive industry waste, which has a daily processing capacity of 165 to 300 tons of MSW. The nominal power is 8 MW and more than half of that is supplied to the grid. The energy consumption of processing 1 ton of waste here is around 100-250 kWh. Another exemplary plant, designed by Westinghouse, is in operation in Rome, Italy, and has a daily capacity of 336 tons of waste. [7, 11]

The demonstration plasma gasification plant built in Morcenx (France) by Europlasma has an electrical output power of 12 MW and a projected capacity of around 35 thousand tons of industrial waste per year and about 15 thousand tons of biomass per year. The plant has already reached Final Acceptance with Reservation status. [7, 11]

It is interesting to note that the amount of processing capacity does not indicate and declare the size of the output electrical power of the plant. This can be caused by different technological procedures, different energy requirements of the technology, or a different type of processed material.

After 2000, units for plasma waste treatment became very widespread, especially with smaller operating capacities around low tens of tons per day, as it is visible, for example, in table 1 in the appendices of this thesis. [7]

Currently, the largest plasma waste processing facility is Air Product's Tees Valley plant in Stockton-on-Tees, UK. Processing capacity is nearly a thousand tons of nonrecyclable waste per day (300 thousand per year) and the facility generates 50 MW of electrical power. [11]

5.3 Realization

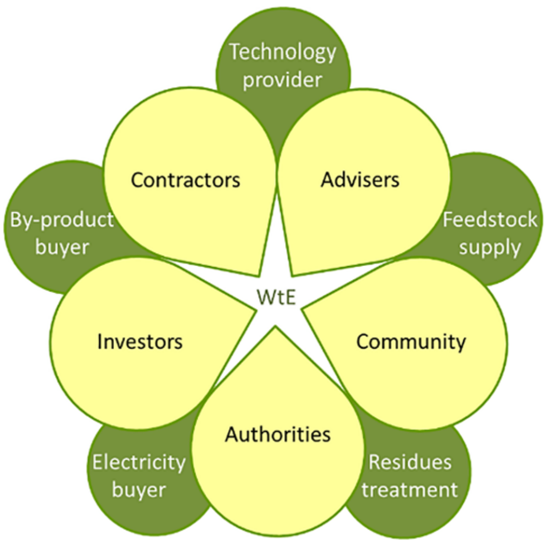

Figure 5.1: Stakeholders of the W2E projects [6]

When assessing a project as W2E, all participants in the project must be considered.

The hierarchy of project membership can be visualized with the figure 5.1.

Stakeholders can be divided into ones directly related to the facility (yellow) and the subordinate, subcontracted actuators (green). [6]

In the case of the implementation of a real commercial project, it is important not to forget any of the necessary.

Of course, it always depends on the specific purpose of the given device. For a general plasma solid waste treatment system, the facility should consist of: [4, 7]

- the plasma reactor with metal and slag collection,
- supplying system for energy, gases, water, and material feeding,
- control and data acquisition equipment,
- auxiliary combustor for higher residence times,
- cooling chamber (depending on the waste),
- cleaning systems (cyclone, gas scrubber, absorbers, filters or separators),
- fan to create negative pressure.

5.4 Perspective applications

As previously mentioned, the motivation for addressing this topic was the assessment of the possibility of plasma waste treatment technology integration into the energy infrastructure. In addition to the technology and process description, related research about power system infrastructure development (and its prediction), the energy market (including legislation, system, and other services that the facility may provide in practice), or the relevant conditions for the project implementation were carried out.

The expected result of this thesis is the following list of proposals for some prospective applications of this technology, specifically concerning the areas of waste management, operation of the energy system, or sale of secondary raw materials. All these areas are connected with technology and can form the basis for determining the financial strategy and economic self-sufficiency of the project. These topics are worth further investigation, for example as the subject of consecutive research, other final theses, or case studies.

5.4.1 Stationary W2E facility

Non-mobile plasma treatment W2E facility would primarily process waste materials for the purposes of energy and material utilization. For suitable input material (with a sufficient content of organic components), the device can theoretically be energetically self-sufficient. In another case, energy would need to be taken from the grid, which would be attractive especially outside peak load (because of the electricity prices). In order to solve the economic question of the potential facility operation, it is necessary to make a case study including all important aspects (including the type of processed waste). Attractive materials for processing are problematic wastes from the perspective of the waste processing industry (for example sewage sludge or MSW). [7]

If the installed plasma waste treatment equipment produced even more energy than it consumed, it would be possible to supply the energy to the grid using one of the known methods, such as gas tubes, steam turbines, or a large integrated gasification cycle using solid lignite as fuel (or potentially also Stirling engines). Cogeneration is also worth considering implementing, as it can increase energy savings by up to 40 %. According to some reports, a plasma waste processing plant with a daily capacity of 2-3 thousand tons can achieve an operational electrical power output of 120 MW. Costs for a facility of these dimensions are estimated from a quarter to half a billion USD. [6, 7, 11]

Moreover, the potential production of other chemicals is also possible. Creating hydrogen from pure synthesis gas is a known process that is relatively easy and efficient. Most of the methanol production (approximately $^3/_4$) is still realized from natural gas. Using the plasma gasification method, this approach can be economically and ecologically replaced. [7]

Note: Regarding the replacement of natural gas for synthesis gas in the field of internal combustion engines and gas turbines, it is important to pay attention to the purity and overall composition. If hydrogen predominates in the mixture, due to its faster burning, it can cause premature engine conditions, knocking, or backfire. To avoid this, the power is usually reduced from 50 to 70 % of the nominal state (for example, a 1063 kW natural gas engine will deliver a maximum of 730 kW on syngas). [11]

5.4.2 Mobile waste processing unit

Small mobile plasma gasification units can be an attractive option, but there is a big trade-off. While this approach significantly eliminates transportation and investment costs, it will significantly increase labor costs (and probably operating costs, as less operating capacity and power will mean greater relative losses). [14]

In general, small stationary gasification units also have problematic properties from a financial perspective. Most challenging is the high-cost contribution of instrumentation, and generally lower efficiency compared to larger systems. This limits the possibilities of the technology downscaling. [11]

5.4.3 Provider of Support services

The individual SuS and their conditions for fulfillment are briefly described and categorized in chapter *Electricity market*. This knowledge is necessary to determine, whether the aggregate containing plasma gasification unit is capable of providing any of the SuS. Furthermore, a general description of the principle of aggregating energy sources is discussed. The general description is sufficient, as for any aggregate or AB it is fundamental to satisfy all demands of the TS (for instance minimum power, start-up time, certification, or testing).

For the reason of a relatively fast ramp-up to maximum power (from seconds to minutes), plasma aggregates are potentially suitable for all types of SuS from the PBS group, except FCR (the system would require a secondary gas power cycle). As the power (considering the case of the semi-operational reactor at IPP CAS) is not sufficient enough to meet the minimum power requirements set by the TS Codex, independent provision of SuS is not possible. The solution might be the connection of more facilities into AB. There are other factors to examine when assessing the ability of aggregates to provide SuS, for example, reliability. Generally speaking, plasma aggregates can provide SuS in the form of AB, when all the conditions for creating, changing, and operating the AB (set out in Part II of the TS Codex), are complied with.

5.4.4 Honorable mentions

In consideration of the energy mix perspective, one fact needs to be mentioned. The expansion of renewable sources in the energy mix (which are often weather-dependent soft sources or do not have the character of torque) can have a negative impact on the stability of the grid and its components, which are typically designed for certain parameters, including the alternating nature of electrical energy.

Plasma reactors are capable to utilize direct current and produce the synthesis gas from the input organic material, enabling energy to be accumulated, whether in the form of conversion to motor fuels, methane, or other chemicals like acetylene, methanol, or ethanol, for example. Moreover, when the fuel or gas (as a secondary product) is later combusted for electricity generation purposes in the secondary aggregate cycle, (alternating) electrical energy can be produced.

Last but not least, this technology can also be potentially incorporated into Space colonization missions in the future. Early in these efforts, the capacity to transport resources and supplies will be very limited. For this reason, it will be necessary to maximize the use of all the material imported, including waste.

5.5 Feasibility

In summary, the future integration of the system using thermal plasma waste treatment technology into the power infrastructure is feasible for the following reasons:

- anticipated changes in the energy mix and tariff structure,
- the geopolitical situation, energy crisis, and uncertainty regarding gas supplies,
- expected stricter conditions for waste disposal (landfilling in particular) or
- the installation of new technologies like AMM.

Other options for improving the potential commercial project (which can strengthen the competitiveness of the plasma processing technology of waste) may include more efficient utilization of waste heat from the process, for example:

- utilizing waste heat for the production of electricity, heat, and cooling: [85]
  - electricity production - organic Rankine cycle,
  - production of cold - absorption cooling,
  - heat production - absorption heat pump,
  - electricity, heat, and cold production - trigeneration,
- utilizing waste heat for drying processed material.

Conclusion

The subject of this master's thesis was the issue of waste treatment using thermal plasma, accompanied by the production of secondary raw materials, for instance, synthesis gas or carbon black. The first chapter is devoted to the description of the plasma reactor equipment and its various configurations, including an introduction to the basics of plasma theory and the thermochemical reactions present inside the reaction chamber, the thermal plasma sources used (plasma torches), and a brief summary of other possibilities of this technology utilization.

An integral part is an experimental activity in the laboratory at the PCHT department at the IPP CAS, which cannot be done without appropriate preceding activities, for example, preparation of material samples and diagnostic devices, calibration, testing of plasma torches, or their subsequent assembly. The experiments that are part of this thesis differ depending on the used plasma torch (HPT or MWPT) or the processed material (SMW or RDF). The HPT experiments were divided into several intervals to test different operating conditions, especially from the perspective of the supply of accompanying oxidizing agents and subsequent chemical analyses of the generated synthesis gas composition. Oxidizing agent in this case was carbon dioxide. The MWPT experiment primarily served to test the operation of a new configuration using this newly tested type of plasma torch.

The most important part of the thesis is the chapter dealing with the results of the experiments and their analysis. One of the best tools to assess a given experiment (including the mutual comparison of plasma torches or processed materials) is the energy balance of the process, which was created using a discrete balance model. From these balances, some characteristic parameters and quantities were subsequently determined. The most important are, for example, the efficiency of energy conversion, usable waste heat (on an industrial scale), or the energy ratio of substances at the output and input of the process. The results of the energy balances are summarized in tables 3.17, 3.18 a 3.19. Tables 3.20, 3.21 a 3.22 offer a mutual comparison of the processes. This part of the thesis may be considered the most beneficial from the perspective of processing the master's thesis, namely also for the research activity at PCH IPP CAS.

The results show that the highest energy conversion efficiency was achieved in the case of operation with HPT during RDF processing, specifically more than 53 % on average (the highest value achieved was almost 58 %). On the contrary, the lowest energy conversion efficiency in the case of MWPT was on average below 40 % (at least around 28 %). In the case of the experiment with HPT and SMW, very similar, slightly better results were achieved than in the case of the MWPT experiment. However, it is necessary to keep in mind that the actual results with MWPT can probably be even worse because of the frequent presence of undesirable combustion during the experiment and therefore an inaccurate estimate of the ratio between carbon black and ash.

Considering the MWPT experiment, the energy of the input material was allegedly more than doubled in one of the time intervals. Although this result is realistic in general (as confirmed, for example, by [16]), it is rather improbable for this specific case, considering all operational complications. In the HPT experiments, at best, the energy of the by-products was almost doubled compared to the energy of the input products, namely during the time intervals of the highest supply of carbon dioxide as an oxidizing agent. On the contrary, these results can be considered quite convincing. On the other hand, if the goal of the process is to maximize the yield of hydrogen, it is desirable not to add carbon dioxide to the process, or to choose a different form of oxidizing agent like water or steam. From this point of view, the MWPT with water vapor as a stabilization medium (which will be tested on IPP CAS in the near future) seems also promising.

The utilization of the waste heat from the experimental process compared to the input energy (and considering the plasma gasification reactor PLASGAS at PCHT IPP CAS) was estimated at 33-37 % in the case of HPT, in the case of MWPT it is only 22-28 % (which is caused by increased flow rates of the stabilizing media, which thereby takes away heat from the process more intensively).

When interpreting these results, it is necessary to keep in mind that the entire experimental process is always influenced by several diverse factors that could not be included in the compilation and calculation of the energy balance models in this thesis. For example, these factors include time-varying heat losses, different atmospheric conditions (especially temperature), different sizes of the input processed material pieces (granularity), the stochastic nature of material feeding, and much more.

Furthermore, because of many complications (either during the experiment or during data processing and computations), balance models serve primarily for an initial orientational comparison of the given processes. Among the fundamental complications can be included the limited amount and character of experimental data (related to the technical possibilities of the laboratory), the overall complexity of the entire experimental facility and the process itself, the interconnection of many technical engineering disciplines (electrical, mechanical, chemical) or the impossibility of some partial calculations corrections because of the hermetic closing of the system during experiments.

Despite the scope of this thesis, it was not possible to either create simulation models (which would test the functionality and behavior of a potential operational system unit) or economic models (which could support or refute the competitiveness of this technology), mainly as a result of time constraints. For this reason, research was also conducted on the topic of the economic aspects of the plasma gasification of waste technology and pilot projects that already utilize it. This research (including related cited sources) confirmed that this technology can be competitive, and even potentially attractively profitable. From this perspective, the accomplishment of the personal goals of this thesis can be considered relatively fulfilled. Also, as intended, proposals for possible commercial projects attractive for possible implementation were presented. However, their subsequent comparison is very brief, only concerning some of the technical aspects.

The main obstacle restraining the development and expansion of plasma gasification technologies in the commercial sector is the legislation still present in the Czech Republic (similarly as for the case of agrovoltaics, for example). Landfilling will soon be strictly limited and significantly more expensive. Along with other changes in the energy sector, this can bring many opportunities for plasma waste treatment technology.

A more detailed focus on the economics of operation, a proposal for specific project implementation, a simulation of a potential industrial system, or a closer investigation of waste treatment processes with thermal plasma (especially with the lately tested MWPT) can be the subject of further work of any type, regardless the author who would follow up on this thesis.

References

1. BITTENCOURT, José A. *Fundamentals of plasma physics*. Springer Science & Business Media, 2004.
2. BOULOS, Maher I..; FAUCHAIS, Pierre; PFENDER, Emil. *Thermal plasmas: fundamentals and applications*. Plenum Press, 1994.
3. PILAŘ, Jakub. *Gazifikace a pyrolýza odpadnıch látek s využitım termického plazmatu*. 2021. B.S. thesis. České vysoké učenı technické v Praze. Vypočetnı a informačnı centrum.
4. HUANG, Haitao; TANG, Lan. Treatment of organic waste using thermal plasma pyrolysis technology. *Energy Conversion and Management*. 2007, roč. 48, č. 4, s. 1331–1337.
5. CHEN, Francis F. *Introduction to plasma physics*. Plenum Press, New York, 1974.
6. RAMOS, Ana; BERZOSA, Joan; ESPI, José; CLARENS, Frederic; ROUBOA, Abel. Life cycle costing for plasma gasification of municipal solid waste: A socio-economic approach. *Energy Conversion and Management*. 2020, roč. 209, s. 112508.
7. SIKARWAR, Vineet Singh; HRABOVSKÝ, Milan; VAN OOST, Guido; POHOŘELÝ, Michael; JEREMIÁŠ, Michal. Progress in waste utilization via thermal plasma. *Progress in Energy and Combustion Science*. 2020, roč. 81, s. 100873.
8. *Introduction to Plasma Physics - YouTube* [online]. [B.r.] [cit. 2023-05-18]. Dostupné z: `https://www.youtube.com/playlist?list=PLogdluxJPZEqNAICx2zBrmoYNr_F_jhM3`.
9. GOMEZ, E; RANI, D Amutha; CHEESEMAN, CR; DEEGAN, D; WISE, M; BOCCACCINI, AR. Thermal plasma technology for the treatment of wastes: A critical review. *Journal of hazardous materials*. 2009, roč. 161, č. 2-3, s. 614–626.
10. An alternative approach to the Boltzmann distribution through the chemical potential. *Il Nuovo Cimento C* [online]. 2016, roč. 38, č. 3, s. 1–10 [cit. 2023-05-18]. ISSN 03905551, ISSN 03905551. Dostupné z DOI: `10.1393/ncc/i2015-15090-5`.
11. HRABOVSKY, Milan; WALT, Izak Jacobus van der. Plasma Waste Destruction. In: *Handbook of Thermal Science and Engineering*. Ed. KULACKI, Francis A. Cham: Springer International Publishing, 2017, s. 1–57. ISBN 978-3-319-32003-8. Dostupné z DOI: `10.1007/978-3-319-32003-8_32-1`.

12. KAVKA, Tetyana. *Study of thermal plasma jets, generated by DC arc plasma torches used in plasma spraying applications.* 2006. Dis. pr. Ph. D. Thesis, Charles University in Prague. APPENDICES.

13. FABRY, Frédéric; REHMET, Christophe; ROHANI, Vandad; FULCHERI, Laurent. Waste gasification by thermal plasma: a review. *Waste and Biomass Valorization.* 2013, roč. 4, s. 421–439.

14. HEBERLEIN, Joachim; MURPHY, Anthony B. Thermal plasma waste treatment. *Journal of Physics D: Applied Physics.* 2008, roč. 41, č. 5, s. 053001.

15. *Plasma torch* [online]. 2021 [cit. 2023-02-04]. Dostupné z: `https://en.wikipedia.org/w/index.php?title=Plasma_torch&oldid=1000778417`. Page Version ID: 1000778417.

16. HRABOVSKY, MKMKV; KONRAD, M; KOPECKY, V; HLINA, M; KAVKA, T; VAN OOST, Guido; BEECKMAN, E; DEFOORT, B. Gasification of biomass in water/gas-stabilized plasma for syngas production. *Czechoslovak Journal of Physics.* 2006, roč. 56, B1199–B1206.

17. *Water-Stabilized Plasma (WSP)* [online]. 2013 [cit. 2023-02-04]. Dostupné z: `https://degradation2.wordpress.com/alternatives/direct-current-dc-plasma/water-stabilized-plasma-wsp/`.

18. *Hybrid Plasma* [online]. 2013 [cit. 2023-02-04]. Dostupné z: `https://degradation2.wordpress.com/alternatives/direct-current-dc-plasma/hybrid-plasma/`.

19. UHM, Han S; HONG, Yong C; SHIN, Dong H. A microwave plasma torch and its applications. *Plasma Sources Science and Technology.* 2006, roč. 15, č. 2, S26.

20. STONIES, Robert; SCHERMER, Susanne; VOGES, Edgar; BROEKAERT, José AC. A new small microwave plasma torch. *Plasma Sources Science and Technology.* 2004, roč. 13, č. 4, s. 604.

21. TACHI, Shinichi; TSUJIMOTO, Kazunori; OKUDAIRA, Sadayuki. Low-temperature reactive ion etching and microwave plasma etching of silicon. *Applied physics letters.* 1988, roč. 52, č. 8, s. 616–618.

22. MOISAN, M; SAUVE, G; ZAKRZEWSKI, Z; HUBERT, J. An atmospheric pressure waveguide-fed microwave plasma torch: the TIA design. *Plasma Sources Science and Technology.* 1994, roč. 3, č. 4, s. 584.

23. *Facilities* [online]. [B.r.] [cit. 2021-04-06]. Dostupné z: `http://www.ipp.cas.cz/vedecka_struktura_ufp/plazmochemicke_technologie/pristrojove_vybaveni/`.

24. ČR, MŽP. *Odpady* [online]. 2008 [cit. 2023-03-28]. Dostupné z: `https://www.mzp.cz/cz/odpady_podrubrika`.

25. *Bulky waste* [online]. 2021 [cit. 2023-04-02]. Dostupné z: `https://en.wikipedia.org/w/index.php?title=Bulky_waste&oldid=1009058474`. Page Version ID: 1009058474.

26. ALEJTECH.CZ. *V Úholičkách zahájila provoz nová třídící linka* [online]. [B.r.] [cit. 2023-03-28]. Dostupné z: `https://www.fcc-group.eu/ceska-republika/novinky/v-uholickach-zahajila-provoz-nova-tridici-linka`.

27. *Refuse Derived Fuels (RDF) in the cement industry - GRUPO SPR* [online]. 2021 [cit. 2023-03-27]. Dostupné z: https://www.grupo-spr.com/en/refuse-derived-fuels-rdf-in-the-cement-industry/.

28. ZHANG, Li; WU, Lihua; TIAN, Feng; WANG, Zheng. Retrospection-simulation-revision: approach to the analysis of the composition and characteristics of medical waste at a disaster relief site. *PloS one*. 2016, roč. 11, č. 7, e0159261.

29. IVO, Meruna. *Návrh dopravnıch cest odpadu plnıcı stanice*. 2019. Dipl. pr. České vysoké učenı technické v Praze. Vypočetnı a informačnı centrum.

30. PIVOŇKA, Marek. *Návrh šnekového dopravnıku*. 2018. Dipl. pr. České vysoké učenı technické v Praze. Vypočetnı a informačnı centrum.

31. *Water - Density, Specific Weight and Thermal Expansion Coefficients* [online]. [B.r.] [cit. 2023-04-15]. Dostupné z: https://www.engineeringtoolbox.com/water-density-specific-weight-d_595.html.

32. *Water - Specific Heat vs. Temperature* [online]. [B.r.] [cit. 2023-04-15]. Dostupné z: https://www.engineeringtoolbox.com/specific-heat-capacity-water-d_660.html.

33. FILIP, Jiří; ORAL, Jaroslav; MENDELOVA ZEMĚDĚLSKÁ A LESNICKÁ UNIVERZITA. *Odpadové hospodářství. II II*. V Brně: Mendelova zemědělská a lesnická univerzita, 2003. ISBN 9788071576822. OCLC: 320586153.

34. *Calorific value of waste* [online]. 2017 [cit. 2023-04-15]. Dostupné z: https://www.igniss.com/calorific-value-waste.

35. VDI E. V. (ed.). *VDI Heat Atlas* [online]. Berlin, Heidelberg: Springer Berlin Heidelberg, 2010 [cit. 2023-03-30]. ISBN 9783540778769 9783540778776. Dostupné z DOI: 10.1007/978-3-540-77877-6.

36. *Characteristic length* [online]. 2023 [cit. 2023-04-15]. Dostupné z: https://en.wikipedia.org/w/index.php?title=Characteristic_length&oldid=1132753797. Page Version ID: 1132753797.

37. *Air - Density, Specific Weight and Thermal Expansion Coefficient vs. Temperature and Pressure* [online]. [B.r.] [cit. 2023-04-15]. Dostupné z: https://www.engineeringtoolbox.com/air-density-specific-weight-d_600.html.

38. *Air - Dynamic and Kinematic Viscosity* [online]. [B.r.] [cit. 2023-04-15]. Dostupné z: https://www.engineeringtoolbox.com/air-absolute-kinematic-viscosity-d_601.html.

39. *Air - Specific Heat vs. Temperature at Constant Pressure* [online]. [B.r.] [cit. 2023-04-15]. Dostupné z: https://www.engineeringtoolbox.com/air-specific-heat-capacity-d_705.html.

40. *Air - Thermal Conductivity vs. Temperature and Pressure* [online]. [B.r.] [cit. 2023-04-15]. Dostupné z: https://www.engineeringtoolbox.com/air-properties-viscosity-conductivity-heat-capacity-d_1509.html.

41. *Tabulka emisivit* [online]. [B.r.] [cit. 2023-04-19]. Dostupné z: http://www.termokamera.cz/tabulka-emisivit/.

42. *Hodnoty emisivity běžných materiálů | Fakulta bezpečnostního inženýrství VŠB-TUO* [online]. [B.r.] [cit. 2023-04-19]. Dostupné z: https://www.fbi.vsb.cz/export/sites/fbi/030/.content/galerie-souboru/studijni-materialy/TechnickaMereni/5_EmisivitaBeznychMaterialu.pdf.

43. *Tabuľka emisivity materiálov* [online]. [B.r.] [cit. 2023-04-19]. Dostupné z: https://www.elso.sk/sk/blog/technologie/tabulka-emisivity-materialov.

44. *Nusselt number* [online]. 2022 [cit. 2023-04-15]. Dostupné z: https://en.wikipedia.org/w/index.php?title=Nusselt_number&oldid=1124648279. Page Version ID: 1124648279.

45. DAY, Jerod C; ZEMLER, Matthew K; TRAUM, Matthew J; BOETCHER, Sandra KS. Laminar natural convection from isothermal vertical cylinders: revisting a classical subject. *Journal of heat transfer*. 2013, roč. 135, č. 2.

46. CIEŚLIŃSKI, Janusz T; SMOLEN, Slawomir; SAWICKA, Dorota. Free convection heat transfer from horizontal cylinders. *Energies*. 2021, roč. 14, č. 3, s. 559.

47. *Promalight | Promat Technical Data Sheet | Adriaoffer* [online]. [B.r.] [cit. 2023-04-16]. Dostupné z: https://www.adriaoffer.hr/wp-content/uploads/2022/09/promat-promalight-product-data-sheet-usa.pdf.

48. *>1500 °C · Průmyslová keramika* [online]. [B.r.] [cit. 2023-04-16]. Dostupné z: https://prumyslova-keramika.cz/katalog/zarobetony-nizkocementove-lcc/%3E1500c.

49. *Rohože Alsiflex a Dalfratherm* [online]. [B.r.] [cit. 2023-04-16]. Dostupné z: https://propec.cz/rohoze-alsiflex-dalfratherm.

50. MICHEJEV, Michail Aleksandrovič. *Základy sdılenı tepla*. Prmyslové vydavatelstvı, 1952.

51. *Gas constant* [online]. 2023 [cit. 2023-04-16]. Dostupné z: https://en.wikipedia.org/w/index.php?title=Gas_constant&oldid=1149201537. Page Version ID: 1149201537.

52. *Air - Molecular Weight and Composition* [online]. [B.r.] [cit. 2023-04-16]. Dostupné z: https://www.engineeringtoolbox.com/molecular-mass-air-d_679.html.

53. *Fuel Gases - Heating Values* [online]. [B.r.] [cit. 2023-04-23]. Dostupné z: https://www.engineeringtoolbox.com/heating-values-fuel-gases-d_823.html.

54. *Solids - Specific Heats* [online]. [B.r.] [cit. 2023-04-23]. Dostupné z: https://www.engineeringtoolbox.com/specific-heat-solids-d_154.html.

55. *Air - Composition and Molecular Weight* [online]. [B.r.] [cit. 2023-04-23]. Dostupné z: https://www.engineeringtoolbox.com/air-composition-d_212.html.

56. *Molecular Weight of Substances* [online]. [B.r.] [cit. 2023-04-23]. Dostupné z: https://www.engineeringtoolbox.com/molecular-weight-gas-vapor-d_1156.html.

57. *Fuel Gases - Heating Values* [online]. [B.r.] [cit. 2023-04-23]. Dostupné z: https://www.engineeringtoolbox.com/heating-values-fuel-gases-d_823.html.

58. *Hydrogen - Specific Heat* [online]. [B.r.] [cit. 2023-04-19]. Dostupné z: https://www.engineeringtoolbox.com/hydrogen-d_976.html.

59. *Methane Gas - Specific Heat vs. Temperature* [online]. [B.r.] [cit. 2023-04-19]. Dostupné z: https://www.engineeringtoolbox.com/methane-d_980.html.
60. *Isobaric Properties for Argon* [online]. [B.r.] [cit. 2023-04-19]. Dostupné z: https://webbook.nist.gov/cgi/fluid.cgi?P=1&TLow=100&THigh=1500&TInc=10&Digits=5&ID=C7440371&Action=Load&Type=IsoBar&TUnit=C&PUnit=bar&DUnit=kg%2Fm3&HUnit=kJ%2Fkg&WUnit=m%2Fs&VisUnit=uPa*s&STUnit=N%2Fm&RefState=DEF.
61. *Carbon Monoxide - Specific Heat vs. Temperature* [online]. [B.r.] [cit. 2023-04-19]. Dostupné z: https://www.engineeringtoolbox.com/carbon-monoxide-d_975.html.
62. *Carbon Dioxide - Specific Heat of Gas vs. Temperature* [online]. [B.r.] [cit. 2023-04-19]. Dostupné z: https://www.engineeringtoolbox.com/carbon-dioxide-d_974.html.
63. *Nitrogen Gas - Specific Heat vs. Temperature* [online]. [B.r.] [cit. 2023-04-19]. Dostupné z: https://www.engineeringtoolbox.com/nitrogen-d_977.html.
64. *Oxygen Gas - Specific Heat vs. Temperature* [online]. [B.r.] [cit. 2023-04-19]. Dostupné z: https://www.engineeringtoolbox.com/oxygen-d_978.html.
65. CHASE, M. W. Nitric oxide, NIST-JANAF Themochemical Tables, Fourth Edition. 1998, s. 1–1951. Dostupné také z: https://webbook.nist.gov/cgi/cbook.cgi?ID=C10102439&Mask=1&Type=JANAFG&Table=on#JANAFG.
66. CHASE, M. W. Nitrogen dioxide, NIST-JANAF Themochemical Tables, Fourth Edition. 1998, s. 1–1951. Dostupné také z: https://webbook.nist.gov/cgi/cbook.cgi?ID=C10102440&Mask=1&Type=JANAFG&Table=on#JANAFG.
67. HIRKA, Ivan. Numerical Modelling of Processes in Thermal Plasma Reactor [online]. 2013 [cit. 2023-05-10]. Dostupné z: https://dspace.cvut.cz/handle/10467/20102.
68. *Koncepce propojení nového designu trhu v elektroenergetice s regulovanými cenami* [online]. [B.r.] [cit. 2022-12-10]. Dostupné z: https://www.eru.cz/koncepce-propojeni-noveho-designu-trhu-v-elektroenergetice-s-regulovanymi-cenami.
69. *Změna, která se dotkne každého. Úřad chystá revoluci v tarifech - Seznam Zprávy* [online]. [B.r.] [cit. 2022-12-10]. Dostupné z: https://www.seznamzpravy.cz/clanek/ekonomika-byznys-rozhovory-postrach-chaluparu-se-vraci-urad-chysta-revoluci-v-tarifech-pro-elektrinu-215396.
70. [Online]. [B.r.] [cit. 2022-12-10]. Dostupné z: https://www.predistribuce.cz/cs/potrebuji-zaridit/zakaznici/zmena-rezervovaneho-prikonu/.
71. *Česká energetika ve 21. století* [online]. [B.r.] [cit. 2023-01-03]. Dostupné z: https://www.cez.cz/cs/o-cez/vyrobni-zdroje/jaderna-energetika/jaderna-energetika-v-ceske-republice/nove-jaderne-zdroje/proc-nova-jaderna-elektrarna/ceska-energetika-ve-21.-stoleti.
72. *V Temelíně vznikne do roku 2032 první malý modulární reaktor v ČR | ČeskéNoviny.cz* [online]. [B.r.] [cit. 2023-01-03]. Dostupné z: https://www.ceskenoviny.cz/zpravy/v-temeline-vznikne-do-roku-2032-prvni-maly-modularni-reaktor-v-cr/2259492.

73. *Zachytávání a ukládání oxidu uhličitého* [online]. 2022 [cit. 2023-01-03]. Dostupné z: https://cs.wikipedia.org/w/index.php?title=Zachyt%C3%A1v%C3%A1n%C3%AD_a_ukl%C3%A1d%C3%A1n%C3%AD_oxidu_uhli%C4%8Dit%C3%A9ho&oldid=21879434. Page Version ID: 21879434.

74. *Information Library - World Nuclear Association* [online]. [B.r.] [cit. 2023-01-03]. Dostupné z: https://world-nuclear.org/information-library/energy-and-the-environment.aspx.

75. *Carbon Dioxide Emissions From Electricity - World Nuclear Association* [online]. [B.r.] [cit. 2023-01-03]. Dostupné z: https://world-nuclear.org/information-library/energy-and-the-environment/carbon-dioxide-emissions-from-electricity.aspx.

76. *Vnitřní trh s energií | Fakta a čísla o Evropské unii | Evropský parlament* [online]. [B.r.] [cit. 2023-01-03]. Dostupné z: https://www.europarl.europa.eu/factsheets/cs/sheet/45/internal-energy-market.

77. *Co je třeba vědět před uzavíráním uhelných elektráren?* [Online]. 2021 [cit. 2023-01-03]. Dostupné z: https://oenergetice.cz/nazory/treba-vedet-pred-uzaviranim-uhelnych-elektraren/.

78. *Potenciál větrné energie ČR - ČSVE - Větrné elektrárny | Větrná energie* [online]. [B.r.] [cit. 2023-01-03]. Dostupné z: https://www.csve.cz/cz/clanky/potencial-vetrne-energie-cr/495.

79. *2040: třetina elektřiny z větru - ČSVE - Větrné elektrárny | Větrná energie* [online]. [B.r.] [cit. 2023-01-03]. Dostupné z: https://www.csve.cz/cz/novinky/507.

80. *Sokolovská uhelná postaví druhý největší solární park v Česku* [online]. [B.r.] [cit. 2023-01-03]. Dostupné z: https://www.e15.cz/byznys/prumysl-a-energetika/sokolovska-uhelna-postavi-za-miliardu-solarni-park-druhy-nejvetsi-v-cesku-1380932.

81. *ČEZ zvažuje výstavbu dvou nových plynovek, říká Cyrani* [online]. [B.r.] [cit. 2023-01-03]. Dostupné z: https://www.e15.cz/rozhovory/zvazujeme-vystavbu-dvou-plynovych-elektraren-rika-pavel-cyrani-z-cez-1381537.

82. *Ministerstvo průmyslu nečekaně podpořilo provozní podporu pro soláry* [online]. [B.r.] [cit. 2023-01-03]. Dostupné z: https://www.e15.cz/byznys/prumysl-a-energetika/ministerstvo-prumyslu-necekane-podporilo-provozni-podporu-pro-solary-cez-zmenu-vita-1381281.

83. *ČEPS, a.s.* [Online]. [B.r.] [cit. 2023-01-03]. Dostupné z: https://www.ceps.cz/cs/kodex-ps.

84. *ČEPS, a.s.* [Online]. [B.r.] [cit. 2023-01-03]. Dostupné z: https://www.ceps.cz/cs/cinnosti.

85. *Využití odpadního tepla pro výrobu elektřiny, tepla a chladu* [online]. 2015 [cit. 2023-01-03]. Dostupné z: https://oenergetice.cz/elektroenergetika/vyuziti-odpadniho-tepla-pro-vyrobu-elektriny-tepla-a-chladu/.

Appendices

Continent/Country	Since year	Type of waste	Capacity ($^{tons}/_{day}$)
Europe			
Moscow, Russia	2002	LRW	6.0-9.5
Kozloduy, Bulgaria	2010	LRW	5.0
Bordeaux, France	1998	MSW ash	10.0
Kedzierzyn-Kozle, Poland	2010	Industrial solid	10.0
Morcenx, France	2001	Asbestos	30.0
Bergen, Norway	2001	Tannery	15.0
America			
Madison/Pennsylvania	2009	Construction	18.0
Alpoca, Virginia	2003	Ammunition	10.0
Hawthorne, Nevada	2006	Munitions	10.0
Montreal, Canada	2001	MSW	2.5
US Army	2011	MSW, HW, industrial	10.5
Richland, Washington	2002	Hazardous	4.0
Honululu, Hawaii	2001	Medical	1.0
US Navy	2004	Shipboard	7.0
Quebec, Canada	2013	Refrigerant	1.2
Asia			
Taiwan	2006	LRW	5.0
Utashinai, Japan	2002	MSW, automobile	300.0
Mihama-Mikata, Japan	2002	MSW, sewage sludge	25.0
Guangdong, China	2016	MSW, fly ash	30.0
Shimonoseki, Japan	2002	MSW ash	42.0
Kakogawa, Japan	2003	MSW ash	30.0
Imizu, Japan	2002	MSW ash	10.0
Maizuru, Japan	2003	MSW ash	6.0
Yongin, Korea	1997	MSW ash	14.0
Hiemji, Japan	2006	MSW ash, e-waste	5.0
Osaka, Japan	2006	E-waste	4.0
Nagpur, India	2010	Hazardous	68.0
Pune, India	2009	Hazardous	68.0
Sichuan, China	2006	Hazardous chemical	3.0
Tainan, Taiwan	2005	Hazardous, industrial	3.0-5.0
Taiwan	2007	Hazardous, industrial	0.5
Taiwan	2011	Hazardous, industrial	1.5
Iizuka, Japan	2004	Industrial solid	10.0
Shanxi, China	2008	POPs, Medical	5.0
Shanghai, China	2014	Medical, fly ash	30.0
Shanghai, China	2013	Medical	1.5

Table 1: Worldwide deployment of some thermal plasma waste treatment facilities [7]